

6101207

UNIVERSITY OF
RESEARCH INSTITUTE
EARTH SCIENCE LAB.*Economic Geology*
Vol. 74, 1979, pp. 339-350SUBJ
MING
EGDI

The Economic Geology and Development of Igneous Phosphate Deposits in Europe and the USSR

ARTHUR J. G. NOTHOLT

Abstract

Phosphate deposits of igneous origin contributed some 19 million metric tons to the total world marketable output of phosphate rock of nearly 116 million metric tons in 1977. Most of this was produced in the USSR from the Khibiny Complex, Kola Peninsula. There was production at the neighboring Kovdor Complex and, in northern Europe, at Grängesberg in central Sweden. In Europe and the USSR, four other igneous complexes are known to be at various stages of development as commercial sources of phosphate.

Most of the igneous complexes reviewed are characterized by assemblages of alkali-rich intermediate and ultrabasic rocks and carbonatite, the intrusions being generally of Siluro-Devonian or Carbo-Permian age, with the notable exception of the Precambrian Siilinjärvi carbonatite in central Finland. The complexes are also invariably located close to or within regional linear fracture zones.

Associated with the igneous complexes in Europe and the USSR is an interesting variety of apatite-bearing rocks. In addition to the remarkable nepheline-apatite orebodies of the Khibiny Complex, there are other deposits, including apatite-forsterite and apatite-forsterite-magnetite rocks, as well as apatite-bearing carbonatites and, particularly, their weathering derivatives, which have their commercially important counterparts in other parts of the world. The phosphate mineral is invariably fluorapatite, with francolite occurring prominently in weathered zones. Other minerals of value or potential economic importance include magnetite, vermiculite, baddeleyite, bastnaesite, pyrochlore, chalcopyrite, fluorite, and barite.

Introduction

PHOSPHATE deposits of igneous origin are of growing importance in several parts of the world, contributing in 1977 some 19 million metric tons of marketable phosphate rock in the form of apatite concentrate, equivalent to about 18 percent of the total world output of phosphate rock in that year of nearly 116 million metric tons. Apatite was produced in Brazil, Rhodesia, South Africa, Sweden, Uganda, and the USSR (Fig. 1), but the increase of some 11 million metric tons from these sources over the last decade is largely due to the significant expansion of operations at the Khibiny apatite mines in the USSR, situated in the Kola Peninsula about 160 km south of the ice-free Arctic port of Murmansk. The Khibiny Complex has been in continuous production since 1929 and output has grown rapidly since World War II, reaching 3.7 million metric tons in 1960, 9.5 million metric tons in 1968, and an estimated 15 million metric tons in 1977. Production is almost entirely in the form of apatite concentrate averaging 39.5 percent P_2O_5 .

In Europe and the USSR, apatite is produced also at the Kovdor Complex in northern Karelia west-southwest of Khibiny and at Grängesberg in central Sweden, but in both these instances output is at present on a limited scale and as a by-product of iron ore

mining. At Grängesberg dephosphorization of iron ore is being undertaken which provides a high-grade apatite concentrate containing 16.8 percent P (38.5% P_2O_5). A plant has been constructed which is capable of producing 160,000 metric tons of apatite concentrate a year; production in 1977 amounted to about 50,000 metric tons. There are, in addition to Khibiny and Kovdor, four other igneous complexes which are known to be at various stages of development. These are the Sokli and Siilinjärvi Complexes in Finland, the Kodal dike in southern Norway, and the Oshurkov Complex in the Buryat region near Lake Baikal, where the large Synnyr intrusive has also attracted considerable interest.

It is the purpose of this contribution to summarize the distribution and mode of occurrence of the more important igneous apatite deposits in Europe and the USSR. These deposits are associated with a group of closely related intrusive alkalic igneous rocks which are not normally regarded as being of common occurrence, are usually of relatively limited extent, and are sometimes difficult to recognize. In view of their existing or potential economic importance, it is hoped that the contribution will serve also to act as a stimulant and guide to exploration for new occurrences, particularly in areas where sedimentary

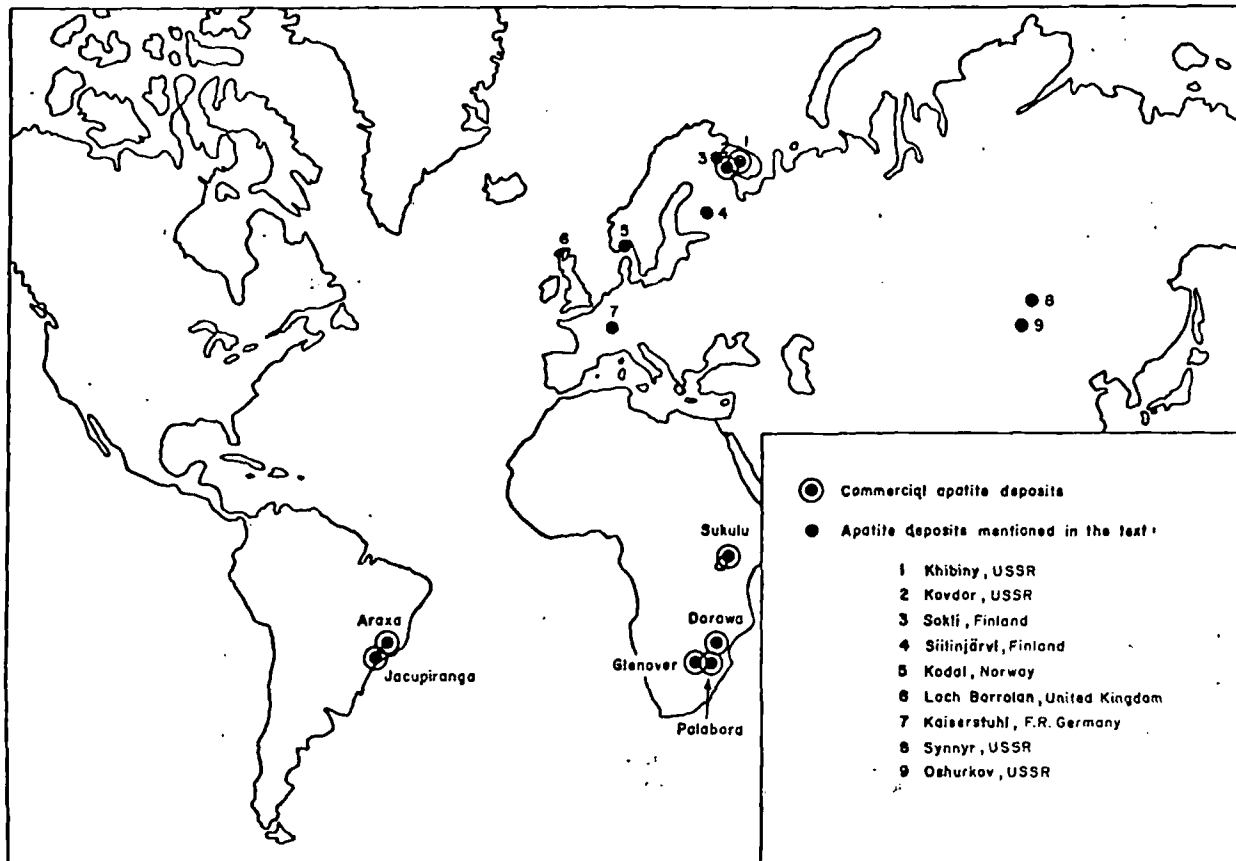


FIG. 1. Distribution of apatite-bearing alkalic igneous complexes and related rocks.

deposits are unknown or not amenable to commercial exploitation at present.

Geological Background

The widespread interest in the USSR in the distribution and nature of apatite mineralization, particularly in alkalic igneous intrusions and carbonatites, is reflected in the numerous examples which have been described in the literature in recent years, including, for example, occurrences recorded from parts of Kazakhstan, Eastern Sayan, Arctic Siberia, Yakutia, and the Maritime Territory of the Soviet Far East (Vorob'eva and Petrov, 1968). Of these, the Synnyr and Oshurkov Complexes near Lake Baikal, in the Buryat region, have attracted considerable interest as a source of phosphate and the latter complex is reported to be undergoing development.

Several interesting alkalic complexes and carbonatites occur also in Europe where, it may be recalled, phosphate deposits in the form of apatite veins and lenses were extensively worked in some countries during the latter half of the 19th century before the advent of cheaper sources of supply from North Africa and North America. In most cases, the com-

plexes have been known for many years and have been the subject of detailed petrological research, while their phosphate potential, if any, has remained unrecognized or largely ignored. For example, the large jacupirangite dike at Kodal in southern Norway was described in 1933 but attracted commercial interest only during the late 1960s. Similarly, the Loch Borrulan intrusion in the Northwest Highlands of Scotland known since at least 1892, has only quite recently been shown to contain significant amounts of titaniferous magnetite and apatite. The discovery in 1967 of the major Sokli Carbonatite Complex in northern Finland, on the other hand, demonstrates the success that can attend the application of modern exploration techniques.

Geologically the igneous apatite deposits of Europe and the USSR are characterized by their association with intrusive complexes which consist of assemblages of alkali-rich intermediate and ultrabasic rocks and carbonatites generally of limited areal extent. Thus, varieties of nepheline-syenite, as well as ijolite and jacupirangite, are prominent, except at Sokli and Sillinjärvi, where carbonatite predominates. The complexes generally intrude Precambrian gneisses and schists and are themselves usually of Caledonian

(Siluro-Devonian) or Hercynian (Carbo-Permian) age, with the notable exception of the Precambrian Sillinjärvi Carbonatite Complex which is probably the oldest in the Baltic Shield. Associated with these igneous complexes is an interesting variety of apatite-bearing rocks.

The remarkable large sheetlike, nepheline-apatite orebodies of the Khibiny Complex appear to be unique, particularly as the high hopes apparently once entertained of finding comparable deposits in the Synnyr intrusion near Lake Baikal have not materialized. However, other deposits represented by apatite-forsterite and apatite-forsterite-magnetite rocks, apatite-bearing carbonatite, and, particularly, the weathering derivatives, have their commercially important counterparts in other parts of the world (Deans, 1968, 1970a). For example, some 24 individual igneous complexes are known in the Kola Peninsula and neighboring Karelia of which at least 12 contain carbonatite (Kukharenko, 1965) and have associated with them apatite deposits essentially similar to those found in some of the carbonatitic alkalic complexes of eastern and southern Africa, Brazil, and Canada.

Structural Setting

The existence of genetic links between alkalic magmatism and other geological events has been recognized for many years, although their precise nature is still a matter of some controversy. The frequent association of alkalic complexes and carbonatites with major, often long-lived, fault zones is well known from many parts of the world, particularly from East Africa and Canada, and a similar relationship appears to hold true for most of the complexes described in this paper. On a continental scale, the presence of a complex rift system linking the carbonatitic alkalic complexes of eastern Canada and Greenland with those of northern Europe and the adjacent parts of the USSR has been postulated, the complexes within this system together forming a North Atlantic alkalic igneous province (Doig, 1970). However, for the intrusions located on the European side of the province, a close relationship with major orogenic episodes may be more significant (Vartiainen and Woolley, 1974).

The Kola Peninsula and Karelia form an integral part of the Baltic Shield within which the location of the associated alkalic complexes may have been controlled by an ancient deep fracture zone (Kukharenko, 1967) extending from the Kola Peninsula in a general southwestward direction through Finland and Sweden to link up with the much younger (Permian) Oslo Graben, a total distance of some 1,500 km. However, the evidence does not appear to be entirely conclusive; a somewhat different

interpretation (Belyayev et al., 1976) places most of the alkalic complexes of the Kola Peninsula along a series of concentric ring faults centered on the Khibiny Complex. Moreover, other major tectonic trends in the Precambrian rocks of the Baltic Shield are discernible, the Sillinjärvi Carbonatite Complex lying at the intersection of a major northwest-southeast trending lineament and north-south fractures developed in the granite gneiss country rock (Puustinen, 1971).

USSR

Khibiny, Kola Peninsula

The USSR is the world's second largest producer of phosphate rock, based largely on the remarkable Khibiny alkalic igneous complex just north of Kirovsk, some 16 km south of Murmansk, where four large mines—Kukisvumchorr (S. M. Kirov), Yukspor, Rasvumchorr, and Tsentralny (Apatite Circus)—have been in operation since 1964. Both apatite and nepheline concentrates are produced, the latter being used for the production of alumina. Marketable apatite production is at present around 15 million metric tons per annum, but there are plans to raise output to some 18 million metric tons by 1980. Reserves within the Khibiny Complex were estimated in 1970 at 2,700 million metric tons averaging 18 percent P_2O_5 .

The geology of the Khibiny Complex and its associated apatite-nepheline deposits are well documented (Ramsay and Hackman, 1894; Polkanov, 1937; Ivanova, 1963; Onokhin, 1965; Galakhov, 1966a, b; Virovlyanskiy and Blagodeteleva, 1966; Minakov, 1967; Gerasimovski et al., 1974). The alkalic rocks of the complex first became known as a result of investigations carried out by W. Ramsay and V. Hackman during the early 1890s. The complex was again studied from 1920 to 1928 during expeditions organized by the Institute for Investigation of the North and by the Academy of Sciences of the USSR under the leadership of A. E. Fersmann, which led to the discovery of the Kukisvumchorr and Yukspor apatite deposits by A. N. Labuntsov and V. J. Vlodavetz in 1927 and 1928, respectively. These and subsequent investigations have shown that the Khibiny pluton, which extends over 1,327 km², is a ring complex about 40 km in diameter, consisting essentially of foyaite surrounded by inward and generally steeply dipping sheets of other varieties of nepheline syenite. The intrusions are horseshoe-shaped, opening and generally wedging out toward the east (Fig. 2). At least seven intrusive phases have been recognized; age determinations indicate that the complex is of lowermost Permian (Sakmarian) or upper Carboniferous (Stephanian) age,

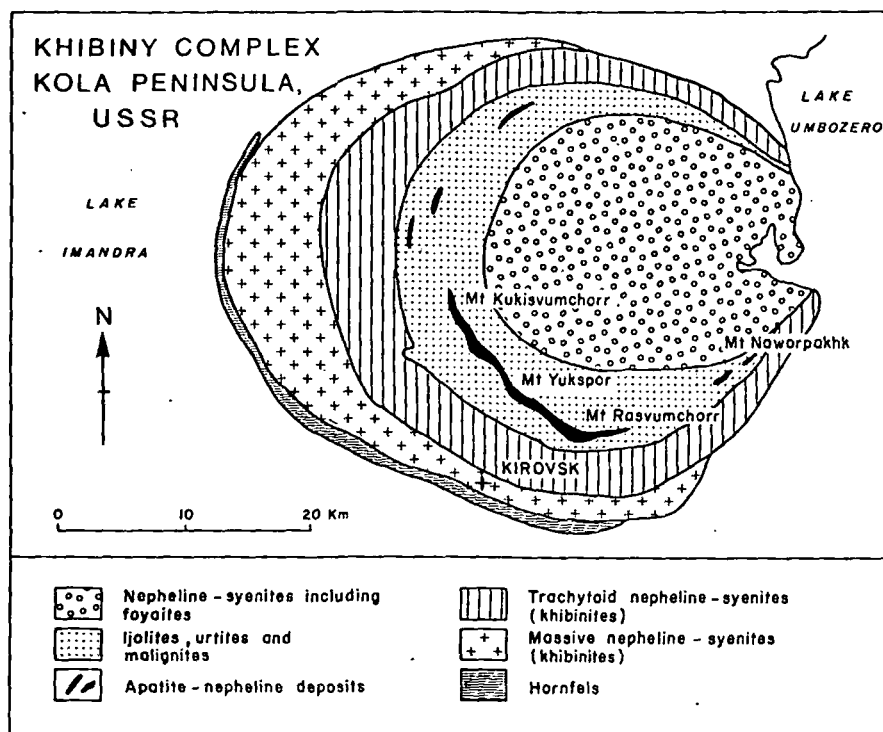


FIG. 2. Simplified geological map of the Khibiny Complex, Kola Peninsula, USSR. (Adapted from Onokhin, 1965, and Gerasimovski et al., 1954.)

although there is some evidence of older (Siluro-Devonian) igneous activity in certain parts of the complex (Virovlyanskiy and Blagodeteleva, 1966).

The apatite-nepheline orebodies of the Khibiny Complex are restricted to a zone of layered ijolitic (nepheline-aegirine-apatite-sphene) rocks which occupy only about 4 percent of the area of the complex. Individual deposits vary from high-grade ores to apatitic ijolites and urtites, generally containing

15 to 75 percent apatite (6-31% P_2O_5), 10 to 80 percent nepheline, 1 to 25 percent aegirine and aegirine-augite, as well as sphene (5-12%), feldspar, and titanomagnetite. The phosphate mineral is fluorapatite, with selected specimens showing up to 11.42 percent SrO and 4.90 RE_2O_3 (Volkova and Melentiev, 1939). However, both the apatite ore (Golovanov et al., 1968) and concentrate contains significantly smaller amounts of these constituents (Table 1).

By far the largest orebody and the source of nearly all the apatite produced to date at Khibiny is an irregular, lens-shaped mass which is overlain by nepheline-syenites and underlain by a variety of ijolites and urtites and dips to the northeast generally between 30° and 40° toward the center of the complex. It has an arcuate outcrop parallel to the southwestern boundary of the intrusion. This orebody has been traced for a distance of some 11 km along the surface, from Mount Kukisvumchorr in the northwest to Mount Rasvumchorr in the southeast, and for more than 2 km along the dip. Its thickness ranges from 10 to as much as 200 m at Kukisvumchorr and averages about 100 m. Typically, there is a bizonal structure, corresponding, respectively, to the upper third of the orebody averaging 23 to 28 percent P_2O_5 and the lower section with 15 to 20 percent P_2O_5 . Mining operations have revealed a variety of internal features, including markedly dif-

TABLE 1. Chemical Composition of Kola Apatite Ore and Concentrate

	Ore	Concentrate
	Percent	
P_2O_5	18.0	39.5
CaO	25.6	50.0
Al_2O_3	13.3	0.71
SiO_2	23.1	2.04
Fe_2O_3	4.8	0.45
FeO	0.5	0.34
TiO_2	1.6	0.42
MnO	0.2	0.42
MgO	0.7	0.10
SrO	1.2	2.14
RE_2O_3	0.4	0.85
NaO	5.5	0.13
K_2O	3.0	0.11
V_2O_5	0.08	0.01
F	1.12	3.00
Moisture	0.3	—
Ignition loss	—	0.15

ferent sets of fold structures and fissure or shear zones along which the rocks have become brecciated and weathered. Such oxidized ores contain a relatively large amount of finely dispersed argillaceous material and occur chiefly in the Rasvumchorr and Yukspor deposits, constituting about 8 to 10 percent of the total apatite-nepheline ore reserves in the Khibiny Complex.

Kovdor

Various apatite-rich rocks occur within the Kovdor alkalic and ultrabasic igneous complex, which is situated in the western part of the Kola Peninsula served by the railway from Kirovsk some 130 km to the east. The complex has been mined by open-pit methods since 1964 as a source of magnetite ore which averages about 50 percent magnetite and 16 percent apatite (6.6% P_2O_5). Reserves of iron ore have been placed at about 708 million metric tons, so that approximately 113 million metric tons of apatite may be present. Electromagnetic separation yields tailings containing about 30 percent apatite (12.5% P_2O_5), which were hitherto dumped as waste. However, beneficiation tests showed that these could provide concentrates containing more than 35 percent P_2O_5 , with a recovery of 73 percent (Golovanov et al., 1968). A recovery plant with a capacity of 900,000 metric tons per annum of apatite concentrate, with by-product baddeleyite, came into operation at the end of 1974. Since 1974 vermiculite has also been produced from the complex as a separate mining operation.

The Kovdor massif (Rimskaya-Korsakova, 1964; Ternovoy et al., 1976), which is of Caledonian, probably Middle Devonian, age, covers an area of about 38 km². It has a concentrically zoned structure (Fig. 3), with an outer belt chiefly of ijolite, an inner semicircular body of melilitic rocks including turjaite, and an ultrabasic core composed of pyroxenites, pyroxene-olivine-rich rocks, and olivinites. These ultrabasic rocks closely resemble the pyroxenites and phoscorites of the Palabora Complex in South Africa, particularly in also containing abundant vermiculite which is mined from the olivinite core and, in the eastern part of the complex, pegmatoid diopside-forsterite-phlogopite rocks. Later intrusive phases consist of apatite-forsterite rocks and magnetite ores, followed by the emplacement of veins and lenses of carbonatite and, finally, thin veins of nepheline syenite.

Apatite-forsterite rocks are concentrated in the southwestern part of the Kovdor Complex at the western end of Kovdoro Lake where, together with the magnetite ores which they enclose, they form an "ore complex" about 1.3 km long and 100 to 800 m wide. This area is characterized by steeply dipping

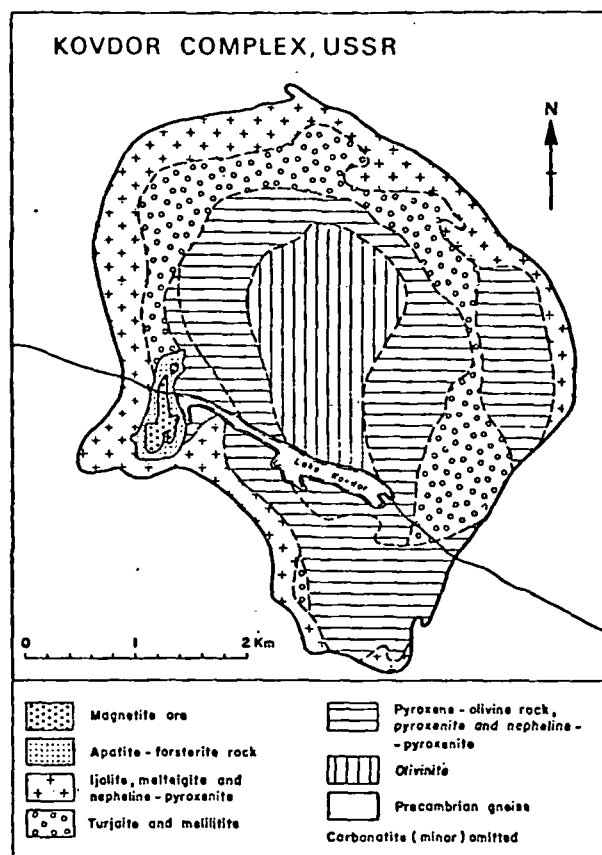


FIG. 3. Generalized geological map of the Kovdor Complex, USSR. (After Rimskaya-Korsakova, 1964.)

vertical veins and lenses of variable thickness chiefly in ijolite and pyroxenite and composed essentially of variable amounts of apatite, forsterite, magnetite, calcite, and phlogopite. In addition to primary apatite, francolite occurs in crush zones as a late alteration product of the magnetite ores and also a result of preglacial and more recent weathering. The chemical composition of the principal apatite-bearing iron ores (Rimskaya-Korsakova, 1964) is shown in Table 2. Not unexpectedly, the high magnesium content of the apatite concentrate is reported to be presenting considerable processing problems at fertilizer plants.

Oshurkov

Apatite deposits discovered by the Buryat Geological Directorate in 1962 (Smirnov et al., 1968) in the upper Proterozoic Oshurkov Complex, an oval-shaped intrusion 9 km² situated in the Buryat Republic some 15 km northwest of Ulan-Ude and close to road and rail links, are being developed to meet the growing regional requirements for fertilizer. Although no large-scale mining appears to have been undertaken as yet, a fertilizer complex based on Oshurkov ore is to be commissioned nearby in 1979

TABLE 2. Chemical Composition of Apatitic Iron Ores, Kovdor Complex

	Apatite-forsterite-magnetite ore ¹	Calcite-bearing magnetite ore ²
	Percent	
P ₂ O ₅	6.02	6.21
CaO	10.27	14.10
SiO ₂	8.69	7.01
Al ₂ O ₃	3.38	2.61
Fe ₂ O ₃	38.60	35.17
FeO	12.61	14.19
MgO	14.50	11.38
Na ₂ O	0.12	0.24
K ₂ O	0.23	0.21
TiO ₂	0.60	0.69
MnO	0.27	0.34

¹ Average of 21 analyses.² Average of 18 analyses.

which, it is reported, will be capable of producing annually about 1.3 million metric tons of apatite concentrate. If so, perhaps some 12 million metric tons of apatite ore will be mined annually by open-pit methods. Reserves were reported in 1970 to be around 1,000 metric tons, of which 500 million metric tons averaging 4 to 4.5 percent P₂O₅ are estimated to occur to a depth of 100 m.

The Oshurkov apatite deposits represent an unusual mode of occurrence, being found as disseminations, pockets, and veinlets in medium-grained biotite-hornblende-diorite, within an irregular, steeply dipping zone which averages 1 km in width and extends over a distance of more than 3.5 km in a northwest to southeast direction. Several varieties of diorite have been identified but on average these contain 4 to 6 percent apatite, 5 to 7 percent biotite, 45 percent plagioclase, 2 to 3 percent diopside, and up to 35 percent hornblende; sphene and titanomagnetite occur as accessory minerals. Most of the apatite is believed to be of metasomatic origin (Andreev, 1968), the mineral being found replacing diopside, hornblende, and plagioclase. Locally, in brecciation zones and zones of intense metamorphism, up to 50 percent apatite may be present. Although the prospective apatite ore is of very low average grade, laboratory tests (Golovanov et al., 1968) have shown that a concentrate with 35 percent P₂O₅ can be produced by flotation, with a phosphate recovery of 94 percent. A concentrate with 35.14 percent P₂O₅ contained also 3.86 percent SiO₂, 2.15 percent Al₂O₃, 0.45 percent TiO₂, and 0.26 percent MgO (Koval'skii and Kostromin, 1968).

Synnyr

The Synnyr alkalic igneous complex (Arkhangel'skaya, 1965, 1968; Nechayeva, 1965), which is situated in the Synnyr Ridge about 120 km northeast of Nizhneangarsk at the northern end of Lake Baikal,

is one of the largest of its type in the USSR, with a diameter of 25 km and occupying an area exceeding 600 km². It was first investigated in detail by the All-Union Scientific-Research Institute of Geology between 1958 and 1961 and attracted particular attention when talus deposits of biotite-pyroxene-apatite rock were discovered by the Buryat Geological Administration in 1963. Synnyr is one of seven alkaline complexes discovered in the Northern Baikalian Highlands in the Baikal Rift System within a narrow belt up to 400 km long extending from the northern end of Lake Baikal northeastward to the middle reaches of the Mama River in Irkutsk. Age determinations indicate that the complexes range from Upper Devonian (Famennian) to upper Carboniferous (Stephanian) in age. A Devonian age has been assigned to the Synnyr Complex (Nechayeva, 1965), which intrudes Precambrian (Proterozoic) rocks and comprises a multiphase ring complex composed chiefly of various potash-rich nepheline-syenites (Fig. 4).

Some 20 individual apatite-bearing deposits have been found within the complex in the form of narrow, semicircular bodies of very variable dimensions composed of medium- to fine-grained melanocratic nepheline-syenites which resemble those found in the ijolite-urtite intrusions of the Khibiny Complex but at Synnyr occupy only about 5 percent of the total area of the complex. In spite of the similarity, apatite deposits comparable with those of Khibiny in terms of tonnage and grade have not been found. The rocks generally contain 3 to 10 percent apatite (1 to 4% P₂O₅) and consist principally of nepheline, analcite, aegirine, aegirine-augite, potassic-sodic feldspar, and biotite, with sphene and titanomagnetite as major accessories. There are richer zones, however, as in the Podledny area, which consist essentially of apatite, pyroxene, and biotite, with admixtures of orthoclase, nepheline, and plagioclase in places, and accessory magnetite and sphene. These zones contain from 5 to 80 percent apatite (2 to 33% P₂O₅). In the Vysodnyy area there are about eight irregular, sheetlike bodies, one of which is up to 3 m thick, dips to the north at 15° to 30°, and contains from 5 to 75 percent apatite. Many of the samples contain 15 to 18 percent P₂O₅ and in places 10 and 20 percent magnetite may be present. As in the Khibiny pluton apatites from the Synnyr Complex are remarkable for their high contents of RE₂O₃ (1.62%) and SrO (2.28%) (Spas-ski, 1970).

Finland

Sokli

A particularly interesting development in Europe has been the discovery, in 1967, of the Sokli Car-

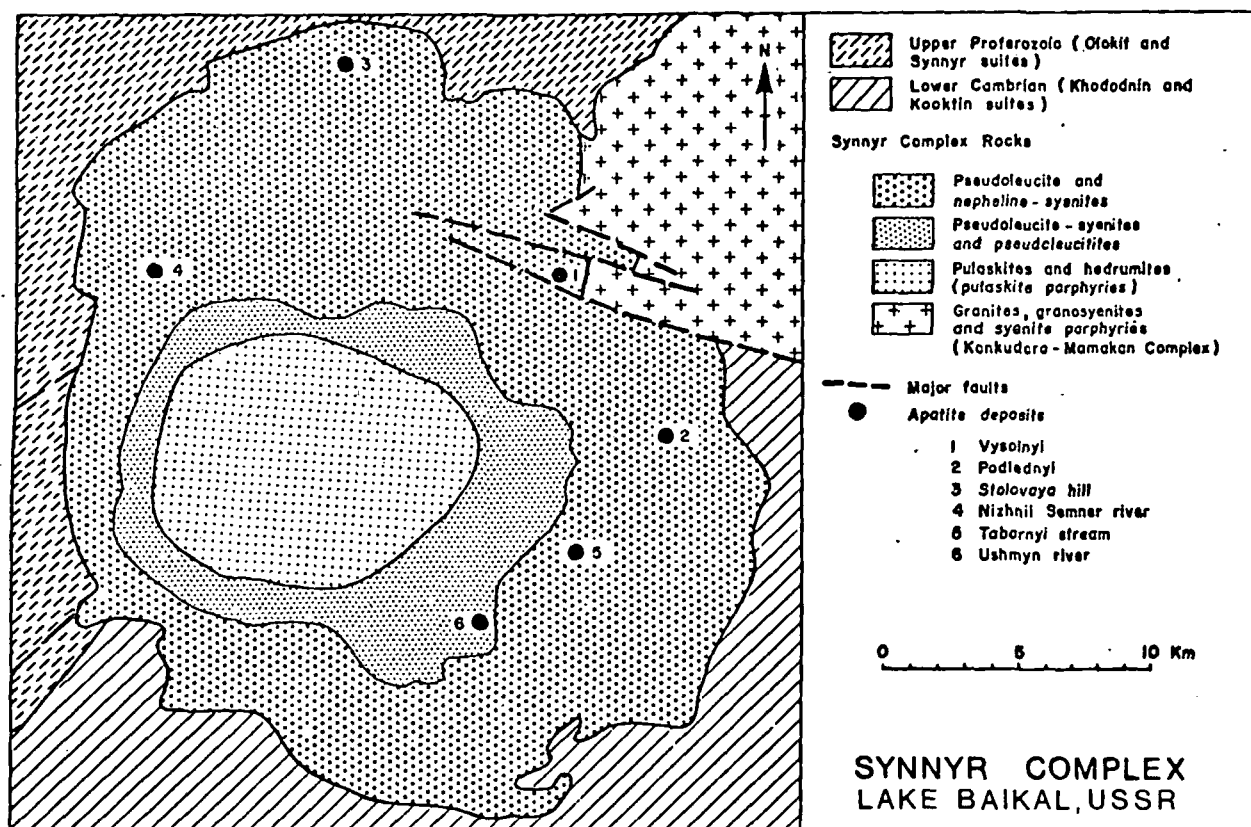


FIG. 4. Simplified geological map of the Synnyr Complex, Lake Baikal, Buryat, USSR. (Based on Ivanova, 1969).

bonatite Complex situated in northern Finland approximately 145 km north of the Arctic Circle and about 80 km northeast of Savukoski. This discovery was the result of a low-level aerial magnetometer and scintillometer survey across structures comparable to those which appear to control the distribution of igneous intrusions in the neighboring parts of the USSR. The survey revealed a circular magnetic anomaly some 5 to 6 km in diameter and also a radioactive anomaly. Since there are virtually no outcrops, the presence of carbonatite was confirmed by the discovery of boulders of carbonatite in stream sections and by trenching. The Sokli Complex is remarkable for its areal extent of 18 km², making it perhaps the largest mass of carbonatite yet known, and for its partial cover of residual, ferruginous phosphate rock of a type hitherto regarded as the product of weathering restricted to the tropical regions of, for example, Africa and Brazil. Drilling by Rautaruukki Oy, the steel and vanadium producer responsible for the discovery and development of the Sokli Carbonatite Complex, has proved over 50 million metric tons of phosphate rock averaging 19 percent P₂O₅, with indicated reserves of 50 to 100 million metric tons of lower grade. In spite of their remote location, the company plans to bring the Sokli

phosphate deposits into commercial production. Preliminary processing tests have shown that apatite concentrates containing up to 37 or 39 percent P₂O₅ can be obtained by washing, magnetic separation, and flotation, a phosphate recovery of about 70 percent being attainable.

The almost circular Sokli Carbonatite Complex (Paarma, 1970; Vartiainen, 1975) occupies a shallow topographical basin some 20 to 30 m deep surrounded by a discontinuous ring of low hills composed chiefly of Archaean (pre-Karelian) granite gneiss, with wide beds of amphibolite and subordinate bodies of olivinite and serpentinite. As shown in Figure 5, the complex comprises mainly carbonatite (söвите), but varieties containing tremolite and phlogopite also occur, the latter mineral being associated with a magnetite-rich type in which serpentine and clinohumite are common and apatite abundant, exhibiting a mineralogy analogous to phoscorite in the Palabora Igneous Complex of South Africa (Hanekom et al., 1965). Surrounding the carbonatite is fenitized bed rock, the boundary being represented by a zone of carbonatite-fenite breccia up to about 500 m wide. A series of age determinations indicates an Upper Devonian age for the carbonatite, which thus falls within the same age range as the intrusions in the

neighboring parts of the USSR including Kovdor, which is situated only some 60 km east-southeast of Sokli.

Fresh carbonatite typically contains 2 to 4 percent P_2O_5 (5–10% apatite), but the most interesting from the economic standpoint are the regolithic deposits resulting from the weathering and dissolution of the underlying carbonatite, followed by secondary deposition of goethite and other iron minerals and of francolite. The main development of secondary phosphate occurs in the northwestern part of the complex north of the Sokli stream (Soklioja), deposits varying from only a few meters to about 70 m in thickness and locally filling steep-sided depressions up to about 100 m wide. In general, quarry sections of the type reproduced in Figure 6 show a zone of weathered carbonatite 5 to 10 m thick and containing 2 to 10 percent P_2O_5 , overlain by predominantly earthy, brown phosphate which consists chiefly of francolite and goethite, together with lesser amounts of primary apatite, magnetite, micas, and amphiboles, and minor amounts of pyrochlore, zircon, and baddeleyite (Deans, 1970b). There are also minor amounts of rhabdophane, an hydrated phosphate of the cerium earths. Francolite partially cements the rock and it may form slabs and irregular blocks of high-grade hard phosphate rock up to 50 cm across. Usually, however, it is fine grained, pale brown or pink to

milk-white in color, forming an incoherent mass in intimate admixtures with goethite and residual minerals liberated from the carbonatite during weathering. The secondary phosphate deposits are masked by glacial drift typically 5 to 6 m thick.

Siilinjärvi

Probably the most advanced phosphate project in northern Europe is that based on the development of the Siilinjärvi Carbonatite Complex, situated in central Finland some 20 km north of Kuopio and adjacent to the phosphoric acid plant operated by the Finnish fertilizer producer Kemira Oy. This plant came into operation in 1969 using Kola apatite and the uncertainty, since 1974, over the future supplies of this raw material from the USSR has no doubt been an important factor in the decision to evaluate the country's domestic phosphate resources. Imported phosphate of African origin has now partially replaced Kola apatite at the Siilinjärvi plant. Mining of a trial quantity of Siilinjärvi carbonatite was begun in 1975, coinciding with the setting up of a 10 metric ton per hour pilot beneficiation plant. A plant capable of producing 250,000 metric tons of apatite concentrate per annum at Siilinjärvi came into operation in late 1978. Preliminary beneficiation tests had indicated that although a concentrate containing 33 percent P_2O_5 (80% apatite) could be obtained, the car-

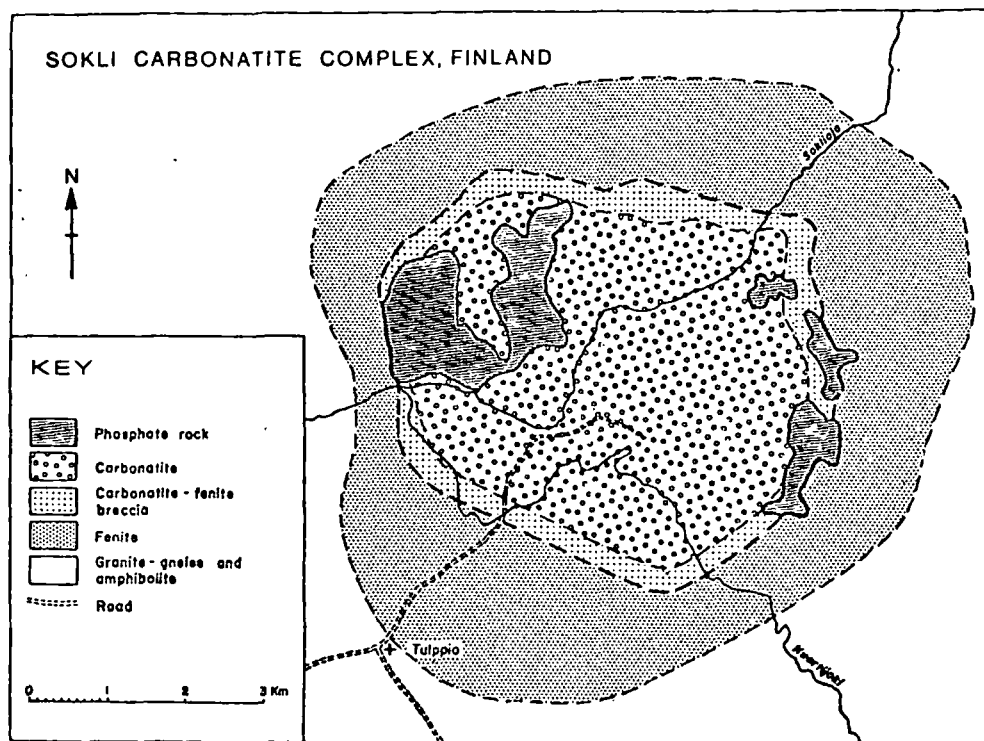


FIG. 5. Generalized geological map of the Sokli Carbonatite Complex, Savukoski, northern Finland. (Adapted from Vartiainen, 1975.)

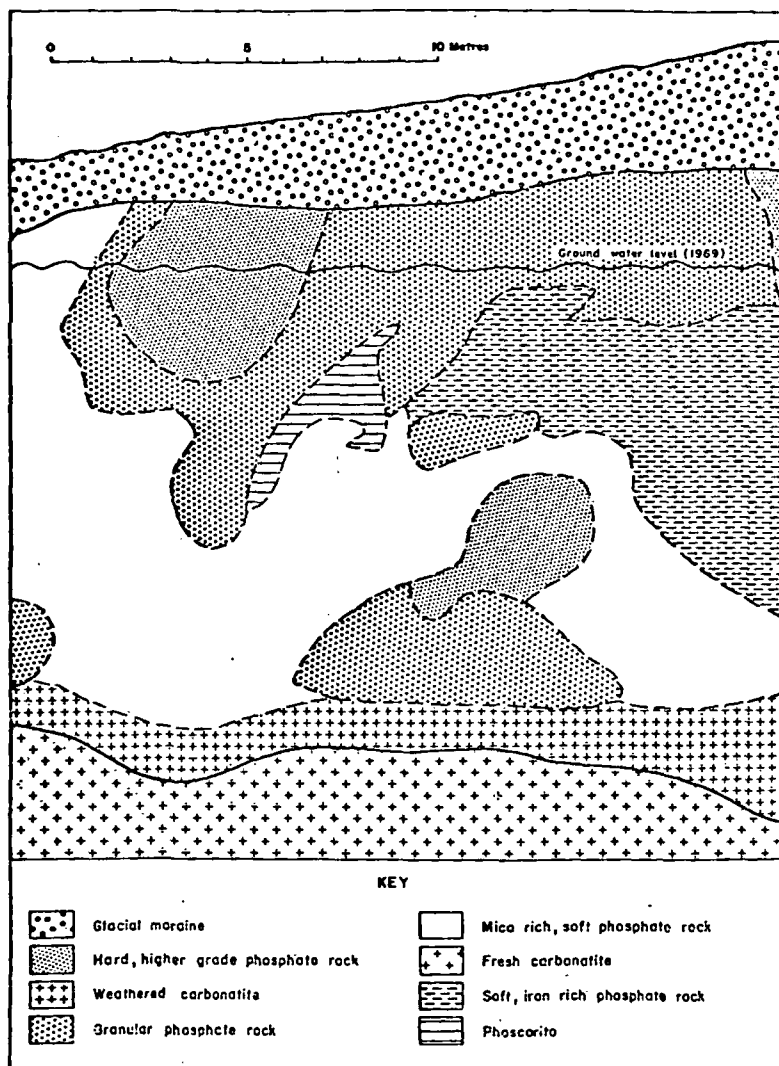


FIG. 6. Quarry section in the Sokli Carbonatite Complex, northern Finland, showing variations in the phosphate-bearing regolithic deposits overlying the carbonatite. (After Vartiainen, 1975.)

bonate content of 20 percent could not be removed easily without also making apatite recovery uneconomical. This problem has since been largely resolved and a concentrate is to be produced which contains about 35 percent P_2O_5 .

The Siilinjärvi Carbonatite Complex (Puustinen, 1971) is unusual because of its elongated shape (Fig. 7), forming an almost vertical tabular body about 16 km long and up to 1.5 km wide, covering an area of 14.7 km². It is notable also for its antiquity, K-Ar age determinations by the Institute of Geological Sciences, London, showing a range of $1,785 \pm 30$ to $2,530 \pm 45$ m.y. The Finnish sector of the Baltic Shield thus contains one of the oldest and, including the Sokli Complex, probably the largest of the carbonatite bodies known. Reserves of carbonatite containing 10 percent apatite (about 4% P_2O_5) have

been placed at 465 million metric tons to a depth of 100 m. Additional resources are indicated by boreholes drilled to a depth of 870 m without reaching the base of the complex.

The carbonatite complex at Siilinjärvi came into prominence as a potential source of phosphate with the discovery, in 1950, of significant amounts of apatite in the carbonatitic rocks of the complex. These comprise a variety of mixed rocks from a few centimeters to tens of meters thick which range in composition from glimmerite, the main constituents of which are phlogopite, alkali amphibole, and apatite, to carbonatite (sövite), consisting chiefly of calcite with accessory phlogopite, alkali amphibole, dolomite, and apatite. The rocks cover an area of nearly 4 km² or 26 percent of the area of the complex, the largest area of carbonatite occurring to the south of Lake

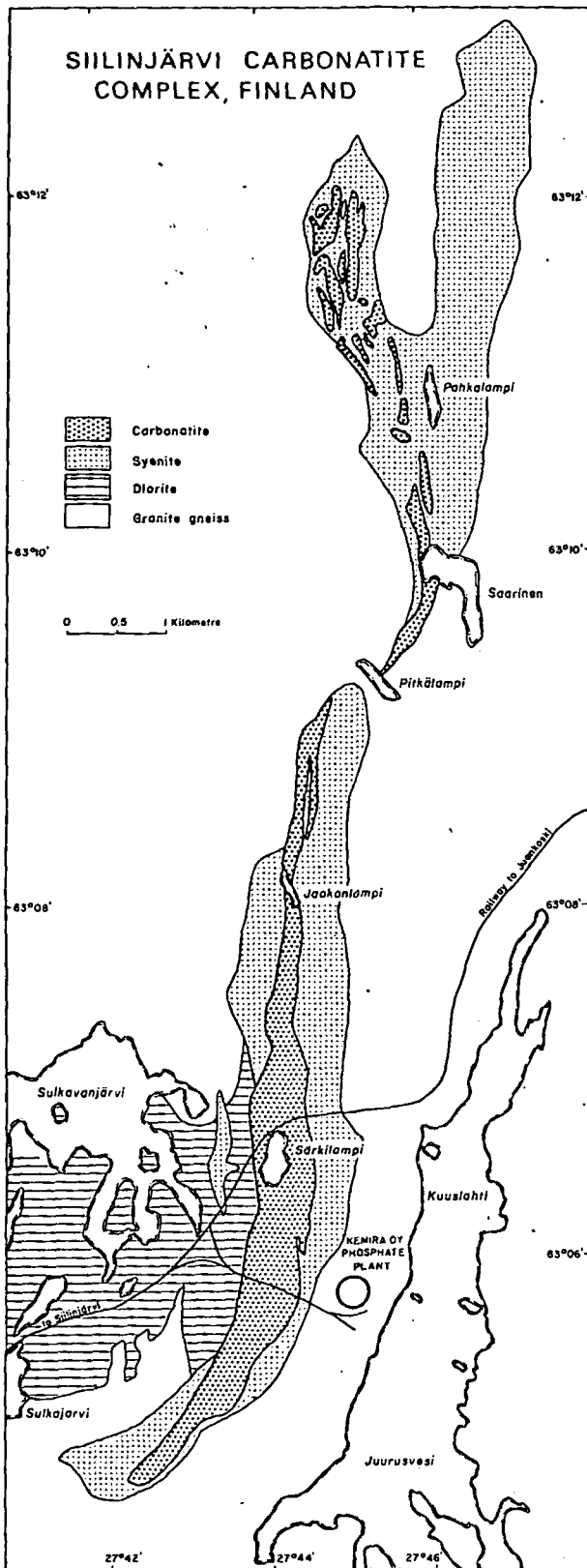


FIG. 7. Simplified geological map of the Siilinjärvi Carbonatite Complex, Kuopio, Central Finland. (Based on Puustinen, 1971.)

Pitkälampi near the Kemira Oy phosphoric acid plant. Apatite is relatively uniformly distributed in the glimmerite-carbonatite rocks, but the highest concentrations are to be found in the carbonate-rich types, a sample of micaceous carbonatite analyzed by the International Minerals and Chemical Corporation, U. S. A., showing the following composition:

	Percent
P_2O_5	24.80
CaO	36.65
SiO_2	14.97
MgO	5.84
K_2O	3.61

Norway

Kodal

Another interesting development in Scandinavia is centered on the jacupirangite dike at Kodal, situated on the west side of Oslofjord some 18 km north of Larvik, one of several occurrences of apatite-bearing jacupirangite and related alkali-rich basic igneous rocks in the Permian Oslo Igneous Province. Investigations carried out by Norsk Hydro a.s. since 1960, including diamond drilling to depths of more than 300 m below the surface, have delineated a steeply dipping and compact sheetlike body some 1.9 km long and varying in thickness from 10 to 35 m, lying within a zone up to 150 m wide which consists of disseminated ore developed in larvikite country rock. Proved reserves in the Kodal deposit total about 30 million metric tons of ore, and it is estimated that there is an additional probable reserve of about 40 million metric tons, together perhaps containing about 12 million metric tons of apatite. In addition, it has been estimated that about 30 million metric tons could be recovered as magnetite concentrate. However, since geophysical surveys carried out by the Geological Survey of Norway indicate that the deposit extends to a depth of at least 1,000 m, twice the stated tonnage may be present.

The compact variety of jacupirangite at Kodal contains 17 to 18 percent apatite, 40 percent titaniferous magnetite, 8 to 9 percent ilmenite, and 30 to 35 percent of various silicates, chiefly aegirine and minor biotite and amphibole, the corresponding chemical analysis (Bergstøl, 1972) showing the following composition:

	Percent
P_2O_5	7.98
SiO_2	11.57
CaO	14.12
TiO_2	8.48
Al_2O_3	3.46
Fe_2O_3	28.48
FeO	17.45
MnO	1.20
MgO	4.49

Accessory minerals are sphene, pyrite, chalcopyrite,

calcite, talc, and traces of rutile and hematite. Apatite occurs as fluorapatite chiefly in the form of euhedral prisms and needles 0.1 to 0.5 mm in diameter. It contains 1.1 percent RE_2O_3 (Nielsen, 1972). The disseminated rock contains between one-third and one-half of the percentages of these various minerals reported for the compact jacupirangite.

After processing tests, a feasibility study was prepared, based on an open-pit mining operation for 15 years, which envisaged an annual output of about 3 million metric tons of compact and disseminated rock. This could yield 330,000 metric tons of apatite, 800,000 metric tons of magnetite, and possibly 80,000 metric tons of ilmenite. Magnetite separation and flotation can produce an apatite concentrate with 39 percent P_2O_5 , but the decision on whether to proceed with mining at Kodal will evidently depend to a large extent on finding suitable market outlets for the titaniferous magnetite. At present Norsk Hydro consumes annually about 400,000 metric tons of phosphate rock, mainly from the USSR, Israel, and the United States, some of which is used in the company's fertilizer plant at Porsgrunn about 25 km southwest of the Kodal deposit.

Western Europe

There are two intrusive igneous complexes in western Europe from which significant amounts of apatite have been reported. The best known are in the Federal Republic of Germany, where apatite-bearing carbonatite bodies cover an area of about 1 km² in the central part of the Kaiserstuhl, a volcanic complex of Miocene age, situated within the Upper Rhine-graben, 15 km northwest of Freiburg. The rocks may contain up to 10 percent apatite (Wimmenauer, 1966), equivalent to 4 percent P_2O_5 , but are not sufficiently extensive within the complex to merit commercial interest.

Loch Borrallan

Although apatite is a widely distributed accessory mineral among igneous rocks in Scotland, the highest concentrations occur in the Loch Borrallan alkaline igneous complex in the Northwest Highlands, approximately 77 km northwest of Inverness. The possible economic significance of the apatite-bearing pyroxenites believed to form the basal layers of the complex was recognized, probably for the first time, during a survey of the phosphate resources of the European Economic Community in 1977. However, a detailed assessment of the phosphate potential of the intrusion has not yet been carried out.

The poorly exposed Loch Borrallan Complex (Shand, 1939), which is 26 km² in extent and intrudes Cambrian strata, consists of quartz syenite, nepheline syenites, and ultrabasic rocks, chiefly pyroxenites, the last named group of rocks having a

limited outcrop on the western margin of the complex. A content of only 2.31 percent P_2O_5 was originally recorded from melanite-pyroxenite (Gem-mell, 1910), but very limited drilling for titaniferous magnetite carried out on magnetic anomalies over the unexposed southwestern part of the intrusion has revealed a suite of rocks consisting predominantly of pyroxenite with gradations to hornblende pyroxenite and hornblendite, these rocks containing an average of 10 percent apatite (Matthews and Woolley, 1977). One borehole, drilled to a depth of 152 m, encountered pyroxenite throughout its entire length which contained extremely variable amounts (5 to over 90%) of titaniferous magnetite (Newman, 1971) and up to 17 percent apatite (Woolley, pers. commun., 1977). It would be tempting to suggest possible comparisons between the Loch Borrallan Complex and some of the other, apatite-bearing, alkaline complexes described in this paper, particularly bearing in mind its age (Lower Devonian) and the presence also of olivine and phlogopite-rich rocks within the complex, but this must be deferred until more detailed investigations have been carried out.

Acknowledgments

The paper is published with the permission of the Director, Institute of Geological Sciences, London. The author is grateful to Mrs. W. Khosla and Mr. A. H. J. Todd for their help in the preparation of the paper and particularly to Dr. T. Deans, a former colleague, for his critical reading of the manuscript. The assistance of Kemira Oy, Norsk Hydro a.s., and Rautaruukki Oy is also acknowledged.

MINERALS STRATEGY AND MUSEUM DIVISION
INSTITUTE OF GEOLOGICAL SCIENCES
EXHIBITION ROAD
LONDON SW7 2DE, ENGLAND
September 28, 1978

REFERENCES

- Andreev, G. V., 1968, Genetic features of the Oshurkov apatite deposit, in Vorob'eva, O. A., and Petrov., V. P., eds., *Apatites*: Moscow, Izdatel'stvo 'Nauka', p. 300-304. (In Russian)
- Arkhangel'skaya, V. V., 1965, Synnyr pluton of alkalic rocks and its apatite: *Akad. Nauk SSSR Doklady*, v. 158, p. 114-117.
- 1968, Structure of the Synnyr alkalic rock massif: *Internat. Geology Rev.*, v. 10, p. 531-540.
- Belyayev, K. D., Urad'yev, L. I., and Shul'ga, T. F., 1976, Patterns of distribution of plutons of the central type of the Kola Peninsula: *Akad. Nauk SSSR Doklady*, v. 226, p. 28-30.
- Bergstøl, S., 1972, The jacupirangite at Kodal, Vestfold, Norway: *Mineralium Deposita*, v. 7, p. 233-246.
- Deans, T., 1968, Exploration for apatite deposits associated with carbonatites and pyroxenites: *Mineral Resources Devel. Ser. No. 32*, United Nations Economic Commission for Asia and the Far East, p. 109-119.
- 1970a, Some recent developments concerning carbonatite complexes and associated phosphate deposits: *Unpub. rept.*, United Nations Economic Commission for Asia and the Far East, 4 p.

- 1970b, Mineralogical notes on niobium bearing phosphorites from the Sokli Carbonatite Complex, Finland: Mineralogy Unit, Institute of Geological Sciences, Rept. 71, 4 p. (Unpublished)
- Doig, R., 1970, An alkaline rock province linking Europe and North America: Canadian Jour. Earth Sci., v. 7, p. 22-28.
- Galakhov, A. V., 1966a, Chemical composition of rocks in the Khibiny alkalic massif: Akad. Nauk SSSR Doklady, v. 171, p. 225-228.
- 1966b, Alkalic-ultrabasic igneous activity in the Khibiny Tundras (Kola Peninsula): Akad. Nauk SSSR Doklady, v. 170, p. 85-87.
- Gemmell, A., 1910, Chemical analyses of borolanite and related rocks: Geol. Soc. Edinburgh Trans., v. 9, p. 417-419.
- Gerasimovskii, V. I., Volkov, V. P., Kogarko, L. N., and Polyakov, A. I., 1974, Kola Peninsula, in Sørensen, H., ed., The alkaline rocks: London, John Wiley & Sons, p. 206-221.
- Golovanov, G. A., Zhelnin, V. S., Kotilevskii, V. I., and Makarov, A. M., 1969, Processing of apatite ores at the ore dressing plants of "Apatite" Complex: 8th Internat. Mineral Processing Cong., 1968, v. 1, p. 489-502. (In Russian)
- Hanekom, H. J., van Staden, C. M. v. H., Smit, P. J., and Pike, D. P., 1965, The geology of the Palabora Igneous Complex: South Africa Geol. Survey Mem. 54, 185 p.
- Ivanova, T. N., 1963, Apatite deposits of the Khibiny Tundra: Moscow, Gosgeoltekhizdat, 287 p. (In Russian)
- 1969, Geological structure and apatite potential of the Synnyr alkaline massif: Leningrad, Izdatel'stvo 'Nauka', 146 p.
- Koval'skii, F. I., and Kostromin, S. V., 1968, Geologic-economic character of the Oshurkov apatite deposit, in Vorob'eva, O. A., and Petrov, V. P., eds., Apatites: Moscow, Izdatel'stvo 'Nauka', p. 304-306. (In Russian)
- Kukharenko, A. A., ed., 1965, The Caledonian complexes of ultrabasic alkaline rocks and carbonatites of the Kola Peninsula and Northern Karelia: Moscow, Izdatel'stvo 'Nedra', 772 p. (In Russian)
- 1967, Alkaline magmatic activity of the eastern part of the Baltic Shield: Zap. Vses. Mineral Obshchestva, v. 96, p. 547-566. (In Russian)
- Matthews, D. W., and Woolley, A. R., 1977, Layered ultramafic rocks within the Borrolan Complex, Scotland: Scottish Jour. Geology, v. 13, p. 223-236.
- Minakov, F. V., 1967, Initial composition and evolution of ijolite-urtite magma of the Khibiny alkalic massif: Geochemistry Internat., v. 4, p. 738-753.
- Nechayeva, I. A., 1965, Apatite-bearing rocks of the Synnyr nepheline-syenite pluton (north Baikal region): Akad. Nauk SSSR Doklady, v. 161, p. 165-167.
- Newman, D., 1971, Recent developments in mineral exploration in the northwest Highlands and Islands of Scotland: Inst. Mining Metallurgy Trans. Sec. B. v. 80, p. 276-288.
- Nielsen, N.-A., 1972, The ilmenomagnetite-apatite deposit at Kodal, S. Norway: Indus. Minerals [London], no. 55, p. 35-37.
- Onokhin, F. M., 1965, Folded structures in the Khibina apatite deposits: Internat. Geology Rev., v. 7, p. 1569-1576.
- Paarma, H., 1970, A new find of carbonatite in North Finland, the Sokli plug in Savukoski: Lithos, v. 3, p. 129-133.
- Polkanov, A. A., ed., 1937, The northern excursion, Kola Peninsula: Internat. Geol. Cong., 17th, Moscow and Leningrad, Chief Editorial Office of the Geological-Prospecting and Geodetic Literature, 119 p.
- Puustinen, K., 1971, Geology of the Siilinjärvi carbonatite complex, Eastern Finland: Comm. géol. Finlande Bull., no. 249, p. 5-43.
- Ramsay, W., and Hackman, V. 1894, The nepheline-syenite region in the Kola Peninsula: Fennia, v. 11, no. 2, 225 p. (In German)
- Rimskaya-Korsakova, O. M., 1964, Genesis of the Kovdor iron-ore deposits (Kola Peninsula): Internat. Geology Rev., v. 6, p. 1735-1746.
- Shand, S. J., 1939, Loch Borolan laccolith, north-west Scotland: Jour. Geology, v. 47, p. 408-420.
- Smirnov, F. L., Kostromin, S. V., and Zhukova, G. V., 1968, Geological structure and presence of apatite in the Oshurkovsk deposit, in Vorob'eva, O. A., and Petrov, V. P., eds., Apatites: Moscow, Izdatel'stvo 'Nauka', p. 295-300. (In Russian)
- Spasski, B. S., 1970, Mineralogical characteristics of apatites from the Synnyrsky Massif (northern Cis-Baikalia): Zap. Vses. Mineral Obshchestva, v. 99, p. 450-457. (In Russian)
- Ternovoy, V. I., Chuera, M. N., Evangulova, E. B., and Belova, A. N., 1976, On the genesis of the Kovdor apatite-francolite deposit: Zap. Vses. Mineral Obshchestva, v. 105, pt. 2, p. 241-247.
- Vartiainen, H., 1975, Sampling in the assessment of the Sokli phosphate ore: Eripainos Vuoriteollisuus, no. 2, p. 1-8. (In Finnish)
- Vartiainen, H., and Woolley, A. R., 1974, The age of the Sokli carbonatite, Finland, and some relationships of the North Atlantic igneous province: Geol. Soc. Finland Bull., no. 46, pt. 1, p. 81-91.
- Virovlyanskiy, G. M., and Blagodeteleva, Y. N., 1966, Late magmatic tectonics of Khibiny apatite deposits in relation to search procedure: Internat. Geology Rev., v. 8, p. 253-265.
- Volkova, M. I., and Melentiev, B. N., 1939, Chemical composition of the Khibiny apatites: Akad. Nauk SSSR Doklady, v. 25, p. 120-122.
- Vorob'eva, O. A., and Petrov, V. P., eds., 1968, Apatites: Moscow, Izdatel'stvo 'Nauka', 424 p. (In Russian)
- Wimmenauer, W., 1966, The eruptive rocks and carbonatites of the Kaiserstuhl, Germany, in Tuttle, O. F., and Gittens, J., eds., Carbonatites: London, John Wiley & Sons Ltd., p. 183-204.

1977.5.18 N6

EXTRACTION OF GERMANIUM FROM SOLUTIONS BY SORPTION

UDC 669.783:661.183

L. E. Slobtsov, L. L. Nikol'skaya,
A. M. Zastavnyi, M. M. Shyakina and V. F. Korotkov

The potential benefits of using sorption technology for extraction of germanium from sulfuric acid solutions have been proved in a number of works [1,2]. It was established that AN-31 anion-exchange resin was the best sorbent, permitting selective extraction of germanium from solutions of complex chemical composition containing up to 50 g/liter free acid. A non-continuous technology has been developed for sorption of germanium from solutions and desorption with hydrochloric acid solutions in columns with a fixed sorbent layer.

The present work gives the results of research¹ to improve this technology involving the development of a continuous process [3], selection of the optimum medium for sorption, and development of a method of hydrochloric acid desorption with simultaneous germanium tetrachloride distillation.

The sorption investigations were carried out in a laboratory installation with a capacity of 1.2 liters/hr consisting of ten sorption units with air mixing (Pachucas) installed in series and counterflow movement of resin and solution.

A prolonged continuous experiment was carried out during which over 300 liters of industrial solution obtained by sulfuric acid leaching of raw material containing germanium were processed. The solution composition (in g/liter) was 0.86 Ge, 7.5 As, 21 S (sulfate), 5.2 Zn, 2.1 Fe, 1.7 Cd, 1.0 Cl, 0.5 Al, 0.4 Cu, 0.35 SiO₂, 0.07 Sb, 0.01 Bi, and 36.2 H₂SO₄.

AN-31 resin in Cl-form (17.5% Cl) was fed into the sorption operation after desorption of germanium with hydrochloric acid and simultaneous tetrachloride distillation. The resin contained 0.48% Ge on average, because germanium desorption in regeneration was 70-75%. The selling ratio of the regenerated resin was 2.55 ml/g.

The counterflow sorption routine, established by preliminary experiments was as follows: number of stages ten, solution and resin contact time in each stage 50 min, and solution-resin flow ratio 6.7:1.

The resin went through 15 sorption-desorption cycles during the experiment; no deterioration in its sorption properties was observed in these circumstances and high germanium extraction figures were obtained.

The average extraction of germanium onto the resin was 98.6%. The spent solution germanium content was 12 mg/liter, with 1.42% in the saturated resin (swelling ratio 2.1 ml/g). The saturated resin also contained (in %) 0.5 As, 16.3 S, 0.04 Cl, 0.3 Zn, 0.14 Sb, and <0.1 of all other elements. AN-31 resin showed itself to be highly selective in relation to germanium and it made it possible to separate germanium from arsenic (separation coefficient 25). There was absorption of silicon dioxide, antimony, and bismuth by the resin during sorption; the antimony and bismuth were not completely desorbed by hydrochloric acid and gradually accumulated in the resin, although the concentration of these elements in the initial solution is very low. These impurities have to be desorbed periodically with alkaline solutions as they accumulate.

Most of the germanium (96.5%) was sorbed in the first six sorption stages.

It is interesting to note that feeding resin from which the germanium has not been completely desorbed into the process caused no deterioration in the sorption figures; this runs counter to the well-known proposition that complete desorption of metal from resin is essential in order to produce a low metal concentration in the spent solution. This apparently due to the fact that the germanium is not desorbed evenly: it is completely desorbed from the outer layers of resin, but the inner layers contain a substantial amount of germanium.

When this resin goes for sorption its outer layers, containing almost no Ge, contact the solution, resulting in a low Ge concentration in the spent solution. There was a considerable sorption of the sulfate ion, and the resin passed from chloride to sulfate form. Since the sulfate concentration in sulfate is extremely high,

Table 1
Effect of Medium Upon Results of Counterflow Sorption of Germanium (six stages)

Test no.	Medium	Content in initial solution		Solution:resin flow ratio	Contact time in each stage, min	Ge content		Ge extraction into resin, %
		Ge, Gmg/l	acid, g-eq/lit			of saturated resin, %	of spent solution, mg/l	
1	Chloride	570	0.65	13.5	40	1.36	7.5	98.7
2	Sulfate	560	0.65	13.5	40	1.04	45.7	91.5
3	Chloride	1075	0.44	12	60	2.85	4	99.6
4	Sulfate	1325	0.39	8.3	60	1.72	62	95.7

¹A. A. Burba, G. Z. Giniyatullin, V. P. Petrushov, A. N. Bykov, Z. F. Kulibaba, A. M. Antonova, and V. N. Titkov participated in the work.

it has a competing effect upon germanium absorption. The germanium should be sorbed from chloride solutions to eliminate this effect.

Comparative experiments on leaching germanium from the raw material with 1N sulfuric and hydrochloric acid solutions and counterflow sorption from the leaching solutions were carried out to check this proposition. Germanium extraction into solution in leaching was the same. In counterflow sorption the germanium content of resin saturated in chloride solution is 1.3 times higher than that of resin produced by processing sulfate solution (Table 1, experiments 1 and 2). The germanium concentration in the chloride solution alters more sharply over the sorption stages and high germanium extraction (98.7%) is achieved in six sorption stages. In the case of sulfate, 8-10 sorption stages are necessary.

Solutions with a higher germanium concentration were used in experiments 3 and 4 (see Table 1). Although the chloride solution contained less germanium the results of processing it are substantially better than in processing sulfate solution.

Thus the continuous sorption of germanium under counterflow conditions using a chloride medium significantly improves the technical and economic results in extraction on to AN-31 resin.

Desorption of germanium from AN-31 resin under dynamic conditions with 6-7 N hydrochloric acid solution is described in collection [1]. Not less than 20 volumes of solution have to be passed through a volume of resin; only four volumes are commercial solutions, the remainder must be used in recirculation. At the same time there are heavy losses of germanium due to the high volatility of the tetrachloride formed.

The results of germanium desorption with hydrochloric acid under static conditions with air mixing of resin and acid are given below. In these circumstances the operations of desorption and tetrachloride distillation into the gas phase are combined, so that the ion-exchange equilibrium continuously shifts in the direction of desorption.

The experiments were carried out in five Drexel vessels installed in series, the last of which was connected to a vacuum pump. The eluting solution and swollen resin saturated in experiments on counterflow sorption from sulfate solution were placed in the first vessel. Water was poured into the subsequent vessels. Air was drawn into the first vessel, where the solution and resin were mixed at a high rate, and then passed through the water absorbers, where germanium tetrachloride and hydrogen chloride were absorbed.

The material balance for the germanium desorption experiment is given in Table 2. The acid concentration fell to 9N due to dilution by moisture from the swollen resin; this is most favorable for tetrachloride distillation.

It follows from the experimental results (Fig. 1) that the speed of germanium desorption is low: 56% Ge is desorbed in the first 4 hr, then the speed decreases. The degree of desorption in 12 hr was ~ 75%, which should be regarded as satisfactory.

The spent acid contains ~1.4 g-eq/liter H_2SO_4 and < 0.2% of the amount of germanium

Table 2
Material Balance for Ge Desorption with Hydrochloric Acid with Simultaneous Tetrachloride Distillation
(Test conditions: 1:2 ratio of swollen resin and hydrochloric acid volumes; 12 hr mixing; room temperature)

Balance headings	Volume liters	Ge content, g/l	Ge distribution, %
Supplied:			
Saturated resin.....	0.1 (47.6 r)	6.19 (1.3%)	100.00
Hydrochloric acid (10.6 N).....	0.2	—	—
Received:			
Regenerated resin.....	0.1 (39.2 r)	1.49 (0.38%)	24.73
Aqueous absorber solutions:			
first.....	0.3	1.41	68.03
second.....	0.3	0.13	6.46
third.....	0.3	0.013	0.64
Spent acid.....	0.2	0.007	0.16
Total.....			100.00
including:			
in solutions (degree of desorption).....			75.27
in absorber solutions (degree of distillation).....			75.11

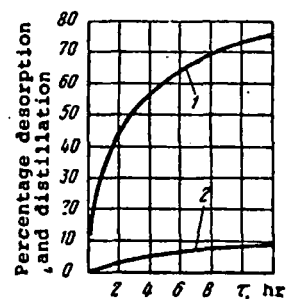


Fig. 1. Kinetics of germanium desorption and tetrachloride and hydrogen chloride distillation: 1 - germanium desorption and tetrachloride distillation; 2 - hydrogen chloride distillation

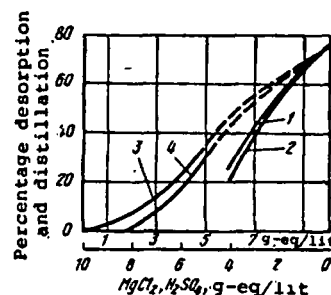


Fig. 2. Relationship of germanium desorption (1, 3) and tetrachloride distillation (2, 4) to eluent composition: 1, 2 - $HCl + H_2SO_4$; 3, 4 - $HCl + MgCl_2$.

in the saturated resin. Consequently the limiting stage in the combined process is desorption of germanium from the resin, not tetrachloride distillation.

A study was made of the effect of sulfuric acid concentration upon germanium desorption, with the proviso that the total concentration of both acids in the eluting solution would be 10 g-eq/liter, to find whether spent acid containing sulfate ions could be used for desorbing germanium from subsequent batches of resin. A study was also made of the effect of the hydrochloric acid concentration at a constant chlorine content in the 9-10 g-eq/liter range. Isonormal series of HCl-H₂SO₄ and HCl-MgCl₂ solutions were prepared for this purpose.

The results of the experiments (Fig. 2) showed that the presence of sulfate ions in the eluting solution had an adverse effect upon germanium desorption. Increasing the sulfuric acid content by 1 g-eq/liter reduces the degree of desorption by ~10%. This is also confirmed by comparing the experiments in the HCl-H₂SO₄ and HCl-MgCl₂ systems. At an identical hydrochloric acid concentration (6N) the degree of germanium desorption in the former system is 15% below that in the latter. For this reason spent acid cannot be recirculated. Desorption must be carried out only with fresh hydrochloric acid.

The tetrachloride distilled off during desorption was trapped in four absorber vessels installed in series. After a germanium dioxide residue had appeared in the solution in the first absorber, this solution was withdrawn for precipitation of germanium concentrate and all the subsequent solutions were transferred to the preceding absorber in each case.

The results of analyses of the absorber solutions at the time of withdrawal of the first solution for concentrate precipitation indicate practically complete absorption and hydrolysis of germanium tetrachloride in this system. The germanium content of each subsequent absorber decreases by ~10 times.

Germanic acid and hydrochloric acid are present in the solution from the first absorber which is withdrawn for concentrate precipitation, as well as a small amount of impurities, because industrial water was used for absorption.

The concentrate was precipitated with 25% ammonia solution at pH = 9.0-9.3 over a period of 3 hr with mixing [4].

The moist residue after filtration contains ammonium chloride. The residue from the first experiment was not washed free of ammonium chloride, the second residue was washed with a small amount of water on the filter, and the third was washed by repulping.

The results of the experiments showed that the degree of germanium precipitation was 94.5-97.5%; the concentrate germanium content is 44-50%, and when washed the content increases due to partial removal of the ammonium chloride. The concentrate obtained is white in color, without tints. Its percentage chemical composition (weighted average sample) is 48.37 Ge, 0.37 As, <0.1 S, 8.56 NH₃, 8 Cl, and the remaining impurities are present at trace levels.

It was established by thermogravimetric, x-ray diffraction, mineralogical, and chemical methods that the principal phases in the unwashed concentrate were ammonium hydrogermanate of composition (NH₄)₃.HGe₇O₆ · x 4H₂O and ammonium chloride. Concentrate which has been washed with water is mostly ammonium hydrogermanate.

The germanium concentrate is easily, quickly, and completely broken down by concentrated acid. It conforms to product grade II in terms of its germanium and impurities content.

The technology developed for desorption of germanium from AN-31 resin using hydrochloric acid with simultaneous distillation of germanium tetrachloride makes it possible to reduce hydrochloric acid consumption tenfold by comparison with desorption under dynamic conditions and to eliminate losses of germanium. This technology also yields high-grade germanium concentrate.

REFERENCES

1. N. M. Sobinyakova, K. M. Starostina, L. N. Aleksandrova, et al., Mineral Raw Materials, Issue 23, Moscow, All-Union Mineral Materials Research Institute, 1972, pp. 59-85.
2. Z. I. Matveeva and P. D. Novikov, Tsvetnye Metally, 1971, No. 12, 46-48.
3. B. N. Laskorin, Zhurnal Vsesoyuznogo Khimicheskogo Obshchestva im. D. I. Mendeleeva, 1970, 15, 388-395.
4. O. D. Lyakh, I. A. Sheka, and A. I. Perfil'ev, Dopovidi Akad. Nauk Ukr. SSR, 1965, No. 12, 1603-1606.

on Experimental Mineralogy and Petrography: Izd. Akad. Nauk SSSR 1973.
 1) O I Arakelyan: Author's Abstract of Thesis: Leningrad VAMI 1957.
 2) S A Shcherban et alia: Izv VUZ Tsvetnaya Metallurgiya 1969, (2), 76.
 3) Kh N Nurmagambetov et alia: Materials of Conference devoted to the 100th Anniversary of the Birth of V I Lenin: Kaz. PTI 1971, pp. 380-383, 366-370, 404-407.

Soo. Non-Fr
1976 v. 4 N3

4) Kh N Nurmagambetov et alia: Zh. Prikl. Khim. 1971, XIV, (7), 1467.
 5) S A Shcherban et alia: Zh. Prikl. Khim. 1970, XIII, (3), 566, 306.
 6) O I Arakelyan: Proceedings of Fifth Conference on Experimental and Technical Mineralogy and Petrography: Izd. Akad. Nauk SSSR, Moscow 1958.
 7) O I Arakelyan: Tr. VAMI 1957, (6), 20.
 8) V A Kolesova: Optika i Spektrosopiya 1959, (6), 20.
 9) P Tarte: Bull. Soc. Franc. Ceram. 1963, 58.

UDC 541.49:542.61:546.6

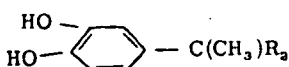
Extraction of gallium, indium, and thallium from an alkaline medium by alkylpyrocatechols

V S Kuznetsova, Yu I. Tarnopol'skii and V F Borbat (Siberian Technological Institute, Krasnoyarsk)

Earlier we showed for the first time that metals of the aluminium subgroup are extracted from alkaline solutions by alkylpyrocatechols¹⁾. In the present work the effect of the contact between the phases, the concentration of the extractant, the diluent, and the temperature on the extraction of gallium, indium, and thallium was investigated for the case of 4-(α - α -dihydroxyethyl) pyrocatechol (DHP), the extracted complexes were isolated, and their composition in the organic phase was studied. The effect of the length of the radical on the extraction characteristics was investigated for a series of alkylpyrocatechols with similar structure.

The alkylpyrocatechols were prepared by the method which we described earlier¹⁾. Their properties are given in table 1. The solid products were crystallised from hexane. Extraction was realised with a freshly prepared solution of the extractant, the volumes of the phases were 10 ml each, the length of contact between the phases in the separating funnel was 5 min, the alkalinity was created with sodium hydroxide, and the concentrations in the initial aqueous phase were as follows - g/l: 0.2 In, 0.2 Tl, 0.1 Ga. The re-extraction of gallium and indium was realised with 1N hydrochloric acid, and that of thallium was realised with 1N sulphuric acid with the phases in a ratio of 1:1. The equilibrium aqueous phase and the re-extract were analysed by a photocolometric method; gallium and thallium were determined with rhodamine B, and indium with PAR²⁾

Table 1: Properties of the alkylpyrocatechols



R	Number of C atoms in radical	bp °C (p, mm Hg)	mp °C	n_D^{20}
n-C ₄ H ₉	10	180-182 (3)	62	-
n-C ₆ H ₁₃	14	203-206 (2)	-	1.5117
n-C ₈ H ₁₇	18	217 (0.5)	57	1.5055
n-C ₁₀ H ₂₁	22	243 (0.5)	-	1.5105
n-C ₁₆ H ₃₃	26	247-248 (0.5)	-	1.4987

The metal-sodium-alkylpyrocatechol triple complexes were isolated by the following method. A 1.5-g sample of the extractant, dissolved in 30 ml of ether, was saturated with an excess of a solution of the metal in 1N sodium hydroxide. The ether layer was removed, evaporated to 5 ml, and added to 50 ml of acetone. The crystalline complex was filtered off, washed with acetone, dried in air, and analysed.

During elemental analysis of the complexes carbon and hydrogen were determined by combustion in a stream of

oxygen, and sodium was determined from the weight of the dry residue after combustion of the sample, which consisted of a mixture of the oxides of the metals contained in the complex. The molecular weight was determined by the Rast method in camphor.

The effect of the alkalinity of the equilibrium aqueous phase on the extraction of gallium in diluents of various types is shown in fig.1. In octyl alcohol, chloroform, toluene, and dibutyl ether insignificant extraction is observed at pH 4-11 and there is a sharp increase in extraction with sodium hydroxide concentrations from 0.01 to 1N i.e., in the region corresponding to the existence of gallates. In decane an additional extraction maximum appears in the neutral region, where gallium separates from the solution in the form of the hydroxide.

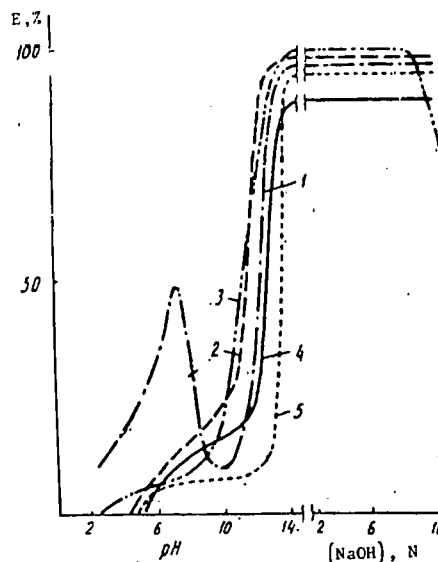


Fig.1 Dependence of the extraction of gallium on the alkalinity of the equilibrium aqueous phase. The organic phase was 1.5% DHP: 1 - In decane with 10% octanol; 2 - in chloroform; 3 - in toluene; 4 - in n-octanol; 5 - in dibutyl ether.

Fig.2 shows the dependence of the extraction of indium on the alkalinity of the equilibrium aqueous phase, and this has a more complex form. In the range of alkalinity of 0.5-2N there is a minimum, the origin of which makes it possible to determine the kinetic and thermodynamic data. In the case of thallium the extraction curves have simpler form (fig.3). As known, thallium (I) exists as a stable cationic form in an alkaline medium.

For all the investigated metals the extraction equilibrium is established in 3 min. With increase in temperature from 20 to 80°C the extraction of all the metals deteriorates. The

exception is the above-mentioned region of the minimum on the extraction curves for indium in the alkalinity range of 0.5-2N, where the extraction equilibrium is not established even after 40 min, but the extraction improves with increase in temperature. It is known that the minima which are encountered in the extraction of chelate compounds in most cases correspond not to the region of the transition from one extracted compound to another but to suppression as the result of competing reactions in the aqueous phase³). For indium such competing reaction may be polymerisation to form a multinuclear "ol" compound⁴). Unlike indium, gallium and thallium do not form polymers in alkaline solutions. All this makes it possible to conclude that the minimum on the extraction curve for indium has non-equilibrium nature, while increase in temperature assists depolymerisation of indium in the aqueous phase to a greater degree than it impairs the distribution coefficient.

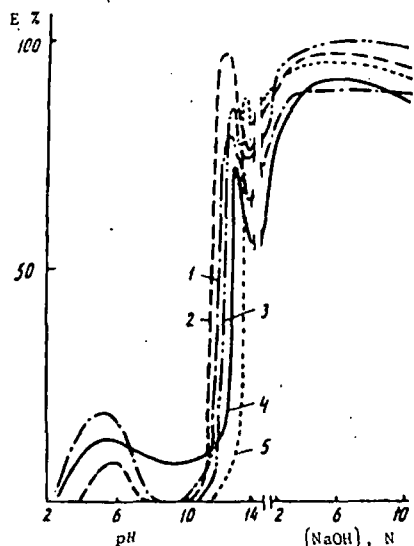


Fig. 2 The dependence of the extraction of indium on the alkalinity of the equilibrium aqueous phase. The designations are the same as in fig. 1.

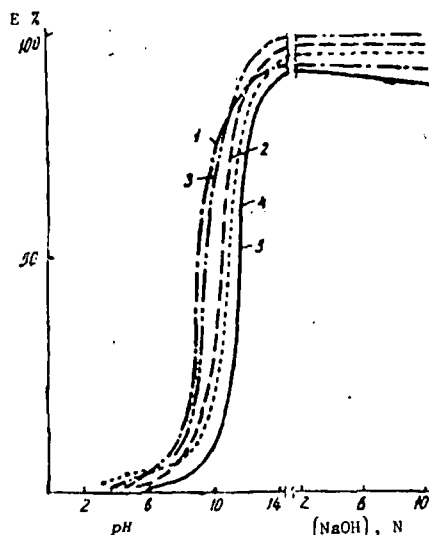
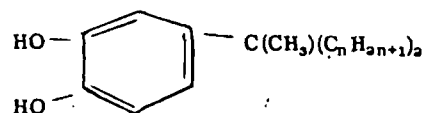


Fig. 3 Dependence of the extraction of thallium on the alkalinity of the equilibrium aqueous phase. The designations are the same as in fig. 1.

The best solvents for the extraction of gallium, indium, and thallium were oxygen-free diluents toluene and chloroform. The extraction goes worst of all in octyl alcohol, and this can be explained by the decrease in the activity of the extractant through the formation of hydrogen bonds with the hydroxyls of the alcohol. To investigate the effect of the length of the hydrocarbon radical in the extractant molecule

the extraction was realised with alkylpyrocatechols having the general formula:



where: $n = 4, 6, 8, 10, \text{ and } 12$.

From comparison of the results (fig. 4) it is seen that gallium is most sensitive to change in the length of the extractant radical. The best extraction is obtained with 18 carbon atoms in the substituent ($n = 8$). If the radical is shortened, the extraction of gallium decreases as a result evidently of the fact that the comparatively small ionic radius of gallium does not assist dissolution of the obtained complexes in the diluent. This is not significant for the extraction of indium and thallium. The extraction of all three metals decreases with increase in the length of the radical as a result, probably, of steric hindrances in the complexing reaction.

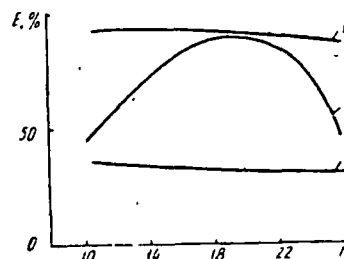


Fig. 4 Dependence of the extraction of the metals on the number of carbon atoms in the hydrocarbon radical of the extractant. The diluent was decane containing 10% of octanol. The Me-DHP ratio was 1:5; 1 - Indium in 5N sodium hydroxide; 2 - gallium in 1N sodium hydroxide; 3 - thallium in 5N sodium hydroxide.

It is known that gallium, indium, and thallium are capable of forming a series of complexes containing sodium or ammonium in the aqueous phase. Thus, for example, the compound $\text{Na}[\text{Ti}(\text{O}_2\text{C}_2\text{H}_5)_4]$ has been described⁵). In the gallium and indium complexes the metal-ligand ratio can amount to 1:1, 1:2, and 1:3 and compounds with the composition $\text{Na}_3[\text{Me}(\text{O}_2\text{C}_2\text{H}_5)_3]$, where Me is the metal, have been isolated^{6,7}).

The composition of the extracted chelate compound depends on the form in which the metal exists in the aqueous solution. Data on the forms of existence of gallium in alkaline solutions are contradictory. Possible forms include the following: $[\text{GaO}_2]^-$, $[\text{GaO}_2]^{2-}$, $[\text{Ga}(\text{OH})_4]^-$, $[\text{Ga}_2(\text{OH})_6]^{2-}$, $[\text{Ga}(\text{OH})_6]^{3-}$. It is doubtful whether gallium gives any specific stable form in alkaline solutions; equilibrium is readily established between the various forms. With an alkalinity of less than 8N indates are unstable. Some time after preparation they dissociate, releasing part of the dissolved indium hydroxide. Only $[\text{In}(\text{OH})_4]^-$ ions are present in such solutions before decomposition⁸).

One of the conditions for determination of the charge of the metal ion in the extracted complex from the slope of the extraction curve against logarithmic coordinates is the absence of hydroxo-complexes of the metal in the aqueous phase. In our case this condition is only observed for thallium. The corresponding slope is unity (fig. 5). Thus, thallium enters into a singly charged anion. For gallium the corresponding slope is 1.2-1.6, depending on the conditions, and for indium it is 2.

We determined the extractant-metal ratio graphically from the dependence of the distribution coefficient on the concentration of the extractant against logarithmic coordinates (fig. 6). For gallium, indium, and thallium it amounts to 3:1, 3:1, and 1:1 respectively. The same result was obtained by the method of isomolar series (fig. 7). The extraction

isotherms (fig.8) confirm the obtained ratios.

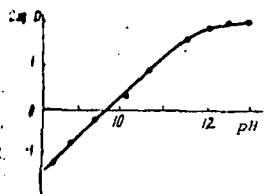


Fig.5 The dependence of the distribution coefficient (D) of thallium (Tl) on the alkalinity of the equilibrium aqueous phase. (DHP) = 0.0413M in toluene, (Tl) = $0.97 \cdot 10^{-3}$ g-ion/l.

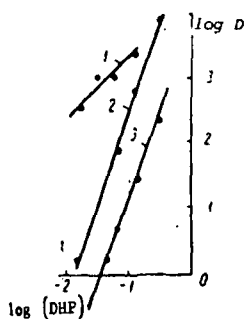


Fig.6 The dependence of the distribution coefficient (D) on the concentration of DHP in toluene: 1 - Thallium ($pH = 13$); 2 - gallium (0.5N sodium hydroxide); 3 - indium (1N sodium hydroxide).

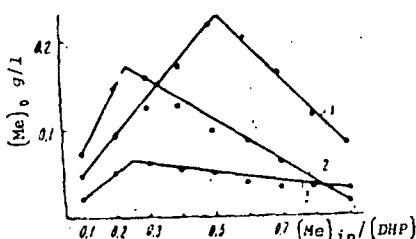


Fig.7 Determination of the composition of the extracted complexes by the method of isomolar series. The diluent was toluene; 1 - thallium (1 N sodium hydroxide); 2 - gallium (1 N sodium hydroxide); 3 - indium (0.1 N sodium hydroxide).

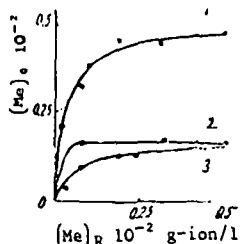


Fig.8 Extraction isotherms. (DHP) = 0.005M in decane with 10% of octanol; 1 - thallium (1 N sodium hydroxide); 2 - indium (5 N sodium hydroxide); 3 - gallium (0.1 N sodium hydroxide)-

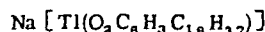
Data on the composition of the complexes in the organic phase agree with the results from elemental analysis, molecular weight determination, and the IR spectra of the complexes isolated in the free form (table 2). The characteristic strong absorption band of the hydroxyls of the alkylpyro-

catechol at 3400 cm^{-1} is absent from the IR spectra of the complexes, and this indicates that all the hydroxyl protons are substituted by the metals.

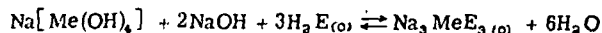
Thus, gallium and indium are extracted from an alkaline medium by DHP in the form of the compounds



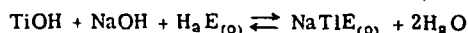
and thallium (I) is extracted in the form of



The extraction of gallium and indium can be described by the equation



where one of the possible forms of existence of gallium in the alkaline solution is given. The extraction equation for thallium has the following form:



In these equations H_2E is the extractant.

Conclusions

1. The effect of the length of contact between the phases, the temperature, the concentration of the extractant, the type of diluent, and the length of the radical in the extractant molecule on the extraction of gallium, indium, and thallium by alkylpyrocatechols was investigated.

2. It was shown that in the extraction of indium, in contrast to gallium and thallium, equilibrium is established slowly at alkalinities of 0.5-2N.

3. The composition of the extracted gallium, indium, and thallium complexes with 4-(α, α -diocetyl-ethyl)-pyrocatechol in the organic phase was studied.

4. The complexes extracted were isolated in the free form. Like the complexes in the organic phase, they have the compositions Na_3GaE_3 , Na_3InE_3 , and $NaTlE$ (where H_2E is the extractant).

References

- 1) Yu I Tarnopol'skii et alia: *Izv. Vuz. Khimiya i Khimicheskaya Tekhno* 1974, (17), 754.
- 2) Z Marchenko: *Photometric determination of the elements* (Russian translation), Mir, Moscow 1971.
- 3) Yu A Zolotov: *Extraction of chelate compounds*. Nauka, Moscow 1968.
- 4) N V Aksel'rud: *Zh. Neorgan. Khim.* 1958, 3, 1738.
- 5) O Tomar et alia: *J. Indian Chem. Soc.*, 1966, 43, (1).
- 6) T N Bevilard: *Bull. Soc. Chem. France* 1955, 1509.

Table 2: Composition and properties of the complexes of gallium, indium and thallium with 4-(α, α -dihydroxyethyl)pyrocatechol

Metal	mp °C	Molecular weight		Calculated %				Formula	Found %				Solvent
		Calculated	Found	C	H	Me	Na		C	H	Me	Na	
Ga	215-220 decomp.	1118	1200	70.86	9.91	5.71	5.65	$C_{78}H_{100}Na_3GaO_6$	69.34	9.77	5.82	5.47	Alcohol, ether benzene, paraffins
In	310-315 decomp.	1426	1285	68.33	9.55	9.07	5.44	$C_{78}H_{100}InNa_3O_6$	66.00	9.18	8.91	5.45	
Tl	94	603	588	49.04	6.85	34.76	3.92	$C_{88}H_{90}NaO_6Tl$	49.28	6.32	34.45	3.90	Paraffins, ether, benzene, chloroform; insoluble in alcohol

SUBJ
MING
EGMN

Economic Geology of the Mishraq Native Sulfur Deposit, Northern Iraq

JAMES M. BARKER, D. E. COCHRAN, AND ROBERT SEMRAD

Abstract

The Mishraq native sulfur deposit is in northern Iraq about 40 km southeast of Mosul and 315 km north of Baghdad. This deposit is the largest known occurrence of stratiform bioepigenetic sulfur, containing at least 100 million tons of elemental sulfur. It underlies a 10 km² portion of the southeast end of a northwest-trending, doubly plunging anticline on the west bank of the Tigris River at its confluence with the Great Zab River. The deposit is in one anticline among many in the folded portion of the Mesopotamian depression and represents part of what may be the largest reserve of elemental sulfur in the world.

Small, tight, en echelon folds are superimposed on the southwest limb of the Mishraq anticline with axial trends similar to the main fold (320°). Faulting is normal and reverse with dominant northwest and subordinate northeast trends. Mining-induced subsidence of 4 to 5 m causes fractures which tend to follow these preexisting directions.

The sulfur mineralization is in three main zones of vuggy and bituminous bioepigenetic limestone in the basal Lower Fars Formation of middle Miocene age and marine origin. The Lower Fars consists of intercalated bituminous marine carbonates (dolomite, limestone, marl) and anhydrite/gypsum with minor shale and sandstone interbeds. The depositional environment was of periodic marine influxes followed by evaporation in a partially barred basin with southern access to the sea.

The sulfur forms by oxidation of hydrogen sulfide produced during metabolism of petroleum and anhydrite/gypsum by anaerobic bacteria (*D. desulfuricans*), a conclusion supported by the ³⁴S and ¹³C fractionation data. Sulfur mineralization is thickest in areas of intense folding and faulting which enhance solution, movement, and mixing of reactants. Combined thickness of the three sulfur-bearing zones is from 2 to 123.9 m, with a maximum ore section of 107.9 m and a grade of 23.14 wt percent sulfur. Seven ore types have been recognized of which predominant coarse crystalline sulfur alternates with bands of secondary limestone.

Hydrologic conditions at the mine are complex with subsurface drainage via karst features, fractures, faults, and vuggy porosity within the ore zones of the productive member. The productive member contains the bulk of the ground water, although up to 13 aquifers have been recognized throughout the section, and it is intersected by the Tigris River. A very steep hydraulic gradient exists with flow southeastward toward the Tigris where it is discharged from springs in and beside the river. Hydrogen sulfide-carbonate waters predominate. Recharge is mainly at the northwest portion of the anticline where the Lower Fars crops out. The ground water connection and flow to the river is important in sulfur generation as it is the pathway by which oxygen is carried into contact with hydrogen sulfide at depth yielding sulfur and water.

The deposit is currently being mined by the Polish hydrodynamic (modified Frasch) process at a rate of about 600,000 tons per annum out of a total capacity of 1,000,000 tons per annum. The maximum capacity has not been reached because of infrastructural constraints related to transportation and because the mine is difficult to operate. Large injection water losses and excessive bitumen contamination are paramount. Water losses are mitigated by the installation of subsurface impermeable screens. Bentonite/sulfuric acid filtration removes the excess bitumen but at a cost of 8 to 25 percent loss of sulfur in filter cake and skim foam.

Initially sulfur was vatted at the mine, crushed, and shipped via rail to the port of Um Qasr about 1,000 km south of Mishraq. Liquid sulfur is currently shipped to the port where vating is done as necessary.

Introduction

THE Mishraq orebody is the largest stratiform sulfur deposit known, containing from 100 to 250 million

tons of bioepigenetic sulfur. The deposit is in northern Iraq about 315 km north of Baghdad and 40 km southeast of Mosul (Fig. 1). It is on the west bank

of the Tigris River, opposite its confluence with the Great Zab River, at about 36° N and 43° 20' E.

Mishraq is in the folded portion of the Mesopotamian depression which separates the nappes and the Zagros Mountains to the east from the unfolded Arabian platform to the west. The Mishraq deposit is in one anticline among many (Fig. 2) which parallel the Zagros Mountains in an area of at least 5,000 km² extending westward from the Tigris River and southward 150 km from Mosul to Al Fatha. Thus Mishraq is one of numerous potential sulfur deposits in northern Iraq which, as a group, may be the largest reserve of elemental sulfur in the world (British Sulphur Corp., 1974).

Sulfur mineralization and hydrogen sulfide springs were noted in the region by English, Italian, and Canadian oil geologists while doing exploration from 1933 to 1935 (Chebanenko, 1969). Sulfur exploration was done in Iraq by Russian geologists during 1960 to 1962. They mapped in detail all the structures in the region but drilled only in the Mishraq and Al Fatha areas. These two were chosen because of existing information from oil wells and their proximity to existing rail, highway, and river transportation. Nine IPC oil wells and 34 Russian sulfur tests were drilled during predevelopment at Mishraq. Initial plans, based on Russian data, called for an open-pit mine.

In early 1969, the Iraqi government established the state-owned National Iraq Mining Company to develop the deposit. A contract for the training of Iraqi personnel and for planning, testing, and construction of a hydrodynamic (Frasch) plant in two stages was made with the Polish Mining Agency, Centrozap, in mid-1969. The second stage of the plant, with a total capacity of 1,000,000 tons per annum, came on stream in 1974. Production in 1977 was 605,000 tons, of which 522,000 tons were exported. The filtered bright sulfur is shipped via standard gauge railroad 1,000 km south to the port of Um Qasr, near Basrah, Iraq (Fig. 1), for export.

Physical Setting

Topography over the Mishraq deposit reflects the underlying structure with low hills and steeper ridges aligned northwest-southeast. Elevations range from 185 m above sea level at the Tigris River near Makhlat to 292 m at the crest of the Mishraq structure, yielding a relief of 107 m.

The eastern side of the orebody terminates in a steep escarpment, about 70 to 80 m high, formed by the westward migration of the Tigris River, which has a seasonal variation in width of from 60 to 200 m. River depth averages 8 to 10 m, with a maximum seasonal range of 10 m. The average annual flow is



FIG. 1. Location map.

about 42 billion cu m with a current velocity of from 0.2 to 2 m per sec.

Ephemeral tributaries of the Tigris River have incised steep rock-filled gorges, some of which have affected the geohydrology of the deposit and the mine facility location and design.

Featherstone and Al-Samarrie (1975) report a mean annual rainfall from 1940 to 1970 of 393 mm, most of it occurring between October and April. The mean monthly temperature varies from 7°C in January to 40°C in July, with evaporation ranging from 2.6 to 16.7 mm/day.

Soil development is minimal, but some marginal agriculture is practiced. Local vegetation is sparse and adapted to semiarid conditions.

Structural Geology

Three broad structural zones occur in northern Iraq (Dunnington, 1958). These are, from west to east, the unfolded zone (Arabian platform), the folded zone (Mesopotamian depression or foredeep), including Mishraq, and the nappe (Zagros) zone. Structures in both the folded and nappe zones are parallel to the Zagros Mountain trend. The folded zone has an average width of about 200 km. Both the individual fold axes and the folded zone itself

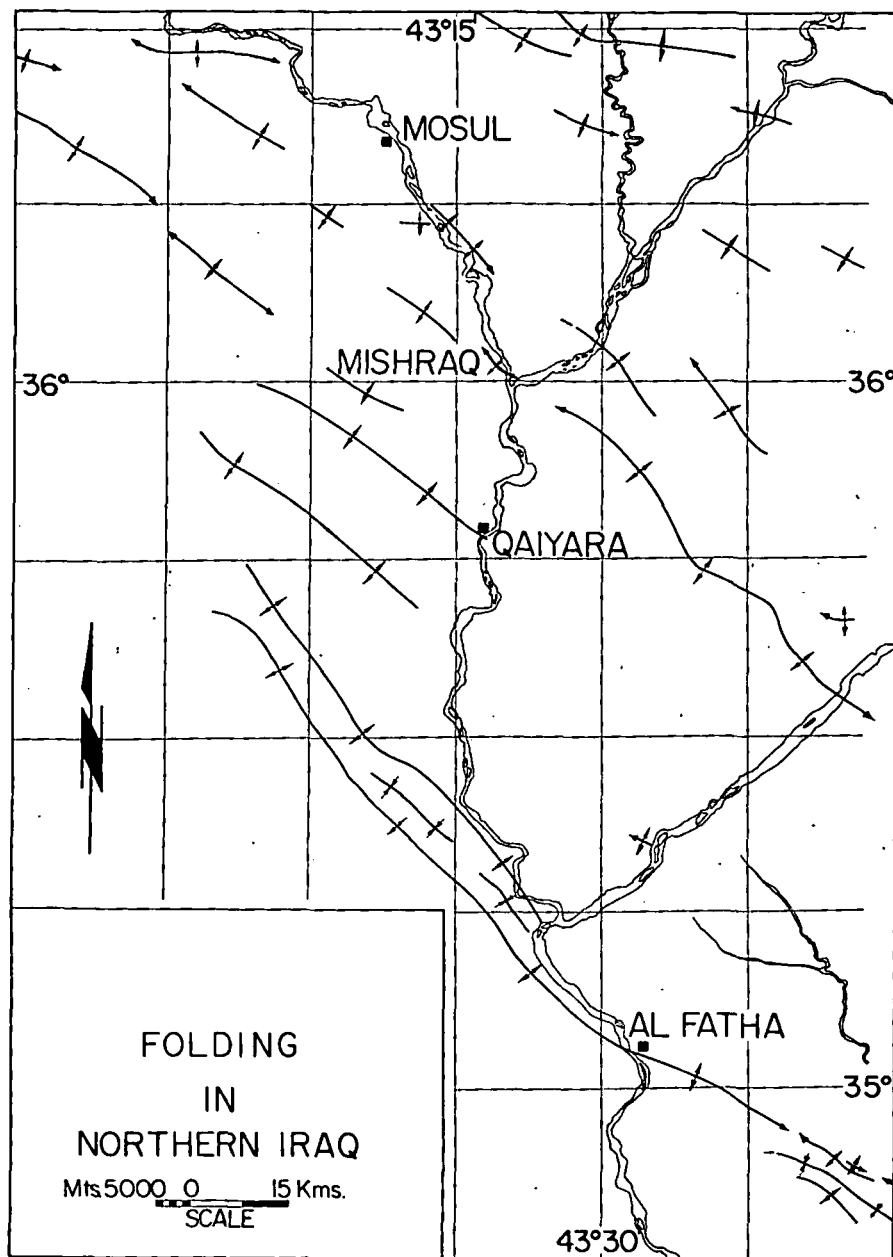


FIG. 2. Folds in northern Iraq.

follow the Zagros Mountain swing from east-west trends in the north to northwest-southeast trends in the south (Fig. 3). Mishraq occurs near the western edge of the folded zone and along the hinge line for this change in direction, which is also followed by the southwestern part of the Great Zab River.

The folded zone has many elongated, northwest-trending anticlines which have variable plunges along their axes. These relationships yield multiple oil and gas structural traps and have a "whaleback" appearance. The topography generally reflects under-

lying structure anticlines forming hills or ridges and synclines forming valleys.

The Mishraq deposit is within a northwest-trending (320°), doubly plunging, broad anticline. The anticline is about 11 km long and 3.5 km wide at the surface with a relief of 107 m in the area of maximum sulfur deposition.

The northeastern flank and the southeastern end of the anticline have been eroded by the local westward migration of the Tigris River induced by the confluence of the Great Zab River. The surface of

the Mishraq structure has been eroded along its axis, giving a rounded, flat-topped profile. Bedding is nearly flat at the axis with dips steepening on the flanks thus yielding a domelike appearance. Localized near-vertical dips occur on the southwest limb, whereas the northeast limb is low dipping (4° to 8°) near the boundary of the deposit.

En echelon folds are superimposed on the southwest limb of the Mishraq anticline. The trend of these folds is parallel to the trend of the main fold axis. These structures are sharply folded with a relief of up to 50 m and minor axes as short as 100 m. The minor folds of the Mishraq anticline have crestal tension-jointing which acted as cross-strata pathways for the dissolution of sulfate rock and mixing of reactants. On the limbs where the zones are more discrete, jointed and tectonically disturbed areas show increased sulfur mineralization in the interbeds between ore zones.

Faulting within the Mishraq orebody is common and is dominantly vertical with both normal and reverse faults present. The most intense faulting and folding is associated with the thickest sulfur accumulations. The main trends are northwest-southeast (normal and reverse faults) and northeast-southwest (normal faults), as shown by Niec and Al Nouri (1976). Normal faults are more common and have a more variable trend than reverse faults. Surface fractures related to mining-induced collapse tend to parallel the preexisting structures. Subsidence caused by sulfur mining at Mishraq is expected to be about 4 to 5 m (Zackiewicz, 1975).

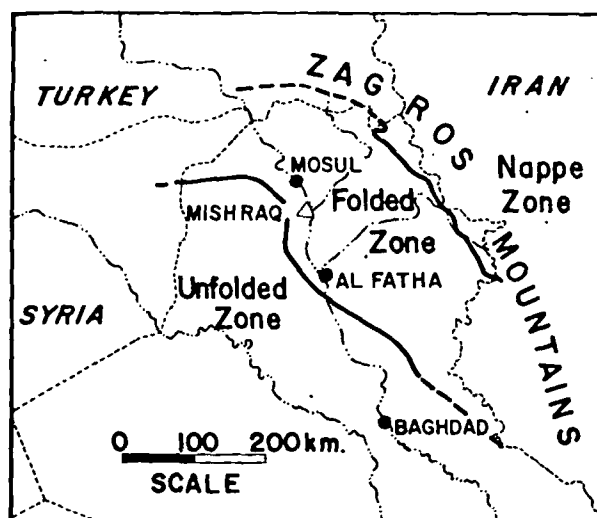


FIG. 3. Structural zones of northern Iraq. (After Dunnington, 1958.)

Stratigraphy

The area west of the Tigris River from Mosul to Al Fatha is underlain by lower to middle Miocene marine evaporites and sediments (mainly carbonates), partially covered by Quaternary alluvium (Table 1). The depositional environment of the Lower Fars Formation was one of periodic desiccation followed by marine influxes. Al Sawaf (1977) considered the area to be a partially barred basin with southern access to the sea.

Surficial rocks in the northern portion of the region

TABLE 1. Tertiary Rocks at Mishraq, Iraq

Age and rock units	Thickness (meters)	Description
Upper Miocene Upper Fars Formation	0 to 34+	varicolored calcareous clay with thin interbeds of gypsum, limestone, marl, and sandstone —paraconformity—
Middle Miocene		
Lower Fars Formation		
Sulfate-clastic member	70 to 100	gypsum/anhydrite, limestone, sandstone, and clay
Carbonate-clastic member	20 to 80	limestone, gypsum/anhydrite, clay, and marl; upper limestone may have sulfur/calcite, bitumen, and vugs
Sulfate member	30 to 55	gypsum/anhydrite with lenses of bitumen and sulfur/calcite locally of ore grade
Productive member	60 to 140	bituminous dolomite, limestone, and marl with three vuggy bioepigenetic sulfur/calcite ore zones which grade laterally into gypsum/anhydrite; banded and coarse crystalline ore predominate; main aquifer
		—transgressiveun conformity—
Lower Miocene		
Euphrates Limestone Burdigalian Stage Aquitanian Stage	280+	biogenic limestone with minor sulfur near top; bituminous

(Mosul to Quiyara) are predominantly from the Lower Fars Formation (middle Miocene). To the south (Quiyara to Al Fatha) surficial rocks are mainly from the Upper Fars Formation (upper Miocene). Alluvial cover rapidly increases in thickness and areal extent to the east of the Tigris River (toward the Zagros Mountains) in both areas. The following data draw heavily from Chebanenko (1969) and unpublished Russian drill logs. More current drill data based on the Iraqi mining-development drilling are unavailable. The Russian data suffer from core recovery problems.

Lower Miocene

The rocks of the lower Miocene transgressively overlie Paleocene limestones which in turn overlie, with erosional unconformity, the Mesozoic carbonate, clastic, and sulfate rocks.

Euphrates Limestone: The Euphrates Limestone comprises 130 m of light gray to tan-gray fossiliferous limestone (Aquitanian Stage) underlying 150 m of similar limestone (Burdigalian Stage) with interbeds of marl and, less commonly, gypsum and anhydrite. Native sulfur with calcite is common throughout the Burdigalian but is best developed in the jointed and vuggy upper portion of this unit. Russian geologists separate these stages, whereas western geologists assign them both to the Euphrates Limestone.

The Euphrates Limestone everywhere underlies the Mishraq structure, varying in depth from 160 m along the crest of the anticline to 310 m on the south-west limb.

Middle Miocene

The middle Miocene rocks are transgressive over the lower Miocene deposits.

Lower Fars Formation: The bulk of the sulfur occurs near the base of the Lower Fars Formation which has been subdivided into four informal lithologic units. These are as follows, with published variations in parentheses: productive (carbonate) member, sulfate member, carbonate-clastic (calcareous-terrigenous) member, and sulfate-clastic (sulfate-terrigenous) member. All four members are easily distinguished in fresh cores but are difficult to differentiate in weathered outcrops. In outcrop only

TABLE 2. Summary of Mishraq Ore Zones (after Chebanenko, 1969)

Ore zone	Depth (meters)	Total thickness (meters)	Ore-grade thickness (meters)	Avg S wt %
3	54.8-134.5	2.8-46.8	2.8-46.8	19.8
2	101.6-170.8	1.4-33.1	1.4-25.9	23.4
1	124.4-303.1	1.9-44.0	1.9-35.2	25.5

TABLE 3. Chemical and Physical Data on Mishraq Sulfur Ore

Parameter ^{1,2}	Low	High
Ore matrix		Percent
CaO	33.59	36.47
MgO	1.58	32.23
CO ₂	26.70	33.00
SO ₂	0.22	1.43
Al ₂ O ₃	0.43	1.97
Fe ₂ O ₃	0.29	1.30
Sulfur		
H ₂ O	1.1	6.3
Ti	0.001	0.03
Va		0.001
Ba		0.1
Sr		1.0
Se		Nil
As		Nil
Specific gravity	2.33	2.70
Bulk density	2.09	2.54

¹ These data are from Cortesini, 1966, who abstracted them from the Russian report of 1962.

² The analyses were performed in Baghdad and checked in Moscow.

two units are differentiated using a pair of limestone markers just above the productive member.

The *productive member* is predominantly fine-grained primary carbonate, coarse-grained secondary calcite with sulfur, and gypsum/anhydrite with a thickness of from 60 to 140 m. It crops out along the west bank of the Tigris River where only the upper part is exposed. The carbonate is commonly argillaceous and bituminous (dispersed) and is composed of dolomite, limestone, and marl. The ore zones of the productive member are highly recrystallized from primary anhydrite/gypsum to secondary (bioepigenetic) calcite and very finely crystalline sulfur, with bitumen concentrations common. To the southwest, the secondary limestone/sulfur grades laterally into fine-grained, dense gypsum/anhydrite.

The productive member has three ore-grade sulfur zones, each about 30 m in thickness, separated by barren or weakly mineralized interbeds of silty dolomite, marl, and shale (Fig. 4, B-B'). Each sulfur zone tends to be massive near the fold axis but splits laterally into multiple sulfur layers separated by barren or near barren interbeds (Fig. 4, A-A'). Coarsely crystalline sulfur or clayey limestone with intermingled bands of calcite and sulfur are the predominant ore types. Tectonically disturbed areas have fracture-filling sulfur and bitumen textures or massive sulfur containing relict carbonate.

In the areas of intense folding, the three ore zones thicken, although later drilling has shown that these layers remain separate (B. Zakiewicz, oral commun., 1978). The width of the sulfur zones decreases upward so that the lowest zone has the maximum lateral extent. Table 2 summarizes Russian data

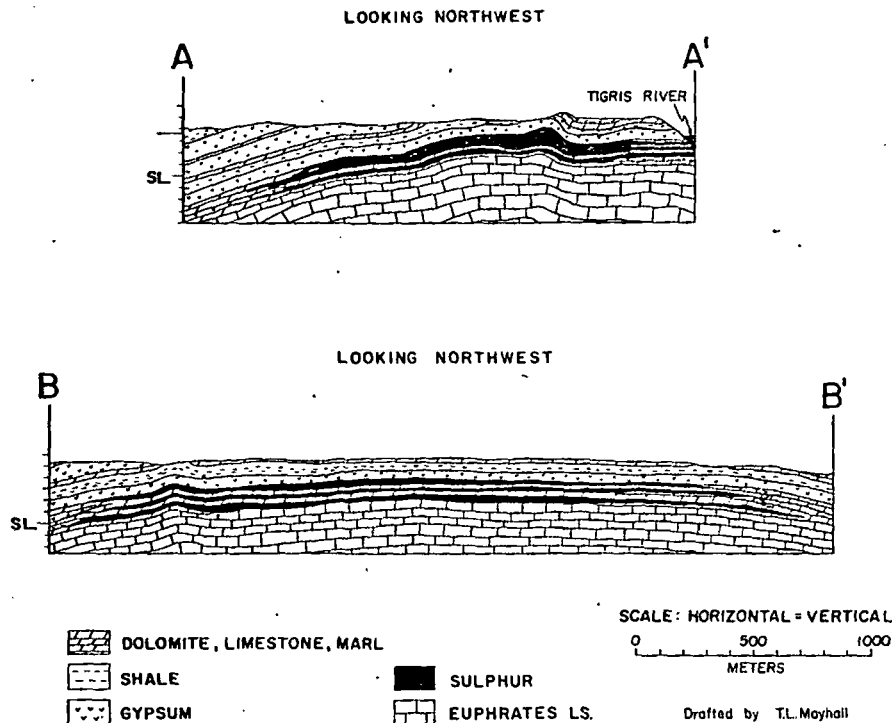


FIG. 4. Cross section A-A' and B-B' at Mishraq, Iraq (based solely on early Russian data after Cortesini, 1966). See Figure 6 for cross-section locations.

(Chebanenko, 1969) from the three ore zones and Table 3 shows matrix and ore analyses (Cortesini, 1966).

Russian core assays indicate that bituminous matter of high asphaltene content comprises up to 10 percent of the rock, with an average of just under 2 percent (Cortesini, 1966). Zakiewicz (1975) reports that actual contamination of sulfur produced during hydrodynamic (Frasch) mining was up to an order of magnitude greater than the 1962 work indicated.

The *sulfate member* is composed of fine- to medium-grained gypsum, anhydrite, and marl. It ranges from 30 to 50 m in thickness and crops out along the Tigris River valley. Interbeds of marl and bituminous, argillaceous, biogenic limestone occur. Individual lenses in the interbeds are permeated with viscous bitumen and have localized sulfur of economic grade and thickness. The limestone in these lenses is very gypsiferous. The basal gypsum/marl layer acted as the seal which kept reactants in the productive member.

The *carbonate-clastic member* is composed of limestone, gypsum, and clay. It is 15 to 75 m in thickness and crops out everywhere except in the deeper wadis where its base has been intersected by the erosional surface.

The limestones of the upper part are recrystallized, vuggy, and sometimes bituminous and sulfur bearing.

Limestones in the lower portions are biogenic, argillaceous, highly bituminous, and are locally recrystallized and sulfur bearing. The sulfur occurs in gypsiferous limestone lenses, similar to those in the sulfate member, containing highly viscous bitumen, mostly in the lower part.

Sandy clay and gypsum are locally interbedded within the limestone. The gypsum is fine to medium grained and sometimes platy. The lower part is bituminous. The sandy clay is gray and calcareous. It may have veinlets of selenite and locally grades into fine-grained sandstone.

The *sulfate-clastic member* consists of light gray, medium- to fine-grained, dense gypsum, with gray fossiliferous (shell) limestone, calcareous polymictic sandstone, and calcareous clay. The member is 70 to 110 m in thickness and is peripheral to the deposit along the southwestern and southeastern boundaries.

Upper Miocene

The clastic rocks of the upper Miocene paraconformably overlie the middle Miocene. Upper Miocene deposits occur only along the southwestern boundary with a maximum thickness of at least 34 m.

Upper Fars Formation: The Upper Fars Formation is composed of varicolored calcareous clay with thin interbeds of gypsum, limestone, marl, and calcareous polymictic sandstone.

Quaternary

Quaternary rocks and sediments are generally absent. Soil and eluvium on divides and alluvium in the wadis and the Tigris River valley are the predominant types present.

The Sulfur Orebody

Sulfur occurs in the lower three members of the Lower Fars Formation and in the Euphrates Limestone. Localized concentrations of ore-grade sulfur are rare except in the productive member of the Lower Fars Formation. Here, the ore is concentrated into three main horizons which are separate although thicker in areas of relatively great tectonic activity (Fig. 5).

Ore reserve calculations are widely variant. The Russian figure was 245×10^6 tons, Cortesini (1966) estimated 239×10^6 tons, Semrad got about 155×10^6 tons, while current Iraqi estimates are about 100×10^6 tons. The later figure is now the accepted reserve figure for Mishraq because the reserve estimate had to be reduced when hydrodynamic mining of the lower two zones rather than open-cast mining

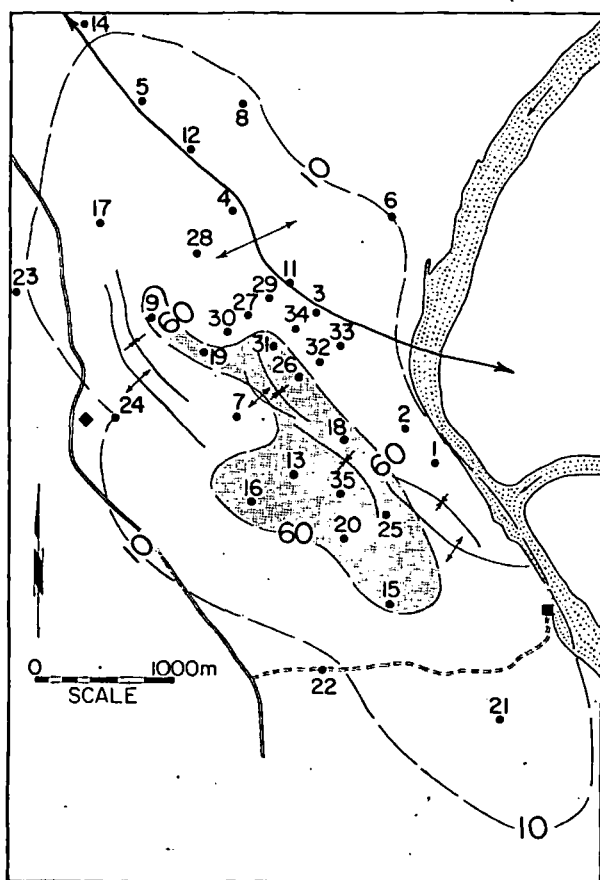


FIG. 5. Isopach of total solid feet of sulfur, zones 1 to 3, as a function of folding at Mishraq, Iraq (based solely on early Russian mapping and drill holes 1-9, 11-35).

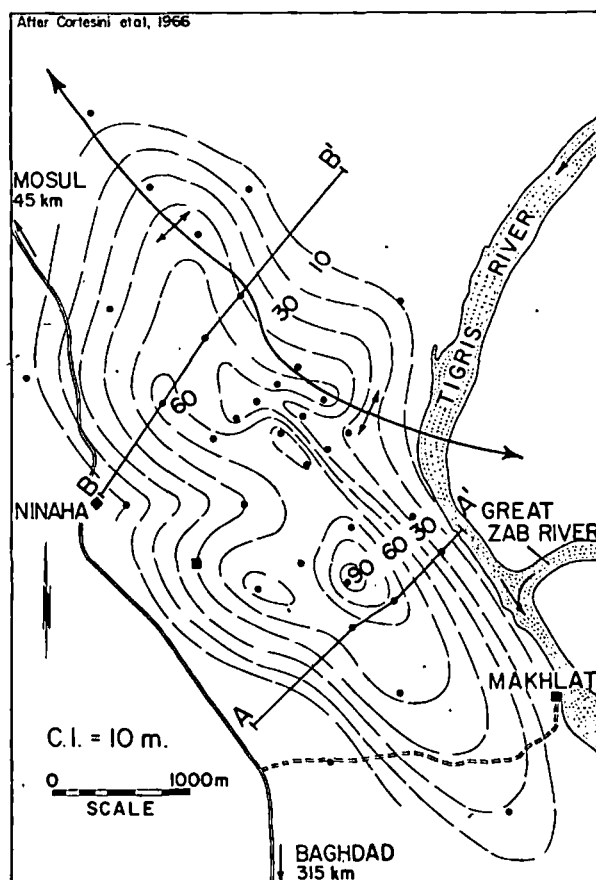


FIG. 6. Isopach of total solid feet of sulfur, zones 1 to 3, Mishraq, Iraq (based solely on early Russian data).

of all three was considered (Zakiewicz, 1975). The mineralization covers about 10 km^2 on the southeast plunge of the Mishraq structure. The lower zone has the greatest lateral extent with zone 2 and zone 3 each smaller in extent than the underlying one.

Cortesini (1966) gave the average composition of the ore matrix (19 holes) as 91.8 percent limestone, 7.7 percent marl and clay, 0.3 percent sandstone, and 0.2 percent sulfate. Sulfur mineralization decreases as sulfate increases so that areas with over 30 m of sulfate have minor sulfur mineralization, thus presenting evidence that the anhydrite is utilized during sulfur generation.

The average sulfur content for the deposit is 23.14 weight percent (Chebanenko, 1969). The total thickness of the three zones together ranges from 2 to 123.9 m with the overburden above the member ranging from 73 to 303.1 m. The maximum total thickness of the economic zones is 107.9 m equivalent to an average of 17 m of solid sulfur (Fig. 6). Porosity determinations in the laboratory ranged from 3 to 13 percent with an average of 5 percent, although this increases during mining. The bulk density of the ore ranges from 2.3 to 2.7 g/cm^3 and is

mainly dependent on the proportions of limestone to sulfur to water-filled porosity.

Niec (1971, in Niec and Al Nouri, 1976) defined seven ore types based on microscopic examination of cores. These are (loosely translated): banded, nested, impregnated, pseudo-brecciated, brecciated, veined, and sparsely veined.

Banded ore is characterized by alternating bands or layers of coarsely crystalline secondary limestone or calcite and finer grained sulfur. Nested ore is composed of irregular nests in sulfur-bearing limestone and ovate nests in dolomitic rocks, often with calcite. Nests may be only partially filled by sulfur yielding a geode structure. Impregnated ore texture shows sparsely distributed, crystalline sulfur concentrations intergrown with calcite. Brecciated ore is brecciated marl and dolomite with interstitial crystalline calcite/aragonite and sulfur. Pseudo-brecciated ore has less angular fragments which are generally blunted and rounded. Veined ore has a variety of vein forms filled with sulfur and/or coarsely crystalline aragonite. More sparsely veined ore has delicate and discontinuous veins up to a few centimeters in thickness.

Chebanenko (1969) describes two main ore occurrences at Mishraq. These are coarsely crystalline and fine-grained laminated. Both types are intimately associated with secondary calcite. Coarsely crystalline ore has crystals ranging from 2 to 5 mm in diameter which normally line vugs, caverns, and fractures. The fine-grained ore has alternating laminations of sulfur and calcite tending to be more massive with fewer vugs and cavities and to have a banded appearance.

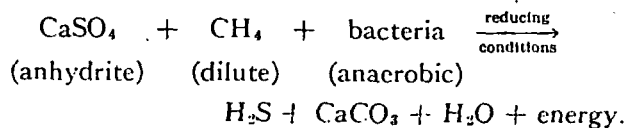
Cortesini (1966) extracted analytical data from the Russian report as shown in Table 3. Contamination other than bitumen was minimal. No systematic analysis of the bitumen concentration was done, but from the 626 samples examined, 278 (44%) had no bitumen. In general, the ore is considered to be bituminous with many sections heavily (>10%) impregnated but with no predictable pattern. Sulfur reaching the surface during mining has over 1 percent dissolved bitumen. Zakiewicz (1975) reports that the bitumen concentration was greater than the Russian estimate of 1962 by an order of magnitude.

Sulfur Origin

A number of well-known conditions are needed for large-scale deposition of sulfur in sedimentary rocks. These are as summarized by Hollister (1977), with appropriate Mishraq characteristics in parentheses: (1) sulfate-bearing rocks, preferably thick and of anhydrite (gypsum and anhydrite in the Lower Fars Formation); (2) proximity to petroleum deposits (a gas field in the northwest portion of the Mishraq

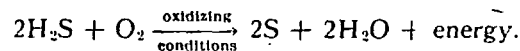
structure and bitumen within the sulfur-bearing rocks); (3) hydrodynamic communication between (1) and (2) which is often accomplished via faulting, jointing, or solution-derived permeability (karst); (4) a stratigraphic or structural trap to contain the precursors of the sulfur-forming reaction (Mishraq anticline); and (5) a reducing environment where petroleum and sulfate are biochemically metabolized, and an oxidizing environment where the sulfur precipitates.

The Mishraq sulfur is derived from the sulfate evaporites of the Lower Fars Formation by reduction of anhydrite/gypsum and bitumen to sulfur and calcite during bacterial metabolism:



Al-Sawaf (1977) has studied the bacteriology of sulfur deposits in northern Iraq and found that both aerobic and anaerobic bacteria were active at Mishraq. The anaerobic bacteria (*D. desulfuricans*) aided the formation of sulfur, whereas the aerobic bacteria (*T. thiooxidans*) destroyed it. No anaerobic bacteria were found subsurface owing to sampling problems, but they were active at the springs along the Tigris River, which interacts with the productive member. Al-Sawaf attributes the lower grade of the upper sulfur zone to sulfur destruction by metabolic activity of the aerobic bacteria.

The H₂S from the anaerobic reaction is oxidized to elemental sulfur and water. Various reactions have been proposed using oxidizers such as SO₄⁻², Ca⁻², and O⁻². The relative shallowness of the Mishraq deposit, porosity developed by solution and folding (tension), and the downdip breaching of the anticline by the Tigris River favor descending oxygenated waters as the H₂S-oxidizing mechanism:



The majority of significant sulfur shows in northern Iraq are in anticlinal structures intersected by the Tigris River, further supporting this view.

Hydrogen sulfide can migrate considerable distances prior to oxidation. At Mishraq, however, the H₂S probably was derived from within the Mishraq anticline. Large amounts (2-5%) of bitumen are in the sulfur ore zones and a commercial sour gas field is on the northwest flank, indicating that the structure is a carbon source and an efficient H₂S trap. The molecular weight ratio of sulfur to diagenetic calcite is 32:136 or 24 percent sulfur (Davis and Kirkland, 1970) as a theoretical maximum in a closed system. The Mishraq deposit con-

tains 23.14 percent sulfur (Chebanenko, 1969) indicating that the reaction is nearly complete and that little H_2S has escaped. Local concentrations of sulfur above 24 percent indicate that internal migration and redeposition of reactants has occurred.

A biological sulfur-forming process should yield fractionations of sulfur ($^{34}S/^{32}S$) and carbon ($^{13}C/^{12}C$) stable isotopes, because biochemical activity tends to increase the concentration of lighter isotopes in the resulting products. Fractionation data are presented as delta (δ) numbers with negative values representing enrichment in lighter isotopes and depletion of heavier isotopes. Lein et al. (1975) measured fractionation in carbonate, sulfate, and sulfur at Mishraq from well 11 (Russian) near the center of the main sulfur-bearing area. The values reported below are from this study unless otherwise labeled.

Carbon ($\delta^{13}C$)

The values of $\delta^{13}C$ in unaltered dolomitized limestone at Mishraq vary from +1 to -6 ppm which are within the range of expected values for unfractionated primary material. Calcite, which, along with sulfur, fills joints, vugs, pores, and fractures, has $\delta^{13}C$ values of -17 to -25 ppm indicating a secondary origin. Carbonate of mixed origin has intermediate values. During microbial reduction of sulfate, light carbon from the organic compounds of the dissolved bitumen was used. This is shown by the strong ^{12}C enrichment in the secondary calcite compared to the primary limestone. The carbon in the bitumen at Mishraq originally had a light $\delta^{12}C$ value which was further lightened by subsequent bacterial partitioning in secondary limestone generated during sulfur formation.

Sulfur ($\delta^{34}S$)

Nonmineralized sulfate rocks from the Lower Fars Formation outside the Mishraq deposit have an average $\delta^{34}S$ value of 19.4 ppm. These rocks appear to be identical to those within the orebody except that sulfur/calcite mineralization has replaced some of the anhydrite/gypsum and limestone. Sulfur samples from the orebody had an average $\delta^{34}S$ value of 15.9 ppm, which is a decrease from unaltered values and represents an increase in the ^{32}S concentration. Sulfur from the Culberson native sulfur orebody in west Texas has a $\delta^{34}S$ value of 15.9 ppm, so the Mishraq value seems typical of large, stratiform sulfur deposits.

Sulfate from within the ore zone had an average $\delta^{34}S$ value of 35.1 ppm indicating an increase of ^{34}S concentration or a depletion of the ^{32}S concentration. The difference between the sulfur and sulfate (gypsum) $\delta^{34}S$ is 19.2 ppm which is a typical fractionation value developed during bacterial reduction of

sulfate (Lein et al., 1975). Isotope fractionation in the Pokorny sulfur deposit in west Texas showed a similar sulfur/sulfate (anhydrite) fractionation value of 19.9 ppm (Davis and Kirkland, 1970).

Hydrocarbons

The recrystallized sulfur-bearing limestone often contains large amounts of black bitumen of a high asphaltene content and with a melting temperature of 30°C. This material fills voids and fractures in the limestone but only rarely pervades the rock laterally. The greatest concentration of asphalt occurs along some of the faults in an irregular fashion (Niec and Al Nouri, 1976).

Dolomite and marl, particularly between the producing horizons, are strongly bituminous, averaging 3.5 percent bitumen. In contrast to the bitumen of the ore zones, it is dispersed throughout, producing a brown coloration (Niec and Al Nouri, 1976).

Overall, the bitumen content averages about 2 percent and ranges up to about 10 percent (Cortesini, 1966). His estimates, based on the Russian drilling of 1960 to 1962, are up to an order of magnitude less than subsequent development drilling has delineated (Zakiewicz, 1975). Current reports indicate that the bitumen content of the wellhead sulfur at the Mishraq mine continues to increase with time.

The northwestern portion of the Mishraq structure is occupied by a low pressure (2-3 atm) sour natural gas field (Chebanenko, 1969) no more than 5 m in thickness (Niec and Al Nouri, 1976). It is in the limestones correlative to the productive member and is at the apical portion of the anticline. The gas is composed of 63 percent methane and ethane with 24 percent hydrogen sulfide and 13 percent carbon dioxide (Niec and Al Nouri, 1976).

The maximum concentration of hydrocarbons occurs in the productive member, but they are of relatively low viscosity. Hydrocarbons of increasing viscosity but decreasing volume upward are associated with the sulfate member and the carbonate-clastic member. None occurs in the sulfate-clastic member or younger units in the Mishraq area.

Hydrogeology

The Mishraq area has complex hydrologic conditions because the Lower Fars Formation has karst features, the area is faulted and folded, and the Tigris River is incised into the eastern side of the anticline. Most of the ground water is within vugs, joints, fractures, channels, and cavities within the limestone, but some occurs in sandstone and fractured claystone (Al-Sawaf, 1977). Calcium sulfate/carbonate waters predominate and often contain hydrogen sulfide. Chebanenko (1969) recognized six aquifers: (1) Recent and early Quaternary alluvium,

(2) sulfate-clastic member, (3) upper part of the carbonate-clastic member, (4) lower part of the carbonate-clastic member, (5) middle part of the sulfate member, and (6) productive member. Of these zones, the productive member contains the bulk of the ground water, with most concentrated in the secondary limestone/calcite (Al-Sawaf, 1977). Niec and Al Nouri (1976) define up to 5 aquifers in the unaltered areas outside the sulfur orebody and up to 8 aquifers within the productive member, of which the three sulfur-bearing zones are dominant.

Al-Sawaf (1977) made a major "study of the quality, temperature, and gas content of groundwater and the distribution of sulfate-reducing bacteria." He found that a tectonically induced interconnection between aquifers was common, particularly in the productive member, although Zakiewicz (1975) found the lower two zones to be separate for hydrodynamic mining purposes. The subsidence associated with mining caused additional fracturing and interconnection between aquifers. Unaltered limestone and anhydrite have low permeability and thus are less important. This conclusion is supported by Featherstone and Al-Samarrie (1975) who got water conductivity in pump tests of 1 m/day in the western portion of the Mishraq deposit and up to 30 m/day near the river where subsurface drainage is better developed. Al-Sawaf (1977) notes a similar relationship with considerable fresh water seepage into ground water near the Tigris River. Core samples showed conductivities of 0.01 m/day (Featherstone and Al-Samarrie, 1975) and pump tests of limestone and anhydrite showed conductivity less than 1 m/day, both supporting a primary flow path via karst and tectonic features. Rock volume decreases

during sulfur formation further enhance porosity and permeability in the productive member relative to unaltered limestone and anhydrite.

Al-Sawaf (1977) calculated ground-water flow in the three sulfur zones of the productive member as follows: zone 1, 3,500 m³/day (or 57% of the total flow); zone 2, 1,500 m³/day (25%); and zone 3, 1,100 m³/day (18%).

Ground water varies widely in temperature, with water in the sulfate and carbonate units ranging from 21° to 25°C. Water in the productive member is warmer, ranging from 25° to 31°C. Mining has raised temperatures to as high as 73°C at springs east of the Tigris River (Al-Sawaf, 1977).

A very steep hydraulic gradient exists with flow southeast toward the Tigris River. Discharge down this gradient, which follows topography, can be so rapid via the karst and tectonic features that turbulent flow and associated acoustical hum can be detected in wells (Zakiewicz, 1975).

It is clear that the orebody is hydraulically connected to the river. Fluctuating water levels in observation wells show a very high correlation with seasonal variations in the elevation of the Tigris River (Featherstone and Al-Samarrie, 1975). The greatest change occurs in wells near the river, with decreasing fluctuations westward. Ground-water communication with the Tigris River is incomplete and may be locally absent. This is indicated by the piezometric head of 20 to 70 m (Niec and Al Nouri, 1976) existing in some wells. Structural and stratigraphic data indicate that river erosion has not penetrated far into the productive member, although intersection of the river channel and the uppermost part of the member has occurred.

TABLE 4. Chemical Analyses of Ground Water and Tigris River Water at Mishraq

Parameter ¹	Tigris River ²	Tigris River ⁴	Tigris River ⁵	Spring sample 5 ³	Overburden sample 3 ³	Overburden ⁴	Ore zone sample 12 ³	Ore zone ⁴
H ₂ S				648	51		415.0	
Free CO ₂				257			304.0	
pH	8.2		7.3	<7			6.5	
Ca	104.0			826	628		561.0	
Mg	46.0	12.3		205	84	72	247.0	224
Na		14.0				60	705.0	1,000
K							15.0	
HCO ₃				869	278		848.0	
SO ₄		171.0	42.0	1,738	1,610	276	1,645.0	2,005
Cl	16.0	45.0	150.0	3,105	435	200	815.0	50
TDS		465.0		9,500	2,794	2,860	4,960.0	2,570
Fe			2.1					
Alkalinity			110.0					
Hardness	150.0	80.0	144.0			640		795
Salinity		184.0				337		2,000

¹ Parts per million except for pH.

² Collected by Semrad in 1966 north of Makhlat and of the main spring.

³ Al-Sawaf, 1977.

⁴ Featherstone and Al-Samarrie, 1975.

⁵ Cortesini, 1966.

Thus discharge is via the Tigris River bed and nearby springs. A large hydrogen-sulfide spring on the east bank of the Tigris north of the Great Zab appears, from water analyses, to be related to the productive member. Sulfate-coated pebbles found in the river bed indicate the existence of more springs under the river.

Ground-water recharge occurs mainly on the northwest portion of the Mishraq anticline where the Lower Fars Formation crops out.

Water quality varies greatly depending on the source (Table 4). Because mine water discharges into the Tigris River, possible pollution was considered but was not found to be significant. During operation of the Mishraq mine, the discharge water

has become more similar to river water due to flushing by the recharge water (treated Tigris River water). Water from the sources listed in Table 4 is suitable for agricultural use except for that directly associated with the productive member (Featherstone and Al-Samarrie, 1975).

Over geologic time, structures intersected by the Tigris River (Mishraq, Al Fatha) have more sulfur than those not intersected (Qalian, Quasab, etc.). This is due primarily to increased oxygenation of the ground water as it flows down to the new hydrologic breach at the river. The dissolved oxygen oxidizes the H_2S to water and sulfur. Thus, the ground-water interaction with the Tigris River has great geochemical significance, over geologic time, relative to sulfur generation and deposition.

Development of the Mishraq Mine

The following account of the developmental history (Table 5) of the Mishraq deposit draws heavily on data from the British Sulphur Corporation (1974 a and b) and Zakiewicz (1975).

Sulfur and hydrogen sulfide were noted in northern Iraq in the mid-1930s by oil geologists. Development was proposed several times and culminated in a strong favorable recommendation by the World Bank in 1951. Following this, Texas Gulf (now Texasgulf, Inc.) formed a subsidiary in Iraq with a \$3 million capitalization. They negotiated with the the government for sulfur exploration and development concessions above 33° N latitude. Profits were to be shared, at 50 percent each, by Texas Gulf and Iraq. This offer was rejected in 1954 as having terms unfavorable to Iraq, although Texas Gulf was unhappy with the government's requirement of 500,000 tons per annum minimum production.

Russian geological and technical aid was utilized in evaluating some areas favorable for sulfur deposition from 1960 to 1962, with several deposits, including Mishraq, delineated. Russian proposals to finance development were not accepted. Little was subsequently accomplished until after the revolution of July 17, 1968, when possible foreign participation in sulfur development effectively ceased.

The Ministry of Oil and Minerals directed investment in sulfur through the National Iraqi Minerals Company (NIMCO). NIMCO (now the State Organization of Minerals) was initially capitalized at \$15 million in February, 1969, with Mishraq picked as the first developmental target.

A contract was signed in May, 1969, between NIMCO and Centrozap of Katowice, the Polish mining engineering institute. Centrozap agreed to develop the mine in two stages of 250,000 and 750,000 tons per annum, respectively, using Hydrokop, the Polish mining construction company.

TABLE 5. Chronology of Development and Production at Mishraq, Iraq (after British Sulphur Corp., 1974, and *Sulphur*, 1974)

Year	Production tons per annum X 1,000	Remarks
1933-1935	0	Sulfur and H_2S noted by oil geologists
1951	0	World Bank strongly recommends development of sulfur
1954	0	Texas Gulf sulfur development proposal rejected
1961	0	Soviet geologists analyze sulfur potential at Mishraq, Al Fatha, Kirkuk, and other areas; Soviet-financed development not undertaken
1966	0	Iraqi government tenders foreign participation offer
1968	0	Revolution on July 17 returns Baatists to power; negotiations with France and U.S. producers cease
1969	0	NIMCO formed in February; contract with Centrozap signed in May
1970	0	Initial equipment dispatched from Krakow, Poland; Hydrokop begins construction and drilling in April
1971	36	First stage completed; trial production in December; sour gas sulfur production begins at Kirkuk (120,000 tons per annum capacity)
1972	100	Mine officially opened on January 6 at 250,000 tons per annum capacity; bitumen removal plant completed
1973	300	Sulfuric acid plant and liquid sulfur transport contracts let
1974	600	Second stage completed, nominal capacity 1,000,000 tons per annum
1975	650	Liquid sulfur shipments begin
1976	610	Installation of new boilers temporarily lowers production
1977	602	Port modifications and mining problems inhibit production

Trial production began in December, 1971, with the mine officially opened at stage one capacity on January 6, 1972. Stage two was completed in the third quarter of 1974.

Shipments of liquid sulfur, by rail, began in 1975, with most destined for export via Um Qasr, a port on the Persian Gulf. Initially, the railroad represented a bottleneck in shipment capacity, but it has now been upgraded. Current bottlenecks are associated with port facilities which are undergoing modification. Negotiations for a rail link across Syria to the Mediterranean are continuing and, if successful, will aid export capacity as well as opening new markets. Exports for 1976 were 407,000 tons and for 1977 were 522,000 tons.

Boiler installation decreased production slightly over 1975 levels, but full capacity, now estimated as 750,000 tons per annum rather than the 1,000,000 planned, will occur in 1980. Complete production data are given for past years in Table 5.

The details of sulfur mining at Mishraq are described by British Sulphur Corporation (1974a) and Zakiewicz (1975).

The Mishraq surface facilities are spread over an area of 40 km² because of the high relief, which prevents convenient access, and the widespread ore occurrence. With subsidence expected wherever mining was done, the facilities had to be kept off the orebody. Utilization of Tigris River water as injection water caused further dispersal of the physical plant to include the intakes at the river.

The two main mining problems at Mishraq are large water losses and hydrocarbon contamination far greater than indicated by the Russian data of 1962.

Water losses were mitigated by emplacement of a subsurface watertight screen about 500 m long and 100 m deep. This was accomplished by subsurface blasting followed by injection of stabilized mud or cement, a process developed by I. B. Zakiewicz in Poland (1975). Following this, a high-temperature steady state was achieved with a low energy expenditure: the recovery of one ton of sulfur requires 7×10^8 BTU and about 11 m³ (2,900 gal) of water. Owing to natural drainage toward the Tigris River, no bleed wells are presently needed at Mishraq, although as mining proceeds to the southeast, relief decreases, and bleed wells and pumps will become necessary.

Molten sulfur reaches the surface with between 1 and 2 percent dissolved bitumen. This is removed in a process developed in Poland by H. Leszczynska. In this process the majority of the bitumen is precipitated using sulfuric acid, with the remainder filtered out of the sulfur by bentonite. Ali and Al-Shahwani (1975) report that up to 8 percent of the

total sulfur feed is lost in skim foam and filter cake. Unofficial reports place this loss at up to 25 percent. The bitumen-removal unit was completed during the first quarter of 1972.

A 15,000 tons per annum sulfuric acid plant was installed to supply the purification plant. Bentonite for Mishraq drilling and screening operations is mined at Qara Tapa, where a mill has been installed. Ground sulfur for agricultural use is also produced at Mishraq.

Initially, sulfur was vatted at the mine and solid sulfur was shipped by standard-gauge railroad. In early 1975, liquid sulfur shipments began, and vating is now done as needed at the port of Um Qasr, near Basrah, about 1,000 km south of Mishraq.

J. M. B.

DEPARTMENT OF MINING AND GEOLOGICAL
ENGINEERING
UNIVERSITY OF ARIZONA
TUCSON, ARIZONA 85721

D. E. C.

DUVAL CORPORATION
4715 EAST FORT LOWELL ROAD
TUCSON, ARIZONA 84712

R. S.

DUVAL CORPORATION
P. O. BOX 1512
PECOS, TEXAS 79772
November 10, 1978

REFERENCES

- Ali, L. H., and Al Shahwani, K. I., 1975, Method for the purification of raw Frasch sulphur from bitumen and ash impurities: *Fuel*, v. 54, p. 221.
- Al-Sawaf, F. D. S., 1977, Sulfate reduction and sulfur deposition in the Lower Fars Formation, northern Iraq: *Econ. Geol.*, v. 72, p. 608-618.
- British Sulphur Corporation, 1974a, Iraq emerges as major sulphur exporter: *Sulphur*, no. 111, p. 36-40.
- 1974b, World survey of sulphur resources, second edition: London, 183 p.
- Chebanenko, V. V., 1969, Geology of the Mishraq native sulphur deposit (Iraq): *Geologia Mestorozhdenii Samorodnoi Sery*, Moscow, Izdatel'stvo Nedra p. 374-379.
- Cortesini, A., 1966, Mishraq sulphur project geologic report: Baghdad, Iraq, Mideast Industries Ltd., unpub. rept., 20 p.
- Davis, J. B., and Kirkland, D. W., 1970, Native sulfur deposition in the Castile Formation, Culberson County, Texas: *Econ. Geol.*, v. 65, p. 107-121.
- Dunnington, H. V., 1958, Generation, migration, accumulation, and dissipation of oil in northern Iraq, in Weeks, L. G., ed., *Habitat of oil*: Tulsa, Am. Assoc. Petroleum Geologists, p. 1194-1251.
- Featherstone, R. E., and Al-Samarrie, A. M., 1975, Geohydrology of Mishraq—groundwater movement study with electrical analogue simulation: *Sulphur*, v. 120, p. 44-49.
- Hollister, V. F., 1977, Potential for the occurrence of sedimentary sulphur deposits in northeastern British Columbia: *CIM Bull.*, v. 70, no. 777, p. 106-108.
- Lein, A. Y., Mamchur, G. P., Zyakun, A. M., Matrosov, A. G., Kudryavtseva, A. I., and Ivanov, M. V., 1975, Origin of native sulphur in Mishraq deposit (Iraq): *Internat. Geology Rev.*, v. 17, p. 881-885.
- Niec, M., and Al Nouri, M., 1976, Złozę siarki Mishraq w polnocnym Iraku: *Przegląd Geologiczny*, v. 24, p. 272-276.
- Zakiewicz, B., 1975, Exploitation of bedded sulphur deposits by the hydrodynamic method: *Sulphur*, no. 120, p. 35-43.

Of the associated sulfides, galena is the best intensifier of dissolution in cyanide solution of both synthesized and natural argentite (Fig. 2). The speed of argentite dissolution in the presence of galena is even higher than when the generally-accepted oxidized lead compounds (litharge, cerussite, and particularly lead nitrate) are added to the cyanide solution.

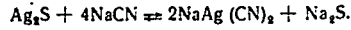
The effect of galena upon the speed and completeness of dissolution in argentite cyanidation is greater than that of oxidizing agents (sodium peroxide, manganese dioxide, potassium ferricyanide, and oxygen). Thus, an addition of 500 mg of sodium peroxide is required for 100% dissolution of synthesized argentite in 24 hours; the same effect is achieved in the presence of 2.5 mg of galena. It has been revealed that sodium peroxide increases the rate of argentite dissolution in the presence of galena and reduces it in the presence of chalcopyrite, and particularly with sphalerite.

Increasing the concentration of protective alkali (lime) in the cyanide solution above 0.04% has an adverse effect upon argentite dissolution in the absence of other sulfides; when galena and sphalerite are added, the solubility of argentite (natural and artificial) increases appreciably with increases in the lime concentrations in the solution (up to 0.08%).

The experiments showed that oxidized zinc minerals (smithsonite) and copper minerals (malachite) in amounts ranging from .5 to 500 mg increased the solubility of argentite somewhat (by 3-17%, according to the amount of minerals added).

Mechanism of Argentite Dissolution in the Presence of Lead, Zinc, and Iron Sulfides. The fact that equivalent results are obtained when argentite dissolves in cyanide solutions in the presence of galena, sphalerite, and pyrite, and in solutions containing only the products of reaction between these sulfides and cyanide (in the absence of the solid phase) indicates that the mechanism of argentite dissolution under these conditions is chemical.

Experiments have shown that zinc and iron cyanide complexes (at a solution metals content of 4-400 mg/liter) do not affect the solubility of argentite; it may be assumed that plumbite, zincate, and ferric hydroxide formed (in amounts depending upon the conditions) by reactions between galena, sphalerite, and pyrite and alkaline cyanide solutions have an intensifying effect upon argentite dissolution. These compounds apparently convert S^{2-} ions to CNS^{-} ions [1, 2]; under these circumstances, the argentite dissolution reaction shifts to the right:



The kinetic curves in Fig. 3 illustrate this fact.

Cyanidation of Pyrargyrite and Proustite. The behavior of silver sulfo salts during cyanidation was studied with artificial single crystals of pyrargyrite and proustite and with natural pyrargyrite. According to spectral analysis, the natural pyrargyrite is remarkably pure, containing 0.03% Pb, 0.003% Cu, and 0.007% Mn. The solubility in cyanide solutions of proustite and pyrargyrite is low (particularly the latter) whether the minerals are synthesized or natural, amounting to 45, 32, and 26.6% respectively in 24 hr at a sodium cyanide concentration of 0.4%.

As in the case of argentite, addition to the cyanide solution of galena, sphalerite, ferric hydroxide, and oxidizing agents (sodium peroxide and potassium ferricyanide) intensifies the dissolution of sulfo salts substantially, proustite dissolving more actively than pyrargyrite in the presence of the additions. Complete dissolution of 25 mg of proustite at a sodium cyanide concentration of 0.2% was achieved in the presence of 50 mg galena in 48 hr; 250 mg of potassium ferricyanide gives 100% dissolution in 24 hr in cyanidation of artificial pyrargyrite. Dissolution of natural pyrargyrite under these conditions amounts of 89.2%.

The investigations confirmed the resistance of sulfo salts which had been noted in the literature [2, 3] and showed that both a preliminary chlorinating roast [3] and certain additions to the solution (galena, oxidizing agents) increase dissolution of silver sulfo salts in cyanidation.

Cyanidation of Mixtures of Various Silver Minerals and Heavy Metal Sulfides. A study was made of cyanidation of mixtures of silver minerals and heavy metals at a sodium cyanide concentration of 0.2% and a lime concentration of 0.02%; the solution volume was 100 ml, and cyanidation time was 24 hr. The results of the experiments (Table 2) show the effect of the mixture composition and its silver content upon the passage of the latter into the cyanide solution.

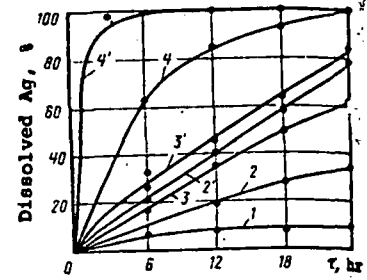


Fig. 3. Effect of additions upon speed of dissolution of synthesized argentite: 1 - no additions; 2 - ferric hydroxide (9.2 mg/liter Fe); 2' - ferric hydroxide (64 mg/liter Fe); 3 - zincate (9.2 mg/liter Zn); 3' - zincate (64 mg/liter Zn); 4 - plumbite (9.2 mg/liter Pb); 4' - plumbite (64 mg/liter Pb).

Cya
re.
sarc
check
avin
chemi
To.4
1.76
1.1 P
2.48
2.66
2.6 M
Lea
sent
want
spha
at a
rial,
The
alkal
tion
am pe
tion
quick
of mi
I. T
spec
to,
te,
Antim
and r
2. T
mani
club
3.
with
the c
their
I. I.
ta
I.
pp
P.
25

Cyanidation of Silver Ore. The results of research on minerals were checked with silver ore having the following chemical composition, %:

76.4 SiO₂ 5.7 Al₂O₃
 1.76 Fe 1.05 K₂O
 0.1 Pb 0.25 Zn
 2.48 CaO 3.5 MgO
 0.66 Na₂O 0.03 Cu
 3.6 Mn 0.32 Stot

Lead and zinc are present in the ore predominantly as galena and

sphalerite; silver is present as native silver and argentite. The ore was cyanided at a sodium cyanide concentration of 0.2%, with the ore ground to 97% -0.074 mm material, a liquid-to-solid ratio of 4:1, and a process duration of 24 hours.

The experiments showed: a) silver extraction from the ore is 81.6% at a protective alkali (lime) concentration of 0.02%, and increasing the protective alkali concentration to 0.08% increases silver extraction to 95.7%; b) adding oxidizing agents (sodium peroxide and potassium ferricyanide) to the cyanide solution reduces silver extraction from the ore from 95.7 to 80.6%; c) the ore is cyanided more completely and quickly (by three times) than its concentration products, which have a higher content of minerals which react with the cyanide solution.

CONCLUSIONS

1. The study showed that the products of the reaction between sphalerite, pyrite, and especially galena and cyanide solution (apparently these are zincate, ferric hydroxide, and plumbite) increase the speed and extent of dissolution of argentite, proustite, and pyrargyrite substantially and do not affect the solubility of native silver. Antimonite and chalcocite have an adverse effect upon the solubility of native silver, and reduce the passage of argentite into the cyanide solution at content of > 300%

2. The effect of galena upon the speed and completeness of argentite dissolution in cyanide solution is greater than that of oxidizing agents. The latter reduce the solubility of argentite in the presence of sphalerite.

3. The speed and extent of dissolution of the principal silver minerals decrease with an increase in the amount of minerals in the initial product which react with the cyanide solution; as a result, the ores can be cyanided more effectively than their concentration.

REFERENCES

1. I. N. Maslenitskii and L. V. Chugaev, Metallurgy of the Precious Metals, Moscow, Metallurgiya, 1972, 367 pp., ill.
2. I. N. Flaksin, Metallurgy of the Precious Metals, Moscow, Metallurgizdat, 1943, 420 pp., ill.
3. F. A. Thompson, Stamp. Milt. Cyanid., New York, McGraw-Hill Book Co., 1915, pp. 255-257.

Table 3
 Dissolution of Silver in Cyanidation of Mineral Mixture

argen- tite	Mixture mineral content, mg									Diss- olved silv- er, %
	chem. pure Ag	elec- trum	gale- na	angle- site	sphal- erite	smith- sonite	py- rite	chalco- pyrite	chalco- cite	
17	9	5	—	—	—	—	—	—	—	100
17	9	5	90	117	165	100	157	80	20	90.6
—	38	—	250	—	900	—	—	—	—	100
—	38	—	140	188	655	376	—	—	—	90.8
—	38	—	—	188	655	376	157	80	20	40
75	—	—	140	188	655	376	157	80	20	94.6
75	38	12	—	—	—	—	—	—	—	63.4
75	38	12	140	188	655	376	157	80	20	78.5

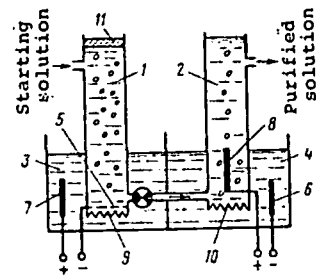
EXTRACTING HEAVY NON-FERROUS METALS FROM SOLUTIONS WITHOUT USE OF REAGENTS

UDC 628.54:669.2

V. K. Makarenko, A. M. Gol'man, and L. I. Mekler

An earlier paper¹ showed that the chemical method of removing heavy metals from solutions, based on the formation of difficult-to-dissolve compounds (primarily hydrates) can be greatly intensified by replacing the extended precipitation operation² by electroflotation without the use of reagent-collectors. However, both with precipitation as well as with electroflotation, the introduction of reagent-precipitants leads to changes in the solution composition (alkalinity, hardness, etc.), which complicates its subsequent use -- for example when organizing water circulation.

The approach suggested by us which avoids the use of reagents eliminates these shortcomings; the essence of our method calls for successive treatment of solutions in cathode and anode cells of the diaphragm electrolytic cell using insoluble electrodes (see Figure). Electrolysis of the water leads to an increase of the alkalinity in the cathode cell and to a combining of metal ions in hydroxides. As they form, these compounds are removed to the liquid surface with the hydrogen bubbles separated at the cathode. Simultaneously, there are separations of fine-dispersed suspended particles, oil, petroleum products, and SAS (surface-active substances). Water is admitted from the cathode to the anode cell where it is acidified to the required pH value; there is also a removal of the organic compounds which are oxidized by the oxygen or chlorine formed at the



Layout of an experimental unit used to remove heavy-metal ions from water without reagents:
 1 - operating cathode cell ($V = 500$ ml, $S = 19$ cm², $H = 26$ cm);
 3, 4 - auxiliary anode and cathode cells (filled with electrolyte - a 10% solution of NaOH);
 5 - operating cathode (grid made of St45, mesh 1.8x1.8 mm, and wire diameter 0.3 mm);
 6 - auxiliary cathode (St 45 plate);
 7, 8 - operating and auxiliary anodes (graphite plates);
 9, 10 - cationite membranes (MK-40);
 11 - flotation froth

Results Obtained After Purifying Industrial Circulating Water by Electrolytic Methods With and Without Reagents

Indices	Composition of circulating water, mc/l		
	before purification	After purification	
		electrolytic method with no reagents	reagent method
pH	3.5-5.5	3.4-5.4	3.5-5.5
Suspended substances	400-700	20-25	10-15
Total iron	100-260	2.7-4.3	0.2-0.5
Zinc	5.0-8.5	0.6-0.7	0.4-0.6
Total hardness, mg-equiv/l.	10.2-10.5	9.2-9.8	16.6-18.2
Sulfate-ion	720-960	420-590	740-990
Dry residue	1480-1800	970-1410	1350-1690
Oleic acid	3.4-5.2	1.6-2.2	3.0-4.5
T-66	9.5-22.0	5.0-11.0	7.5-16.0
Chemical use of oxygen	52.0-96.0	34.0-56.0	48.0-77.0

Preliminary tests on sulfate and chloride solutions of copper, zinc, and iron in distilled water showed that with an original metal concentration of 50-100 mg/l and a pH of 3-5, treatment of solutions for 6-12 minutes (total duration of treatment in cathode and anode cells) at a current density of 1.5 A/l (40 mA/cm²) provides a rather high metal recovery (92-96%) and maintains the original pH value. In most of these tests, the residual concentration of the metal, determined by the incomplete extraction of the hydrated deposit in the operating cathode cell, was 3-5 mg/l. It was established by subsequent research that an improvement in the apparatus design and in the treatment schedule, as well as the shift to actual industrial solutions containing organic substances, make it possible to reduce the residual concentration of metals to 1-2 mg/l and below; this is fully admissible for circulating-water quality.

¹ A. M. Gol'man, L. I. Mekler, M. I. Gorodetskii, and A. A. Elizarov. Tsvetnye Metally, 1971, No. 4, pp. 81-83.

² B. I. Kogan and A. I. Gutman. In the book: Purifying the Sewage from Metallurgical Plants. Moscow, "Tsvetmetinformatsiya," 1970, pp. 31-40.

A study of various treatment schedules showed that the current density in the cathode cell is a basic parameter, determining the intensity and thoroughness of the purification. With low current densities (15-20 mA/cm²), considerable time is needed for alkalization. Moreover, a fine-dispersed hydrated deposit forms which separates poorly during electrofiltration. At current densities of 50-60 mA/cm² and higher, the alkalization rate is high, a floccular deposit of hydroxides forms; however, intensive mixing of liquids by bubbles has an unfavorable influence on the electroflotation of deposits.

In this connection, it was proposed that treatment in the cathode cell be conducted in two stages: alkalization at high current densities of 50-60 mA/cm² (2-2.5 A/l), and the formed deposit is separated at current density values which are optimum for electroflotation (15-20 mA/cm²). The introduction of flocculants, for example polyacrylamide (0.5-1 mg/l) to a solution prior to flotation will greatly accelerate the process. Shifting to a two-stage treatment with the use of flocculants, makes possible a 25-30% reduction in the purification period and an increase in metals recovery of to 98% and more.

A high metals recovery was obtained even when purifying the circulating water from tin finishing plants. Its treatment in a cathode cell was conducted at a current density of 50 mA/cm² (2 A/l) for 5-13 minutes with complete extraction of the hydrated deposit at a current density of 16 mA/cm² (0.6 A/l) for 2-3 minutes. Water is treated in the anode cell for 3-4 minutes at a current density of 2 A/l. For comparison, water was also purified by a method which includes liming, 2-hours precipitation, and acidification of the decantate with sulfuric acid. Comparing the purification results with these two methods (see Table) confirms the fact that with a considerably more rapid electrolytic method, using no reagents, one can completely avoid any increase in water hardness. Moreover, there is a marked drop in its mineralization and it is more thoroughly purified of organic substances.

When using the electrolytic method without reagents to recover heavy metals from solutions, the electric-power consumption depends on the original acidity of the solutions, its electroconductivity, the construction of the apparatus, and a series of other factors. According to approximate calculations, performed from data on laboratory research, the electric-power consumption is about 0.5-3 kW·hr/m³.

BDC 66

In i
not ex
counte
reases

It i
by pre

The
up the
To eli
soluti
mainte

The
fill t

To f
of the
flow

The
as fol

where
produc
R - th
When
with c
sumpti

where
When
preate
If I
calcul
in the

The

where
The

All
tion.
Sol
= Fg
of so
The
the t

Aft
ing b
tor p
tions
tions
evapo

V. A
tion

Sov. Mining Sci.
N2, 1967UNIVERSITY OF UTAH
RESEARCH INSTITUTE
EARTH SCIENCE LAB.

UDC 622.341:542.61

EXTRACTION OF IRON FROM OXIDIZED ORES
BY LEACHINGN. A. Chinakal, F. A. Baryshnikov,
and I. L. Ruzinova

The present paper deals with extraction of iron from ores, by-passing the blast-furnace process [1-3].

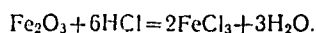
Direct extraction of iron from ores is of great importance in the case of oxidized iron ores as found in the Bakchark, Lisakovsk, Nizhne-Angarsk, and other deposits. Such ores are very difficult to concentrate owing to the presence of very fine intergrowths of ore and nonore minerals and to the very slight difference between the densities of the ore and the rock.

The reserves of oxidized iron ores are enormous, reaching hundreds of billions of tons in the West Siberian basin alone [4]; it is therefore of great importance to develop an efficient method for their concentration or the direct extraction of the iron.

Present methods (gravity, gravity-flotation, gravity-magnetic and the use of a strong magnetic field) of concentrating oxidized iron ores are ineffective because the iron content of the concentrates is 44-49% [5, 6].

Laboratory experiments and industrial tests have shown that the most technologically advanced method of concentrating oxidized iron ores is the reducing-roasting-magnetic method [4-6]. The methods of direct reduction [1-3] and direct leaching of iron from the ores [7] may also be of considerable promise. An earlier paper [1] gave the conditions for using the direct reduction of iron from oxidized ores, and approximate economic data.

The essential feature of the method of leaching iron from ferruginous minerals in oxidized ores is selective solution of iron from crushed ore, with HCl solutions



The solution of ferric chloride is evaporated to dryness and the iron in the residue recovered in a powdered state by reduction with hydrogen. Hydrochloric acid is regenerated during the process.

To confirm the feasibility of leaching and elucidate the process conditions, the Mining Institute of the Siberian Branch of the Academy of Sciences of the USSR has made a laboratory study of Bakchark iron ores. Under percolation conditions, a study was made of the effect of the following factors on iron solution: the HCl concentration, the solids: liquid ratio, the contact time of the solvent with the ore, the solution temperature, the fragment size of the ore, and the mixing of the ore with the solvent.

The mineralogical composition of a sample is given in Table 1.

It will be seen from Table 1 that all the ferruginous minerals in the ore are soluble in HCl, the quartz and feldspars are insoluble in HCl, and only traces of other soluble minerals are present.

The chemical composition of the sample was as follows: Fe_{Tot} - 36.30%; FeO - 16.35%; Fe_2O_3 - 33.75%; H_2O - 2.28%; losses on ignition - 16.34%; TiO_2 - 0.33%; SiO_2 - 22.82%; Al_2O_3 - 5.18%; S - 0.02%; P - 0.31%; P_2O_5 - 1.09%; MnO - 0.29%; Cu - absent; Pb - absent; CO_2 - 2.20%; As - 0.02%; Cr - absent; CaO - 0.48%; MgO - 0.82%; Ni - absent; Co - 0.007%; ZnO - 0.82%; V_2O_5 - 0.32%.

Iron was extracted from ore of the 1 + 0 mm class by allowing the liquid to flow through funnels with taps.

The experiments showed that at solvent temperature 18-20°C and a 3:1 stoichiometric ratio of the amount of HCl solution to the iron content in the ore (liquid: solids), maximum iron extraction from the ore is observed only when leached with 35% acid for 5 h. In the case of 10% and 17.5% acid, extraction of iron is very low (Table 2). The optimum leaching time was taken as 5 h.

Mining Institute, Siberian Branch of the Academy of Sciences of the USSR, Novosibirsk. Translated from Fiziko-Tekhnicheskie Problemy Razrabotki Poleznykh Iskopaemykh, No. 2, pp. 88-91, March-April, 1967. Original article submitted November 10, 1966.

TABLE 1. Results of Mineralogical Analysis

Mineral	Amount of mineral in the sample, %	Fe content in the mineral, %
Hydrogoethite.	20-24	60.9
Hydrohematite	1-2	64-69
Goethite	2-3	62.9
Ferruginous chlorites (leptochlorites, chamosite). . .	28-30	27-38
Glauconite.	1-2	-
Siderite.	18-20	48.2
Quartz	14-16	-
Feldspars	1-2	-
Clay minerals (kaolinite, chlorite, hydroschists, phosphates, etc.).	4-6	-
Rutile	0.5-1	-

TABLE 2. Comparison of the Extraction of Iron with HCl

Time, h	HCl		
	10%	17.5%	35%
1	6.49	7.16	55.2
2	8.2	9.3	63.7
3	11.0	10.6	70.3
4	11.1	11.8	77.0
5	14.1	14.3	85.6

TABLE 3. Extraction of Iron from Bakcharsk Ore at 80°C

Time, h	Extraction of Fe with HCl, %		
	10%	17.5%	35%
1	22.9	52.2	-
2	-	67.9	-
3	-	74.0	-
4	55.0	83.9	-
5	62.0	93.0	100.0
6	62.4	92.7	-

Under these experimental conditions, with a change in the solids : liquid ratio and using 35% acid, extraction of iron into the solution reaches the following values: at a 5 : 1 stoichiometric ratio 89.2%, at a 4 : 1 ratio 87.4%, 3 : 1 - 85.6%, 2 : 1 - 79.1%, and at a 1 : 1 ratio 42.8%. The optimum stoichiometric ratio is 3 : 1.

To elucidate the effect of temperature on extraction of iron into the solution, the experiments were performed in a thermostat. With a 3 : 1 ratio, 17.5% acid and contact time 5 h, an increase in the solution temperature from 18-20 to 80°C leads to an increase in iron extraction from 14.3 (cf., Table 2) to 93% (Table 3). Under these conditions, leaching with 35% acid gives 100% extraction.

The effect of the fragment size of the ore on Fe extraction was studied by allowing a 3-fold amount of acid to flow over the ore in a funnel for 5 h at 18-20°C. Treatment of the -1 + 0 mm size class gave 85.6% Fe extraction; in the case of the -3 + 1 mm and the -6 + 3 mm size classes, Fe extraction was 70.1% and 63.69%, respectively.

TABLE 4. Comparison of Impurity Content in Iron Ore and in the Ferric Chloride Residue

Impurity	In the ore, from chemical analysis data, %	In ferric chloride, from spectral ana. data, %
Si	9.5	0.005 - 0.002
Al	2.73	0.01 - 0.005
Ca	0.34	0.02
Mg	0.49	0.05
P	0.31	-
V	0.089	-
S	0.02	-
Zn	0.65	0.06

At 80°C and leaching with 17.5% acid, Fe extraction was as follows: for the -1 + 0 mm class 93%, the -3 + 1 mm class 72.0%, and the -6 + 3 mm class 65.9%, respectively.

With increasing size of the ore fragments, Fe extraction falls markedly. An increase in solvent temperature to 80°C enables us to obtain the same Fe extraction with 17.5% acid as that obtained with 35% acid at 18-20°C.

To elucidate the effect of the leaching method on Fe extraction, in addition to the percolation method we performed leaching experiments with and without mixing of the ore and the solvent, at preselected optimum parameters.

The experiments showed that higher Fe extraction is obtained with leaching by percolation for 5 hours' contact of solvent and

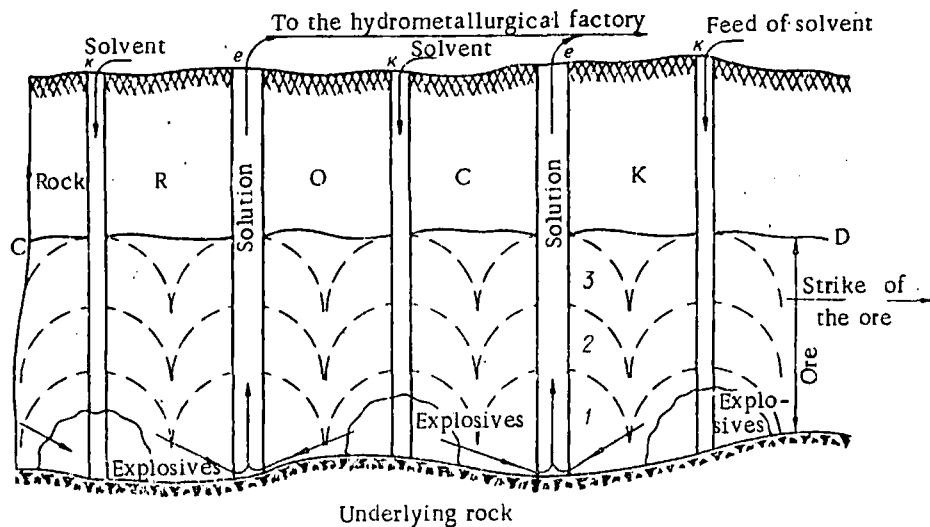


Fig. 1. Working a deposit via boreholes, with underground crushing and leaching out of the iron.

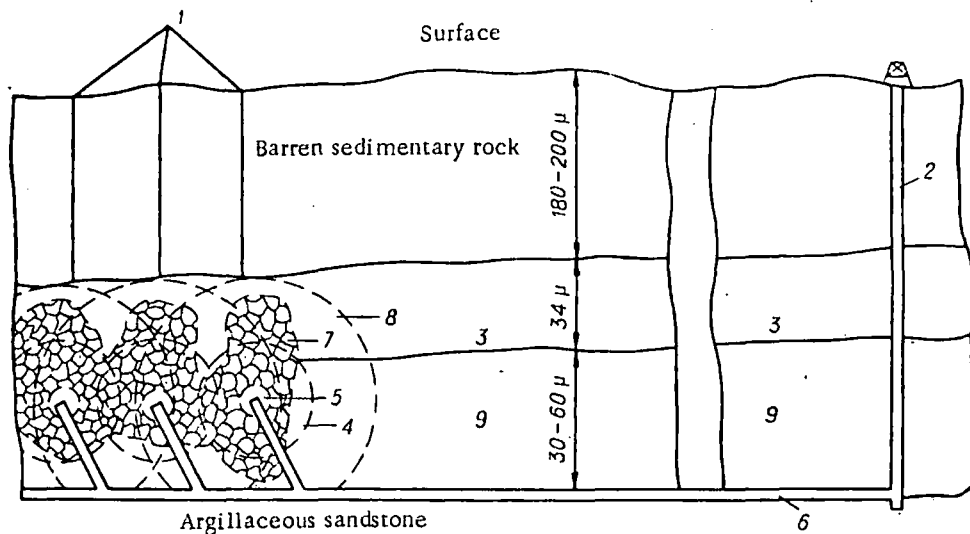


Fig. 2. Working a deposit by the combined method: underground crushing and leaching out of iron. 1) Boreholes for feeding the solutions; 2) shaft; 3) ore body; 4) crushing zone; 5) nuclear charges; 6) drainage road; 7) caving zone; 8) boundary of fissure formation; 9) poor iron ores.

ore (86.4-88.7%); mixing of the ore and solvent with a stirrer gives 85.0-86.2% extraction. Under these conditions, extraction of iron without mixing and without percolation is only 47.7%.

To determine the content of impurities, the ferric chloride solution thus obtained was evaporated to dryness and the content of impurities in the residue determined (Table 4). It will be seen that iron powder with minimum content of impurities can be obtained by leaching iron with HCl.

Thus the investigations established that leaching is an effective method of extracting iron from oxidized ores of the Bakchark type. It is applicable to winning of ore and its processing on the surface in hydrometallurgical factories, and can also be used in underground conditions without winning of the ore. The decisive factors governing the applicability of leaching in underground conditions are the porosity or water permeability of the ore body and the feasibility of fine crushing of the ore in the underground workings.

Leaching out of iron in underground workings can be performed in several ways.

Boreholes are drilled from the surface, along and across the strike of the ore body, at a specific distance and to a specific depth (Fig. 1). Shaped charges or small nuclear charges are placed in these holes. Blasting leads to

disintegration and fragmentation of the ore body. The solvent is then fed under pressure from the surface. The iron-containing solutions thus obtained flow to the central boreholes and are pumped to the surface; they are then transported to the hydrometallurgical factory for conversion to iron powder [7].

According to data from Alberta (Canada), the production of high-grade iron powder by the leaching method is profitable because the powder fetches a high price and the solvent is recovered during the process [8].

In the case of the Bakchar'sk deposit, a factor favoring the use of the leaching method is the presence of natural gas and peat in the vicinity. The gas can be used for obtaining large amounts of hydrogen to reduce the iron from the chloride precipitate and as a fuel for heating the solvent; the peat can be used as a metallurgical fuel and reducing agent.

LITERATURE CITED

1. N. A. Chinakal, F. A. Baryshnikov, and O. F. Baryshnikov, On the Concentration of Oxidized Iron Ores by Direct Reduction and Magnetic Separation, *Fiziko-Tekhn. Problemy Razrab. Polezn. Iskopaemykh*, No. 3 (1966).
2. A. A. Shitov, Direct Manufacture of Iron from Ores in the USA, *Metallurgicheskaya i Gornorudnaya Promyshlennost'*, No. 1 (1962).
3. W. Lucken, Preparation of Crudes for Blast-Furnace Smelting [Russian translation], Translated from the German by I. S. Gokhman, Edited by Ya. I. Dashevskii, Moscow, Gosgortekhzdat (1959).
4. N. Kh. Belous, Geological Reserves and Forecasts of the West Siberian Iron Ore Basin, In: *The West Siberian Iron Ore Basin* [in Russian], Novosibirsk, RIO SO AN SSSR (1964).
5. A. S. Finkel'shtein, D. B. Indenbom, and A. B. Patkovskii, Review of Experiments and Selection of Alternative Methods of Ore Preparation, The Oolitic Iron Ores of the Lisakovsk Deposit of the Kustanai Region [in Russian], Moscow, Izd. AN SSSR (1962).
6. A. G. Gerasimov, G. F. Suslikov, and P. A. Taupenko, Industrial Beneficiation of Iron Ores of the Nizhne Angarsk Deposit [in Russian] (manuscript proof copy), Krasnoyarsk (1958).
7. B. I. Nifontov, D. D. Protopopov, I. E. Sitnikov, and A. V. Kulikov, Underground Nuclear Explosions [in Russian], Moscow, Atomizdat (1965).
8. Present Trends in the Iron Industry, *Express-Informatsiya*, No. 34 (1964).

AN EXAMINATION OF THE INTERACTION OF GOLD TELLURIDE WITH AQUEOUS SOLUTIONS OF CHLORINE

UDC 669.213

I. A. Kakovskii, V. V. Gubailovskii, and D. A. Pirmagomedov

Ores containing gold tellurides can be classified as stable. Extraction methods such as gravitation and amalgamation do not apply to them. It is possible to subject telluride ores to cyanidation, but various complications result: a sharp drop in the dissolution rate as compared with metallic gold, an increased consumption of reagents — particularly cyanide (1).

This paper gives the results of studies into the kinetics of dissolution in aqueous solutions of chlorine for the most stable of the gold tellurides — the synthetic alloy which corresponds in composition to the calaverite mineral AuTe_2 . Preparation of the alloy was described in an earlier work (1); its composition was checked by chemical and x-ray-structural analyses, the tests conducted by the rotating disk method.

In conducting the tests, it was noted that rather thick films form on the disk surface. Analysis of these films and of the solution for gold and tellurium showed that alloy components pass into solution in amounts different from their ratio in the solid phase, i.e., dissolution occurs incongruently and depends on the solution composition, basically on its acidity. Where there is low solution acidity on the disk surface, tellurium films form which complicate the diffusion of chlorine to gold telluride and reduce the rate of dissolution for the latter in time (Fig. 1).

Interaction between gold telluride and aqueous solutions of chlorine occurs in the diffusion system, which follows from the directly proportional relationship between the dissolution rate and the mixing intensity and the presence of characteristic etching figures on the disk surface (2-4).

In the aqueous solutions of chlorine, without their acidification with hydrochloric acid, the ratio of the gold and tellurium concentrations fluctuates (due to the instability of tellurium passage to solution) from 1:0.56 to 1:0.76, rather than 1:2. Chemical analysis of the films, taken from the disk following the test ($t = 25^\circ\text{C}$, $n = 515$ rpm, $[\text{Cl}_2] = 0.015$ mole/lit), provided the following atomic relationship between tellurium and gold: 5.9 without acidification of the solutions and 4.3 with acidification, using HCl (0.1 mole/lit), i.e., the films were very rich in tellurium, as was noted above.

As solution acidity increased, there is an increase in the tellurium dissolution rate with a comparatively slight reduction in the rate of gold dissolution (see Table). For the last test, use of chlorine is about 45% of theoretical, which also confirms the diffusion nature of the process, somewhat complicated by formation of films,

Let us consider the causes for the incongruent dissolution of gold telluride. At the low solution acidity, tellurium is found in films as TeO_2 — compounds which dissolve comparatively poorly in water while the rate of its passage into a solution is lower than that of gold. As solution acidity rises, there is formation of readily-soluble tellurium compounds — TeCl_4 and H_2TeCl_6 . However the standard potentials for the reactions of AuCl_4^- and TeCl_6^{2-} formation differ: +0.995 and 0.55 V, respectively. Consequently, there is formation on the disk surface of galvanic micropores, in which gold is the cathode and tellurium the anode. This causes more intensive tellurium dissolution and some drop in the gold-dissolution rate as the solution acidity increases (and possibly also the precipitation of gold by tellurium; as in the instance of the dissolution of silver amalgams (5)).

As confirmation of that kind of electrochemical mechanism for the process, one can use the reaction of metallic gold chlorination, the rate of which increases ten-fold

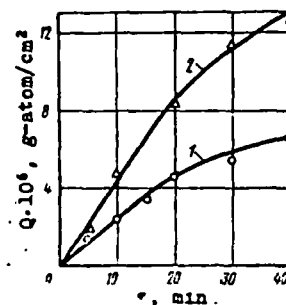


Fig. 1. Kinetic dissolution curves for AuTe_2 in aqueous solutions of chlorine, mole/lit: 1 — 0.015 Cl_2 ; 2 — 0.026 Cl_2 ; 0.1 HCl.

Rates of Gold and Tellurium Passage into Solution in Relation to Solution Acidity ($t = 25^\circ\text{C}$, $n = 515$ rpm; $[\text{Cl}_2] = 0.015$ mole/lit)

[HCl], mole/l	$v \cdot 10^3, \frac{\text{g-atom}}{\text{cm}^2 \cdot \text{sec}}$		$v_{\text{Au}} \cdot v_{\text{Te}}$
	Au	Te	
0	4.05	2.5	1:0.62
0.1	3.80	5.2	1:1.37
0.33	3.20	10.4	1:3.25
0.66	3.00	18.0	1:6.0

with an increase in the hydrochloric acid concentration of the solution, in contrast to the process of gold telluride chlorination. Formation of films on disk surfaces is accompanied by some reduction in the experimental constant of the dissolution rate, as compared with the calculated theoretical level and equalled 4.2×10^{-7} lit/cm² with $1/2 \text{ rev}^{1/2}$. Depending on the solution acidity, the experimental rate constant is from 21 to 45% of the theoretical level.

A study was also made into the effect of the chlorine concentration of the solution (Fig. 2) and the temperature on the rate of gold telluride dissolution. Given a solution acidification with over 0.1 mole/lit HCl, the rate of gold dissolution to solution was directly proportional to chlorine concentration (first order reaction in chlorine); without acidification, there is a slight deviation from the linear relationship (a more intensive formation of films when there is an increased chlorine concentration in the solution). The effect of temperature on the rate of gold passage to solution was studied in two series of tests: without acidification and with acidification of the solution to 0.1 mole/lit HCl. The values of the reaction rate, calculated from these data, were identical in both series of tests. In view of the good correspondence of

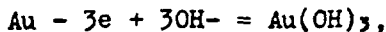
results, instead of the Arrhenius graph, we use the equation $\log K = -3.508 - \frac{1060}{T}$, and an experimental activation energy of 4.85 kcal/mol characteristic for diffusion processes, complicated by the formation of films on the surface (4).

Calculation of the rate of gold passage to solution (in view of the incongruity of gold telluride dissolution, we consider the more valuable component - gold) can be conducted by using the conventional equation (2-4) of:

$$v = \frac{Q}{St} = Kcn^{1/2}$$

Given low concentrations of acid and chlorine in the solution, the constant of the reaction rate at 25°C equals $8.6 \cdot 10^{-8}$ l/cm² with $1/2 \text{ rev}^{1/2}$; for other temperatures, it can be calculated from the above cited equation or the activation energy, equal to 4.85 kcal/mole.

Let us consider the advantages of the chlorination process for gold telluride, as compared with cyanidation. First of all, unlike cyanidation, the chlorination process occurs in a diffusion mode even where there is a large number of disk revolutions; this makes possible its intensification by means of mixing. The reason that the gold dissolution process does not occur in chloride solutions in the kinetic mode should be searched for in the surface charge of the metal. Gold is more inert in chloride solutions than in cyanide (the standard potentials are +0.995 and -0.543 V). Given so positive a surface charge there will be no formation on it of oxidized passivated films, since the process potential is:



which according to Peshchevitskii equals +0.59 V and according to our calculations equals +0.53 V.

There will be a less marked slowing down of the dissolution rate as a result of the formation of films on the gold telluride surface when chlorinating pulps, as a result of the wearing away of the films by the gangue particles. Secondly, chlorine is a much cheaper reagent than cyanide; it would be simpler to separate gold from chloride solutions. Thirdly, since chlorine is also a complex-former and an oxidizer, when employing chlorination it is possible to achieve a much greater maximum dissolution rate than with cyanidation, when the process is limited by the solubility of the oxygen in the solution -- which is much lower than the solubility of chlorine.

According to our research (1), when using pulp with low alkalinity, the constant of the reaction rate for the cyanidation of gold telluride was $5.6 \cdot 10^{-9}$; at 25°C, it was much lower than the constant for the chlorination reaction rate of $8.6 \cdot 10^{-8}$. During cyanidation, the obtainment of larger dissolution rates is possible as a result of an increase in the cyanide concentration of the solution (to 0.5-1%). However, the maximum achieved dissolution rate when blowing pulp with air at $n = 600$ rpm was 7×10^{-10} g-atom/cm²-sec (1, Fig. 1, curve 4); however, using the same amount of revolutions and a chlorine concentration of 0.03 mole/lit (7 times lower) the chlorination rate was $8.2 \cdot 10^{-9}$, i.e., an order higher.

If cyanidation is conducted at lower cyanide concentrations, compensating this by an increase in solution alkalinity (1, Fig. 5), then the cyanidation rate totals (2-2.2).

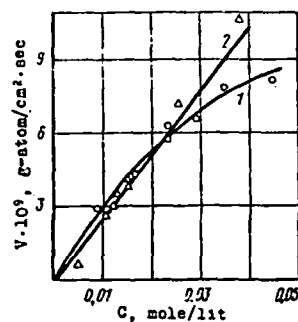


Fig. 2. Relationship between the rate of gold passage to solution and the Cl concentration: 1 - without acidification; 2 - 0.1 mole/lit HCl.

.10-10, i.e., it is of one- and one-half times lower than when employing chlorination, not counting the fact that the latter process can be accelerated by increasing the chlorine concentration in the solution.

The comparative review given for the cyanide and the chlorination process shows the latter to have marked advantages over the former. The known negative aspects of chlorination can be partially compensated for by combining the flotation of gold telluride with the last chlorination of the obtained concentrates; given a correct and possibly selective flotation system, the yield would be low. Prior to chlorination, it would be useful to regrind the concentrate since gold telluride is very brittle.

Evidently, the optimum chlorination conditions for gold tellurides would be as follows: fine grinding, intensive mixing, a slight acidification of the pulp; and an adequate chlorine concentration in the solution. An increase in temperature does not produce any special effect -- only a comparatively small activation energy.

References

1. I. A. Kakovskii and N. I. Sorokina, Izv. Vuz., Tsvetnaya Metallurgiya, 1972, vol. 15, No. 3, pp. 96-103.
2. I. A. Kakovskii and Yu. B. Kholmanskikh, Izv. AZ SSSR, OTN, Metallurgiya i Toplivo, 1969, No. 5, pp. 207-218.
3. I. A. Kakovskii and Yu. B. Kholmanskikh, Izv. AZ SSSR, OTN, Metallurgiya i Toplivo, 1960, No. 5, pp. 207-218.
4. I. A. Kakovskii and V. V. Gubailovskii, DAN SSSR, 1969, vol. 184, No. 5, pp. 1157-1160.
5. I. A. Kakovskii and S. A. Kuligin, Scientific Works from Uralmekhanobr, No. 13, Sverdlovsk, 1967, pp. 200-216.

SUBJ
MNG
EIS

UNIVERSITY OF UTAH
RESEARCH INSTITUTE
EARTH SCIENCE LAB.

**National and international
management of mineral
resources
London May 1980**

UNIVERSITY OF UTAH
RESEARCH INSTITUTE
EARTH SCIENCE LAB.

Paper 4

J. C. Agarwal and J. C. Burrows

Economic impact of *in-situ* solution mining of copper

The Institution of Mining and Metallurgy

This preprint has been prepared for distribution to registrants for the joint meeting of the Institution of Mining and Metallurgy, the Society of Mining Engineers of AIME and the Metallurgical Society of AIME, to be held in London in May, 1980. All papers that are presented at the conference will be included, together with discussion, authors' replies, name and subject indexes, in the volume *National and international management of mineral resources*. The volume, which will be published in April-May, 1981, may be obtained from The Institution of Mining and Metallurgy, 44 Portland Place, London W1N 4BR, England.

Economic impact of *in-situ* solution mining of copper

J. C. Agarwal D.Ch.E.

J. C. Burrows Ph.D.

Charles River Associates, Boston, Massachusetts, U.S.A.

Synopsis

Conventional mining for copper involves the moving of hundreds of tons of overburden and ore to produce one ton of copper. Large amounts of energy, capital and labour are expended in crushing, grinding, concentrating and smelting of the ore and concentrate. In-situ solution mining, if successfully developed, would have an immense economic impact in decreasing capital and operating costs and increasing the resource base. The economic impact of the development of this technology is examined with particular reference to copper.

The United States and most other developed countries historically have faced the spectre of ever-increasing demand for metallic minerals coupled with decreasing ore grades. Until recently, U.S. companies have been able to hold down the costs of producing metallic materials by taking advantage of economies of scale and relatively more effective management, and by investing in more efficient technologies. In the past few years, however, the United States has begun to face severe competitive pressures from foreign sources in a variety of mineral markets. In the absence of major technological changes in mining and smelting, it is likely that the United States will not only face rising costs for the mineral resources essential to its economy but will become increasingly dependent on imported mineral supplies. Rising costs for one of the most important factors of production in our economy are likely to have an adverse effect on our standard of living and on inflation. Increasing dependence on foreign supplies will reduce the ability of the United States to pursue an independent foreign policy and will increase the risk of supply crises, such as the OPEC embargo and oil price increases, the sharp escalation of IBA bauxite taxes since 1974, and the critical shortage of cobalt that is currently being faced by the industrialized world. Finally, if the decline in U.S. mineral production continues, it will significantly affect the economies of a number of states, including New Mexico, Arizona, Utah and Nevada.

The reasons for these problems are complex,

but the following four factors are dominant and must be considered: (1) the United States has relatively lower-grade ores than most of its foreign competitors; (2) costs of complying with government regulations, particularly in the environmental area, are relatively high in the United States; (3) capital costs, particularly construction costs, are higher in the United States; and (4) incremental technological change to reduce costs is possible but limited and is quickly diffused to competitors abroad, who are using higher-grade ores.

In-situ solution mining offers attractive potential solutions to all of these problems. Conceptually, the process involves the following basic five steps: (1) drilling of injection and production wells in the orebody; (2) injection of a liquid (or a mixture of liquid and gas) to dissolve the desirable metal out of the host rock; (3) recovery of the pregnant solution; (4) purification and recovery of metal(s) from the recovered pregnant solution; and (5) recycling of the barren solvent.

In-situ solution mining differs from conventional dump leaching, vat leaching or heap leaching in two important aspects, i.e. no movement of solids occurs and the leaching solution has to be more oxidizing to recover copper from sulphide mineralization.

In contrast to present copper-producing methods in which rock is drilled, blasted, moved, crushed, ground and beneficiated, and the concentrate smelted, no disturbance of earth takes place and only liquid moves through the rock. For example, in the U.S. copper industry, approximately 500–800 tons of rock are processed in this way for every ton of copper that is produced. These kinds of mining, crushing, grinding and flotation operations consume nearly one-half of the total energy that is required to produce copper as well as nearly two-thirds of the capital costs. This condition places the United States, which has relatively low-grade ores, at a distinct economic disadvantage in relation to other countries that have higher-grade ores.

In-situ solution mining can decrease the capital and operating costs for processing minerals by as much as one-half by eliminating the processing of large amounts of solids. Additionally,

environmental costs due to scarring the earth in open-pit mining and from unsightly tailings (waste) ponds are completely eradicated. Valuable minerals and metals can be recovered even in areas where natural surroundings would normally prohibit such operations, because no movement of earth occurs.

Because massive earthmoving mining and processing equipment is not used in *in-situ* solution mining, the scale of operation can be much smaller. Therefore, smaller and lower-grade ore deposits and even deep-lying ore deposits, which would normally be uneconomical to exploit, can be brought into production quickly and profitably. Availability of *in-situ* technology will also increase the reserves of the metal thus recovered.

The most important distinction between *in-situ* solution mining and conventional mining is that one of the normal criteria of economical viability—ore grade—is not critical for *in-situ* operations. Therefore, given enough ore reserves, it is possible to recover many minerals and metals that would otherwise be uneconomical to recover either from new deposits, old depleted mines or tailings.

In-situ solution mining is currently being used in shallow deposits of uranium and for copper oxide ores. Kennecott Copper Corporation has done extensive development work for *in-situ* mining of porphyry copper sulphides, but *in-situ* solution mining is also applicable to most other non-ferrous metals, e.g. nickel, molybdenum, vanadium, manganese, chromium, zinc, lead, gold, silver, etc.

If *in-situ* solution mining can be proved to be economically and technically feasible, it could greatly increase over the long run the supply of a number of minerals, providing significant benefits not only to U.S. metals industries but to many parts of the world where low-grade deposits occur. The development of commercially viable *in-situ* processes for minerals other than uranium is still in its infancy, however, and many fundamental problems need to be resolved. The necessary research, field testing and development is expensive. To date, only one firm has invested significantly in the *in-situ* solution mining of copper, and even that effort has recently been abandoned because of lack of funds. But the eventual payoff is so great that the technology *will* be developed. It is highly likely that the petroleum companies will take the lead because major uncertainties and the required development work are in the area of the petroleum companies' expertise in drilling and completion of wells, reservoir engineering and secondary recovery of oil. So it will not be surprising to see the development of *in-situ* mining technology led by oil companies, which have the technical skills, the economic resources and, most important, a history and the fortitude to take risks.

Important technical and economic factors

Although we use the term *in-situ* mining, the technical requirements for success for *in-situ* solution mining are very different from those for the conventional mining and winning of metals, at least until the copper is in solution. *In-situ* solution mining will not be technically and economically successful unless (1) drilling costs can be minimized; (2) solution flow can be controlled reasonably to contact desired minerals; (3) the pregnant solution contains enough metal concentration by proper selection of chemical processes to minimize the metal recovery costs in relation to its projected selling price; (4) adequate reserves are available (or an adequate recovery of the metal in the available reserves is possible); (5) chemical and power costs are not likely to be prohibitive in relation to the selling price of metal(s); and (6) injected chemicals will not damage the natural or induced permeability of the deposit by undesirable chemical reactions.

These considerations lead to four major areas of importance: (1) deposit characterization and suitability; (2) leaching behaviour of desired minerals; (3) recovery of the desired metal(s) from pregnant liquid; and (4) environmental compliance.

Desirable deposit characteristics

In-situ mining has many attributes that make desirable deposit characteristics for it significantly different from those of conventional mining. For example, permeability and porosity of the deposit and their variations within the deposit are of little or no significance in conventional mining, whereas they are of immense importance in *in-situ* mining, whether the permeability and porosity of the deposit is induced or natural. Ore grade is of less importance in *in-situ* mining because the ore is not moved from the deposit and it is the solution contact with the mineral grain that is important, regardless of the surrounding host rock, which may or may not 'see' the solution.

Without going into a detailed discussion of their interrelationships, the following parameters are important in defining acceptable deposits: (1) profile of ore grade, lateral and vertical; (2) configuration of deposit; (3) mineralogy to predict leaching and loss of copper to ion-exchangers; (4) profile of permeability to predict solution flow; (5) porosity of deposit to predict hold-up of solution; (6) location of dykes and thief zones to anticipate abnormal flow behaviour; (7) stratigraphic behaviour of rock to control drilling; (8) extent of ore reserves to determine mine life; and (9) suitability of ore deposit to enhance permeability, if needed.

It should be emphasized that it is highly likely that a large fraction of the desired information on geological characterization of deposits will not be available because the development of *in-situ*

technology for metals is still in its infancy.

Leaching of copper

Increased concentration of copper in solution has the largest single beneficial impact on *in-situ* solution mining. Even if copper sulphide minerals have been oxidized at an adequate rate and have gone into solution, dissolved copper could be lost by the following methods, thereby decreasing the copper loading in the pregnant liquor: (1) loss to ion-exchangers; (2) loss by precipitation because of dilution by groundwater; and (3) loss by excursions in chemical regime, i.e. pH and solution chemistry.

Copper loading is also dependent on the residence time of the solution and the amount of copper-bearing minerals contacted. Therefore, it is important to minimize the shortcircuiting of the flow of leaching solution and create selective fracturing or permeability to achieve better access to the copper minerals. It should be noted that copper loading will inevitably decline in any block of ore being leached, so new blocks of ore must be brought into production periodically to maintain annual production within a narrow range of variation.

Chemicals, oxygen and power are the major cost elements on leaching, which can be either acidic or ammoniacal. If the calcite content of the host rock is high, it may be desirable to avoid acidic leaching because of high acid consumption and gypsum formation.

Dissolution and recovery of such by-products as molybdenum, gold and silver are also important to economics, but it may not be possible to recover gold and silver in the same solution as copper or molybdenum. Therefore, it is highly likely that those deposits which have economically important gold and silver content as *by-products* would be extracted by two different chemical solvents or not be exploited at all by *in-situ* solution mining.

Recovery of metals from pregnant solution

Copper is recovered from solution by liquidation exchange followed by electrowinning. Thus, most of the required technology for this sector of the process is conventional or available with minor modifications.

Environmental considerations

In-situ solution mining does not have to contend with tailings disposal and sulphur dioxide abatement problems. It does, however, have to contain the leaching solutions within the orebody so that no contamination of groundwater occurs. In addition, when the deposit has been depleted, post-mining restoration must be done that would involve continued pumping out of the solution, rendering it environmentally safe and returning it to the ground. This is an expensive and long operation and cannot be overlooked in economic evaluation.

Economic analysis

The most important factors in economic feasibility are: (1) concentration of metal in pregnant liquors; (2) number of wells needed for desired annual production; (3) solution flow control and environmental requirements (especially with the use of toxic chemicals); (4) solution hold-up in the deposit; and (5) percentage recovery of metal(s) from the deposit.

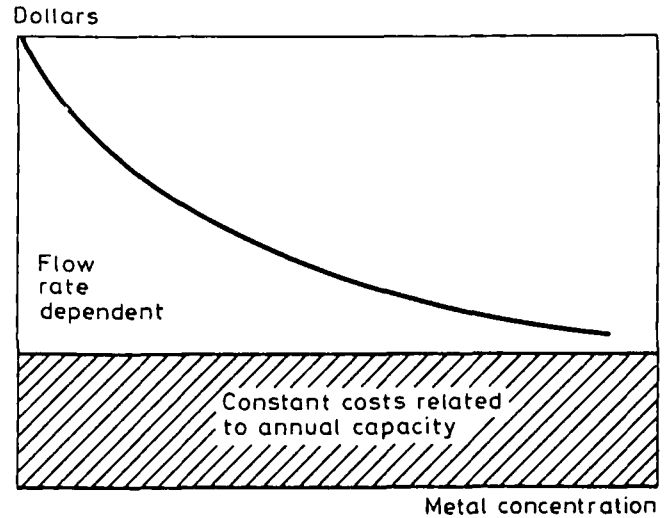


Fig. 1 Structure of capital cost

These five factors are interrelated in determining the optimum area of economical operation. It is easy to see the desirability of high concentration of metal(s) in the pregnant liquor and small number of wells for a desired annual production, but the economic relationships become very complex when the cost and impact of solution hold-up, surface plant requirements and power costs are taken into account. There are two major categories of cost components in *in-situ* mining (see Figs. 1 and 2). One of the major categories of costs is determined by the desired annual production capacity and is fixed. The other, which is variable, is determined in large part by the concentration of the desired metal(s) in the pregnant liquor.

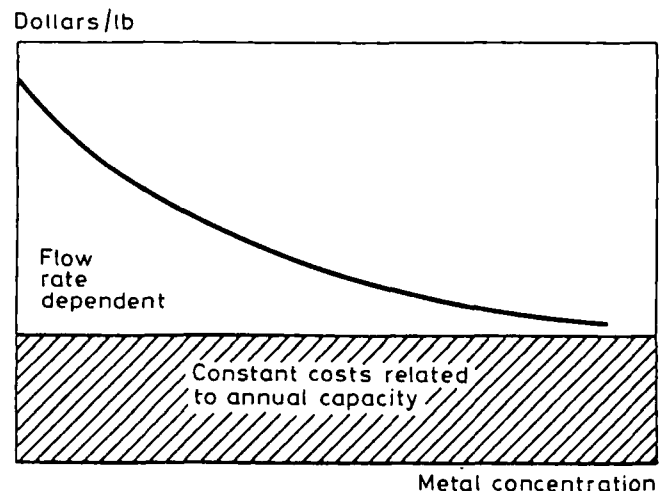


Fig. 2 Structure of operating cost

Table 1

	\$/annual ton of copper
(1) Deposit preparation and wells	300-600
(2) Solution preparation and injection	450-900
(3) Metal recovery	1100-1300
(4) Off-sites and ancillaries	700-1000
Sub-total	2550-3800
(5) Working capital	300-400
(6) Mine development expense (including solution hold-up)	1350-1100
Total	4200-5300

Capital costs for the *in-situ* solution mining plant can be divided (1979 dollars) as shown in Table 1.

The mine development costs require explanation for *in-situ* solution mining. The minimum cost will be that required to fill the pore spaces in the ore block that is being extracted. Additional expenses will be incurred as the solution concentration increases to the desired level with time. The reason for displaying mine development costs separately is that some portion of these costs could be treated as expense and some capitalized, depending on existing laws.

The capital costs for conventional mining and smelting (in 1979 dollars) range between \$6700 and \$7700 per annual ton. Approximately two-thirds of those costs are for mining, milling and concentration, and one-third are for smelting and refining. Mines that have high-grade ores will have a much lower capital cost because mining and milling costs are lower in spite of the same smelting and refining costs. Additional infrastructure costs in foreign countries would offset higher pollution abatement investment in the United States.

We believe that these investment costs for *in-situ* solution mining are achievable through further development work. The cost of recovery of copper cathodes from dilute solutions is well known. The cost of pumping solution against a given pressure drop is easily estimated. Even the cost of a single completed well can be estimated accurately: what is not known is the number and frequency of wells. The investment estimates are given for a well field layout that assumes that a single well can be made to produce approximately 50-100 gal/min at a copper concentration of 2-6 g/l.

Turning to operating costs, *in-situ* solution mining requires less labour and, as was demonstrated earlier, is less capital-intensive. It does, however, require more chemicals, but less energy per pound of copper. The capital costs for using this energy are also less because in *in-situ* mining the energy is used for pumping liquids and electrowinning whereas in conventional mining,

smelting and refining most energy is used in milling and smelting.

Cash operating costs are projected in cents per pound in 1979 dollars (Table 2).

Table 2

	¢/lb Cu
Process materials	12-14
Utilities	12-20
Labour-related costs	5-7
Capital-related costs	9-13
Overhead	3-4
	41-58

In any extraction process for the recovery of copper from chalcopyrite or other sulphide minerals, sulphur must be oxidized. The preferred oxidant for *in-situ* solution mining for deep-lying deposits is gaseous oxygen in acidic medium or ammoniacal medium. The choice between acid or ammoniacal solvent with oxygen for *in-situ* solution mining is dependent on many technical and economic factors, some of which are: (1) cost of oxidant; (2) amount of calcite in the host rock, which may neutralize sulphuric acid; (3) amount of oxidation of ammonia; (4) pyrite to chalcopyrite ratio (to generate additional acid); and (5) loss of copper to natural zeolites.

If significant loss of acid to the host rock can be prevented, most of the acid that is required can be generated by the oxidation of sulphides. Similarly, if ammonia oxidation can be controlled, the cost of ammonia can be minimized by recycling most of the ammonia in the lixiviant. In arriving at these cost numbers we have assumed that approximately 4 lb of oxygen will be required per pound of copper, which is approximately 80% more than the stoichiometric requirement for oxidation of sulphur in chalcopyrite. The cost of tonnage oxygen is assumed to be \$0.06-\$0.08/lb of copper, and the remainder of the process material costs are for miscellaneous chemicals.

In many commercial copper oxide leaching processes the acid consumption has been reported to be between 10-15 lb of acid per pound of copper. The acid consumption is high—primarily because the surface area of crushed ore exposed to the acid is high. For *in-situ* mining of copper from sulphide minerals the major cost for process chemicals is for oxygen to oxidize the sulphide minerals, regardless of whether acid or ammoniacal lixiviant is used. It is assumed that ammonia oxidation or the neutralization of acid by the host rock can be minimized by further development. Only pilot-plant tests under long-term operation can provide pertinent data on firm operating costs.

The most important aspect of these costs is that they are not so sensitive to manpower-related costs, and it should be possible to automate a

number of operations. In addition, the impact of a slowdown of demand and production would be felt less severely because a turndown on pumping of solution is more easily achieved than that in conventional mining and smelting.

Potential implication of in-situ mining process

As was discussed earlier, there are many situations in which *in-situ* leaching or mining of minerals would be economical. These are: (1) currently unexploitable deposits because of (a) low grade, (b) depth and configuration of deposit, (c) high stripping ratio, (d) water-table, (e) small reserves, (f) inaccessible terrain and (g) possible destruction of scenic beauty; (2) to increase reserves; (3) to provide a competitive edge; and (4) to produce metals such as nickel and manganese for which the United States is totally dependent on foreign sources.

The situation regarding the copper industry in the United States is very similar to that of the oil industry. A more appropriate analogy is in the iron ore industry. By developing the taconite pellet industry, starting with a low-grade and then unexploitable deposit, the United States was able to limit the amount of iron ore that was imported and to put an upper limit on the price that the United States had to pay for iron ore.

A low-grade copper deposit cannot compete with a high-grade copper deposit on an equal footing; therefore, either the prices have to rise to accommodate the higher investment and operating costs for the low-grade deposits or the production from 'marginal' deposits would eventually be curtailed. We need a technological breakthrough for the copper industry in the United States. The development of *in-situ* solution mining would provide that not only for the copper industry but also for such other metals as nickel, molybdenum, chromium, uranium and manganese.

nitude of the chemical potential of the strongly magnetic impurity along the length of the tube, as a result of which there is a change in the values of the diffusion characteristics proportional to the product $H(\partial H/\partial x)^2$. In fields greater than 20 000 Oe the δ/D ratio becomes extremely small, the exponential term in equation (3) decreases, and the K_{eff} value becomes closer and closer to the equilibrium value.

In addition, in a non-uniform magnetic field any paramagnetic particle is acted upon by the force F , determined by the expression:

$$F = mXH(dH/dX) \quad (4)$$

where: M is the mass g; X is the magnetic susceptibility of the sample cm^3/G ; H is the strength of the magnetic field Oe; dH/dX is the intensity gradient of the magnetic field Oe/cm, which pulls this particle towards the region of higher strength. In our magnetic fields the magnitude of this force can have an appreciable effect on the move-

ment of the nickel in the melt, giving rise to a directional drift towards the crystallisation front.

Conclusions

1. A method was developed for investigation of the effect of a magnetic field on the degree of purification of copper from nickel by the crystallisation method.
2. It was shown that with a crystallisation rate of 0.3mm/min the effective distribution coefficient of nickel in copper is increased by 1.5 times in a magnetic field with intensity $15.25 \cdot 10^3$ Oe.

**UNIVERSITY OF UTAH
RESEARCH INSTITUTE
EARTH SCIENCE LAB.**

References

- 1) W Pfann: Zone melting: Mir 1970.
- 2) A I Belyaev et alia: Metallurgy of pure metals and elementary semi-conductors: Metallurgiya 1969.
- 3) V V Sychev: Complex thermodynamic systems: Energiya, Moscow 1970.

*Sov. Non-Fe metals Research
v6 N6 1978*

UDC 669.536:546.723.66.066.2

The effect of individual parameters on the hydrolytic precipitation of iron, copper and zinc from sulphate solutions

N A Zapuskalova and E V Margulis (North-Caucasian Mining-Metallurgical Institute) *yeg*

Under specific concentration and temperature conditions the minimum pH value at which hydrolytic precipitation of metal ions (Me^{n+}) is possible is pH_{in} . As for any process¹, the concept of the possibility of hydrolytic precipitation has thermodynamic and kinetic significance. As a kinetic characteristic $(pH_{in})_k$ signifies the minimum pH value at which the precipitation rate becomes sufficient to detect the process by the selected method of detection at a given temperature, at a given concentration of the salt being hydrolysed, and with a given concentration of the salt background. As thermodynamic characteristic $(pH_{in})_t$ signifies the minimum pH value of a solution at a given temperature, a given concentration of the salt being hydrolysed, and with a given salt background where the solution can coexist in equilibrium with the precipitate formed during hydrolysis of the salt. It is clear that $(pH_{in})_t < (pH_{in})_k$.

The hydrolytic precipitation of Fe(III), Cu and Zn as a stable hydroxide only occurs with low concentrations in the solution: with concentrations of Me^{n+} above a certain critical value $(c_{Me})_c$ the basic salts are precipitated in stable form. Thus, at 22°C $(c_{Cu})_c = 1.1 \cdot 10^{-3}$ g/l, $(c_{Zn})_c = 15.2 \cdot 10^{-3}$ g/l², and $(c_{Fe})_c \approx 0.1$ g/l. We note that at a considerable ionic strength in the solution it is more accurate to use $(a_{Me})_c$ and not $(c_{Me})_c$. In hydrometallurgical practice the concentrations of the hydrolytically deposited metals $c_{Me} > (c_{Me})_c$. Under these conditions Fe(III) is precipitated in the form of the amorphous basic sulphate $2Fe_2O_3 \cdot SO_3 \cdot xH_2O$ ³, copper is precipitated in the form of $CuSO_4 \cdot nCu(OH)_2$, where $n = 2-3^6$, and zinc is precipitated in the form of $ZnSO_4 \cdot nZn(OH)_2 \cdot qH_2O$, where $n = 3-4$ and $q = 4-5^6$.

The relationship $(pH_{in})_t = f(c_{Me})$ was mentioned by Britton⁷, and it was subsequently discussed and investigated in a series of papers⁸⁻¹³ and others¹⁴. This relationship for the basic salt $MeSO_4 \cdot nMe(OH)_2$ is given by the equation:

$$(pH_{in})_t = \frac{1}{2n} \lg AP - \lg K_w - \frac{n+2}{2n} \lg(\gamma_{\pm} \cdot c_{Me}) - \frac{1}{2n} \lg(\gamma_{\pm} \cdot c_{SO_4}) \quad (1)$$

where: AP is the activity product of the basic salt; K_w is the ionic product of water, and γ_{\pm} is the activity coefficient. As applied to the precipitation of impurities from zinc sul-

utions, it can be assumed that $c_{SO_4} \approx$ constant, and $(pH_{in})_t$ then becomes a function of one variable $\gamma_{\pm} c_{Me}$.

The $(pH_{in})_k = f(c_{Me})$ relationship for zinc sulphate solutions can be expressed in terms of the equation¹⁵:

$$(pH_{in})_k = B + \lg(K_w \cdot K^{1/n_2}) - \frac{n_1}{n_2} \lg c_{Me} \quad (2)$$

where: B is a constant which depends on the sensitivity of the method for the detection of the beginning of precipitation; K is the precipitation rate constant; n_1 and n_2 are the partial kinetic orders of the precipitation reactions with respect to c_{Me} and c_{OH^-} respectively.

The attainment of equilibrium between the solution and the precipitate is usually lengthy (from several hours to many days). Although it is a conditional characteristic which depends on its method of determination, the $(pH_{in})_k$ value is closer to the practical conditions for the precipitation of Me^{n+} than $(pH_{in})_t$. The $(pH_{in})_k$ value is therefore a convenient characteristic of the boundary conditions beyond which hydrolytic precipitation of Me^{n+} is realised in practice. Subsequently, only $(pH_{in})_k$ will be considered, and for brevity it will be denoted as pH_{in} .

The absence of published data on the dependence of pH_{in} on the method of its determination and also the absence of systematic data on the pH_{in} for the main impurities (iron, copper) in zinc sulphate solutions gave rise to interest in the determination of the conditions for pH_{in} and to determination of pH_{in} by a single method as a function of the concentration and temperature over a wide range of variation in these parameters and for the formulation of pH for zinc. The present work was devoted to this problem. The conditions attached to pH_{in} were determined by comparison of pH_{in} for Fe(III) and Cu in experiments in which the following parameters differed with other conditions equal: 1) neutralisers (KOH and ZnO); 2) the method for detection of the beginning of formation of a precipitate (by the change in light dispersion and by a decrease of c_{Me} by a specific value Δc_{Me}); 3) the time from the moment of the attainment of a given pH in the solution to the beginning of the formation of a precipitate ($\tau_0 = 15$ min and 2h); 4) the salt background (without a salt and with $ZnSO_4$ at $c_{Zn} = 100$ g/l). Investigations according to point 1 were not undertaken for Fe(III), since the pH_{in} values differ considerably with the use of KOH and ZnO as neutralisers, and this is due not to the effect of the conditions on the hydrolytic pre-

precipitation process but to difference in the chemical mechanism of the process. [Jarosite and not the amorphous basic sulphate is precipitated by KOH at pH_{in}^{14}].

The procedure for these investigations was as follows: the initial materials were Fe(III) and Cu sulphates, ZnO, and KOH of chemical purity or analytical purity. The experiments were carried out in closed thermostated ($\pm 0.5^\circ C$) flasks with mechanical agitation at 20-90°C.

Two series of experiments were set up for each c_{Me} and $t^\circ C$. The experiments in each series differed in a narrow range by the successively increasing amount of the given neutraliser. The series were identical in the set of neutraliser-sulphate ratios. In one series of experiments the pH was determined immediately after the sulphate solution was mixed with the neutraliser and the composition of the mixture had averaged (complete dissolution of ZnO or non-equilibrium precipitates formed locally at the point where the KOH entered), and this together with measurement of the pH required not more than 5 min. In the other series of experiments the optical density was determined after the elapse of a given holding period τ_0 (15 min or 2h), and the pH and c_{Me} values were determined in the filtered solution. In the described series of experiments we found the pair of mixtures, closest in composition, where precipitation was not yet detected in one mixture while the beginning of precipitation was detected in the other by a sharp increase in optical density D or by a decrease in c_{Me} by a given value Δc_{Me} . The pH values of these mixtures, determined after the composition had averaged, determined the limits within which the pH_{in} value lies under the selected conditions and with the given method for the determination of this quantity. These limits differed by not more than 0.2 pH unit, i.e. pH_{in} was determined with an accuracy of ± 0.1 pH unit.

The pH was measured by means of a glass electrode on a pH-340 instrument with an accuracy of ± 0.05 pH unit. The optical density D of the neutraliser-sulphate solution mixtures was measured on a photo-electric FEK-M colorimeter. The solutions were analysed for copper by iodometric titration and for Fe(III) and Zn by a complexometric method with Trilon B (EDTA). At Fe and Cu concentrations c_{Me} of 0.5-50g/l the beginning of precipitation was characterised by Δc_{Me} values between 0.1 ± 0.05 and 1.0 ± 0.2 g/l, depending on c_{Me} .

With other conditions equal the effect of the neutraliser (KOH and ZnO on pH_{in} was determined from the Cu in the zinc solutions and the beginning of precipitation was determined from Δc_{Cu} . The results showed that the pH_{in} values with the use of KOH and ZnO practically coincided over the whole range of c_{Cu} and t .

The effect of the method of detection of the beginning of precipitation (by the increase in D and by Δc_{Me}) for $\tau_0 = 15$ min with other conditions equal was checked against Fe and against Cu in the zinc solutions. In the case of Fe the neutraliser was zinc oxide, and in the case of Cu the neutraliser was potassium hydroxide. It was established that both methods give coinciding pH_{in} values for Cu over the whole range of c_{Cu} and t° and differing pH_{in} values for Fe (fig. 1). From fig. 1 it is seen that the pH_{in} value obtained from Δc_{Fe} is higher than pH_{in} obtained from the change in the light scattering. Moreover, the difference in pH_{in} increases with decrease in t , particularly in the region of $t \leq 50^\circ C$.

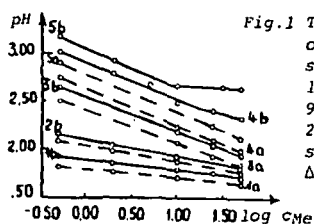


Fig. 1 The dependence of pH_{in} for Fe(III) on the concentration c_{Fe} in zinc solutions ($c_{Zn}=100$ g/l) for $\tau_0 = 15$ min and temperatures $^\circ C$: 1 - 90, 2 - 70, 3 - 50, 4 - 35, 5 - 20. a) pH_{in} according to light scattering; b) pH_{in} according to Δc_{Fe} .

The effect of the zinc sulphate background on pH_{in} was checked on Cu and Fe with other conditions equal by the method for determination of pH_{in} from Δc_{Me} with $\tau_0 = 15$ min. It was found that for Cu the pH_{in} value was practically the same both in zinc solutions and in solutions without zinc. The pH_{in} value with zinc sulphate was 0.1 pH unit higher than without zinc sulphates only at 90°C and with low c_{Cu} concentrations (~ 0.5 g/l).

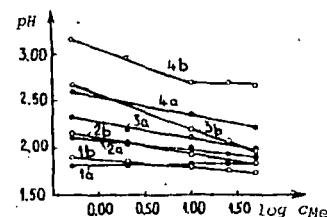


Fig. 2 The dependence of pH_{in} for Fe(III) on the concentration c_{Fe} in solutions at temperatures $^\circ C$: 1 - 90, 2 - 70, 3 - 50, 4 - 20. a) Without zinc sulphate in the solution; b) with zinc sulphate in the solution ($c_{Zn} = 100$ g/l). The pH values were obtained from Δc_{Fe} for $\tau_0 = 15$ min.

For Fe the pH_{in} values in solutions with and without zinc sulphate differ (fig. 2). The effect of the zinc sulphate background becomes stronger with decrease in temperature and with decrease in c_{Fe} . This results in the fact that with other conditions equal the pH_{in} value is higher in solutions with zinc sulphate than in solutions without zinc sulphate.

The effect of the holding time τ_0 on the pH_{in} value was checked for iron and copper. The pH_{in} value was determined from Δc_{Me} for $\tau_0 = 15$ min and 2h. For copper the difference in τ_0 has practically no effect on pH_{in} . For iron the effect of τ_0 is considerable and increases with increase in temperature and with increase in c_{Fe} (table).

Table: The effect of the holding time (τ_0) on pH_{in} for iron(III) from zinc sulphate solutions (neutraliser ZnO, $c_{Zn} = 100$ g/l)

$^\circ C$	c_{Fe} g/l	pH_{in}	
		$\tau_0 = 15$ min	$\tau_0 = 2$ h
90	0.5	1.90	1.55
	50.0	1.70	0.80
20	0.5	3.17	2.95
	50.0	2.63	2.22

The pH_{in} values for Fe and Cu as functions of the concentration and temperature were determined by a single method in zinc sulphate solutions ($c_{Zn} = 100$ g/l). The neutraliser was zinc oxide, and the beginning of the formation of the precipitate was determined by the decrease of c_{Me} by $\Delta c_{Me} = 0.1 \pm 0.05$ to 1.0 ± 0.2 g/l for c_{Me} values in the range of 0.5-50g/l. The pH_{in} value for zinc in zinc sulphate solutions ($c_{Zn} = 80-180$ g/l) with zinc oxide as neutraliser was determined from $\Delta c_{Zn} = 1.0 \pm 0.2$ to 2.0 ± 0.5 g/l.

The results made it possible to determine the numerical coefficients in equation (2) with allowance for the effect of temperature, and this led to the following analytical equations, formulated as a result of the identity of the methods for the determination of the $pH_{in} = f(c_{Fe}, t)$ values for Fe(III) and Cu(II) in the range of $c_{Me} = 0.5-50$ g/l and $t = 20-90^\circ C$ (for $c_{Zn} = 100$ g/l):

$$pH_{in Fe} = 3.43 - 0.018t - (0.588 - 0.006t) \lg c_{Fe} \quad (3)$$

$$pH_{in Cu} = 5.45 - 0.018t - (0.511 - 0.0024t) \lg c_{Cu} \quad (4)$$

and for Zn in the range $c_{Zn} = 80-180g/l$ and $t = 20-90^{\circ}C$

$$pH_{in, Zn} = 7.60 - 0.021t - (1.02 - 0.005t) \lg c_{Zn} \quad (5)$$

The conditions attached to pH_{in} were assessed for the case of Fe(III) and Cu(II), of which Fe^{3+} belongs to the strongly hydrolysing and Cu^{2+} belongs to the weakly hydrolysing ions. The strongly hydrolysing ions are characterised by a susceptibility for transition of the hydrolysed forms into sols and gels with increased values of c_{Me} .

The difference in the mechanism of the formation of the basic sulphates of iron and copper is the reason for the fact that the pH_{in} values obtained from the change in light scattering and from the decrease of c_{Fe} coincide with copper and differ for iron. The formation of the precipitate of $2Fe_2O_3 \cdot SO_3 \cdot xH_2O$ is preceded by the following stages: 1) conversion of the hydrolysed iron into a sol; 2) the formation of a gel; 3) the formation of a precipitate^{3,4)}. With sufficiently large c_{Fe} values these stages are reflected in the variation of the optical density D of the solutions, as seen from fig. 3 in curve 2a, where stages 1, 3 and 2 correspond to sections de, eg and ik. During the precipitation of copper (fig. 3, curves 1b and 2b) and iron with small c_{Fe} values (fig. 3, curve 1a) the sol and gel of the hydrolysed forms of Me^{n+} do not accumulate. The sols and gels cannot be separated from the solution by normal filtration, and their appearance is not therefore detected by the change in c_{Me} but is detected by the increase in D. Therefore, for strongly hydrolysed Me^{n+} the method for determination of pH_{in} from the change in light scattering is more sensitive than the method based on Δc_{Me} . For weakly hydrolysing Me^{n+} these methods are equivalent.

The effect of the holding time τ_0 from the setting of the pH in the solution before the beginning of precipitation on pH_{in} for strongly hydrolysing ions (Me^{3+}) is due to the presence of an induction period during their precipitation in the region of pH_{in} . For Cu^{2+} the precipitation hardly has any induction period at all, and τ_0 does not therefore affect pH_{in} .

The effect of the salt background zinc sulphate on the pH_{in} for iron is explained by the stabilising effect of zinc sulphate as an electrolyte on the iron sol, and this hinders the formation of the precipitate and requires large pH values for the beginning of precipitation. The absence of a sol during the precipitation of copper is the reason for the identical pH_{in} value of copper both with and without zinc sulphate.

The results on the effect of the conditions of the beginning of precipitation and the method of determination of the beginning of precipitation on the pH_{in} value not only agree with the formulated theories about the hydrolytic precipitation of metal ions but also characterise the degree of this effect quantitatively.

The analytical expressions $pH_{in} = f(c_{Me}, t)$ for iron (III), copper (II), and zinc in zinc solutions, obtained on the

Thermodynamic properties of zinc-strontium alloys¹⁰⁾

A V Volkovich, A V Krivopushkin and I F Nishkov (Novomoskovsk Branch, Moscow Chemical Technology Institute - Department of Electrochemistry)

In the literature¹⁾ the solubility of strontium in liquid zinc was given, and the existence of an intermetallic compound with the composition $SrZn_{13}$ in the Zn-Sr system was indicated. There are no published data on the thermodynamic characteristics and phase diagram.

The present work sets out the results from an investigation into the thermodynamic characteristics of liquid solutions in the Zn-Sr system by the emf method in the range

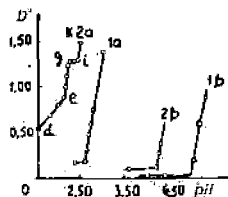


Fig. 3

The variation of optical density D' of zinc sulphate solution as a function of pH when precipitating a) Fe(III) at 35°C and b) Cu(II) at 20°C. Elementary concentration $C_0 Me^{n+} = 0.5$ (1), 25.0 (2).

basis of a single method, make it possible to calculate comparable pH_{in} values for these metals and, thereby, to determine the conditions for possible precipitation of these metals as applied to the hydrometallurgy of zinc.

Conclusions

1. The effect of the precipitation conditions and methods for detection of the beginning of precipitation on the pH_{in} value for Fe(III) and Cu(II) in zinc sulphate solutions was investigated. It was shown that the method and conditions for determination of pH_{in} have a considerable effect on the magnitude of this characteristic during the precipitation of iron and have practically no effect during the precipitation of copper.

2. On the basis of experimental data obtained by a single method equations were derived, determining the pH_{in} values for Fe(III), Cu(II) and Zn in zinc sulphate solutions as a function of the concentration of these metals in the solution and of temperature.

References

- 1) E V Margulis and G I Chufarov: Zh. Fiz. Khim. 1971, 45, (5), 1261.
- 2) E V Margulis and L I Beisekeeva: Zh. Prikl. Khim. 1970, 43, (12), 2746.
- 3) E V Margulis et alia: Izv. VUZ Tsvetnaya Metallurgiya 1977, (5).
- 4) E V Margulis et alia: Zh. Prikl. Khim. 1977, 50, (7), 1457.
- 5) E V Margulis et alia: Zh. Neorgan. Khim. 1965, 10, (8), 1782.
- 6) E V Margulis et alia: Zh. Neorgan. Khim. 1965, 10, 906.
- 7) H T Britton: Hydrogen ions: ONTI-Khimteoret. Leningrad 1936, 285.
- 8) B V Gromov: Zh. Prikl. Khim. 1948, 21, (260).
- 9) I M Korenman: Zh. Obshch. Khim. 1951, 21, (1), 10.
- 10) N V Akselrud and V G Patsenko: Ukr. Khim. Zh. 1951, 17, (6), 845.
- 11) P N Kovalenko: Zh. Prikl. Khim. 1953, 26, (8), 814.
- 12) V L Kheifets and A L Rotinyan: Zh. Obshch. Khim. 1954, 24, (6), 930.
- 13) G N Dobrokhotov: Zh. Prikl. Khim. 1954, 26, (10), 1056.
- 14) E V Margulis et alia: Zh. Prikl. Khim. 1976, 49, (11), 2382.

UDC 541.55:891/541.134

of 948-1048°K with measurement of the concentration of strontium between 0.1 and 4.0at.-%:

It is not possible to measure the emf of the $Sr|SrCl_2-KCl|Zn-Sr$ cell directly, since metallic strontium has high solubility in the molten salt. In addition, an exchange reaction $Sr + 2K^+ \rightleftharpoons Sr^{2+} + 2K$ occurs between the metal and the potassium ions. The potentials of the alloys were therefore measured with reference to a chlorine reference electrode with

tallurgy
g Industry)

The dependence of the rate constant for the dissolution of nickel oxide in sulphuric acid on temperature

°C	γ	α mg/cm ²	K
60	0.101	0.041	20563
70	0.094	0.143	113
80	0.084	0.209	39459
90	0.078	0.526	376

effective-
ion-ferrous
l schemes
amounts
aim of
and incl
SUBJ
MNG
ELC

the values of the activation energy for the dissolution of nickel oxide and the high value of the temperature coefficient show that the kinetics of the dissolution process in sulphuric acid are controlled by the rate of the true chemical reaction at the interface.

The dependence of the dissolution rate of nickel oxide on the sulphuric acid concentration in the solution was studied at 70°C with sulphuric acid concentrations varying between 0.36 and 1.5 mole/l. The results are shown in fig. 2. The variation of the dissolution rate of nickel oxide with the sulphuric acid concentration is curvilinear, and an increase in the dissolution rate is observed with increase in the sulphuric acid concentration in the solution. It is clear that the factor which controls the dissolution of nickel oxide in this case is the rate of the heterogeneous chemical reaction at the interface.

The investigations into the dissolution of nickel oxide in sulphuric acid show that there are considerable kinetic hindrances to this process.

UNIVERSITY OF UTAH
RESEARCH INSTITUTE
EARTH SCIENCE LAB.

200. Non-F
1978 v.6 N6

Effect of lead compounds on the behaviour of indium in zinc sulphate solutions

M V Kravets and E V Margulis (North-Caucasian Mining-Metallurgical Institute - Department of General, Physical and Analytical Chemistry)

The existing technology for the extraction of indium from zinc raw material involves the leaching of Waelz oxides with sulphuric acid solutions. Here up to 30% of the indium contained in the Waelz oxides remains in the leaching residue (the lead cake)¹. It has been noted that during the leaching of indium-containing intermediate products with sulphuric acid increase in the lead content of the materials reduces the extraction of indium in the solution².

investigated cases was capture of the indium by the precipitate observed.

During the leaching of two industrial intermediate products (Waelz oxides and zinc cakes) containing 10.3% Pb and 0.019% In and 3.2% Pb and 0.006% In respectively at 92-95°C with an initial sulphuric acid concentration of 160-180g/l and a solid-liquid ratio of 1:10, the extraction of indium into solution amounted to 90.1 and 88.4%. Consequently, the presence of lead compounds is not the reason for the losses of indium with the lead cakes.

In this connection, in the present work we studied the effect of lead compounds on the behaviour of indium. During a check on the suggestion about adsorption capture of indium by lead compounds the authors started from the fact that under production conditions adsorption occurs on the already formed surfaces of the lead compounds: PbO; 4PbO · PbSO₄; 3PbO · PbSO₄; PbSO₄. The synthesis of the known lead oxosulphates was realised in accordance with published recommendations³. A series of solutions containing 100g/l Zn₂SO₄ and 50g/l of In with pH values of 0.0, 0.3, 0.7, 1.0 and 1.3 were thermostated at 20, 50 and 90°C. On the attainment of the given temperature in the solutions a sample of lead oxosulphate from the above-mentioned series was added in the quantity required for the creation of a solid-liquid ratio of 1:5. After holding at the given temperature for 20 min with vigorous stirring the solutions were filtered, and their indium contents were determined. In none of the in-

References

- 1) K A. Bolshakov (Ed.): Chemistry and technology of rare and trace elements: Vysshaya shkola, Moscow 1976, p. 304.
- 2) A T Drobchecko et alia: Tr. In-ta Unipromed' Sverdlovsk Metallurgizdat 1958, (3), 154.
- 3) V G Khlopin: Selected works: Izd. Akad. Nauk SSSR, Moscow-Leningrad 1957, 1.
- 4) B A Nikitin: Selected works: Izd. Akad. Nauk SSSR, Moscow-Leningrad 1956.
- 5) E V Margulis: Investigation of basic lead sulphates: Izv Akad. Nauk SSSR, Neorganicheskie Materialy 1972, 8, (2), 393.

Refining of aluminium alloys of the Al-Si-Cu system from iron

V M Grigorenko, V A Popov, and A A Ofengenden (All-Union Scientific-Research Institute of Secondary Non-Ferrous Metals Production)

An increased content of deleterious metal impurities and of iron, in particular, is observed in alloys obtained from secondary raw material (GOST 1583-73). A characteristic feature of alloys of the AK5M2 and AK5M7 types of the Al-Si-Cu system without modifying additions is their satisfactory casting characteristics. The phase composition of alloys of the AK5M2 type¹ in the casting state is as follows: Si + Mg₂Si + CuAl₂ + AlSiMnFe + α -solid solution. The W(Al_xMg₅Si₄Cu₄) phase may form on cooling. Alloys of the AK5M7 type are distinguished by their increased copper content.

During the experiments the aim was to determine the effect of the following factors on the degree of purification of the alloys from iron (the final content of iron in the alloy C) and on the yield of the filtrate (ϕ): filtration temperature of the alloy t; the initial iron content of the alloy C₀; the ratio of the amount of manganese to iron ψ ; the height of the filter layer H; the metallostatic pressure over the filter h; the weight of filtered metal m. The experimental procedure and the treatment of results have been described before².

Approximating functions for the final iron content of the alloy C and the yield of usable filtrate ϕ were given in the literature³. A comparison of the data calculated by means of the published formulae³ and the experimental data is given in the table.

The present article gives the results from laboratory investigations into the refining of cast aluminium alloys of the AK5M2 and AK5M7 type from iron by filtration through a volume filter⁴ consisting of a layer of granulated salt NaCl and heat-treated aluminium filings.

UDC 669.714.2

given sample and the smaller the consumption of collector needed for its extraction. Consequently, the same relationship was traced for activated ZnS as for lead, copper, and iron sulphides.

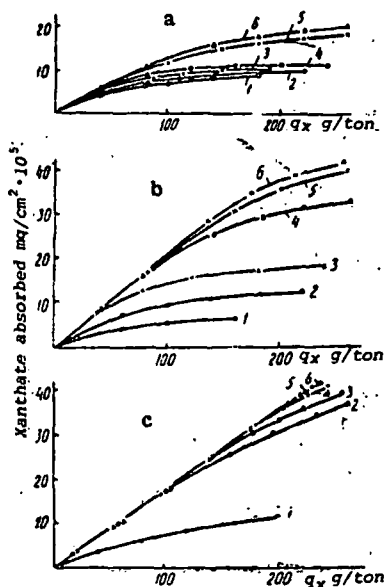


Fig. 1 Curves for the absorption of xanthate by samples of spherulite from the deposits: a) Naugarzanskoe; b) Sikhali (light modification); c) Sikhali (dark modification); activated with copper sulphate at initial concentrations mg-l: 1-0.0; 2-2.5; 3-5.0; 4-10.0; 5-20.0; 6-50.0.

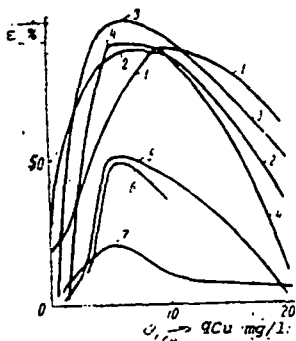


Fig. 2 Effect of the copper sulphate consumption (xanthate consumption 20g/ton) on the flotation extraction of samples of spherulite from the deposits: 1 - Naugarzanskoe; 2 - Sikhali (dark); 3 - Sikhali (light); 4 - Akatuiskoe; 5 - Savin; 6 - Buron; 7 - Sadon.

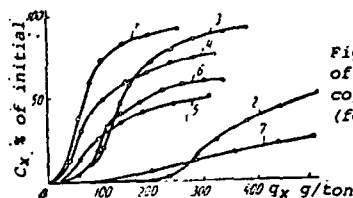


Fig. 3 Curves for the saturation of spherulite, activated by copper sulphate, with xanthate (for legend see fig. 2).

Soo. Nev-Fe
1975 0.3 N5

Electrochemical mechanism of the dissolution of sulphides

A V Baev and A I Orlov (Irkutsk Polytechnical Institute)

In recent years a considerable amount of work has been carried out on the leaching of sulphide materials in aqueous media. It is stressed that the least understood is the first step of oxidation, which is accompanied by rupture of the bonds in the crystal lattice of the sulphide. Here the views of individual authors on the mechanism of the reaction of

Additions of cyanide to copper sulphate⁵⁾ showed a positive effect on the variation in the absorptive capacity of the mineral towards xanthate in minerals for which activation required a considerable consumption of copper sulphate (e.g., for the light modification of spherulite from the Sikhali deposit). By considerably increasing the absorption of copper (fig 4a, b), the cyanide thereby promotes increase in the absorptive capacity towards xanthate for the same copper sulphate consumption rates (fig. 4c, d). An analogous effect is observed for spherulite from the Sadon and Naugarzanskoe deposits.

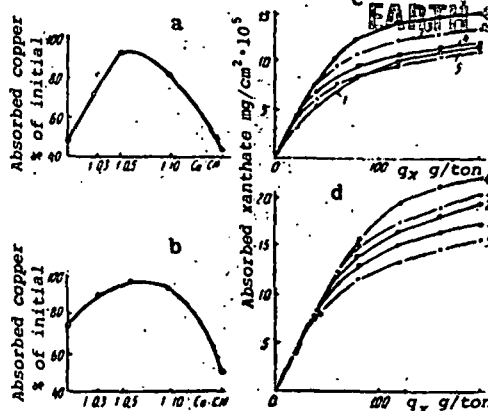


Fig. 4 The effect of cyanide additions to copper sulphate (a, c - 2.5mg/l; b, d - 5.0mg/l) on the variation in the absorptive capacity of the light modification of spherulite from the Sikhali deposit towards copper (a, b) and xanthate (c, d) ions. Molar ratio of copper to cyanide: 1 - 1:0.0; 3 - 1:0.5; 5 - 1:1.5; 2 - 1:0.3; 4 - 1:1.0.

The need for individual selection of the optimum reagent conditions during flotation is determined by the individuality of properties in the samples of spherulite from various deposits.

References

- 1) L V Marasanova et alia: Izv. Vuz. Tsvetnaya Metallurgiya, 1973, (2).
- 2) A M Okolovich et alia: Collection: Problem of the treatment of solid minerals. Moscow, Nauka 1973.
- 3) A M Okolovich et alia: Tsvetnye Metally 1973, (7).
- 4) A A Shvidenko et alia: Collection: Control of the ionic composition of the ore pulp during flotation. Nauka 1974.
- 5) I N Plaksin et alia: Activating action of cyanide in the flotation of sulphide polymetallic ores of Central Asia, Dushanbe, Izd. DONISH, 1970.

UDC 669:541.138

3) Adsorption reaction of oxidation of the solution
3) Reaction of sulphide, tal sulphide
4) Electro
For the the dissol
the tempo
sulphide i
the initial
typical of
the mechanis
In the s
by mecha
passage o
the oxidiz
reaction
majority
must cle
2.5 · 10⁻⁸
more qui
practice
These
tively ea
dissolut
The m
of disso
the soli
surface
heterog
minera
are rea
cells. I
of the f
absenc
differe
to 50-
ence i
proces
rate of
From
the di
oxidis
be rep
occur
MeS
2Fe
MeS
In t
of ox
latte
oxyg
The
tion
of a
(O₂)
at c
puri
Su
ano
inv
det
cas
pol
ele
pol

UNIVERSITY OF TASHKENT
RESEARCH INSTITUTE
EARTH SCIENCES LAB

SUBJ
MNG
EMD

- 2) Adsorption of the oxidising agent on the sulphide, chemical reaction of the sulphide with the oxidising agent, subsequent oxidation with participation of water molecules, and passage of the soluble products into solution³⁾;
- 3) Reaction of the sulphide and acid to form hydrogen sulphide, which is oxidised by the oxidising agent to elemental sulphur⁴⁾;
- 4) Electrochemical mechanism of oxidation of sulphides^{5,6)}.

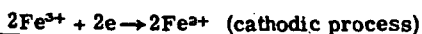
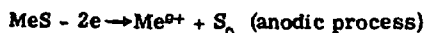
For the case of copper sulphides it can be supposed that the dissolution of minerals by mechanism 3 is unlikely at low temperatures, since no significant release of hydrogen sulphide is observed in the absence of the oxidising agent. The initial stage of adsorption of the oxidising agent is typical of mechanisms 2 and 4 and is not essential for mechanism 1.

In the simplest case the rate of dissolution of the sulphide by mechanism 1 is determined by the slowest stage, i.e., passage of the solid substance into solution, diffusion of the oxidising agent and reaction products, and the chemical reaction itself in solution. The solubility product of the majority of sulphides is very low, and the dissolution rate must clearly be determined by this quantity. Since $SP_{Cu_2S} = 2.5 \cdot 10^{-20}$ and $SP_{CuS} = 4.10^{-26,20}$, coveline should dissolve more quickly than chalcosine, but this is not observed in practice.

These and other contradictions can be explained comparatively easily from the standpoint of the electrochemical dissolution of sulphides.

The main requisite for the electrochemical mechanism of dissolution is an oxidation-reduction type of reaction at the solid-liquid boundary. Under leaching conditions the surface of the reacting particles can have clearly defined heterogeneity, since the various faces of one and the same mineral have different potentials. In this case conditions are realised for the functioning of macro and microgalvanic cells. Of course, the dissolution rates of minerals on account of the functioning of local galvanic pairs are low in the absence of depolarisers, since in the best case the potential difference of copper minerals in the steady state amounts to 50 - 70 mV. With the use of an oxidising agent the difference in the equilibrium potentials of the anodic and cathodic processes can amount to 300 - 500 mV, and the dissolution rate of the mineral increases considerably.

From the standpoint of the electrochemical mechanism the dissolution reaction of sulphides in solutions of an oxidising agent (e.g., in solutions of trivalent iron) can be represented as the sum of two independent processes occurring in conjunction:



In the anodic process there can be an increase in the degree of oxidation of the metal and sulphide sulphur, where the latter can be oxidised either to elemental sulphur or to oxygen compounds, depending on the process conditions. The cathodic reaction can take place not only with participation of cations (Fe^{3+} , Cu^{2+} , Ce^{4+}) but also with participation of anions (MnO_4^- , $Cr_2O_7^{2-}$, $S_2O_8^{2-}$) and neutral molecules (O_2 , Cl_2). The reduction of the oxidising agent takes place at cathodic sections, which can be both more positive impurities and the investigated mineral itself.

Such an approach makes it possible to investigate the anodic and cathodic processes separately by electrochemical investigations. Here the retardation of the process will be determined by the total resistance, which can in the general case be represented as the sum of the anodic and cathodic polarisabilities and the resistance of the mineral and the electrolyte, including the resistance of the contacts. The polarisabilities of the anodic and cathodic processes are

the most significant factors determining the kinetics of the dissolution of the sulphide.

During examination of the combined polarisation curves of the anodic and cathodic process (fig.1) it is possible to note the following means for increasing the dissolution rate of sulphides: 1) the use of a solvent with a possibly higher oxidation-reduction potential (φ_0^0); 2) the use of complexing agents in order to reduce the anodic potential of the sulphide (φ_A^0); 3) reduction in the polarisability of the anode; 4) reduction in the polarisability of the cathode; 5) reduction in the resistance of the cell.

In spite of the fact that a comparatively large series of oxidation-reduction systems have a high oxidation-reduction potential ($> 1.0 V$), only the salts of trivalent iron, divalent copper, and oxygen can be used for leaching owing to the short supply of many reagents and the economic expediency of their utilisation. Chlorine, chlorates, and ozone can be of specific interest in hydrometallurgy. However, the approach to strong oxidising agents must be cautious, since oxidation of the sulphide sulphur not to elemental sulphur but to a higher degree of oxidation is possible.

It should be noted that the use of ferric chloride will be preferably to the sulphate. Ammonium salts can be used in the leaching of copper minerals.

Means for reducing the polarisability of the anode and cathode depend on the form of polarisation. With chemical polarisation, i.e., retardation of the electrode process on account of the difficulty in the occurrence of the reaction itself, it is expedient to raise the temperature. In the case of concentration polarisation agitation plays a more important role. However, diffusion limitations cannot always be removed by intensification of the agitation. In fact, if the mineral dissolves in stages, the secondary sulphides which form cover the reacting surface with a fairly compact film, through which the oxidising agent and the soluble reaction products have to diffuse. In this case it is necessary to remove the films of secondary products in order to intensify the process. Determination of the form of polarisation is of great importance for solution of purely practical problems, since it makes it possible to determine in which region (kinetic or diffusion) the reaction occurs.

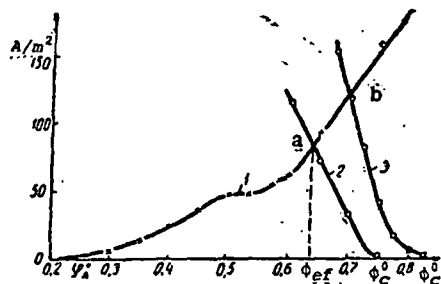
There are various methods for investigating electrochemical reactions. In our investigations we mainly used two methods, i.e., measurement of the electrode potential of the sulphides in various media and recording the polarisation potentiostatic curves. The method for the preparation of the samples and the realisation of the experiments was described in⁶⁾.

Analysis of the polarisation curves for chalcosine in sulphuric and hydrochloric acids shows that this mineral dissolves in stages, forming the secondary sulphide CuS . The polarisability of cupric sulphide is considerably greater than that of cuprous sulphide, since monovalent copper is oxidised in the first stage of dissolution, and the sulphide sulphur only begins to be oxidised in the second stage. The oxidation rate of the secondary sulphide is considerably lower than that of chalcosine but higher than the dissolution rate of the mineral coveline.

According to the electrochemical mechanism, increase in the concentration of the oxidising agent leads to an increase in the equilibrium potential of the cathodic process. During the functioning of the galvanic cell the potential difference of the anode and cathode increases, and the cathodic polarisability decreases. This gives rise to additional polarisation of the anodic sections, and, accordingly, increases the dissolution rate of the mineral (fig.1, point b).

To increase the dissolution rate of the sulphide it is necessary to raise its potential, i.e., by using an oxidising agent with a higher oxidation-reduction potential. Measurements of the potential of the mineral in various oxidising

agents show that in some of them the potential is close to the oxidation-reduction potential of the solution, while in others it differs considerably. This effect can be explained only from electrochemical standpoints. In the equilibrium state the anodic and cathodic currents are equal to each other and are called the exchange current, which is determined by the nature of the electrode and the reagent and depends on the concentration and temperature of the solution. For various oxidation-reduction systems the exchange current can vary within very wide limits ($1 \cdot 10^{-11}$ A/cm²).



Polarisation curves for anodic oxidation of bornite (1) in HCl and for the cathodic reduction of Fe³⁺ with concentrations of 10 and 150g/l (2 and 3).

During polarisation of the electrode the equality of the currents of the anodic and cathodic processes is destroyed, and the electrode potential is shifted to one or the other side from the equilibrium state, depending on the sign of polarisation. During the functioning of the galvanic cell, as a result of polarisation of the electrodes, the preferred process will be oxidation of the sulphide at the anode and reduction of the oxidising agent at the cathode.

If the areas of the anodic and cathodic sections are approximately the same, at the cell current the polarisation of the electrode at which the occurring reaction has the lowest exchange current will be greater. Consequently, a sulphide in a solution of oxidising agent will have a potential which is closer to the oxidation-reduction potential of the solution, the lower the dissolution current of the sulphide at a potential close to the oxidation-reduction potential compared with the exchange current of the oxidising agent. From this potential difference it is possible to assess the polarisability of the sulphide and the relative ease of occurrence of the process. For example, in solutions of trivalent iron chalcopyrite has a potential of this solution.

The exchange current of the $0.1 \text{ N Fe}_2(\text{SO}_4)_3 + 0.1 \text{ N FeSO}_4$ system is $1 \cdot 10^{-6}$ A/cm², and according to the polarisation curves the dissolution current of chalcopyrite at the respective potential amounted to $5.3 \cdot 10^{-6}$ A/cm². As a result the potential of chalcopyrite in solutions of Fe³⁺ differs from the oxidation-reduction potential by 5-10 mV. In potassium permanganate solutions the same mineral has a potential 0.5 V lower and in potassium bichromate solution 0.27 V lower than the oxidation-reduction potential, and the exchange current of these systems is considerably lower than the dissolution current of chalcopyrite at potentials close to the oxidation-reduction potential of the oxidising agent. Thus, the dissolution rate of the sulphides is determined not only by the oxidation-reduction potential of the oxidising agent but also by the exchange current of

the respective oxidation systems.

No less interesting is the question of determining the activation energy of the dissolution processes in the sulphides from electrochemical standpoints. During investigations the calculation of activation energy is usually associated with the specific conditions, and its variation is not subsequently taken into account. During a periodic process the activation energy will clearly be different at the beginning and at the end of the process. Since in such processes the concentrations of the oxidised and reduced forms of the oxidising agent vary and the oxidation-reduction potential of the solution decreases, the polarisation of the electrodes also varies; in accordance with this the activation energy varies. It was established⁹⁾ that the activation energy of the anodic oxidation of bornite varies from 5.2 to 9 kcal/mole and that of chalcopyrite from 4.3 to 6.2 kcal/mole as a function of the polarisation of the sulphide electrode from 0.5 to 0.1 V. The activation energy of the reduction process lies within the limits of 2.8 - 3.7 kcal/mole in unagitated solutions and 3.5 - 4.5 kcal/mole with an electrode rotation rate of 300 rpm and identical overpotentials.

By means of the electrochemical method of investigation it is considerably simpler to establish the stage character of the dissolution process, since it is possible to select mineral dissolution potentials where secondary sulphides will not dissolve completely or their oxidation rate will be low. As a result of this it is possible for a quantity of the secondary products required for mineralogical, X-ray, and other analyses to accumulate. We confirmed the stage character of the dissolution of chalcopyrite, where coveline and cubanite were detected as intermediate products.

The electrochemical mechanism of the dissolution of the sulphides requires further investigation of the electrochemical characteristics of both the oxidising agents and the sulphide minerals. On the basis of the investigation of these properties it is possible to predict the behaviour of the mineral in one or the other oxidising agent and also to select the form of oxidising agent, its concentration, the temperature, and where necessary also the respective conditions for realisation of the process. The determination of the electrochemical and electrophysical characteristics of minerals and oxidising agents will undoubtedly assist the development of hydrometallurgical processes in the treatment of sulphide ores and concentrates.

References

- 1) G. N. Dobrokhotov: Zh. Prikl. Khim., 1959, 32, 11.
- 2) A. L. Tseft and A. P. Serikov: Tr. IPI, Vysh. 18, Irkutsk 1963.
- 3) I. N. Plaksin: Izv. Akad. Nauk SSSR, Seriya Tekhnicheskaya 1950, 12.
- 4) V. D. Ponomarev et alia: Collection: Alkaline hydrochemical methods for the treatment of polymetallic products. Nauka, Alma-Ata 1969.
- 5) A. V. Baev: Tr. IPI, Vysh. 67, Irkutsk 1971.
- 6) A. V. Baev et alia: Tr. IPI, Vysh. 67, Irkutsk 1971.
- 7) A. V. Baev et alia: Tr. IPI, Vysh. 67, Irkutsk 1971.
- 8) N. Ya. Eune and Ya. M. Kolotyrykhin: Zh. Fiz. Khim., 1961, 35, 7.
- 9) A. V. Baev: Author's abstract of thesis, Irkutsk 1973.
- 10) Concise Manual of Physicochemical Values, Vol. 5, Leningrad, Khimiya 1967.

EXTRACTION OF MOLYBDENUM FROM COAL TREATMENT WASTE

UDC 669.283:622.613

A. N. Zelikman, N. N. Rakova, L. A. Zekel',
N. V. Krasnobaeva, and M. Ya. Shpirt

The recovery of rare metals from secondary raw materials is becoming a matter of increasing importance.

Iron-molybdenum catalysts, a mixture of ammonium paramolybdate and iron sulfate, are used in the process of hydrogenation of brown coals mixed with high-sulfur petroleum products to obtain valuable chemical products and low-sulfur boiler fuel [1]. The catalyst composition includes 0.2-0.3% Mo relative to the initial coal mass [2]. The scales of coal treatment by the hydrogenation method planned for the long term will require substantial amounts of molybdenum.

It is essential to extract the molybdenum from the coal hydrogenation process waste, in view of the relatively high cost and scarcity of molybdenum compounds. During coal treatment the molybdenum present in the catalyst passes almost entirely into the slime (> 1% Mo) remaining after hydrogenation (see Fig.). To extract the molybdenum, the slime is ignited in a cyclone chamber with removal of molten slag at 1500-1700°C. The molybdenum compounds which distil off are trapped in a bag filter; 95% of the Mo present in the slag passes into the trapped volatile product, and 5% remains in the slag [2].

The chemical composition of the volatile ash product (in %) is as follows: 11-19 SiO₂, 3-5 Al₂O₃, 10-13 Fe₂O₃, 23-36 CaO, 9-15 MoO₃, 29-31 other.

The rational composition of the volatile ash product was studied in order to choose the optimum method for molybdenum extraction.

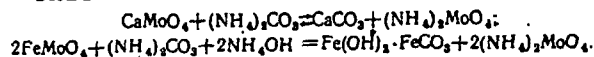
Investigations using a method based upon differences in the solubility of molybdenum compounds (MoO₃, MoO₂, MoS₂, CaMoO₄, etc.) have established that molybdenum is present in the volatile ash products as the trioxide (60-70%), calcium and iron molybdates (15-20%), and the dioxide (5-10%).

Ammonia leaching, which is widely used in processing molybdenum calcines, can be employed for products of this type [3].

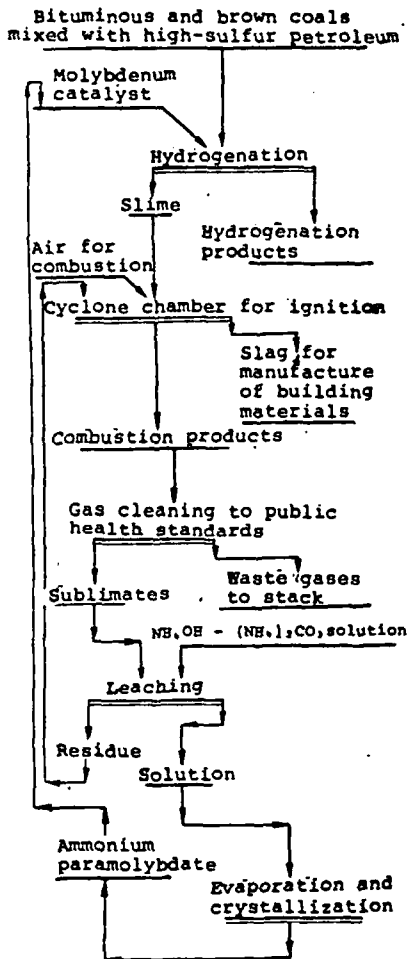
A series of experiments in which the temperature, reagent consumption, and leaching time were varied was mounted to find the optimum routine for leaching molybdenum from the volatile ash products.

Molybdenum was measured in the solution and the residue by a method employing the reagent "Rezarson" [4]. According to the experimental data (see Table) the ammonia solutions extract ~ 60% of the Mo present in the ash product as a result of dissolution of MoO₃ in ammonia.

Since the molybdenum in the calcium and iron molybdates is not extracted to any significant extent by ammonia solutions, additions of ammonium carbonate were made. This reacts as follows:



Under optimum conditions (t = 40°C, leaching time 1



Process scheme for recovery of molybdenum from volatile products.

Effect of Various Factors Upon Molybdenum Leaching*

Serial no.	t, min	t, °C	Mo, %	Serial no.	t, min	t, °C	Mo, %
1	30	20	58.5	5	180	40	60.70
2	30	40	59.1	6	30	40	92.4
3	30	40	50.6	7	60	40	95.0
4	45	40	59.93	8	160	40	94.8

*Batch 15 g; solid-to-liquid ratio 1:4; volatile ash contains 6.07% Mo; solutions No. 1-5 contained 10% (by mass) NH₃; No. 6-7 contained 8% NH₃ and 5% (NH₄)₂CO₃.

hr, solid-to-liquid ratio 1 : 4) solutions of 8% ammonia with the addition of 5% (by mass) $(\text{NH}_4)_2\text{CO}_3$ extracted > 95% of the molybdenum from the volatile ash product.

The ammonium molybdate solutions produced by leaching were evaporated, with subsequent crystallization of ammonium paramolybdate; the crystals were used for catalyst preparation. The residue from leaching the volatile ash product is returned to the process. The process scheme for recovery of molybdenum from volatile ash products is shown in the Figure.

This scheme provides for a closed process without discharges, which will make it possible to save expensive and scarce molybdenum.

REFERENCES

1. A. A. Krichko, Fuel Chemistry and Processing, Moscow, IGI (Fossil Fuel Institute), 1972 (Proceedings, Vol. 28, No. 1), pp. 57-66.
2. Yu. K. Pisarev, V. M. Ivanov, L. S. Grishina, et al., Theory and Technology of Reductive Breakdown of Fuel, Moscow, IGI, 1974 (Proceedings, Vol. 29, No. 2), pp. 62-67.
3. A. N. Zelikman, Molybdenum, Moscow, Metallurgiya, 1970, 440 pages, illustrated.
4. I. V. Avgushevich, A. M. Lukin, N. A. Kaslina, et al., Khimiya Tverdogo Topliva, 1975, No. 3, 87-90.

EXTRACTING MOLYBDENUM AND IRON FROM NITRATE AND SULFATE SOLUTIONS

UDC 659.28

A. N. Zelikman, G. M. Vol'dman, and V. N. Bulgakov

Polyalkylphosphonitryl acid (PAPNA) is a new type of phosphorus- and nitrogen-containing polymer cation-exchanger (1), obtained during the alkylation of the phosphonitryl-chloride $(\text{PNCl}_2)_n$ with alcohol (2).

A series of works have already described the use of PAPNA for the extraction of non-ferrous metal ions (1, 3), the separation of heavy metals by extraction with PAPNA from ammonia-carbonate solutions (2), and the extraction of molybdenum from solutions of mineral acids with low concentration (4).

This paper gives the results of laboratory research into the extraction of molybdenum and iron with PAPNA solutions in kerosene from synthetic solutions with high and moderate concentrations of mineral acids (sulfuric and nitric) and industrial mother liquors following the nitric acid decomposition of the molybdenum concentrates.

Extraction was conducted in separatory funnels at an o:a phase ratio of 1:1. It was established by preliminary tests that equilibrium is established in the extraction system after 3-5 minutes for molybdenum and 7-9 minutes for iron. The contacting time in the tests on extracting iron and molybdenum from synthetic solutions was 15 minutes.

It was established that there is a change in the nature of the relationships for the distribution coefficients D of molybdenum and iron where there is a shift from nitric to sulfuric acid and it is practically equal for both metals (Fig. 1). In sulfate solutions, the D_{Mo} is reduced monotonously with increases in the acid concentration due to suppression of PAPNA dissociation. Prior to concentration in solutions of 2 g-equiv/lit HNO_3 , the distribution coefficients are low; however, with a further increase in acidity it increases sharply. This attests to the changes in the extraction mechanism, in all probability, with a shift from cation exchange to a solvate or a mixed mechanism. Given an identical character for the curves, the value of D_{Mo} will be much higher than for D_{Fe} in the entire range of concentrations for both acids -- which makes it possible to separate molybdenum and iron.

For the extraction, use was made of a 10% (volum.) or a 0.24-N. solution of PAPNA in kerosene.

As is evident from Fig. 2, successful separation of molybdenum and iron is possible within the entire range of acidities studied; however, a concentration of 2-5 g-equiv/lit HNO_3 (H_2SO_4) is optimum. The maximum difference in the extractability of the metals ($\beta = 1230$) is noted in solutions with 2.5 g-equiv/lit HNO_3 .

When decomposing molybdenite concentrates with nitric acid, the mother liquors contain about 3 g-equiv/lit ($\text{HNO}_3 + \text{H}_2\text{SO}_4$), which corresponds to optimum conditions for the separation of molybdenum and iron. The possibility was checked of extracting molybdenum with PAPNA directly from the mother liquor obtained after nitrate decomposition of Almalyk semimanufactures, containing (in g/l): 9.7 Mo, 8.64 Fe, 0.0077 W, and an acidity of 196.5 (in conversion to HNO_3). Extraction was conducted with a 15% (volum) solution of PAPNA in kerosene, at an o:a ratio of 2:1 and an extraction period of 7 minutes. The raffinates contained 0.2 g/l Mo and 5.4 g/l Fe. 98% Mo and 37% Fe per contact were extracted to the organic phase. When conducting extraction in a countercurrent cascade, the best extractable element - molybdenum - should be recovered to a greater degree, while the least extractable element - iron - should be recovered to a lesser degree. Thus, even from these complex industrial solutions, containing to 10 g/l Fe, it would be possible to almost completely recover molybdenum by extraction with

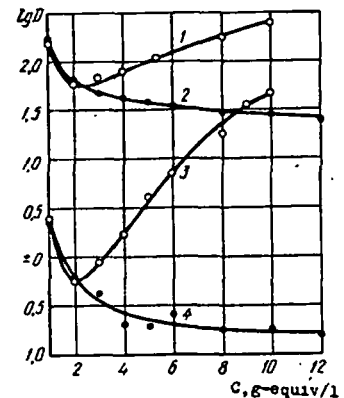


Fig. 1. Relationship of Mo and Fe distribution coefficients ($C_{\text{init}} = 1 \text{ g/l}$), when present separately, to the concentration of HNO_3 and H_2SO_4 :
1, 2 - Mo ($C_{\text{PAPNA}} = 0.15 \text{ g-equiv/l}$); 3, 4 - Fe ($C_{\text{PAPNA}} = 0.24 \text{ g-equiv/l}$).

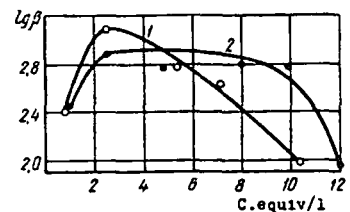


Fig. 2. Relationship of Mo and Fe separation coefficient ($C_{\text{init}} = 1 \text{ g/l}$), when both are present, to the concentration of nitric 1 and sulfuric 2 acids.

PAPNA.

When re-extraction is performed with an ammonia solution, with the addition of ammonium nitrate for a better separation of the phases (10% NH_3 +2.5% NH_4NO_3), the molybdenum is more completely extracted from the organic phase after two contacts, while the iron remains in the organic phase, forming a fine-dispersed suspension or a colloidal solution, which is confirmed by the brown color of the organic phase (characteristic of the colloidal solutions of tetravalent iron hydroxide). The ammonia re-extracts contain 10-20 g/l mg/l Fe and 10-50 g/l Mo, depending on the ratio of the phase volumes during re-extraction.

In connection with the fact that iron is not extractable with ammonia solutions, it is possible to obtain molybdenum re-extracts which are pure with respect to iron; however, when using a closed cycle of extraction-reextraction, iron can accumulate in the organic phase and reduce the D_{Mo} . It is clear from Fig. 3 [$C_{\text{init}}(\text{Mo, Fe}) = 5 \text{ g/l}$ $C(\text{H}_2\text{SO}_4) = 100 \text{ g/l}$] that iron, accumulating in an extractant, will intensively worsen the extraction of molybdenum. In this connection, following the re-extraction of molybdenum, it is necessary to re-extract iron in order to regenerate the extractant.

Our research has shown that iron is not extracted from the organic phase with solutions of nitric and sulfuric acids within a concentration of 2-6 g-equiv/lit: the iron content in the first washing solution does not exceed 0.2 g/l and is reduced with each succeeding washing. The complete separation of iron from the organic phase is achieved when the extractant is treated with a soda solution and an addition of NaOH. The formed iron hydroxide is separated together with the soda solution, while the extractant can be returned to the process.

References

1. A. N. Asabin, O. P. Avraamova, V. S. Strizhko, and M. D. Ivanovskii, Izv. Vuz, Tsvetnaya Metallurgiya, 1973, No. 2, pp. 25-27.
2. B. N. Laskorin, V. A. Kuznetsov, E. A. Filippov, and D. I. Skorovarov, USSR Patent No. 181812, Izobr. Promyshl. Obraztsy i Tov. Znaki, 1966, No. 10, p. 80.
3. B. N. Laskorin, D. I. Skorovarov, E. A. Filippov, and A. V. Lomonosov, USSR Patent No. 211786, Otkr. Izobr. Promyshl. Obraztsy i Tov. Znaki, 1969, No. 8, p. 180.
4. L. S. Chernikova and S. V. Khryashchev, Scientific Proceedings (Sibtsvetmetnii-proekt), No. V., Krasnoyarsk, 1972, pp. 155-159.

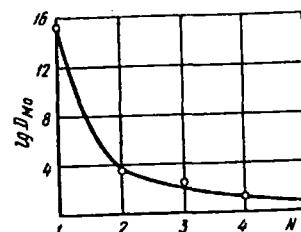


Fig. 3. Relationship of distribution coefficient for Mo ($C_{\text{init}} = 5 \text{ g/l}$) to the number of extraction-reextraction cycles.

The Effects and Mechanisms of Oxidation Reactions at Solid Surfaces During Leaching

A. R. BURKIN

Department of Metallurgy,
Imperial College of Science & Technology,
London S.W.7. England

The reactions used in leaching minerals and other solids are, in many cases, similar to those which occur during the natural weathering and alteration of minerals. When an insoluble product is formed, the situation closely resembles that existing when metals corrode. The thermodynamic aspects of leaching can, therefore, be conveniently considered in terms of Pourbaix diagrams, which give the regions of stability of solid and solute species in a particular environment as the pH and oxidation potential are changed. However, the reaction rates are controlled by many factors, particularly when some material is insoluble, so that as in the case of metal corrosion, the kinetics rather than the thermodynamics of the system may be of overriding importance.

Two kinds of behaviour are considered in this paper. 1. Unexpected compounds are formed as a result of a side-reaction due to the leaching conditions. This is exemplified by the much greater stability of potassium niobate solutions formed by leaching columbite compared with solutions formed by leaching niobium pentoxide. 2. Metastable iron oxides form which control the kinetics of the leaching process. Three kinds of reaction have been found: a. The rate of removal of chromium from chromite is controlled by the rate of diffusion of chromium ions through the lattice, which does not break down readily. b. The reaction of wolframite with dilute alkali is stopped when too great an oxygen pressure is used, due to the formation of magnetite; a passivation effect. c. The reaction of pyrite with dilute alkali is hindered by the formation of metastable iron oxides under certain

conditions. The effects of temperature and of the degree of perfection of the pyrite crystals on the formation of this metastable compound are mentioned.

STABILISATION OF SOLUTIONS

Columbite is decomposed by potassium hydroxide solutions to give a solution from which $K_8Nb_6O_{19} \cdot xH_2O$ may be crystallised (1). The value of x is variable but equals 15 immediately after the solid is separated from the mother liquor. The alkali concentration necessary is about 2 to 5N and the temperature 200–300°C, depending on this concentration. If leaching is carried out in nitrogen, oxygen having been completely displaced from the autoclave and solution, no columbite is decomposed. Thus removal of niobium from the solid requires that some iron is oxidised. Oxidising agents other than oxygen may be used; for example if no oxygen gas is present, nitrate ion is reduced to ammonia. This shows the very strong reducing power of ferrous ions in such alkaline solutions. In the presence of some oxygen, however, the conditions are strongly oxidising and commonly used organic reagents, added in an attempt to dissolve the iron or stabilise the niobium in solution, are oxidised to oxalate and very probably, but more slowly, to carbonate.

As a result of a study of the kinetics of dissolution of chromium sesquioxide, Cr_2O_3 , in alkali solutions in the presence of oxygen, it has been suggested² that oxidation of lattice ions at the solid-liquid interface occurs with formation of peroxide ions either directly or by combination of hydroxyl radicals. Peroxides have often been found in solutions in which an oxidising leaching reaction was carried out, and were present in the solutions obtained by leaching columbite. The evidence for this was that permanganate solutions were reduced and potassium iodide solutions oxidised by the leach liquor at the appropriate pH. In most cases approximately the same amount of each reagent was decomposed, but some leach liquors gave no detectable reaction and a few were strongly oxidising toward the iodide, apparently because of manganese in the solution. The rapid decomposition of organic reagents in the autoclave may be explained in terms of acceleration in the presence of the reacting mineral surface. Potassium niobate solutions hydrolyse slowly, precipitating niobium pentoxide or an insoluble metaniobate, depending on the conditions, the rate of decomposition being greater the higher the temperature.

10 g of niobium pentoxide were dissolved completely in 1 litre of 3.5*N* potassium hydroxide solution after 4 hours at 220°C, but if the temperature was then raised to 300°C for 2 hours all of the niobium reprecipitated. No niobium pentoxide dissolved in 3.5*N* potassium hydroxide at 300°C. Addition of hydrogen peroxide to the solutions did not affect these results. However, 50 g of columbite in 1 litre of 3.5*N* potassium hydroxide gave 23 g of niobium pentoxide in solution after 4 hours at 220°C using 400 p.s.i.g. of air (at 20°C). When the experiment was repeated and the temperature then raised to 300°C for 2 hours, 24 g of niobium pentoxide remained in solution. If the same run was carried out at 300°C throughout, 26.5 g of niobium pentoxide was in solution after 6 hours. Thus although the same niobate crystallised at room temperature from the solutions prepared from niobium pentoxide and from columbite, the solution from columbite was more stable at 300°C immediately after formation.

These observations can be explained in terms of the reaction mechanism for the decomposition of columbite. Oxidation of iron occurs at the solid surface and peroxide ions are produced in consequence, at the solid-liquid interface and so very close to niobium ions which are in suitable positions for escape from the solid. This leads to the incorporation of peroxide groups in the niobate ion, which is then stabilised against hydrolysis and precipitation, the peroxide groups at the same time being stabilised against decomposition. After cooling and filtering the suspension the concentration of peroxide found was always much lower than that of niobium in solution, often by a factor of fifty.

It has not proved possible to determine the oxidation potential in an autoclave at high temperature, but an upper limit under oxidising conditions can be set by the observation that no purple ferrate has been observed under any leaching conditions employed.

METASTABLE IRON OXIDE FORMATION. DIFFUSION OF CHROMIUM IN CHROMITE

Chromite reacts with 5*N* or stronger sodium hydroxide solutions in the presence of oxygen to give soluble alkali chromate. A temperature above 230°C is necessary and the reaction is slow. The chromium content is dissolved much more quickly, at a lower temperature, after reduction of the chromite to ferrochrome. Dissolution of Cr_2O_3 is even more rapid, particularly if the solid has not been heated. Thus

the low rate of chromium removal from chromite must be due to the structure of the solid.²

When fairly large particles of chromite (>200 μ diameter) were leached, and less than about 10% of the chromium present was in solution, the particles remained moderately highly reflecting and no ferric oxide was seen on the surface or in solution. When much smaller particles of chromite were treated, and 50% or more of the chromium was in solution, ferric oxide was produced. In order to oxidise the chromium to chromate, a fairly high oxidation potential is necessary and it seems unlikely that any compound of iron (II) could be stable under the leaching conditions. The slow rate of oxidation must, therefore be due to a rate controlling process with a high activation energy.

A well-formed octahedral single-crystal of chromite (from Sierra Leone) was cut across the central, square plane, giving two square pyramids. One was leached in 7.5*N* sodium hydroxide with 500 p.s.i.g. air pressure (at 20°C) at 260°C for three hours. After washing, it was mounted beside the unleached pyramid, square faces uppermost, and these faces were polished, finishing with 0.5 μ diamond. The leached

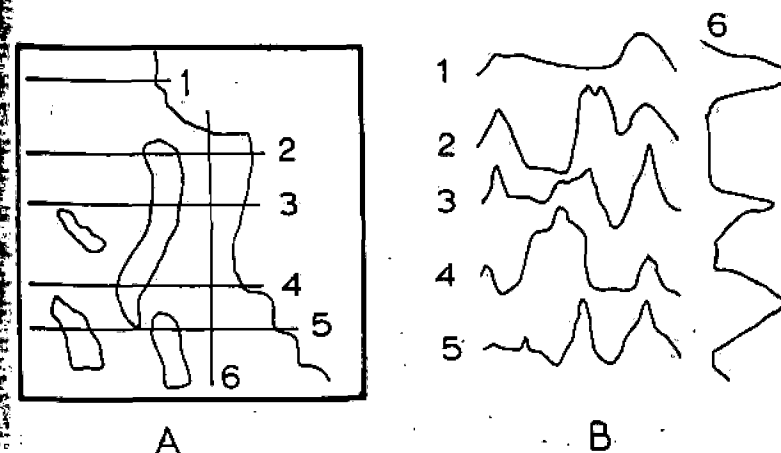


Fig. 1. Electron probe microanalyser view of chromite crystal surface after polishing. A shows areas of high reflectivity outlined and lines of scan numbered. The edge of the crystal is the approximately vertical line to the right. Drawn from a photograph, magnification $\times 1700$ as submitted. B shows iron content variation along the lines scanned, arbitrary ordinate. Areas of high reflectivity have higher iron content than other areas. High iron content at the crystal edge is caused by leaching.

specimen appeared tarnished, and microscopic examination showed a thin, adherent film of a black solid around the edge of the polished face. No such film was visible on the unleached sample. Using the Cambridge electron probe micro-analyser, the latter was found to have a very thin layer of an iron rich phase around the outside, almost certainly magnetite formed by weathering. Both halves had a very uneven distribution of iron and chromium over the polished surface as shown in Fig. 1. The edge of the leached specimen showed a

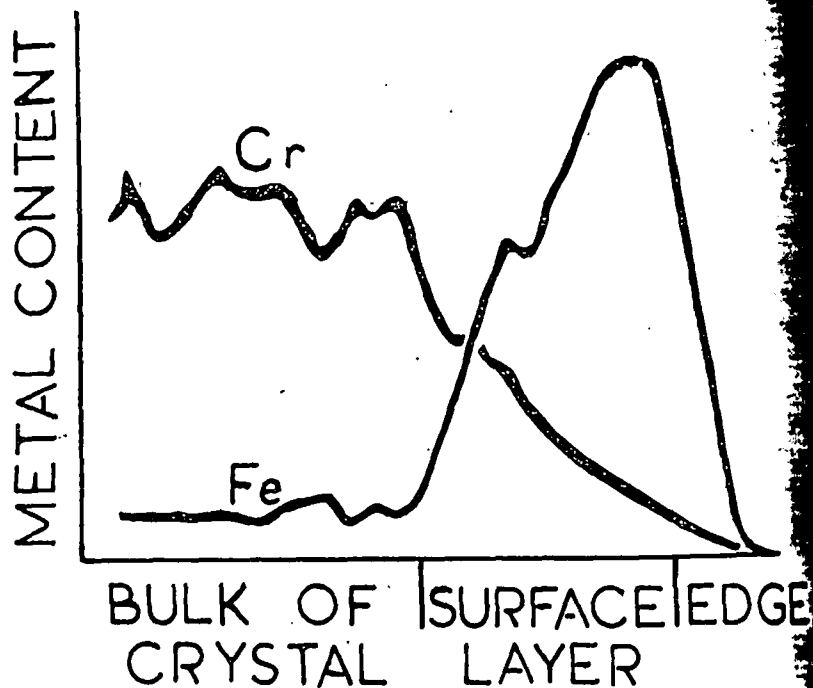


Fig. 2. Iron and chromium content at edge of leached chromite crystal. Arbitrary metal content scale. Thickness of surface layer, about 24 microns.

systematic variation of iron and chromium content, illustrated in Fig. 2, drawn from an enlargement of a photograph of the trace on a cathode ray tube. The thickness of the lines indicates the statistical variation in counting rate over a number of scans.

The chromium content of the outside layer of the crystal decreased sharply at the edge of the unaltered chromite and then more slowly, becoming effectively zero at the solid-liquid boundary. As the chromium content fell, the iron content rose, reaching a maximum at the

edge of the solid. There was no gap apparent between the chromite and the outer solid layer. These facts can be interpreted as follows. The inverse spinel lattice of chromite comprises a close packed oxygen structure with iron and chromium in some of the holes. Removal of chromium from the solid leads to a deficiency of positive charge which is compensated by oxidation of some of the iron to the ferric state. This leaves a chromium activity gradient down which the metal diffuses to the solid-liquid boundary from which it can be removed into the alkali solution. The iron also diffuses so as to maintain what may be regarded as a magnetite structure containing chromium. The rate of leaching of chromite is, therefore, controlled by the rates of diffusion in the spinel structure.

It is known that the rate of oxidation of magnetite under leaching conditions is slow, so the formation of ferric oxides does not occur until a thick layer of the alteration product has built up around the chromite particles and reaction has continued for a long time. That is, until a fairly large proportion of the chromium is in solution.

INSOLUBLE LAYER FORMATION WITH COLUMBITE

The reaction between columbite and potassium hydroxide solution slows down more rapidly as reaction proceeds than would be predicted from changes in surface area and reagent concentrations.¹ Under some conditions the reaction may stop completely after a time and the niobium content of the solution then falls as precipitation occurs. Typical curves are shown in Fig. 3. The rates fit the Arrhenius equation when the initial reaction is considered, and also when a given proportion of the columbite has been decomposed. Values of the activation energy, or critical increment, differ somewhat between different samples of columbite, but typical values are, for the initial reaction, $E_A = 14 \text{ kcal mole}^{-1}$, and, when the reaction is slowing down considerably, 4 kcal mole^{-1} between 200 and 220°C in 3.5*N* potassium hydroxide solution.

It can be concluded that the initial reaction rate is controlled by a chemical process, but after an appreciable proportion of the columbite has been decomposed, a diffusion process becomes rate controlling. When a sample of columbite which had been leached until reaction ceased, was washed with mineral acid and then leached again, reaction proceeded as though the columbite were freshly ground. This was true whether the original or fresh leach liquor was used. Thus the

first leaching reaction stopped because a coating of an insoluble material, removed by the acid washing, had been produced.

Although a ferric oxide formed after a considerable proportion of the columbite had decomposed, and some remained attached to the particles, most of it broke away and remained in suspension. The

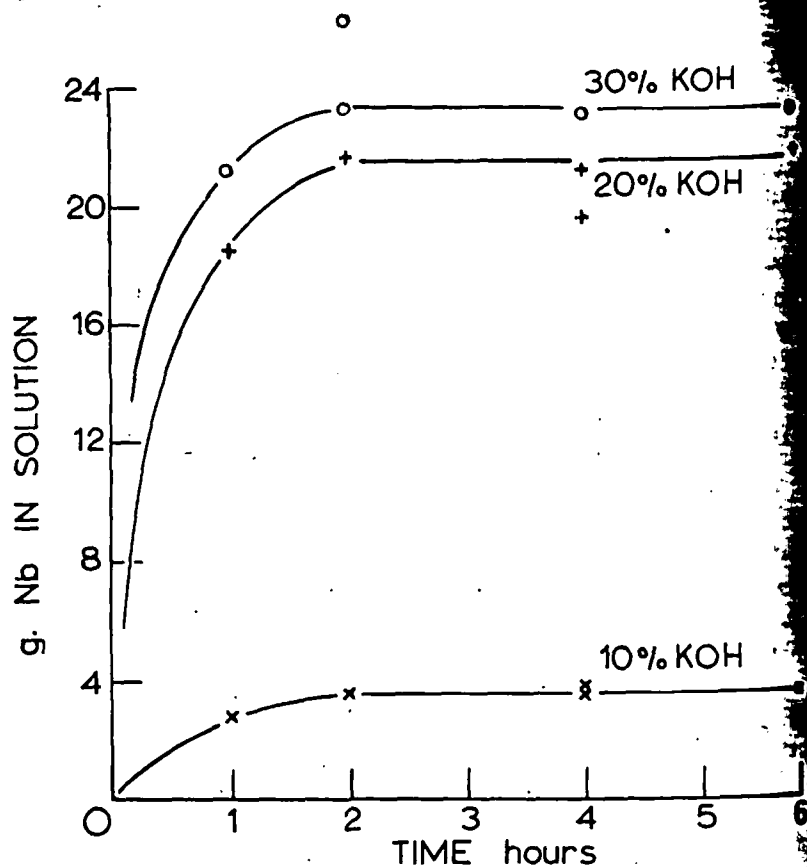


Fig. 3. Rate of solution of niobium from 50 g of columbite in 1 litre of potassium hydroxide solution of the concentration given. Temp. 220°C.

residual columbite was more magnetic than the unleached solid, indicating that the layer of insoluble product which hindered and finally prevented diffusion of the reactants to the columbite surface, was probably magnetite, possibly with a diffusion layer also, as in the case of chromite.

5 g of columbite, of particle size about 1 mm was leached in 3.5N potassium hydroxide with 200 p.s.i.g. air pressure (at 20°C) at 260°C for 3 hours. After washing and drying, the particles were mounted as a thin layer in resin, and polished. The electron probe microanalyser showed the edges of most particles to be rich in iron and low in columbium and manganese, a typical series of curves is given for a single field, in Fig. 4. Experimental points are given for iron only, to prevent confusion; those for the other elements fit the lines equally well. The shape of the columbium line differed widely with different fields of a single particle, and with different particles, usually showing a step such as that seen in Fig. 4 but occasionally being a straight line from the value within columbite to almost zero near the solid edge.

As in the case of chromite, manganese is leached out since fairly concentrated alkali and strongly oxidising conditions were employed. Tantalum does not dissolve appreciably and the results with this element show a constant value and demonstrate the slope of the line corresponding to a sharp edge as seen on the microanalyser.

PASSIVATION EFFECTS WITH WOLFRAMITE

The reaction of wolframite with dilute sodium hydroxide solution shows the effect of oxygen partial pressure on the nature of the mineral surface during leaching, and so on the reaction rate.³ Using 0.5N sodium hydroxide solution at temperatures between 100°C and 150°C, the rate of decomposition of the wolframite increased with increasing oxygen partial pressure up to about 1.5 to 3 p.s.i. O₂ (at 20°C). With the slightly weathered solid used in the experiments described, reaction took place in the absence of oxygen, becoming slow after some time when a coating had formed over the surface. At temperatures above 100°C increasing the oxygen partial pressure to 10 or 50 p.s.i. caused less tungstic oxide to dissolve than with 3 p.s.i. oxygen, under equivalent conditions of alkali concentration, time, temperature and stirring. For example using 0.5N sodium hydroxide at 150°C for 2 hours, the percentage of tungstic oxide dissolved fell from 71% at 1.5 p.s.i. oxygen, to 32% at 50 p.s.i. oxygen. Wolframite showing no extensive surface oxidation was hardly attacked by the alkali solutions in the absence of dissolved oxygen. Above about 3 p.s.i. oxygen pressure, further increase had no effect on the rate of decomposition of this wolframite.

Rate curves using 0.5N sodium hydroxide with up to 10 p.s.i. oxygen

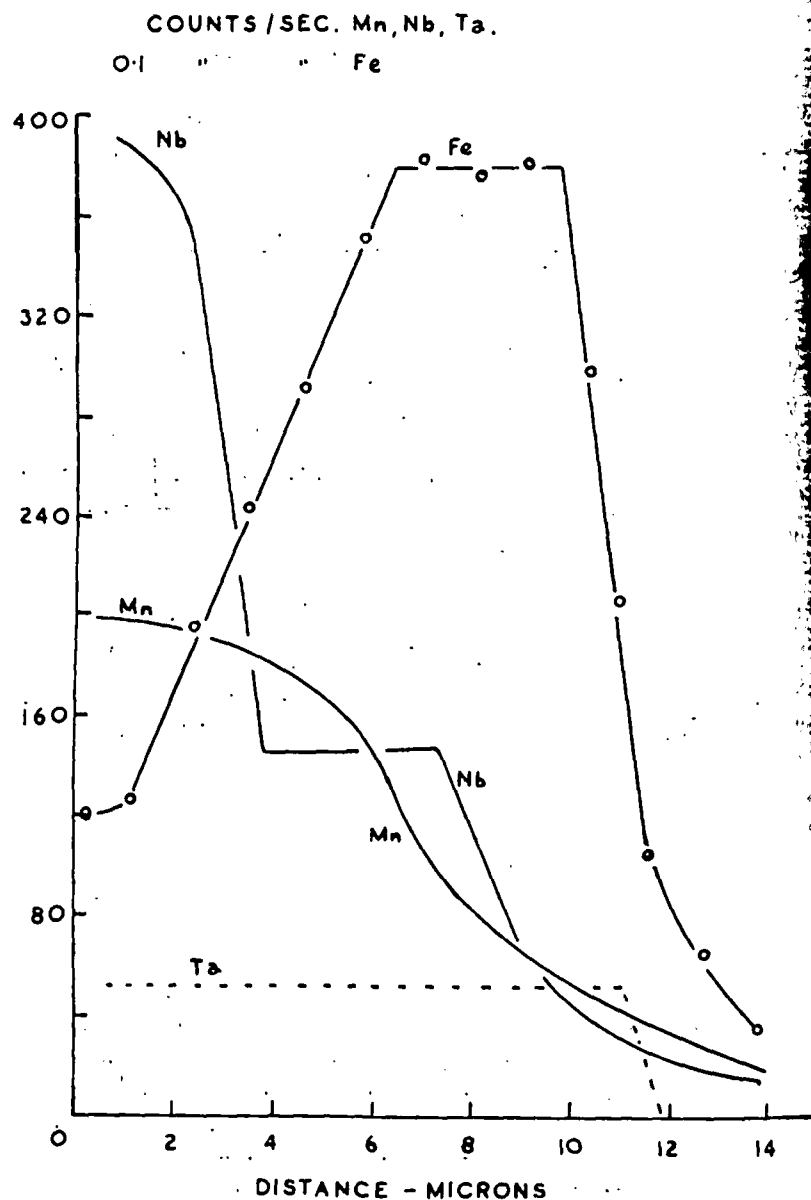


Fig. 4. Metal content variation near edge of leached columbite crystal.

at temperatures between 100°C and 150°C had shapes somewhat similar to those for columbite, Fig. 3, indicating an extremely rapid initial reaction, with the rate falling as a surface coating formed. This explanation was supported by the fact that if just sufficient of a complexing agent capable of chelating iron in the leach solution, was



Fig. 5. Wolframite particle partly decomposed by leaching with 2% sodium hydroxide at low oxygen pressure. Note penetration.

present, complete decomposition of the wolframite occurred rapidly. The complexing agent used was "Detarex C" (F. W. Berk & Co. Ltd.) which is diaminoethane-tetra-acetic acid "modified with a buffering agent."

Microscopic examination and X-ray microanalysis of polished sections of leached wolframite showed heavy coatings of a solid containing iron and manganese in the same ratio as in the parent wolframite, and little or no tungsten (Figs. 5 to 8). No diffusion gradients were observed. X-ray powder photographs showed no lines other than those of wolframite. Attack had occurred readily along grain boundaries and other defects, so that the effective surface area was much larger than that calculated from the particle size. The sequence of oxidation products appeared to be the same within the cracks as

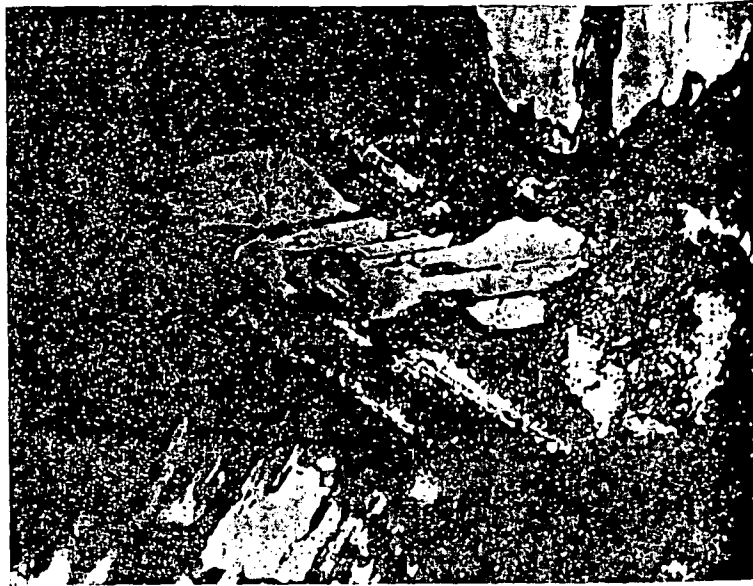


Fig. 6. As Fig. 5 using 3 p.s.i.g. oxygen. Uneven attack and formation of some magnetite along one edge of the central particle.

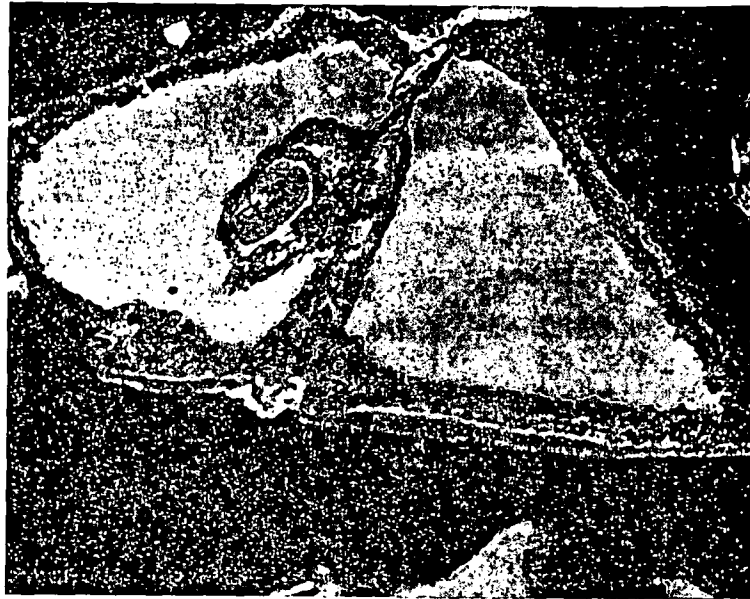


Fig. 7. As Fig. 5 using 50 p.s.i.g. oxygen. Thin coherent band of highly reflecting magnetite formed around the particle.

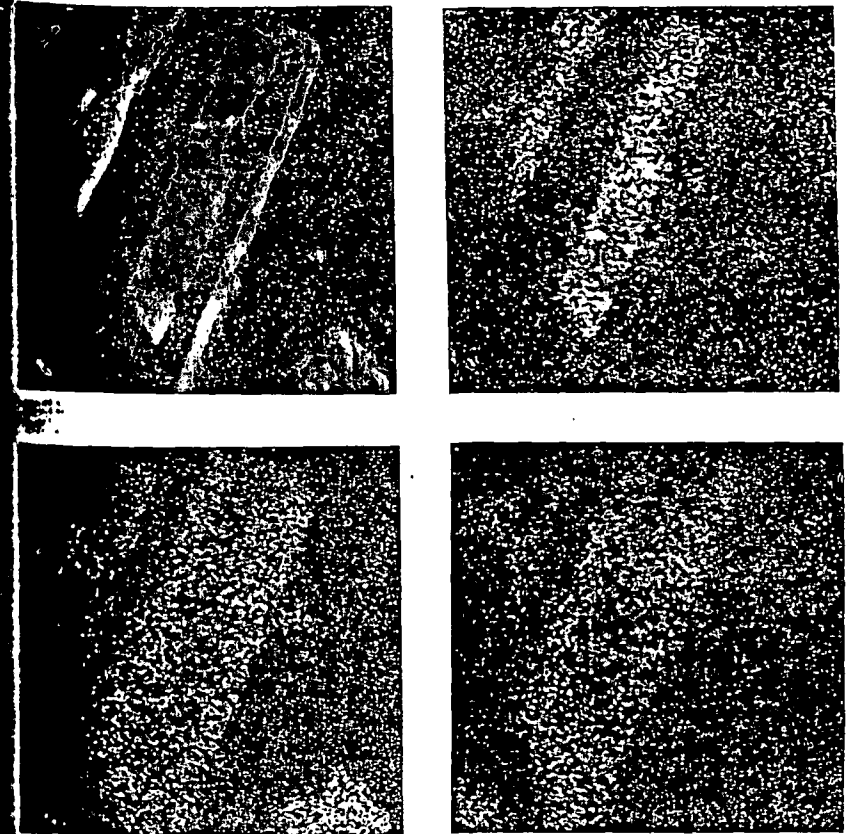


Fig. 8. Composition of coatings around leached wolframite particle; *a* electron reflection view of field. The narrow light band is caused by a relief effect; *b* tungsten distribution shown by characteristic X-rays emitted. Coating contains very little tungsten; *c* iron content; *d* manganese content. The coating contains more iron and manganese than does the wolframite.

at the outside of the particle, under any leaching conditions, and the absence of tungsten from the products proved that diffusion was rapid.

The results indicate that the initial solid produced when tungsten is removed from the mineral may be formed by a topotactic reaction. When the oxygen concentration was greater than that required for maintenance of the reaction at the wolframite surface, the iron was oxidised to give a solid impervious to reactants and soluble products, so that when the layer attained an appreciable thickness, reaction ceased. Ferrous hydroxide is transformed non-topotactically to goethite

(α -FeOOH) in strongly alkaline solutions, non-topotactically to magnetite, and topotactically to δ -FeOOH. The experimental conditions used in the leaching experiments outlined above, favoured the formation of magnetite and the presence of this in the products is suggested by the strongly magnetic properties of the material. However, this could not be confirmed from X-ray powder photographs.

TOPOTACTIC REACTIONS INVOLVING PYRITE

The rate curves obtained on leaching pyrite in dilute sodium hydroxide solutions in the presence of oxygen at temperatures between 60° and 150°C, differed in shape under some conditions, depending on the nature of the pyrite used. One sample was from Rio Tinto and had a highly imperfect solid structure, being agglomerates of small particles and containing considerable amounts of As, Pb, Cu, and Zn. The other was from the Cassandra mine, Greece, and contained the same impurity elements but in trace quantities only. It was obtained as cubic crystals of side about 1 cm. In each case the solid was dry ground and the 40–120 μ fraction used for leaching. In the absence of dissolved oxygen no pyrite was decomposed in 0.5*N* sodium hydroxide at temperatures up to 160°C. In the presence of oxygen, sulphate formed, together with iron oxides. Thus under these conditions the reaction was simple, no sulphur-containing ions other than sulphate being detectable, and no sulphur-containing compounds of iron being formed. The rate of decomposition of the pyrite increased with increasing oxygen partial pressure, and no upper limit was found above which reaction stopped.

In the case of the Cassandra pyrite the reaction rate curves were smooth at all temperatures between 80° and 150°C. The Rio Tinto pyrite, however, showed two kinds of behaviour. At 100° and at higher temperatures the rate curves were smooth, but at 90° and at lower temperatures the reaction proceeded normally for between 40 and 90 minutes and then slowed down sharply. The point of inflexion in the rate curve appeared at a shorter time and larger percentage decomposition, the higher the temperature.

The different kinds of behaviour are due to the formation of an adherent coating around particles of Rio Tinto pyrite shown by X-ray powder photographs to contain maghemite (γ -Fe₂O₃). The solid product retains precisely the shape of the original pyrite crystals and appears as a dense, highly reflecting material. It must, therefore, have

been produced directly by reaction on pyrite and not by re-deposition from solution. It was usually separated from remaining pyrite by a thin band of solid which was heavily cracked, usually 1 to 2 microns thick. X-ray microanalysis showed that the outer dense layer contained 3% or less of sulphur and the fall in sulphur content from about 53% in pyrite to this low value occurred over the region of broken down solid. The iron content rose sharply as the sulphur value fell.

The order of reaction with respect to sodium hydroxide concentration is zero between 0.5 and 4*N*; and 0.5 with respect to oxygen partial pressure under the conditions used. The rate controlling process is assumed to be transport of oxygen atoms through the layer of solid product to the pyrite surface and oxidation of sulphide to sulphur. This is subsequently oxidised to sulphate at the liquid-solid interface.

It is suggested that the reactions in the solid state may proceed as follows. When an oxygen atom oxidises sulphide groups to sulphur, the oxide ion formed occupies the position in the crystal lattice previously occupied by the S₂⁻ group. Thus an initial metastable wustite (FeO) structure is set up, this and pyrite having the sodium chloride structure. When the metastable phase reaches a certain thickness it alters to magnetite and, finally, maghemite in which only ferric ions occur in the close packed cubic arrangement of oxide ions. When the initial ferrous oxide begins to oxidise, decomposition of pyrite slows down, and the position of the inflexion in the rate curve depends on the stability of the wustite layer under the leaching conditions employed. Thus a series of topotactic alterations occurs; in the first the ferrous ions retain their lattice positions, in the others the oxide ions remain stationary. The change in lattice dimensions on going from pyrite to wustite must lead to strain so that the solid at the interface with residual pyrite tends to shatter on cooling and storage.

The thick layers of product discussed above are not found on particles of Cassandra pyrite leached under similar conditions. Penetration into the crystals occurred only along occasional defects, and only for very small distances around these was a visible layer of product bound to the outside surface of the particles. It was shown by electron diffraction, however, that a single face of a pyrite crystal was roughened slightly after leaching for ten minutes in 0.5*N* sodium hydroxide with 150 p.s.i.g. of air at 85°C and retained a very thin layer of very small crystals of maghemite, which were in random orientation.

After prolonged leaching $\alpha\text{-Fe}_2\text{O}_3$ was found to be present on the surface also. Thus, so far no direct evidence for topotactic reaction or of epitaxy have been found, although oxidation of pyrite in water vapour at higher temperatures (around 600°C) gives oriented crystals of $\gamma\text{-Fe}_2\text{O}_3$, that is, epitaxy. The individual crystals in pieces of Rio Tinto pyrite are so small that they cannot be examined satisfactorily by electron diffraction. Thus the topotactic nature of the pyrite-wustite stage of the reaction series is not proven.

References

1. Burkin, A. R., Paper submitted for publication.
2. Farrow, C. J. & Burkin, A. R., Paper submitted for publication.
3. Burkin, A. R. & Edwards, A. M., Paper submitted for publication.
4. Burkin, A. R. & Edwards, A. M., Paper in press.
5. Bernal, J. D., Dasgupta, D. R. & Mackay, A. L., *Clay Minerals Bulletin*, 4, 15, 1959.

Discussion

P. G. Thornhill:* Would the author please give details of the leaching conditions under which the pyrite was oxidized?

I calculate the volume of the Fe_2O_3 resulting from the oxidation of FeS_2 to amount to only about 63% of that of the FeS_2 reacted. Such shrinkage does not seem consistent with observations in this work of dense iron oxide coatings, and I wonder if the author would care to comment on this?

A. R. Burkin: The pyrite was leached in 0.5M sodium hydroxide solution at 90°C , using 200 p.s.i.g. air (at 20°C), for 1 hour. The term "dense" was used to describe that part of the iron oxide layer produced around Rio Tinto pyrite which showed up after polishing as large areas of solid having no apparent microstructure. This was distinguished from "broken down" solid which was also $\gamma\text{-Fe}_2\text{O}_3$ but very much cracked, as though it had shattered under strain.

If the sequence of reactions which I put forward is accepted, the shrinkage referred to by Dr. Thornhill occurs during the change from pyrite to wustite; the subsequent series of topotactic alterations during the oxidation of the iron oxides involves only small changes in lattice dimensions. Because of the relatively large change in interionic spacings during the pyrite to wustite reaction the oxide tends to break away, and does so in the case of Cassandra pyrite. Only a very thin coating of $\gamma\text{-Fe}_2\text{O}_3$ is found by electron diffraction in this case except in defects in the crystals. The Rio Tinto pyrite has so many flaws that the oxide produced is "keyed in" and thick layers build up. At the oxide-pyrite interface the product is under strain because of the poor fitting and so tends to shatter easily, as is seen visually. A truly protective coating is never produced, but the degree of protection depends on the conditions of leaching, being shown by the discontinuities found in the rate curves under conditions of slow reaction, that is at low temperatures.

* P. G. Thornhill, Falconbridge Nickel Mines Limited, Thornhill, Ontario.

Studies on Hypochlorite Leaching of Molybdenite

ROSHAN B. BHAPPU
Metallurgist

DEXTER H. REYNOLDS
Research Chemist

WILLIAM S. STAHMANN
Technical Assistant

New Mexico Bureau of Mines and Mineral Resources
New Mexico Institute of Mining and Technology
Socorro, New Mexico

This paper is to be presented at the "International Symposium on Unit Processes in Hydrometallurgy," at the Annual Meeting of the American Institute of Mining, Metallurgical, and Petroleum Engineers Inc., Dallas, February, 24 to 28, 1963.

Abstract

The response of molybdenite to hypochlorite leaching has been known for some time. However, sufficient information on the mechanism of the process has not been available for this technique to be utilized effectively in practice for exploiting low-grade molybdenum deposits. Experimental data are presented which reveal that nine moles of hypochlorite are consumed in leaching one mole of molybdenite, both with pure concentrates and with natural low-grade ores. The leaching rates and extractions of molybdenum as a function of hypochlorite concentration and ore particle size have also been established. Molybdenum extractions of 50 to 70 percent can be expected from sized ($-\frac{1}{2}$ inch) low-grade ores in 48 hours of leaching time at moderate concentrations of hypochlorite.

INTRODUCTION

Increased importance of molybdenum in high-temperature alloy applications, as evidenced by the recent rise in price and demand, has resulted in increased interest in the recovery of this metal from low-grade sources. These include porphyritic, or disseminated, copper ores of the Southwest from which molybdenum is recovered as a by-product;

Five case histories of feasibility studies show what mine owners, operators, or loan officers must know when judging the economic worth of proposed mining ventures.

(Part 2 of a two-article series)

Evaluating Mining Ventures Via Feasibility Studies

UNIVERSITY OF UTAH
RESEARCH INSTITUTE
EARTH SCIENCE LAB.

F. Milton Lewis and Roshan B. Bhappu, Mountain States Mineral Enterprises, Inc.

In Part I of this article, published in the September issue of *MINING ENGINEERING*, Edward S. Frohling and Robert M. McGeorge of Mountain States Mineral Enterprises, Inc., reviewed the general overall financial aspects and methods of raising the necessary capital for developing the mine. In Part 2 of this two-article series, we will present several case histories to show how realistic feasibility studies are used for evaluating the choices and options entailed in mining ventures.

Basically, after a potential ore body has been discovered, and the necessary funds obtained for the development of the deposit, the next major problem is one of ascertaining what specifically is to be produced, and the costs of production. The profit potential of the mining venture can then be accurately assessed by the mine owner, operator, or loan officer.

Mining companies and lending institutions use various yardsticks to judge the basic viability of a proposed project. First, they must have a specific return on investment below which the venture would have to be rejected. In calculating the return on investment, one must choose a certain base price for various products. Alternately, return on investment may be calculated at several price levels to determine at what price the venture becomes viable. Also, many use three to four years for return of investment for a mine with six to ten years mine life.

It should be noted that the depth of feasibility study and capital cost estimate depends upon the requirements of the decision-making body seeking the estimate: mine owner, corporate management, bank and lending institution, public financing, or governmental agency.

In the case histories presented here, we have selected typical examples of problems which a mine owner, a plant operator, or manager of a company may face in his efforts to evaluate mining ventures. These examples include: (1) economics of a copper mining venture consisting of open-pit mining, flotation concentration and custom smelting; (2) selection of the optimum process for treating oxide-copper ores; (3) economic viability of a marginal gold deposit requiring conventional cyanidation processing; (4) economic recovery of silver and gold values from tailings; (5) feasibility of in-situ extraction of uranium from lower-grade ores.

Economics of a Copper Mining Venture

Mountain States Mineral Enterprises has been estimating costs within the copper industry in the United States for the past three years. During this period, the capital cost for developing an open-pit mine and constructing a concentrator has increased approximately 45%, and the operating cost has increased about 40%. At the end of 1974, Mountain States' studies indicated that

the weighted average cost for producing copper from 27 large copper mines in the United States (based on the assumption that all were on full production) was \$0.54 per lb, including credits for by-products. The cost at eight of these mines was over \$0.63, and two were near that figure.

Based on the price of \$0.63 per lb for extracting copper, it would be very difficult to justify developing a new open-pit porphyry deposit averaging 0.6% copper in the Southwest.

Mountain States' evaluation reveals that with a 300-million-ton copper deposit averaging 0.60% copper, and a 40,000-tpd operation, the net sales of the copper, plus by-product credits, must equal \$0.70 in order to return the capital outlay in full at an average compound interest rate of 15% on the expected average cash flow for the life of the mine, discounted to present worth.

The details concerning the above feasibility study for the copper mining venture investigation, are shown in Tables 1 through 3.

Selection of Optimum Process

The hydrometallurgical processes currently available for treating oxide-copper ores include several variations. Basically, these processes involve ore preparation for leaching, solution application to broken or unbroken ore, and recovery of copper from pregnant solutions. Dump leaching, heap leaching, vat leaching, agitation leaching,

Table 1—Capital Cost Estimate
(Thousands of Dollars)

Mine Production: Tons per operating day	40,000
Operating days per year	355
Tons per year	14,200,000
Total Tons of Ore	284,000,000
Life of Mine	20 Years
Preproduction Mine Cost	
Tons overburden	35,500,000
Cost for removing overburden (\$0.35 per ton)	\$12,400
Mobile equipment	14,400
Property acquisition cost	500
Exploration and development	2500
Environment studies and hearings	2000
Buildings	3000
Contingencies and interest during construction	5200
	\$40,000
Concentrator Cost:	
Crushing	\$20,500
Grinding	36,900
Flotation	20,800
Filtering	1300
Reagents, storage, preparation and handling	1300
Tailings disposal	6300
Buildings	2200
Contingencies and interest during construction	13,400
	\$102,500
Supporting Facilities	
Roads, railroad, landscaping, etc.	\$1500
Total Capital Investment	\$144,000

and in-situ leaching or solution mining (in combination with the conventional cementation process, or the recently developed solvent extraction-electrowinning system) have all been employed or investigated for recovering copper from oxide ores. Of these processes, dump, heap and vat leaching have been practiced successfully for processing oxide copper ores. On the other hand, agitation leaching is relatively a newcomer, having been adopted from the experiences of uranium and gold processing. Finally, the in-situ leaching technique is the latest process to be proposed for possible treatment of oxide copper ores.

From the viewpoint of metallurgical effectiveness, in general, dump and heap ore gives the lowest extraction of copper, amounting to about 60% in several weeks to months, depending on the ore size and height of the dump or heap. On the other hand, agitation leach gives the highest extraction of copper, amounting to about 90% in four to twenty-four hours, followed by vat leaching with an extraction of about 80% in a six to eight-day leaching cycle. In-place leaching is comparatively slow and may provide 50 to 60% extraction of copper in a variable leaching period, depending on the nature of the deposit and type of operation practiced.

From the viewpoint of economics, the net return from a mining venture using a specific process will depend upon the quality and quantity of copper extracted from the ore. Since the cost of the unit operation (mining and crushing), unit process (leaching, solvent extraction-electrowinning) and reagents (H₂SO₄ and scrap iron) would dictate the overall economics of the operation, they should be evaluated carefully. The overall profitability will also be affected by the initial capital investment. For these reasons, the economic feasibility of any new venture and process must be considered in light of all these and many more pertinent factors.

Table 2—Operating Cost Estimate

Ore Copper	0.60%
Overall Copper Recovery (Concentrator and Smelter)	85%
Tons per Operating Day	40,000
Tons per Year (355 Operating Days)	14,200,000
Stripping Ratio	1.5 to 1.0
Pounds Copper Recovered per Ton Ore	10.2
Pounds Copper Recovered per Year	144,840,000

	Cost		
	Per Year*	Per Ton Ore	Per Pound Copper
Mining (\$0.38 per ton material)	13,470	\$0.95	\$0.093
Concentrating	21,300	1.50	0.147
Smelting, freight and refining	36,210	—	0.250
General ¹	8,998	0.63	0.062
Total operating	79,978	—	0.552
Non-operating ²	11,215	0.79	0.077
By-product credits ³	<10,428>	<0.74>	<0.072>**
Total	80,765		0.557

* Thousands of dollars.
 Notes: (1) Includes local administration expense, local taxes, hazard insurance, and payroll burden.
 (2) Includes depreciation, sales expense, and administration expenses allocated from headquarters. Federal income tax not included.
 (3) By-product credits include secondary copper recovered from mine dumps, molybdenum recovered from copper concentrate and gold and silver credits from refinery.
 Secondary copper cost \$0.40 per lb. Profit \$0.23 per lb.
 Molybdenum \$2.25 per lb.
 Gold \$160.00 per troy oz.
 Silver \$4.50 per troy oz.

** Recovered per ton ore	Value per ton ore
Secondary copper 1.5 lb	\$0.345
Molybdenum 0.12 lb	0.270
Gold 0.0001 oz	0.016
Silver 0.023 oz	0.104
Total value per ton ore for by-products	\$0.735
Total value per pound of copper	0.072

In the final analysis, selecting the optimum process for a given oxide copper ore would depend on the tonnage and grade of the deposit under consideration, as well as on the prevailing price of copper. The validity of this statement is illustrated in the second case history, which involves the selection of the optimum method for processing oxide copper ore from a 16.5-million-ton deposit averaging 0.5% copper; a 5000-tpd operation with a 10-year mine life is projected and the price of copper is set at a low of \$0.60 per lb and a high of \$0.80 per lb.

The available processes under consideration are: (a) heap leaching of crushed (minus 3-in.) ore with cementation; (b) heap leaching of crushed (minus 3-in.) ore with solvent extraction-electrowinning; (c) modified vat leaching with solvent extraction-electrowinning; (d) agitation leaching with solvent extraction-electrowinning; (e) in-situ leaching (ore broken in place) with solvent extraction-electrowinning.

The vat leaching system under consideration involves an inclined trough with truck loading and unloading, and not the usual Inspiration type. Such a conventional vat system is rather expensive to build and to operate, while

Table 3—Financial Analysis (Thousands of Dollars)

Capital Investment	\$144,000
Working Capital (Operating Cost—three months)	20,000
Total	\$164,000
Tons Ore per Year	14,200,000
Pounds Copper per Year (10.2 lb/ton ore)	144,840,000
Life of Mine	20 yr
Minimum Acceptable Rate of Return on Investment Discounted to Present Worth	15%
Average Annual Cash Flow = 164,000 $\left[\frac{0.15 (1.15)^{20}}{(1.15)^{20} - 1.0} \right]$	= \$26,209
Sales	
144,840,000 lb copper at 63.0 cents	\$ 91,249
By-Products at 7.2 cents per lb copper	10,428
Total Sales	\$101,677
Expenses	
Total Operating	80,765
Depletion 15% (101,677 - 36,210)*	9820
Total Expenses	\$ 90,585
Net Operating Income	11,092
Federal Income Tax (48%)	5324
Net Income	\$ 5768
Investment Credit**	2884
Depreciation (straight line), 144,000 ÷ 20	7200
Depletion	9820
Recovery of Working Capital (Discounted to present worth)**	537
Average Annual Cash Flow	\$ 26,209

* Total sales minus annual cost of smelting, freight and refining.
 ** Averaged over 20 years.

Table 4—Copper Ore—1,650,000 TPY

Operating days per year	330
Tons ore treated per operating day	5000
Production	
Pound copper recovered per year—in thousands of pounds	0.50
Ore-percent copper	
Heap leaching (60% recovery)	9900
Vat leaching* (80% recovery)	13,200
Agitation leaching (90% recovery)	14,850
In-situ leaching (60% recovery)	9900
Annual Sales (Thousands of Dollars)	
Copper—%	0.50
Copper—Price, \$/lb	0.60 0.80
Heap leaching	5940 7920
Vat leaching	7920 10560
Agitation leaching	8910 11880
In-situ leaching	5940 7920

* The vat system employed is a modified method using an inclined trough and truck loading and unloading.

Table 5—Copper Ore—1,650,000 TPY; Capital Cost Estimates
(In Millions of Dollars)

Type of Leaching Recovery Method	Heap Cementation	Heap SX-EW	Vat SX-EW	Agitation SX-EW	In Situ SX-EW
Copper, %	0.50	0.50	0.50	0.50	0.50
Mining	2.0	2.0	2.0	2.0	2.0
Crushing	2.2	2.2	3.1	3.1	—
Ore Handling	0.5	0.5	0.7	0.3	—
Grinding	—	—	—	4.4	—
Leaching	0.5	0.5	2.8	2.6	0.7
Metal Recovery	1.0	4.5	5.5	6.0	4.5
Supporting Facilities	0.2	0.2	0.2	0.2	0.2
Total	6.4	9.9	14.3	18.6	5.4
Dollars per Ton Day*	880	1,580	2,460	3,320	1,080

* 5,000 tons per operating day. Mine capital is not included.

Notes:

(1) Cost of developing mine not included.

(2) Cost of developing a tailings disposal area and equipment for handling tailing not included.

the modified system employed here has lower capital and operating costs.

The desired information for selecting the optimum process is achieved by making an economic evaluation of the available processes, considering capital costs, operating costs, cash flow analyses, pay-out periods, and return of investment for each of the five processes, as shown in Tables 4 through 8.

The above feasibility study clearly indicates that for the copper deposit under consideration (16.5-million-ton reserve averaging 0.5% copper) at a copper price of \$0.60 per lb, the only process showing an attractive return on investment is in-situ leaching. On the other hand, at \$0.80 per lb copper, both heap and vat leaching with solvent extraction-electrowinning (SX-EW), in addition to in-situ leaching, appear to be economically viable.

Viability of Gold Mining Venture

The current \$150 to \$170 per oz price range for gold has generated considerable interest and activity in the gold mining camps in the US and throughout the world. Under these economically favorable conditions, many of the older gold mines are being reactivated and a major exploration effort is underway to find new deposits. For both the older mines and the new ones, the paramount make-or-break question is the best method for extracting gold, especially from the submarginal and low-grade ores that are now becoming so economically attractive.

The treatment methods applicable to comparatively higher-grade ore—averaging better than 0.2 oz gold per ton and having a cutoff grade of about 0.07 oz per ton—include: gravity concentration, amalgamation, flotation, cyanidation, or direct smelting. Such processes involve

Table 6—Copper Ore—1,650,000 TPY;
Summary of all Direct Operating Costs
(Cost per Ton Ore Treated)

Type of Leaching Recovery Method	Heap Cementation	Heap SX-EW	Heap SX-EW	Agitation SX-EW	In Situ SX-EW
Copper, %	0.50	0.50	0.50	0.50	0.50
Mining*	0.900	0.900	0.900	0.900	0.150
Crushing	0.216	0.216	0.307	0.307	—
Ore Handling	0.159	0.159	0.318	—	—
Grinding	—	—	—	0.913	—
Leaching	0.381	0.347	0.348	0.369	0.190
Metal Recovery	2.055	0.490	0.580	0.628	0.455
Supervision	0.038	0.096	0.096	0.112	0.053
Administration	0.202	0.278	0.358	0.436	0.176
Total	3.951	2.486	2.907	3.665	1.024
Cost per Pound Copper	0.650	0.415	0.364	0.407	0.171

* Stripping ratio 1:1.

Ore and waste cost \$0.45 per ton of material mined.

high capital investments as well as high operating costs. A conventional cyanidation plant used in processing lode gold ores usually includes crushing, fine grinding, and agitation leaching in cyanide solution, countercurrent decantation in thickeners for separating the pregnant solution, clarification of this solution by filtering, de-aeration by vacuuming, and precipitation of the gold by zinc powder. It is obvious that such a treatment scheme would be costly from the viewpoint of capital investment and of operating cost. For this reason, such processes are not economically justified in the processing of lower-grade ores below 0.07 oz gold per ton.

However, many of the known and newly discovered domestic gold deposits are quite low in gold content, have limited reserves, or contain detrimental clays and other components that make processing by conventional gravity and cyanidation methods impractical. Such

Table 7—Copper Ore—1,650,000 TPY; Cash Flow (In Thousands of Dollars)
0.50% Copper—Copper at \$0.60 Per Pound

Type of Leaching Recovery Method	Heap Cementation	Heap SX-EW	Vat SX-EW	Agitation SX-EW	In Situ SX-EW
Capital	6400	9900	14300	18600	5400
Net Sales	5940	5940	7920	8910	5940
Cost and Expenses:					
Total operating (Table 12)	6523	4104	4798	6048	1690
Mine amortization ¹	50	50	50	50	—
Depreciation ²	640	990	1430	1860	540
Depletion ³	891	891	1188	1337	891
Total	8104	6035	7466	9293	3121
Operating Income	<2164>	<95>	454	<383>	2819
Federal Income Tax	—	—	218	—	1353
New Income	<2164>	<95>	236	<383>	1466
Cash Flow	<583>	1836	2904	2864	2897
Pay-Out in Years	—	5.4	4.9	6.5	1.9
Percent Rate of Return ⁴	—	14.0	16.3	9.4	54.5

Notes:

(1) Cost of developing mine prior to production \$500,000. Amortize this cost during the life of the mine—10 years.

(2) Depreciation—Straight-line, 10 years.

(3) Depletion—15% sales.

(4) Average compound interest rate, discounted to present worth, to return the capital in full.

Table 8—Copper Ore—1,650,000 TPY;
Cash Flow (In Thousands of Dollars)
0.50% Copper—Copper at \$0.80 per lb

Type of Leaching Recovery Method	Heap Cementation	Heap SX-EW	Vat SX-EW	Agitation SX-EW	In Situ SX-EW
Capital	6400	9900	14300	18600	5400
Net Sales	7920	7920	10560	11880	7920
Cost and Expenses:					
Total operating	6523	4104	4798	6048	1690
Mine amortization*	50	50	50	50	—
Depreciation*	640	990	1430	1860	540
Depletion*	1188	1188	1584	1782	1188
Total	8401	6332	7862	9738	3418
Operating Income	<481>	1588	2698	2142	4502
Federal Income Tax	—	762	1295	1028	2161
Net Income	<481>	826	1403	1114	2341
Cash Flow	1397	3054	4467	4806	4069
Pay-Out in Years	4.6	3.2	3.2	3.9	1.3
Percent Rate of Return*	18.3	29.4	29.6	23.3	75.0

* See Table 7 Notes 1, 2, 3, and 4.

lower-grade and refractory deposits pose the big challenge to modern extraction technology. Such projects involve large-volume mining, ore handling, and processing and this, in turn, usually results in substantial surface disturbances, possible land-use conflicts, and probably some environmental considerations. For this reason, in recent years considerable efforts have been focused on developing low capital, low operating cost, and environmentally attractive processes for such ore.

The newly developed cyanide heap leaching-carbon adsorption-electrowinning process, as well as conventional vat leaching or several of its modifications also using the carbon adsorption-electrowinning step, may be applicable to the treatment of lower-grade gold deposits. One of the attractive modifications involves an inclined trough with truck loading and unloading. Such a system is less expensive to build and operate than the conventional vat leaching system.

Compared to heap leaching procedures, vat leaching incurs higher capital expenditures and operating costs, but with inherent advantages of equal or higher recoveries in a comparatively shorter period. The vat leaching technique also has an advantage over heap leaching when the mine is located at higher elevations and the problem of freezing is encountered. The vat can be covered and operated throughout the year, while the heap leaching may have to be discontinued during winter months.

It should be noted that the above heap leaching and vat leaching systems can only be successfully applied if the gold mineralization occurrence is favorable. In this case, the free gold occurs in fracture fillings and is readily exposed by fragmentation or coarse crushing. In this example, gold values are very intimately associated

with gangue and a fine grind (such as 65-mesh) is required for effective liberation; thus, the recovery by heap and vat leaching is not applicable. A conventional agitation leach with countercurrent decantation (CCD) and Merrill-Crowe procedure is one of the systems that can be used effectively for treating such an ore, provided its grade is sufficiently high to sustain higher capital and operating costs associated with the agitation leach (cyanidation) process.

A recent study by Mountain States Research and Development¹ has projected the following comparative capital and operating cost schedule for the four available process alternatives for treating lower-grade gold ores, taking the conventional process as the base:

Process	Cost Factor	
	Capital	Operating Direct & Indirect
Conventional agitation leach with CCD-Merrill Crowe	1.00	1.00
Agitation leach with charcoal-in-pulp electrowinning	0.75	0.94
Vat leaching-charcoal adsorption-electrowinning	0.52	0.79
Heap leaching (with crushing) charcoal adsorption-electrowinning	0.32	0.66

In a subsequent contribution on the economics of gold ore processing at different grades and gold prices, Mountain States Research and Development² surmised that for a 5,000 tpd operation with ore grades of 0.04 and 0.10 ounce gold per ton, economic operations using different processes may be feasible at the following gold prices:

Table 10—Estimated Capital and Operating Costs for Agitation Leach-CCD-Merrill Crowe Process (Thousands of Dollars)

Table 9—Details Concerning Orebody and Operating Data

Gold Ore	
Total tons of ore	10,000,000
Total ore mined per year	1,650,000
Life of project	6 years
Processing Plant	
Operating days per year	330
Tons treated per operation day	5000
Production	
Ounces of gold per ton	0.04
Total ounces gold per year	66,000
Recovery in ounces per year:	61,380
Agitation leaching (93%)	
Net Sales (Thousands of Dollars)	
Value of gold \$80 per oz	4910
Value of gold \$100 per oz	6138
Value of gold \$120 per oz	7366
Value of gold \$140 per oz	8593
Value of gold \$160 per oz	8920

Capital Costs		Operating Costs	
Mining ¹	\$2000	Mining ³	\$1000
Crushing	3100	Crushing	400
Grinding	4400	Grinding	1300
Leaching	2600	Leaching	311
Gold Recovery	2800	Gold Recovery	551
Supporting Facilities ²	500	Mil Supervision	180
		Administration	616
Total	\$15,400	Total	\$4358
		Cost per ton ore processed	2.64
		Cost per ounce gold recovered	71.00

Notes:
(1) Cost of mine development not included.
(2) Supporting facilities include sub-station, change house, general offices, warehouse, etc., but does not include tailing disposal costs.
(3) Mine operating cost, \$0.60 per ton of ore.

Process Alternatives	Gold Price for Feasible Operation	
	Grade 0.04 oz per ton	0.10 oz per ton
Heap leaching-carbon adsorption-electrowinning	\$120	\$35
Vat leaching-carbon adsorption-electrowinning	120	35
Agitation leach-carbon adsorption-electrowinning	140	55
Agitation leach-CCD-Merrill Crowe	160	75

In the third case history, efforts have been made to present a feasibility study for a given gold deposit containing 10 million tons of minable ore reserve and averaging 0.04 oz gold per ton. The gold mineralization of this ore is such that fine grinding (minus 65-mesh) is required to liberate the values, thereby precluding the application of heap and vat leaching and necessitating the employment of the conventional agitation leach (cyanidation)-CCD-Merrill Crowe process. The study is based on estimated capital costs, operating costs, cash flow analysis, pay-out time, and return on investment projections, as shown in the following Tables 9, 10, and 11. Since, in this feasibility study a six-year mine life is assumed, the pay-out period for the investment should be less than three years in order to make the process economically attractive.

From the succeeding cash flow analysis in Table 11, it is quite evident that the proposed process is economically unattractive for all gold prices up to \$160 per oz, since the pay-out period is more than the acceptable three-year limit. It is also obvious that the deposit can be worked profitably if the price of gold is above \$160 per oz.

Silver and Gold Recovery from Tailings

Since the improvement in the price of silver above \$4.00 per oz, considerable interest has been shown in retreating tailings to recover residual gold and silver values. These tailings, originating from older gravity, flotation, and cyanidation operations, still contain sufficient silver and gold values to make their reprocessing attractive. The economics of retreating tailings look especially favorable: mining costs are minimal, and the processing does not require crushing and grinding. In some cases, however, additional grinding may be necessary to liberate residual silver values:

In general, residual silver values may be recovered by either flotation, cyanidation, or a combination of the two in which the flotation concentrates are ground and cyanided, with or without the flotation tailings. If cyanidation is the preferred or the ultimate process, silver extraction from leached pulp may be accomplished by

Table 12—Capital Cost Estimate Summary
Alternate I (Carbon-in-Pulp), and
Alternate II (CCD-Merrill Crowe)

	Alternate I	Alternate II
Total Direct Cost	\$1,737,730	\$2,029,300
Freight on Equipment (5% of equipment cost)	30,180	35,460
Indirect Cost (15% direct cost)	260,860	304,400
Total Direct plus Indirect Cost	2,028,570	2,369,160
Contingency (20% direct plus indirect)	405,710	473,830
Escalation (10% direct plus indirect)	202,860	236,920
Contractor's Overhead (2.5% direct plus indirect)	50,710	59,230
Contractor's Fee (8% direct plus indirect)	162,290	189,530
Total Estimated Installed Cost	\$2,850,140	\$3,327,670

Table 11—Cash Flow Analysis at Different Gold Prices Agitation Leach-CCD-Merrill Crowe Process (Thousands of Dollars)
(Ounces Gold recovered per Year—61,380¹)

	Price of Gold				
	\$80	\$100	\$120	\$140	\$160
Capital	15400	15400	15400	15400	15400
Net sales	4910	6138	7366	8593	9320
Costs and Expenses:					
Operating	4358	4358	4358	4358	4358
Mine amortization ²	42	42	42	42	42
Depreciation ³	2567	2567	2567	2567	2567
Depletion ⁴	737	921	1105	1289	1473
Total	7704	7888	8072	8258	8440
Operating Income	(2794)	(1750)	(706)	337	1380
Federal Income tax, 48%				162	662
Net Income	(2794)	(1750)	(706)	175	718
Cash flow	552	1780	3008	4073	4800
Payout in years	27.9	8.7	5.1	3.8	3.2
Rate of return, ⁵ %	Neg	Neg	5.4	18.7	23.5

Notes:

- (1) 0.04 oz gold per ton of ore, 93% recovery.
- (2) \$250,000 mine preproduction expense. Amortized in 6 yr.
- (3) Straight line depreciation. Life of mine, 6 yr.
- (4) Depletion—15% of net sales.
- (5) Average compound interest rate, discounted to present worth, to return the capital in full.

conventional countercurrent decantation (CCD) followed by Merrill-Crowe precipitation, or by the newly developed carbon-in-pulp process. This latter process is especially effective for slimy tailings which do not settle well and thus do not respond to the conventional CCD circuit. Recent applications of the carbon-in-pulp systems by Homestake^{3,4} both at Lead, S.D., for gold extraction from slimes, and at Creede, Colo., for silver extraction from flotation plant tailings, have demonstrated the operating as well as economic effectiveness of this process.

The fourth case history concerns the recovery of residual values from the tailings of a previous flotation plant operation. The tailings, amounting to about 4,000,000 tons, contain 2.0 oz per ton silver and 0.03 oz per ton gold. Laboratory tests indicated that 1.0 oz. per ton silver and 0.02 oz per ton gold are recovered by cyanidation of the tailings after regrinding. Flotation concentration, on the other hand, was not effective in reclaiming the residual values from the tailings.

Since cyanidation appears to be an attractive process for treating the tailings under investigation, a preliminary feasibility study is justified in determining the economic viability of the process. Also, since the laboratory tests had indicated the presence of appreciable slimes in

Table 13—Operating Cost per Ton of Tailings.
(300,000 tpy)

	Alternate I	Alternate II
Mining ¹	\$0.300	\$0.300
Supervision	0.170	0.170
Labor	0.340	0.259
Reagents:		
Lime—6.7 lb at \$0.02	0.134	0.134
Cyanide—0.6 lb at \$0.36	0.216	0.216
Charcoal—0.1 lb at \$1.05	0.105	
Steel Wool—0.01 lb at \$0.50	0.005	
Zinc Dust—0.04 lb at \$0.60		0.024
Flux	0.008	0.002
Power	0.239	0.248
Grinding balls, 1.5 lb at \$0.18	0.270	0.270
Fuel Oil	0.016	0.002
Maintenance—3% of Capital	0.281	0.333
Tailings Disposal ²	0.050	0.050
Miscellaneous Supplies	0.050	0.050
Total Operating Cost	\$2.184	\$2.058

Notes:

- (1) The tailings will be reclaimed by contract and dumped in receiving bin at mill.
- (2) Once each year it will be necessary to rise the tailings dam and the discharge line at an estimated cost of \$15,000.

40 \$160
100 15400
183 9320

158 4358
42 42
167 2587
189 1473
156 8440
137 1380
62 662
75 718
173 4800
3.8 3.2
6.7 23.5

In 6 yr.

to present

followed
y devel-
ss is es-
nt settle
nal CCD
ulp sys-
gold ex-
ilver ex-
onstrated
ss of this

ry of re-
fotation
ut 4,000,-
3 oz per
per ton
y cyanid-
concen-
reclaim-

process
prelimi-
the eco-
laboratory
slimes in

lings.

Alternate II

\$0.300
0.170
0.259
0.134
0.218
0.024
0.002
0.248
0.270
0.002
0.333
0.050
0.050
\$2.058

pumped in
illings dam
0,000.

Table 14—Financial Analysis for Treatment of Au-Ag Tailings (300,000 tpy)

	(Thousands of Dollars)	
	Alternate I	Alternate II
Capital	\$2850	\$3328
Net Sales ¹	1932	1932
Cost and Expenses:		
Total operating	655	617
Depreciation ²	428	500
Depletion ³	290	290
Total	1373	1407
Operating Income	559	525
Federal Income Tax ⁴	268	252
Net Income	291	273
Cash Flow ⁵	1009	1063
Pay-out in Years	2.8	3.1

Notes:

- (1) Net Sales:
Silver: 300,000 oz at \$4.00 per oz. = \$1200
Gold: 6000 oz at \$150.00 per oz. = 900
Total \$2100
Cost of refining Doré bullion (8%) 168
Net sales \$1932
- (2) Depreciation: Straight-line for 6.66 years of mine life.
- (3) Depletion: 15% of sales.
- (4) Federal income tax: 48% of operating income.
- (5) Cash flow: Net income plus depreciation and depletion.

the tailings, which resulted in a rather difficult-to-settle pulp, a carbon-in-pulp cyanidation appeared to be a more attractive alternative to conventional CCD-Merrill Crowe cyanidation procedure. For this reason, the current feasibility study includes the evaluation of both the above alternatives. Table 12 shows the capital cost estimate for the two alternates, while Table 13 gives the operating costs for the two procedures under consideration. The cash flow analysis for the two alternates is shown in Table 14.

As can be seen, both the above alternates for treating the gold-silver tailings appear to be promising, with the carbon-in-pulp system showing more favorable economics. It should be noted that for a seven-year mine life, a pay-out period of less than 3.5 years is considered economically attractive. Similarly, a profitability index of above 25% makes the mining venture economically viable.

Feasibility of In-Situ Leaching of Uranium

In-situ mining of lower-grade uranium ores has become increasingly attractive in recent years because of the favorable price of uranium in the free market. An in-place extraction technique of considerable promise is the so-called "borehole" mining which recovers uranium by drilling into the orebody, circulating a lixiviant fluid to dissolve the mineral, extracting uranium values from the pregnant solution, regenerating the lixiviant and finally, recycling the fluid. Such a technique is economically and environmentally attractive in extracting uranium values from deeper, lower-grade reserves.

In the evaluation of a block of uranium-mineralized zone as a potential producer by in-place leaching using the borehole mining technique, it is first necessary to establish a grade-thickness product which will cover development costs and operating costs with something left over for recovery of investment in plant and equipment and profit. This grade-thickness product is then a cutoff parameter for determination of whether a hole is included in reserves or excluded.

To calculate the grade-thickness product of a hole, it is necessary to establish a second cutoff, the grade at which operating costs are just covered. Amortization of development and plant and equipment costs are not included in calculating this grade. No sample interval of a grade less than this operating break-even grade can be

included in calculation of the grade thickness product of the hole for determination of the potential contribution of the hole to reserves.

Once the holes have been classified as potential ore or waste, the reserves in each potential block can be estimated, for example, by the ore outline method.

Development costs for determination of whether or not a hole is a potential contributor to ore, or not, include: (1) costs of drilling and casing injection and production wells; (2) pumps; (3) surface piping and electrical requirements to bring an ore block into production.

Operating costs in the field include: (1) operating and repair costs of injection of solvent and of reagent required to convert uranium minerals to soluble form; (2) operating and repair costs of pumping pregnant solution from formation to ion exchange plant.

Now an injection and production well pattern can be finalized and any necessary adjustments to development costs made. The capital cost for the piping to carry the solution from the ore blocks to the ion exchange plant, the capital cost of the ion exchange and precipitation plant, and other required equipment can be estimated.

A cash flow analysis is now made to determine whether the project has satisfactory profit potential. At this stage, it is necessary to arrive at a realistic estimate of the true thickness of strata which will be penetrated by solution. Large amounts of reagents will often be consumed in reactions in sub-ore grade zones above and below the "ore interval." Also, there will often be one or

Table 15—In-Situ Uranium Leaching Operation

Type of Operation	Borehole mining
Deposit	30-ft ore zone at 200-ft depth
Reserves	4,000,000-ton deposit at 0.1% U ₃ O ₈
Contained U ₃ O ₈	8,000,000 lb
Recoverable U ₃ O ₈	5,600,000 lb at 70% recovery
Plant Capacity	1,000,000 lb U ₃ O ₈ per yr 2,750 lb per day
Production Life	5.6 yr
Type Process	Ion exchange-precipitation
Type Leaching	Acid at 100 lb H ₂ SO ₄ per ton of ore
Leaching Rate	500 gpm
Solution Grade	0.45 gallons per liter U ₃ O ₈
Capital Cost, Leaching	\$1,500,000
Capital Cost, IX-PPT	\$2,700,000
Total Capital Cost	\$4,200,000
Operating Cost, Leaching	\$1.50 per lb U ₃ O ₈
Operating Cost, IX-PPT	\$2.00 per lb U ₃ O ₈
Total Operating Cost	\$3.50 per lb U ₃ O ₈
Cut-off Grade Based on:	
	Operating cost at \$8.00 per lb 0.031% U ₃ O ₈
	Operating cost at \$16.00 per lb 0.016% U ₃ O ₈
	Operating cost at \$24.00 per lb 0.010% U ₃ O ₈

Table 16—In-Situ Uranium Leaching Economics (Bore Hole Mining—IX-PPT) Cash Flow (In Thousands of Dollars)

	\$8/lb	Price of U ₃ O ₈		\$24/lb
		\$10/lb	\$4200	
Capital Cost	\$4200	\$4200	\$ 4200	\$ 4200
Net Sales (at 70% Extraction)	8000	8000	16,000	24,000
Net Sales (at 35% Extraction)				
Costs and Expenses:				
Total Operating	3500	3500	3500	3500
Depreciation	750	750	750	750
Depletion	1760	1760	3520	5280
Indirect Cost	175	175	175	175
Total	6185	6185	7945	9705
Operating Income	1815	1815	8055	14,295
Federal Income Tax	871	871	3866	6862
Investment Credit	294	294	294	294
Net Income	1238	1238	4483	7727
Cash Flow	3748	3748	8753	13,757
Pay-Out in Years	3.4	1.1	0.9	0.5
Return on Investment	30%	30%	107%	184%

Notes:

- (1) Depreciation, Straight-line, 5.6 yrs
- (2) Depletion, 22% of net sales
- (3) Indirect cost, 5% of total operating cost
- (4) Federal income tax, 48%
- (5) Investment credit, 7% of capital cost for the first year

more sub-ore zones within an ore interval which will also consume reagents.

As a general principle, it should be anticipated that even after careful geologic and engineering studies, and after months of actual experience in a field, it wouldn't yet be possible to predict leaching rates or total recovery from one block to the next with anything approaching accuracy. For example, one block may yield 120% of the estimated recoverable uranium in three to six months. The adjacent block, although apparently geologically identical, may never yield over 60% of its estimated recoverable uranium, regardless of the number of months it is leached. It is necessary, therefore, to be fairly generous in setting the pounds of U_3O_8 which must be present in a block to justify leaching.

Table 15 gives the details of the capital and operating costs for the third case-history involving the feasibility of extracting uranium values from a given sandstone deposit. Table 16 shows the financial analysis for the project under consideration.

As can be noted, the bore hole mining technique appears to be a very attractive method for extracting uranium from lower grade ores. Even at the old price of \$8.00 per lb, the return on investment is 30%. Similarly, the same return is obtainable at \$12.00 per lb of uranium with only 35% extraction, rather than the anticipated 70%.

References

- ¹ McAllister, Lewis, and Bhappu, "Leaching of Low Grade Gold Ores—Economic Evaluation of Available Processes," Paper presented at the AIME Annual Meeting, Dallas, February 1974.
- ² Bhappu and Lewis, "Gold Extraction From Low Grade Ores—

Economic Evaluation of Processes," *Min. Cong. J.*, January 1975, pp. 38-41.

³ Hall, Kenneth B., "Homestake Carbon-in-Pulp Process," Presented at local AIME meeting, Lead, S.D., July 1974.

⁴ Salisbury, et al. "Silver Recovery From Flotation Trails by Carbon-in-Pulp Cyanidation," Paper presented at the AIME Annual Meeting, New York, February 1975.

About the Authors

F. Milton Lewis is an internationally known mining and metallurgical engineer. For the past five years, he has been a consultant in both of these categories of expertise to Mountain States Mineral Enterprises, Inc. (P.O. Box 17960, Interstate 10 & Vail Rd., Tucson, AZ 85731). For many years prior, he served as assistant to the general manager of the Copperhill, Tenn., operations of Cities Service Co. Before that, "Doc" Lewis was superintendent of mills with the responsibility for the various concentrators operated by Cities Service in the Copperhill area.



Roshan B. Bhappu is vice-president and general manager of Mountain States Research & Development, a subsidiary of MSME. He holds a D.Sc. in metallurgy and mining and an M.S. in metallurgical engineering from Colorado School of Mines. Before joining MSME, Dr. Bhappu was senior metallurgist at the New Mexico State Bureau of Mines and Mineral Resources, research professor at New Mexico Institute of Mining and Technology, and resident metallurgist at Miami Copper Co. A member of several professional organizations, and extremely active in SME-AIME affairs, Dr. Bhappu is listed in American Men of Science and is a special consultant to the United Nations.



The Greening of the Oquirrh

Christine Alexander, Environmental Editor



Twenty years ago, the northern Oquirrh Mountains overlooking Salt Lake City were bare. Heavy logging and overgrazing combined with erosion and uncontrolled forest fires had severely denuded the mountains by the turn of the century. As a final coup de grace, a copper smelter was built there in 1906, and for the next 50 years its sulfurous fumes killed off what little vegetation remained.

In 1956, Paul Rokich, a biology student at the University of Utah, started to surreptitiously restore the mountains. For the next 17 years, Rokich devoted his spare time and money to replanting the Oquirrh, with the result that several thousand acres of the mountains are green again, and animals have returned: deer, elk, and rabbits thrive among olive, maple, and fruit trees, wheat grass, and sunflowers.

Working Alone

For the first four years, Rokich carried out his work without the knowledge of the smelter officials—trespassing on their land in the dead of night to plant experimental plots of grasses and shrubs. He would leave his car where no one could see it, and then hike into

Paul Rokich examines black locust trees growing in the Kennecott greenhouse on the University of Utah campus. The trees will later be planted around Kennecott's smelter in the Oquirrh Mountains overlooking Salt Lake City.

The Effect of Nonelliptical Cracks on the Compressibility of Rocks

GERALD M. MAVKO AND AMOS NUR

*The Rock Physics Project, Department of Geophysics, Stanford University, Stanford, California 94305*SUBJ
MNG
ENCC

Dislocation theory is used to study the deformation of nonelliptical thin cracks in a loaded elastic material. The cracks considered are two-dimensional with nonblunted, tapered ends such that opposite faces are tangent to each other at points of contact. Under compression the cracks shorten by closing near the crack tips, the proportion of crack surface area in contact becoming gradually larger. Some cracks make contact between the crack tips, becoming multiple cracks. Normal stresses on the crack surface vary rapidly over the closed portions from zero near the open surfaces to a peak value at the original crack tip. Stresses remain finite everywhere. At a given load the effective rock compressibility due to arbitrarily shaped, tapered cracks depends only on crack length, giving results identical to a distribution of elliptical cracks of the same lengths. However, at different loads the varying length causes the modulus to vary. As a result, interpretation of features like porosity and modulus under varying applied stress will depend on the specific crack model chosen. In particular, a single aspect ratio of a simply tapered crack yields the same nonlinear effect as a flat distribution of elliptical cracks. Consequently, estimates of crack spectra from nonlinear strain data are totally nonunique.

INTRODUCTION

The mechanical behavior of rocks depends strongly upon the geometry of pore space. In particular, long narrow cracks, ranging from microcracks to joints and fractures, can drastically reduce the effective moduli of a rock system. The closing of microcracks, for example, can account for the typically observed increase in modulus with increasing confining pressure below several kilobars [Birch, 1960; Brace, 1965; Simmons *et al.*, 1974]. Similarly, Nur [1971] attributed the directional dependence of seismic velocity in nonhydrostatically stressed samples to the anisotropic closure of cracks.

Theoretical models for the mechanical behavior of rocks containing cracks (both dry and fluid saturated) have been presented by a number of authors. Many of these models incorporate the known analytic solution for the deformation of individual cracks under applied stress. Consequently, only two-dimensional elliptical cracks and three-dimensional ellipsoidal cracks have been considered [Walsh, 1965a; O'Connell and Budiansky, 1974; Budiansky and O'Connell, 1976], since solutions for more realistic crack shapes are generally not available in closed form. The more general problem of an ellipsoidal elastic inclusion [Eshelby, 1957; Kuster and Toksöz, 1974] has the dry or fluid-saturated crack as a special case.

Both visual inspection and common sense suggest that almost no cracks in situ are ellipsoidal cavities. We expect that instead, typical cracks are irregular in shape, possessing in particular a wide range of edge configurations. Cracks may terminate with blunt edges, such as the ellipsoidal case, or with very fine edges, such as those at a contact of two slightly irregular parallel surfaces. The compliance of the latter cracks over a range of pressures will be quite different from that of ellipsoidal ones, leading to a different overall stress-strain behavior of the rock. It is therefore important to determine the elastic response of a rock with nonellipsoidal cracks and compare the results with the ellipsoidal case.

In this paper we examine the influence of a broad class of nonelliptical, two-dimensional cracks on the effective compressibility of rocks. In the section that follows we compute the deformation of an almost arbitrarily shaped thin crack using the well-developed theory of elastic dislocations. A particularly simple set of closed form polynomial solutions is

obtained in a manner similar to that of Delameter [1974]. In the next section the effective compressibility is computed as a function of crack deformation. The general case as well as specific examples are presented. The remainder of the paper gives a discussion of the model in comparison with the elliptical crack results, including the interpretation of a typical stress-strain curve.

CALCULATION OF CRACK DEFORMATION
UNDER HYDROSTATIC PRESSURE

We approximate the rock as an isotropic elastic solid containing a distribution of randomly oriented (dry) cracks or pores of the type shown schematically in Figure 1. For mathematical convenience the pores are treated as two-dimensional cracks in plane strain, and the separate pores are assumed not to interact. Furthermore, only flat planar cracks are considered, with aspect ratio $\alpha \ll 1$ (where $\alpha = b/c$ and c and b are the half length and maximum half width of the crack). By limiting our study to flat, two-dimensional cracks we can easily solve for the crack deformation under varying hydrostatic pressure by applying two-dimensional elastic dislocation theory [Bilby and Eshelby, 1968; Landau and Lifshitz, 1959].

The problem of opening a crack under tension is conceptually simpler and more conveniently posed than the problem of crack closing under pressure. Therefore in the derivation of crack closure that follows we first close the crack with a large confining pressure and then study the crack shape as the stress is relaxed. For hydrostatic stress the crack shape is a single-valued function of applied stress, so that the crack closing problem is exactly equivalent to the opening problem.

Consider a thin crack of shape $U_0(x)$ and length $2c_0$ (Figure 1), where $U_0(x)$ and dU_0/dx are continuous functions of x . (We define these as the reference state of zero stress and strain regardless of the stress history leading to the formation of U_0 .) In our analysis we will emphasize nonblunted cracks with tapered ends such that $dU_0(\pm c_0)/dx = 0$. The effect of these cracks will be compared specifically with elliptical cracks for which solutions already exist [Walsh, 1965a; Berg, 1965].

Imagine that a hydrostatic stress $-P'$ (stress is defined as being positive in tension) is applied that is just great enough to close the crack completely. The strain field is a superposition of the uniform hydrostatic strain and the perturbation due to the closed crack. This perturbation is just the strain field due to

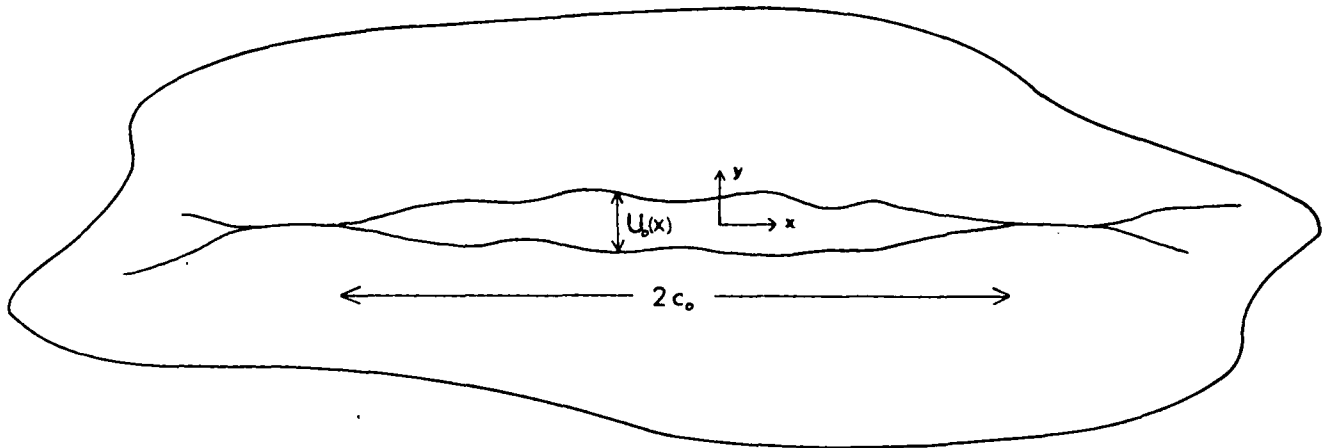


Fig. 1. A flat two-dimensional crack with tapered ends. The width, given by $U_0(x)$, is shown exaggerated.

a continuous distribution of infinitesimal elastic edge dislocations with density function

$$B_0(x) = (d/dx)U_0(x) \tag{1}$$

Likewise, the stress field is given by

$$\sigma_{ij} = -P'\delta_{ij} + \sigma_{ij}^c$$

where σ_{ij}^c is the stress due to the closed crack. In particular, the normal stress on the plane $y = 0$ is

$$\sigma_0(x) = -P'(x) + \sigma_0^c(x)$$

where

$$\sigma_0^c(x) = \frac{\mu}{2\pi(1-\nu)} \int_{-c_0}^{c_0} \frac{B_0(z)}{x-z} dz \tag{2}$$

[Bilby and Eshelby, 1968]. Here μ is the intrinsic shear modulus of the rock material and ν is Poisson's ratio. Because $U_0(x)$ is smooth and $B_0(\pm c_0) = 0$, the stresses are finite everywhere including the crack tips, and $\sigma_0^c \rightarrow 0$ very far from the crack.

If the hydrostatic stress is now slightly relaxed by an amount τ (which is equivalent to superimposing a tension τ), the crack will begin to reopen over a region $-c < x < c$, where $c \leq c_0$, with shape $U(x, P)$, where $P = (P' - \tau)$. (We have assumed for simplicity that the original crack is symmetric, i.e., $U_0(x)$ is an even function of x . This assures that the deformed crack at any value of $P \geq 0$ is also symmetric.) The crack opening $U(x, P)$ at this point can be thought of as a new distribution of infinitesimal elastic edge dislocations with density function

$$B(x, P) = -\partial U(x, P)/\partial x \tag{3}$$

The problem of finding the deformed crack shape reduces to finding the distribution of dislocations $B(x, P)$ subject to the conditions that the opened crack faces are stress free, i.e.,

$$\sigma_0 + \tau + \sigma^c = 0 \quad |x| \leq c \tag{4}$$

where σ^c is the stress due to the crack opening dislocations:

$$\sigma^c = \frac{\mu}{2\pi(1-\nu)} \int_{-c}^c \frac{B(z, P)}{x-z} dz \tag{5}$$

and $U(x, P) = B(x, P) = 0$ for $|x| \geq c$. The density function $B(x, P)$ is found by solving the integral equation obtained by combining (4) and (5):

$$\int_{-c}^c \frac{B(z, P)}{x-z} dz = -\frac{2\pi(1-\nu)}{\mu} [\sigma_0^c(x) - P] \quad |x| \leq c \tag{6}$$

where the right-hand side of (6) is a known function of the original crack shape $U_0(x)$ and the applied hydrostatic pressure P . The condition that a solution to (6) exist with finite stresses everywhere is given by [Muskhelishvili, 1953]

$$\int_{-c}^c \frac{\sigma_0^c(x) - P}{(c^2 - x^2)^{1/2}} dx = 0$$

Using the integral ((B3), see Appendix B), this becomes

$$P = \frac{1}{\pi} \int_{-c}^c \frac{\sigma_0^c(x)}{(c^2 - x^2)^{1/2}} dx = \frac{\mu}{2\pi^2(1-\nu)} \int_{-c}^c \frac{1}{(c^2 - x^2)^{1/2}} \int_{-c_0}^{c_0} \frac{dU_0(z)}{dz} (x-z)^{-1} dz dx \tag{7}$$

For a given original crack shape U_0 with length $2c_0$, (7) gives a relation between the applied hydrostatic pressure P and the reduced length c . We will see with some numerical examples in a later section that for cracks with tapered ends (i.e., no stress singularities), crack closing from hydrostatic stress is accompanied by crack shortening.

The solution of (6) is given by

$$B(x, P) = \frac{2(1-\nu)}{\pi\mu} (c^2 - x^2)^{1/2} \int_{-c}^c \frac{\sigma_0^c(z) - P}{(x-z)(c^2 - z^2)^{1/2}} dz \quad |x| < c \tag{8}$$

[Muskhelishvili, 1953], where c is given by (7). The actual crack shape is found by integrating $-B(x, P)$:

$$U(x, P) = \frac{-2(1-\nu)}{\pi\mu} \int_{-c}^x (c^2 - t^2)^{1/2} \int_{-c}^c \frac{\sigma_0^c(z) - P}{(t-z)(c^2 - z^2)^{1/2}} dz dt \quad |x| < c \tag{9}$$

Equations (8) and (9) can be slightly simplified by dropping P (or adding any constant) from the integrand, since

$$\int_{-c}^c \frac{dz}{(t-z)(c^2 - z^2)^{1/2}} = 0 \quad |t| < |c|$$

Hence the shape $U(x, P)$ is determined by (9) once half length c is specified.

The normal stress on the plane $y = 0$ is zero over range $|x| < c$, but for $|x| > c$ it is given by

$$\sigma = \sigma_0^c - P + \sigma^c \tag{10}$$

Substituting for σ_0^c and σ^c from (2) and (5), this gives

$$\sigma = -P + \frac{\mu}{2\pi(1-\nu)} \int_{-c_0}^{c_0} \frac{B_0(z) + B(z, P)}{x-z} dz \quad (11a)$$

$|x| > c$

or

$$\sigma = -P + \frac{\mu}{2\pi(1-\nu)} \int_{-c_0}^{c_0} \frac{\partial}{\partial z} \frac{[U_0(z) - U(z, P)]}{x-z} dz \quad (11b)$$

$|x| > c$

where $B(x, P) = U(x, P) = 0$ for $c \leq |x| \leq c_0$.

It should be pointed out that (7), (9), and (11) are strictly valid only for single isolated cracks. As we will see in a later section, certain cracks make contact at their centers before completely closing, forming two adjacent cracks. In this case, (7), (9), and (11) apply only before the center makes contact. More general expressions for the multiple-crack cases are given in Appendix A.

Levels of applied stress outside the range $-P' \leq \sigma \leq 0$ (i.e., outside the range $0 \leq P \leq P'$), where $-P'$ is the closing stress (or P' is the closing pressure) require additional care. Crack deformation in tension with respect to the reference state of stress cannot be found unless additional information is given for the stress or strength in the plane $y = 0$ for $|x| > c_0$. On the other hand, calculation of the stress and strain fields for levels of compression greater than the crack closing pressure, i.e., $P > P'$, are straightforward. The strain field for continued hydrostatic loading after crack closure is the superposition of the uniform hydrostatic strain due to P and the strain due to the distribution of dislocations $B_0(x)$. Likewise, the stress field is given by $\sigma_{ij} = -P\delta_{ij} + \sigma_{ij}^c$, where σ_{ij}^c is the stress due to the closed crack. In particular, the normal stress on the plane $y = 0$ is

$$\sigma_0(x) = -P + \sigma_0^c(x)$$

where σ_0^c is given by (2).

Equations (2)-(11) can be quite difficult to evaluate for arbitrary crack shapes, usually requiring numerical solution. However, a broad class of analytic solutions can almost trivially be found when polynomials are used to express U_0 and σ_0^c . In particular, the properties of Chebyshev polynomials simplify considerably the necessary integral relations. Such closed form solutions are useful in quickly assessing the effects of various crack features on the properties of rocks. In the remainder of this section a specific method of polynomial solution of the crack problem is discussed, and two simple illustrative examples of crack closure are presented.

When the crack shape $U_0(x)$ is smooth with tapered ends and continuous derivative $B_0(x)$, the corresponding $\sigma_0^c(x)$, given by (2), is continuous and finite over the interval $-c_0 \leq x \leq c_0$. We can therefore approximate σ_0^c to arbitrary accuracy over this interval by a polynomial of sufficiently large degree n :

$$\sigma_0^c(x) \approx R_n(x) = \sum_{k=0}^n r_k x^k \quad |x| \leq c_0 \quad (12)$$

where the r_k are constants. (For simplicity we once again assume symmetric cracks.) For computational purposes this polynomial form for $\sigma_0^c(x)$ is a convenient starting point for generating crack solutions (as well as for other dislocation applications like fault slip). However, it is often necessary or desirable to start with a prescribed crack shape $U_0(x)$. In this

case the function σ_0^c can be obtained from (2) by using a numerical Hilbert transform. Alternatively, the shape $U_0(x)$ can be approximated with some convenient form like

$$U_0(x) \approx (c_0^2 - x^2)^{1/2} S_m(x)$$

where $S_m(x)$ is an even polynomial such that the derivative $B_0(\pm c_0) = 0$. The Hilbert transform, (2), can then easily be found by using (16).

With the polynomial form, (12), in hand, the relation between applied pressure and crack length, (7), becomes

$$P = \frac{1}{\pi} \sum_{\substack{k=0 \\ \text{even}}}^n r_k c^k \gamma_k \quad (13)$$

where the constants γ_k are given in Appendix B. Similarly, the expression (equation (8)) for $B(x, P)$ becomes

$$B(x, P) = \frac{-2(1-\nu)}{\mu} \left[1 - \left(\frac{x}{c} \right)^2 \right]^{1/2} \cdot \sum_{\substack{k=2 \\ \text{even}}}^n b_k U_{k-1} \left(\frac{x}{c} \right) \quad |x| \leq c \quad (14)$$

where the $U_n(x)$ are Chebyshev polynomials of the second kind [Hochstrasser, 1964] and the constants b_n are defined in Appendix B. Finally, the crack shape $U(x, P)$ is found by integrating (14):

$$U(x, P) = \frac{2(1-\nu)}{\mu} \int_{-c}^x \left[1 - \left(\frac{t}{c} \right)^2 \right]^{1/2} \cdot \sum_{\substack{k=2 \\ \text{even}}}^n b_k U_{k-1} \left(\frac{t}{c} \right) dt \quad |x| \leq c \quad (15)$$

In order to find the normal stress on $y = 0$ outside the crack opening this expression for B is substituted into (5) and (10):

$$\sigma = \sigma_0^c - P - \frac{1}{\pi} \int_{-c}^c \frac{[1 - (z/c)^2]^{1/2}}{x-z} \cdot \sum_{\substack{k=2 \\ \text{even}}}^n b_k U_{k-1} \left(\frac{z}{c} \right) dz \quad |x| > c \quad (16)$$

The last term in (16) is given by

$$\text{sgn}(x) \left\{ \left[\left(\frac{x}{c} \right)^2 - 1 \right]^{1/2} \sum_{\substack{k=2 \\ \text{even}}}^n b_k U_{k-1} \left(\frac{x}{c} \right) - Q(x) \right\} \quad |x| > c$$

where $Q(x)$ is a polynomial obtained by expanding $[(x/c) - 1]^{1/2}$ as a polynomial in x , multiplying term by term with $\sum b_k U_{k-1}(x/c)$ and discarding all negative powers of x [Muskhelishvili, 1953]. The same technique is used to find $\sigma_0^c(x)$ for $|x| > c_0$.

To illustrate some important features of nonsingular crack closure, two simple crack shapes are now computed. Consider a crack of the form

$$U_0(x) = 2b[1 - (x/c_0)^2]^{3/2} \quad (17)$$

where c_0 is the crack half length and b is the maximum half width. From (2) the stress $\sigma_0^c(x)$ is computed:

$$\sigma_0^c(x) = - \frac{3\mu b}{\pi(1-\nu)c_0} \int_{-c_0}^{c_0} \frac{z [1 - (z/c_0)^2]^{1/2}}{x-z} dz$$

Integrals of this form can be evaluated by expressing the polynomial factor in the integrand in terms of Chebyshev polynomials U_n and using (B5) (see Appendix B).

Hence σ_0^c becomes

$$\sigma_0^c(x) = \frac{-3\mu b}{2(1-\nu)c_0} \left[2\left(\frac{x}{c_0}\right)^2 - 1 \right] \quad |x| \leq c$$

which is of the convenient polynomial form given by (12). Substituting this expression into (13), we obtain the relation between applied pressure P and crack length c :

$$P = \frac{-3\mu b}{2(1-\nu)c_0} \left[\left(\frac{c}{c_0}\right)^2 - 1 \right] \quad (18a)$$

or

$$c = c_0 \left[1 - \frac{2(1-\nu)c_0}{3\mu b} P \right]^{1/2} \quad (18b)$$

Finally, the deformed crack shape is obtained from (15):

$$U(x, P) = 2b(c/c_0)^2 [1 - (x/c)^2]^{3/2} \quad |x| \leq c \quad (19)$$

From (19) we see that at crack closure, i.e., $U \rightarrow 0$, the crack length $c \rightarrow 0$. Substituting $c = 0$ into (18), we obtain the closing pressure P' :

$$P' = \frac{3\mu b}{2(1-\nu)c_0} = \frac{3}{4(1-\nu^2)} \alpha_0 E$$

where α_0 is the original aspect ratio b/c and E is Young's modulus. This is consistent with the usual rule of thumb that the crack closing pressure is numerically $\sim \alpha_0 E$. The exact numerical factor will vary with the crack shape. In comparison, Berg [1965] found that the pressure required to close an elliptical crack of aspect ratio α_0 is

$$P_e' = \frac{1}{2(1-\nu^2)} \alpha_0 E$$

The ratio of tapered crack closing stress to elliptical crack closing stress for identical aspect ratios is

$$P'/P_e' = 3/2$$

Hence the tapered crack is stiffer than an elliptical crack of the same dimensions, in terms of the closing stress.

The stress on $y = 0$ outside the crack is computed from (16):

$$\sigma = -P' 2 \left(\frac{c}{c_0}\right) \left(\frac{x}{c_0}\right) \operatorname{sgn}(x) \left[\left(\frac{x}{c}\right)^2 - 1 \right]^{1/2} \quad c \leq |x| \leq c_0$$

$$\sigma = -P' 2 \left(\frac{x}{c_0}\right) \operatorname{sgn}(x) \left\{ \left(\frac{c}{c_0}\right) \left[\left(\frac{x}{c}\right)^2 - 1 \right]^{1/2} - \left[\left(\frac{x}{c_0}\right)^2 - 1 \right]^{1/2} \right\} \quad |x| \geq c_0$$

where $-P'$ is the closing stress.

Figure 2a shows the crack shape, (19), plotted for several levels of applied stress. The most prominent feature of the deformation is the crack shortening accompanying closing. For example, the inner contour (Figure 2a) shows the crack at 0.75 of the closing pressure. In this case the crack width is reduced to ~ 0.1 of the original width, while the crack length is reduced by a half. The relative changes in width and length are described by the aspect ratio α , where $\alpha = U(0, P)/c$ and is obtained from (18) and (19):

$$\alpha = \alpha_0(c/c_0)^2 = \alpha_0 [1 - (P/P')]$$

Here α_0 is the original aspect ratio. As suggested by the figure, α decreases (the crack gets flatter) with increasing pressure. Although both $U(0, P)$ and c approach zero with closing, their ratio also goes to zero.

A major consequence of the crack shortening under pressure is the elimination of stress singularities at the crack tips, which occur, for example, with an infinitesimally thin elliptical crack. Bounded stress concentrations, however, do appear. Figure 2b shows the normal stress on the plane $y = 0$ plotted for several levels of applied stress. For all open cracks the stress over $|x| < c$ is zero, as expected for free surfaces. Over the range $c < |x| < c_0$ the stress rapidly increases to a peak compressive stress at the original crack tip, greater than the applied pressure. For $|x| > c_0$ the stress falls off and asymptotically approaches the applied stress far from the crack. In each case the stress is quite nonuniform over the closed portions of the crack. This result differs substantially from the case of an elliptical crack which does not shorten under pressure. Berg [1965] and Walsh [1965b] have extended the solution for elliptical crack deformation to pressures at which an elliptical crack is effectively closed. Their results suggest that an elliptical crack closes uniformly over its entire length and that the normal stress over the closed crack faces is uniform. Such extrapolations of linear elastic solutions must be viewed with caution, since strains are not infinitesimal at the crack tip. Nevertheless, the uniform stress result has been used to compute the frictional sliding of crack faces under applied deviatoric stress [Walsh, 1965b, 1966].

As a second example, consider a crack with shape

$$U_0(x) = 2b \left[1 - 0.3 \left(\frac{x}{c_0}\right)^2 - 1.3 \left(\frac{x}{c_0}\right)^4 \right] \left[1 - \left(\frac{x}{c_0}\right)^2 \right]^{1/2}$$

where c_0 is the crack half length and b is the maximum crack half width. The dislocation stress corresponding to the closed crack is obtained from (2):

$$\sigma_0^c(x) = \frac{-10\mu b}{41(1-\nu)c_0} \left[27 \left(\frac{x}{c_0}\right)^4 - 12 \left(\frac{x}{c_0}\right)^2 + \frac{33}{8} \right]$$

which is once again in the convenient polynomial form given by (12). The relation between applied stress and crack length is given by

$$P = \frac{-\mu b}{(1-\nu)c_0} \frac{10}{41} \left[\frac{81}{8} \left(\frac{c}{c_0}\right)^4 - 6 \left(\frac{c}{c_0}\right)^2 - \frac{33}{8} \right] \quad (20)$$

Finally, the deformed crack shape is

$$U = \frac{-2b}{41c_0} \left\{ 54 \left(\frac{x}{c_0}\right)^4 + \left[27 \left(\frac{c}{c_0}\right)^2 - 40 \right] \left(\frac{x}{c_0}\right)^2 + \left[-81 \left(\frac{c}{c_0}\right)^4 + 40 \left(\frac{c}{c_0}\right)^2 \right] \right\} (c^2 - x^2)^{1/2} \quad (21)$$

Figure 3 shows the crack shape, (21), plotted for several levels of applied stress. Once again the crack shortens as it closes, although the shortening is slower than that in the previous example. In addition, as the applied pressure increases, the crack faces touch in the center, forming two adjacent cracks, before completely closing. The overall crack width at this stage is obtained by setting $x = 0$ in the expression for U in (21) and equating $U = 0$, giving $c = 0.7c_0$. Using this value in (20), the applied pressure causing initial contact is

$$P' = 1.12\mu b / (1-\nu)c_0$$

Deformation beyond initial contact cannot be described with

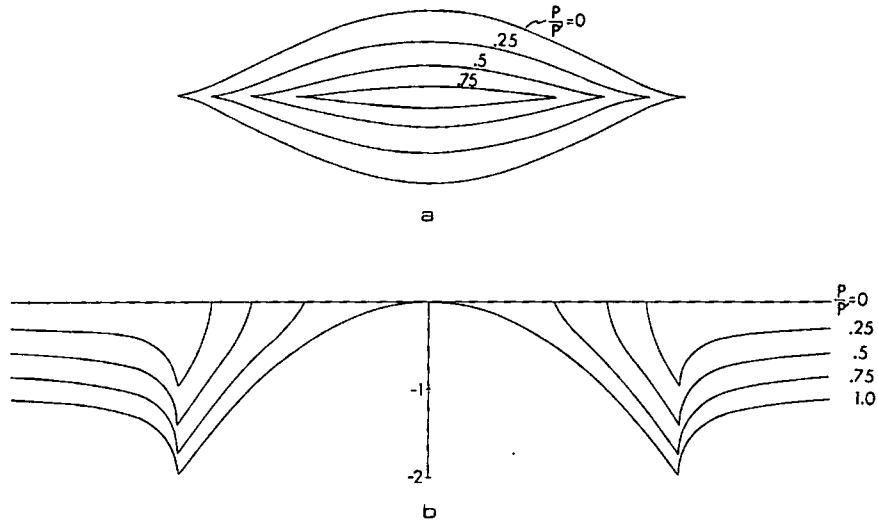


Fig. 2. (a) The deformation of a simple crack under several values of applied pressure P . (b) The normal stress in the plane of the crack for the same values of applied pressure.

the single-crack expressions in (20) and (21). The multiple-crack theory outlined in Appendix A can, in principle, be used to extend the results. However, the simple solutions made possible for single cracks by the Chebyshev polynomials are no longer available. Nevertheless, we expect qualitatively that the normal stress on the closed portions of the crack will increase from zero at the crack tips to peak stress concentrations at the center as well as at the original crack tips, with a falloff to the applied stress far from the crack. The central contact should result in an abrupt stiffening of the crack and rock at the contact stress.

CALCULATION OF BULK MODULUS

To find the effective bulk modulus of the porous rock, we follow the example of Walsh [1965b] and Jaeger and Cook [1969] and use the Betti-Rayleigh reciprocity theorem. The theorem states that for an elastic body acted upon separately by two sets of tractions, the work done by the first set of tractions acting through the displacements produced by the second set of tractions is equal to the work done by the second set of tractions acting through the displacements produced by the first set of tractions.

To apply the reciprocity theorem, consider the two sets of tractions shown in Figure 4. The rock with volume V has a distribution of N noninteracting flat cracks of the type shown in the figure. The system on the left is loaded by an externally applied stress, $-\delta P$, resulting in crack deformation $\delta U(x)$. The crack faces are stress free. (The deformation $\delta U(x)$ is an incremental change in crack shape defined as being positive in opening and is given by $\delta U(x) = \delta P \cdot [\partial U(x, P) / \partial P]$.) The system on the right has the same uniform stress, $-\delta P$, applied to both the external surface and the crack faces. In this case the system, at least externally, behaves like a solid block without cracks. Applying the reciprocity theorem, we can write

$$\delta P \cdot \frac{\delta P}{K} V = \delta P \cdot \frac{\delta P}{K'} V + \delta P \sum_{i=1}^N d_i \int_{-c_i}^{c_i} \delta U_i(x) dx$$

where V is the volume of the rock sample, K is the intrinsic bulk modulus of rock material, K' is the effective bulk modulus of the porous rock, and d_i is the crack length into the page of the i th crack. The summation is over all cracks in the rock.

Rearranging the equation, we obtain

$$\frac{1}{K'} = \frac{1}{K} - \frac{1}{V} \sum_{i=1}^N d_i \int_{-c_i}^{c_i} \frac{\delta U_i}{\delta P} dx$$

which gives the effective compressibility (equal to the inverse effective bulk modulus) in terms of the crack deformation δU , as found in the previous section. In the limit as $\delta P \rightarrow 0$, the effective compressibility becomes

$$\frac{1}{K'} = \frac{1}{K} - \frac{1}{V} \sum_{i=1}^N d_i \int_{-c_i}^{c_i} \frac{\partial U_i(x)}{\partial P} dx \tag{22}$$

Since $U(x, P) = 0$ at $x = \pm c$, the derivative can be taken outside the integral. Hence (22) can be written as

$$\frac{1}{K'} = \frac{1}{K} - \sum_{i=1}^N \frac{d_i}{V} \frac{d}{dP} \int_{-c_i}^{c_i} U(x, P) dx \tag{23}$$

As an example, consider the case of a rock containing a distribution of N identical cracks of the form given by (17) and plotted in Figure 2. To find the compressibility at some level of applied stress P , we compute the derivative

$$\frac{\partial U}{\partial P} = \frac{\partial U / \partial c}{dP / dc}$$

where P and U are given by (18) and (19). Therefore

$$\frac{\partial U}{\partial P} = - \frac{2c(1 - \nu)}{\mu} \left[1 - \left(\frac{x}{c} \right)^2 \right]^{1/2}$$

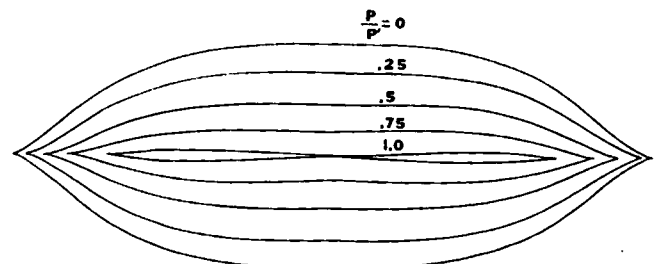


Fig. 3. The deformation of a tapered crack which makes contact in its center before completely closing.

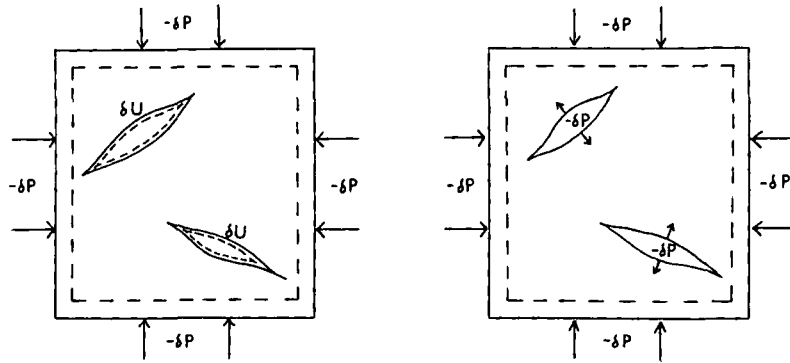


Fig. 4. Two sets of applied stresses and the resulting displacements on a rock with a distribution of cracks.

Substituting into (22), the compressibility becomes

$$\frac{1}{K'} = \frac{1}{K} + \frac{N}{V} \frac{(1 - \nu)}{\mu} \pi c^2 d$$

or, expressing μ in terms of K , as

$$\frac{1}{K'} = \frac{1}{K} \left[1 + \frac{2\pi}{3} \frac{(1 - \nu^2)}{(1 - 2\nu)} \frac{Nc^2d}{V} \right] \tag{24}$$

The effective compressibility given by (24) is a function only of the crack dimensions c and d and the number of cracks N . In fact this result is exactly the same as that for an elliptical two-dimensional crack in plane strain with the same dimensions [Walsh, 1965a; Jaeger and Cook, 1969]. The generality of this result is shown as follows.

Suppose that the rock contains a distribution of noninteracting, arbitrarily shaped, flat nonsingular cracks with dimensions c and d . Using (3), we can write

$$\begin{aligned} \frac{\partial U(x, P)}{\partial P} &= - \int_{-c}^x \frac{\partial B(z, P)}{\partial P} dz - \frac{\partial c}{\partial P} \cdot B(-c, P) \\ &= - \int_{-c}^x \frac{\partial B(z, P)}{\partial P} dz \end{aligned} \tag{25}$$

since $B(\pm c, P) = 0$. It can be shown (Appendix C) for arbitrary (symmetric) flat, tapered cracks that

$$\frac{\partial B}{\partial P} = - \frac{2(1 - \nu)}{\mu} \frac{x}{(c^2 - x^2)^{1/2}} \tag{26}$$

Therefore substituting (26) into (25), we obtain

$$\frac{\partial U(x, P)}{\partial P} = \frac{-2(1 - \nu)}{\mu} (c^2 - x^2)^{1/2} \tag{27}$$

Finally, using (27) in (22), the compressibility can be written as

$$\frac{1}{K'} = \frac{1}{K} + \frac{\pi(1 - \nu)}{\mu} \frac{Nc^2d}{V}$$

or, expressing μ in terms of ν and K , as

$$\frac{1}{K'} = \frac{1}{K} \left[1 + \frac{2\pi}{3} \frac{(1 - \nu^2)}{(1 - 2\nu)} \frac{Nc^2d}{V} \right] \tag{28}$$

Once again the compressibility given by (28) for an arbitrary shape is exactly the same as that for a distribution of flat 2-D elliptical cracks in plane-strain with the same dimensions. This is a remarkable result which says that although different crack shapes deform and shorten differently under varying levels of hydrostatic stress, the overall compressibility at any given value of stress is independent of crack shape (assuming flat,

symmetric, noninteracting, nonsingular 2-D cracks). Hence any convenient crack shape, including the ellipse, can be used for computing the compressibility in terms of the crack dimensions. However, as a consequence, nothing about crack shape can be inferred from the compressibility at a single value of pressure.

The result that dry rock compressibility is independent of crack shape is perhaps hinted at by the results of Walsh [1965a] and O'Connell and Budiansky [1974] that the effect of ellipsoidal cracks on moduli is independent of aspect ratio. However, it has not been previously demonstrated that the numerical coefficients remain the same when nonellipsoidal shapes are modeled. A complementary result by O'Connell and Budiansky [1974] which should be distinguished from this discussion of (2-D) cross-sectional shapes is that moduli appear to be very weakly dependent on the plan view crack shape as long as their density is characterized by

$$\epsilon = (2N/\pi)(A^2/P)$$

Here N is the number of cracks, A is the crack area, and P is the crack perimeter.

DISCUSSION

The derivation of effective compressibility in the previous section is based upon the calculated incremental volumetric strain $d\epsilon$ resulting from infinitesimal excursions of stress $d\sigma$ about a given hydrostatic load, i.e.,

$$d\sigma = K' d\epsilon \tag{29}$$

Such excursions might result, for example, from passing a wave through a statically loaded sample; the incremental modulus would ideally be the local slope of the quasi-static stress-strain loading curve. However, in practice the agreement between the static and the dynamic modulus is often poor.

To trace out the entire stress-strain curve, we substitute the crack-dependent effective bulk modulus into (29) and integrate:

$$\int_0^\epsilon d\epsilon = \epsilon = \frac{1}{K} \int_0^{-P} \left[1 + \frac{2\pi}{3} \frac{(1 - \nu^2)}{(1 - 2\nu)} \sum_{i=1}^N \frac{c_i^2 d_i}{V} \right] d\sigma \tag{30}$$

An essential feature of the penny-shaped crack or 2-D elliptical crack model considered by Walsh [1965a] is that while a given crack is open, its length c is independent of stress. Hence over any interval of stress in which no cracks close, the integrand of (30) is a constant, and stress-strain relation is linear. If we generalize to nonelliptical shapes but constrain the crack length to be constant, the stress-strain relation remains linear. When the increasing applied pressure reaches the closing pres-

sure of one or a set of elliptical cracks (the closing pressure is determined by the shape and aspect ratio), those cracks suddenly stop contributing to the summation in (30), and the compressibility takes a discontinuous jump. The jump will be small if only one of many cracks closes at a time. Hence a distribution of elliptical cracks can give an approximately 'continuous' compressibility. In fact, with this model the only way to achieve a smoothly varying compressibility is to have a smooth distribution of aspect ratios. For a more detailed discussion of the relation between aspect ratio distribution and the pressure dependence of elastic constants, see Nur [1971] and Simmons *et al.* [1974].

Nonsingular cracks, on the other hand, change length with varying stress. Hence the integrand in (30) is not constant, and the stress-strain curve is not linear. Consider, for example, a rock with N identical cracks of the type given by (18). Substituting into (30) and integrating, we obtain

$$\epsilon = \frac{-P}{K} - \frac{\beta}{K}P + \frac{\beta}{2KP'}P^2 \quad P \leq P' \quad (31)$$

where

$$\beta = \frac{2\pi(1 - \nu^2)}{3V(1 - 2\nu)} Ndc_0^2$$

The first term in (31) is just the intrinsic linear compressibility of the rock material. The second term, also linear, makes the rock more compliant and is equivalent to the effect of a distribution of elliptical cracks of the same original dimensions. The last term makes the rock less compliant and is due to the crack shortening; i.e., the modulus at a given pressure depends only on the crack length, so that the crack shortening causes stiffening. Equation (31) is plotted in Figure 5a and is compared with the linear intrinsic and equivalent elliptical crack curves. At very low stresses the quadratic term is negligible, so the stress-strain curve follows the elliptical crack curve. At larger pressures the quadratic term becomes significant, and the curve deviates substantially from the elliptical crack line. At P_e' the equivalent elliptical cracks close, causing an abrupt change in slope of the elliptical curve. If no other cracks were present, the new slope would be the same as that of the intrinsic crack curve. Above P_e' the tapered crack curve continues smoothly to P' , where the tapered cracks just close. The slope at P' is equal to the intrinsic slope. Hence there is no abrupt change in modulus at crack closure.

The exact shape of the stress-strain curve will differ for different crack shapes. However, for any tapered crack we expect the curve to be nonlinear and to take on smoothly the intrinsic slope when all cracks are completely closed. As a result, interpretation or prediction of features like porosity and modulus under varying confining pressure will depend upon the specific crack model chosen. Furthermore, the inversion of velocity or modulus data to obtain crack distributions [Simmons *et al.*, 1974; Toksöz *et al.*, 1976] is inherently nonunique.

To illustrate this nonuniqueness, we can find separate distributions of elliptical and nonelliptical cracks which give identical stress-strain curves. Consider, for example, the middle curve in Figure 5 given by (31). As we have already seen, this stress-strain behavior corresponds to a distribution of N identical cracks of the type given by (17) and Figure 2, with unstressed dimensions c_0 and d . The aspect ratio distribution function is $N(\alpha) = N\delta(\alpha - \alpha_0)$. In contrast, the same stress-strain curve is obtained from a set of N elliptical cracks (with

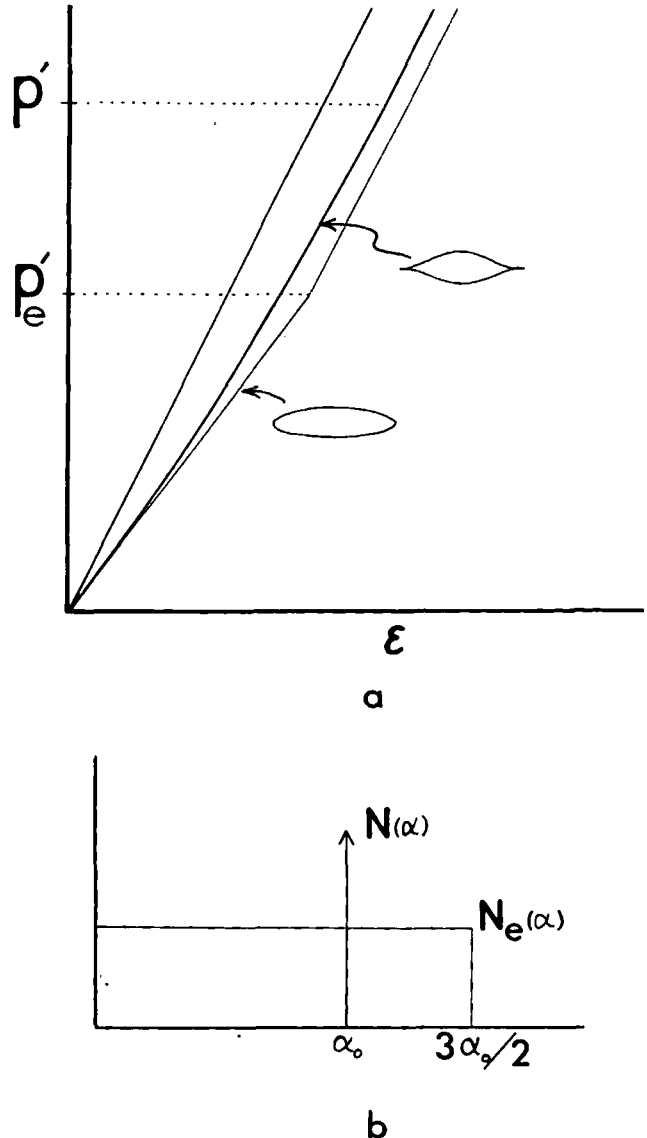


Fig. 5. (a) Applied pressure versus volumetric strain for a rock with a distribution of cracks. The upper curve is for the uncracked rock. The middle curve is for a distribution of identical tapered cracks. The lower curve is for a distribution of identical elliptical cracks with unstressed dimensions equal to those of the unstressed tapered cracks. (b) Two separate aspect ratio distributions, both of which give the middle stress-strain curve in Figure 5a. $N(\alpha)$ is the monodistribution of nonelliptical cracks. $N_e(\alpha)$ is a flat distribution of elliptical cracks.

the same dimensions c_0 and d) having a flat aspect ratio distribution, $N_e(\alpha) = 2N/3\alpha_0$ ($0 < \alpha < 3\alpha_0/2$). These two distributions, shown in Figure 5b, are drastically different. This difference suggests that the error in estimating aspect ratio spectra for rocks assuming elliptical cracks can be so great that such estimates may be essentially meaningless.

The inherent nonlinearity in the stress-strain curve resulting from tapered cracks offers a more reasonable explanation to observed nonlinearity at very low pressures. With the elliptical crack model, stiffening at confining pressures from, say, 1 bar to 100 bars can only be explained by invoking unreasonably small aspect ratios of 10^{-4} – 10^{-6} . In contrast, the slight shortening of a tapered crack, independent of aspect ratio, can account for the same stiffening.

Under nonhydrostatic conditions, cracks under shear,

whether partially or totally closed, may undergo frictional sliding at contact points and crack tips. Since the normal stress varies continuously over the crack faces in contact, the frictional stress will also vary. The spatial extent of sliding will depend on the level of applied shear. Again this differs from the elliptical crack which has frictional sliding only after the crack is completely closed. After closure the frictional stress is uniform across the crack, since the normal stress is uniform. For either crack model, frictional sliding will produce hysteresis in the stress-strain curve and dissipation of the mechanical energy.

The static saturated rock bulk modulus K_s can be obtained from the dry rock modulus using *Gassmann's* [1951] relation

$$K_s = K \frac{K' + Q}{K + Q}$$

where

$$Q = \frac{K_f(K - K')}{\phi(K - K_f)}$$

Here K' , K , and K_f are the bulk moduli of the dry porous rock, of the intrinsic rock material, and of the fluid, respectively, and ϕ is the porosity. Substituting for K' from (28), we obtain

$$\frac{1}{K_s} = \phi / \left[\frac{K\phi V(1 - 2\nu)}{2\pi(1 - \nu^2) \sum_i c_i^2 d_i} + \frac{K_0 K_f}{K_0 - K_f} \right]$$

This result assumes that the pore pressure is uniform everywhere throughout the rock. This situation could arise when (1) all pores are interconnected and sufficient time has passed for pressure equilibration or (2) all pores are exactly ellipsoidal with the same ratios of semiaxis lengths.

The importance of the nonelliptical crack model is not only in interpreting the bulk modulus of rock but also for predicting the closure of cracks with depth in the earth's crust [Brace, 1975] and the flow of fluids in the cracks. Elliptical cracks close at confining pressure P_c of order $P_c = \alpha E$ [Berg, 1965], where α is the aspect ratio and E is Young's modulus. Consequently, it is often suggested that fine cracks cannot exist at depth within the crust, since they are totally closed owing to confinement.

This conclusion becomes less obvious when we consider the more realistic nonelliptical cracks. Their closure is gradual, and the pressure or depth of closure depends on their unstrained initial shape. It is conceivable, for example, that some cracks such as joints with somewhat irregular surfaces may never close completely under confining pressure. Instead, only portions of the cracks may close, leaving irregular and more equidimensional cavities which are resistant to further deformation. Therefore so long as rock in the crust is brittle and sufficiently strong, it should be able to support porosity to depths of perhaps several kilometers.

Finally, the fluid pressure in an elliptical crack, induced by abrupt changes in compression of the rock, is uniform throughout the crack [Eshelby, 1957]. Consequently, no local flow is induced within the crack. Any other crack shape, however, will produce instantaneous nonuniform compression, with subsequent fluid flow. Although the magnitude of such flow is not yet clear, it may play a role in attenuation of seismic waves in rock [Mavko and Nur, 1978]. Such an effect does not exist in elliptical cracks.

CONCLUSION

We have used dislocation theory to study the deformation of rock with flat nonelliptical cracks under hydrostatic stress. The

general expression for crack shape as a function of pressure has been developed in terms of a triple integral involving the original crack shape and the applied stress. Evaluation of these integrals is particularly simple when the original crack shape is appropriately described in terms of polynomials.

The most prominent feature of the deformation of tapered cracks under compression is crack shortening. A consequence of the shortening is the elimination of stress singularities at crack tips. However, bounded stress concentrations do occur. The normal stress on the closed portions of the cracks increases rapidly but continuously from zero at the open face to a peak value at the original crack tip. In contrast, a thin elliptical crack simply flattens under compression. The length stays constant until, at sufficiently high pressure, the crack abruptly closes, making contact simultaneously over the entire crack surface. The stress concentration is unbounded outside the crack tips, and after closure the normal stress is exactly uniform over the closed crack faces.

The compressibility of a rock containing a distribution of arbitrarily shaped, flat tapered cracks is exactly the same as that for a distribution of flat elliptical cracks with the same lengths. Therefore at a given value of pressure the compressibility is independent of the (2-D) crack model chosen. Consequently, nothing about crack shape can be inferred from the compressibility at a single value of pressure. However, at different confining pressures the varying length causes the modulus to vary. As a result, interpretation or prediction of features like porosity and modulus under varying load will depend on the specific crack model chosen.

APPENDIX A

The multiple-crack case can be treated following *Muskhelishvili* [1953]. Consider a set of coplanar thin cracks with tapered ends, each of the type treated separately in the text of this paper. The original shape of the i th crack is U_{i0} with tips at a_{i0} and b_{i0} as shown in Figure 6. If the hydrostatic stress $-P'$ is applied large enough to close all of the cracks, the normal stress on the plane $y = 0$ is

$$\sigma_0(x) = -P' + \sigma_0^c(x)$$

where

$$\sigma_0^c(x) = \frac{\mu}{2\pi(1 - \nu)} \sum_{i=1}^N \int_{a_i}^{b_i} \frac{B_{i0}(z) dz}{x - z} \quad (A1)$$

and

$$B_{i0}(x) = \frac{d}{dx} U_{i0}(x) \quad (A2)$$

If the compression is relaxed to $P < P'$, some of the cracks will reopen over the range $a_i < x < b_i$, where $a_i > a_{i0}$ and $b_i < b_{i0}$, with shape $U_i(x, P)$. The crack opening $U_i(x, P)$ corresponds to a distribution of infinitesimal elastic edge dislocations with density function

$$B_i(x, P) = -\frac{\partial}{\partial x} U_i(x, P) \quad (A3)$$

The integral equation for B_i expressing the condition of stress-free crack faces is

$$\sum_{i=1}^N \int_{a_i}^{b_i} \frac{B_i(z, P)}{x - z} dz = \frac{-2\pi(1 - \nu)}{\mu} [\sigma_0^c(x) - P] \quad (A4)$$

$$a_i \leq x \leq b_i \quad i = 1, 2, 3, \dots, N$$

The condition that a solution to (A4) exist with finite stresses

everywhere is given by

$$\sum_{i=1}^N \int_{a_i}^{b_i} \left\{ [\sigma_0^c(x) - P] / \left[\prod_{j=1}^N (x - a_j)(b_j - x) \right]^{1/2} \right\} dx = 0 \quad k = 0, 1, 2, \dots, N-1 \quad (A5)$$

The solution of equation (A4) is given by

$$B(x, P) = \frac{2(1-\nu)}{\pi\mu} \left[\prod_{j=1}^N (x - a_j)(b_j - x) \right]^{1/2} \sum_{i=1}^N \int_{a_i}^{b_i} \left\{ [\sigma_0^c(z) - P] / (x - z) \left[\prod_{j=1}^N (z - a_j)(b_j - z) \right]^{1/2} \right\} dz \quad (A6)$$

$a_i \leq x \leq b_i \quad i = 1, 2, 3, \dots, N$

The actual crack shapes are found by integrating $-B(x, P)$:

$$U_i(x, P) = -\int_{a_i}^x B(z, P) dz$$

APPENDIX B

Given the polynomial form, (12), the expressions for crack length, (13), and $B(x, P)$, (14), are found as follows. Substituting (12) into (7),

$$P = \frac{1}{\pi} \int_{-c}^c \sum_{k=0}^n \frac{r_k x^k}{(c^2 - x^2)^{1/2}} dx \quad (B1)$$

or setting $z = x/c$,

$$P = \frac{1}{\pi} \sum_{k=0}^n r_k c^k \int_{-1}^1 \frac{z^k}{(1 - z^2)^{1/2}} dz = \frac{1}{\pi} \sum_{k=0}^n r_k c^k \gamma_k \quad (B2)$$

The integral in (B2) is given by

$$\begin{aligned} \gamma_k &= \int_{-1}^1 \frac{z^k}{(1 - z^2)^{1/2}} dz = \pi \quad k = 0 \\ \gamma_k &= \int_{-1}^1 \frac{z^k}{(1 - z^2)^{1/2}} dz = 0 \quad k = 1, 3, 5, \dots \\ \gamma_k &= \int_{-1}^1 \frac{z^k}{(1 - z^2)^{1/2}} dz = \frac{k-1}{k} \cdot \frac{k-3}{k-2} \dots \frac{1}{2} \pi \quad k = 2, 4, 6, \dots \end{aligned} \quad (B3)$$

Similarly, substituting (12) into (8), $B(x, P)$ becomes

$$B(x, P) = \frac{2(1-\nu)}{\pi\mu} (c^2 - x^2)^{1/2} \int_{-c}^c \frac{R_n(z) - P}{(x - z)(c^2 - z^2)^{1/2}} dz \quad |x| \leq c$$

or setting $t = z/c$,

$$B(x, P) = \frac{2(1-\nu)}{\pi\mu} \left[1 - \left(\frac{x}{c} \right)^2 \right]^{1/2} \int_{-1}^1 \frac{R_n(ct) - P}{[(x/c) - t](1 - t^2)^{1/2}} dt \quad |x| \leq c$$

By expanding the polynomial $R_n(ct)$ in terms of Chebyshev polynomials of the first kind, $T_n(t)$, i.e.,

$$R_n(ct) = \sum_{k=0}^n b_k T_k(t) \quad |t| \leq 1 \quad (B4)$$

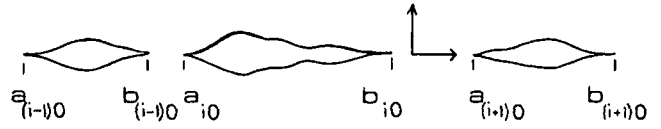


Fig. 6. A set of flat two-dimensional coplanar cracks with tapered ends.

the expression $B(x, P)$ can be written as

$$B(x, P) = \frac{2(1-\nu)}{\pi\mu} \left[1 - \left(\frac{x}{c} \right)^2 \right]^{1/2} \left\{ \sum_{k=2}^n b_k \int_{-1}^1 \frac{T_k(t) dt}{[(x/c) - t](1 - t^2)^{1/2}} + (b_0 - P) \int_{-1}^1 \frac{dt}{[(x/c) - t](1 - t^2)^{1/2}} \right\} \quad |x| \leq c$$

But

$$\begin{aligned} \int_{-1}^1 \frac{T_n(t) dt}{(z - t)(1 - t^2)^{1/2}} &= -\pi U_{n-1}(z) \quad n \geq 1 \quad |z| \leq 1 \\ \int_{-1}^1 \frac{T_n(t) dt}{(z - t)(1 - t^2)^{1/2}} &= 0 \quad n = 0 \quad |z| \leq 1 \\ \int_{-1}^1 \frac{(1 - t^2)^{1/2} U_{n-1}(t) dt}{z - t} &= \pi T_n(z) \quad |z| \leq 1 \end{aligned} \quad (B5)$$

where the $U_n(x)$ are Chebyshev polynomials of the second kind [Hochstrasser, 1964]. Hence $B(x, P)$ becomes simply

$$B(x, P) = \frac{-2(1-\nu)}{\mu} \left[1 - \left(\frac{x}{c} \right)^2 \right]^{1/2} \cdot \sum_{k=2}^n b_k U_{k-1} \left(\frac{x}{c} \right) \quad |x| \leq c \quad (B6)$$

APPENDIX C

The independence of compressibility from crack shape is shown as follows. Through algebraic manipulation it can be shown that for symmetric tapered cracks the solution given by (8) is equivalent to

$$B(x, P) = \frac{2(1-\nu)}{\pi\mu} \frac{1}{(c^2 - x^2)^{1/2}} \int_{-c}^c \frac{[\sigma_0^c(z) - P](c^2 - z^2)^{1/2}}{x - z} dz \quad (C1)$$

Differentiating, we obtain

$$\begin{aligned} \frac{\partial B}{\partial P} &= \frac{2(1-\nu)}{\pi\mu} \left\{ -\frac{c(\partial c / \partial P)}{(c^2 - x^2)^{3/2}} \int_{-c}^c \frac{[\sigma_0^c(z) - P](c^2 - z^2)^{1/2}}{x - z} dz \right. \\ &\quad - \frac{1}{(c^2 - x^2)^{1/2}} \int_{-c}^c \frac{(c^2 - z^2)^{1/2}}{x - z} dz \\ &\quad \left. + \frac{\partial c / \partial P}{(c^2 - x^2)^{1/2}} \int_{-c}^c \frac{[\sigma_0^c(z) - P]c}{(x - z)(c^2 - z^2)^{1/2}} dz \right\} \end{aligned}$$

Using both (8) and (C1), this can be written as

$$\begin{aligned} \frac{\partial B}{\partial P} &= \frac{-c}{c^2 - x^2} B(x, P) \frac{\partial c}{\partial P} - \frac{2(1-\nu)}{\pi\mu(c^2 - x^2)^{1/2}} \\ &\quad \cdot \int_{-c}^c \frac{(c^2 - z^2)^{1/2}}{x - z} dz + \frac{c}{c^2 - x^2} B(x, P) \frac{\partial c}{\partial P} \\ &= \frac{-2(1-\nu)}{\pi\mu(c^2 - x^2)^{1/2}} \int_{-c}^c \frac{(c^2 - z^2)^{1/2}}{x - z} dz \quad (C2) \end{aligned}$$

The integral in (C2) can be evaluated to give

$$\frac{\partial B}{\partial P} = \frac{-2(1-\nu)}{\mu} \frac{x}{(c^2-x^2)^{1/2}} \quad |x| < c \quad (\text{C3})$$

Acknowledgments. This work was supported by grants from the National Science Foundation, Earth Sciences Division; and the Energy Research and Development Administration, Division of Basic Energy Sciences. Gerald Mavko was supported in part by a National Science Foundation graduate fellowship.

REFERENCES

- Berg, C. A., Deformation of fine cracks under high pressure and shear, *J. Geophys. Res.*, 70(14), 3447, 1965.
- Bilby, B. A., and J. D. Eshelby, Dislocations and the theory of fracture, in *Fracture: An Advanced Treatise*, vol. 2, edited by H. Liebowitz, p. 99, Academic, New York, 1968.
- Birch, F., The velocity of compressional waves in rocks to 10 kilobars, *J. Geophys. Res.*, 65, 1083, 1960.
- Brace, W. F., Some new measurements of linear compressibility of rocks, *J. Geophys. Res.*, 70, 391, 1965.
- Brace, W. F., Dilatancy related electrical resistivity changes in rocks, *Pure Appl. Geophys.*, 113, 207-217, 1975.
- Budiansky, B., and R. J. O'Connell, Elastic moduli of a cracked solid, *Int. J. Solids Structures*, 12, 81-97, 1976.
- Delameter, W. R., Weakening of elastic solids by arrays of cracks, Ph.D. dissertation, Dep. of Appl. Mech., Stanford Univ., Stanford, Calif., 1974.
- Eshelby, J. D., The determination of the elastic field of an ellipsoidal inclusion, and related problems, *Proc. Roy. Soc., Ser. A*, 241, 376, 1957.
- Gassmann, G., Über die Elastizität poröser Medien, *Vierteljahressch. Naturforsch. Ges. Zuerich*, 96(1), 1-21, 1951.
- Hochstrasser, U. W., Orthogonal polynomials, in *Handbook of Mathematical Functions*, edited by M. Abramowitz and I. A. Stegun, p. 771, Dover, New York, 1964.
- Jaeger, J. C., and N. G. W. Cook, *Fundamentals of Rock Mechanics*, Methuen, London, 1969.
- Kuster, G. T., and M. N. Toksöz, Velocity and attenuation of seismic waves in two-phase media, I, Theoretical formulations, *Geophysics*, 39(5), 587, 1974.
- Landau, L. D., and E. M. Lifshitz, *Theory of Elasticity*, 144 pp., Addison-Wesley, Reading, Mass., 1959.
- Mavko, G. M., and A. M. Nur, Wave attenuation in partially saturated rocks, submitted to *Geophysics*, 1978.
- Muskhelishvili, N. I., *Singular Integral Equations*, edited by J. R. M. Radock, p. 256, P. Noordhoff, Groningen, Holland, 1953.
- Nur, A., Effects of stress on velocity anisotropy in rock with cracks, *J. Geophys. Res.*, 76(8), 2022, 1971.
- O'Connell, R. J., and B. Budiansky, Seismic velocities in dry and saturated cracked solids, *J. Geophys. Res.*, 79(35), 5412, 1974.
- Simmons, G., R. W. Siegfried II, and M. Feves, Differential strain analysis: A new method for examining cracks in rocks, *J. Geophys. Res.*, 79(29), 4383, 1974.
- Toksöz, M. N., C. H. Cheng, and A. Timur, Velocities of seismic waves in porous rocks, *Geophysics*, 41(4), 621, 1976.
- Walsh, J. B., The effect of cracks on the compressibility of rock, *J. Geophys. Res.*, 70(2), 381, 1965a.
- Walsh, J. B., The effect of cracks on the uniaxial elastic compression of rocks, *J. Geophys. Res.*, 70(2), 399, 1965b.
- Walsh, J. B., Seismic wave attenuation in rock due to friction, *J. Geophys. Res.*, 71, 2591-2599, 1966.

(Received September 14, 1977;
revised February 24, 1978;
accepted April 12, 1978.)

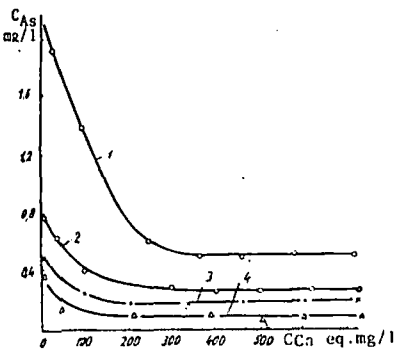
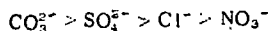


Fig. 4
The solubility of arsenic-containing precipitates based on hydroxylapatite as a function of the concentration of calcium in the solution and of the ageing time. pH = 7-7.5; amount of precipitate 500 mg/l; contact time 96 h; temperature 20-22°C. Holding time of precipitate in mother solution, days: 1 - 1; 2 - 12; 3 - 24; 4 - 35.

The salt composition of the water during the precipitation of the arsenic determines not only the effectiveness of the precipitation but also the solubility of the compounds which form. Thus, anions are capable of competing with the arsenic during the sorption on the hydroxylapatite precipitate. According to their effect on the precipitation of arsenic, the anions can be arranged in the following order:



i. e., the precipitation of the arsenic becomes worse with increase in this series. It is most difficult to precipitate arsenic from carbonate waters by this method, whereas the presence of even small amounts of fluorine in the system considerably improves the precipitation of arsenic and reduces the solubility of the precipitate. In the general case it is possible to purify water with a salt content of not more than 5 g/l effectively by precipitation of the arsenic in the form of poorly soluble compounds based on hydroxylapatite. The results from the investigations were brought into use during the introduction of the method for the purification of effluents from the slime accumulator at one of the copper-smelting combines of the Urals.

Conclusions

1. A compound of the hydroxylapatite type, corresponding

Extraction of noble metals from the tailings from the sorption cyaniding of ores

A S Romanov, N V Svistunov and V F Nechetalenko (North-Caucasian Mining-Metallurgical Institute - Department of the Metallurgy of Noble, Rare and Light Metals)

The sorption cyaniding of gold ores is finding wider and wider use particularly in the treatment of clay and ocherous ores. While possessing a series of advantages over the normal cyanide process, it also has disadvantages characteristic of the latter; stubborn gold (combined with sulphides and tellurides, coated by films insoluble in cyanide) is lost in the cyaniding tailings. The same applies to silver to an even greater degree. Methods which make it possible to extract the stubborn forms of noble metals from the tailings from sorption cyaniding by flotation of the gold and silver containing materials, in particular, are therefore of interest.

Examples of the flotation of the tailings from direct cyaniding have been described in the literature^{1,2}). The need for such a combination of processes arises when the ore contains gold tellurides and also other valuable minerals (lead, bismuth, etc.), the loss of which with the cyaniding tailings is undesirable.

Gold tellurides are readily floated in a lime-cyanide medium²), but other sulphide minerals are greatly depressed in the cyaniding process and must be activated before flotation. Washing out the depressers (lime and cyanide) with water is not always sufficiently effective. Acid treatment of the cyaniding tailings is therefore sometimes practiced²). Pyrite is activated in a soda medium by copper

to the composition $\text{Ca}_5(\text{PO}_4)_3\text{OH}$ and distinguished by low solubility, is formed initially in the $\text{Ca}_2\text{P}_2\text{O}_7$ system.

2. Arsenic is precipitated as a result of the replacement of hydroxyl groups by arsenic anions with the formation of a compound of the hydroxylapatite type, which changes into a crystalline form with time.

3. The proposed mechanism was confirmed by data on the solubility of arsenic-containing precipitates having a hydroxylapatite structure by the IR spectra and by X-ray, thermographic, and derivatographic methods of analysis.

References

- 1) A V Nikolaev et alia: Izv. SO Akad. Nauk SSSR, Ser. Khim. Nauk 1970, 3, (7), 115.
- 2) V P Porubaev et alia: Tr. in-ta Kazmekhanobra Sb. 1972, 10, 110.
- 3) Yu O Grigor'ev et alia: Proceedings of Scientific-technical conference on "Methods for the high purification of effluents". Sverdlovsk 1975.
- 4) A V Nikolaev et alia: Izv. SO Akad. Nauk SSSR, Ser. Khim. Nauk 1972, 5, (12), 121.
- 5) A V Nikolaev et alia: Izv. SO Akad. Nauk SSSR, Ser. Khim. Nauk 1974, 5, 12, 30.
- 6) B I Shramban et alia: Khimicheskaya Promyshlennost' 1974, (5), 396.
- 7) A K Babko et alia: Photometric analysis. Methods for the determination of non-metals. Khimiya, Moscow 1974.
- 8) Yu Yu Lur'e et alia: Chemical analysis of industrial effluents. Khimiya, Moscow 1974.
- 9) A V Kazakov: Tr. In-ta Udobrenii i insektofungitsidov 1973, 139.
- 10) A V Valyashko et alia: Geokhimiya 1968, (1), 26.
- 11) H M Pootare et alia: J. Colloid. Sci., 1962, 17, (3).
- 12) U A Dir et alia: Rock-forming minerals. Mir, Moscow 1966, 5.
- 13) M V Akhmanova: Uspekhi Khimii 1959, 27, (3), 312.
- 14) H A Schleede et alia: Elektrochemie 1932, 38, 633.
- 15) B P Nikol'skikh (editor): Chemists Handbook; Khimiya, Leningrad 1964, 2.

UDC 669.213.6+622.765.06

sulphate and sodium sulphide. An essential condition for the flotation of copper sulphides from the cyaniding tailings is considered to be the absence of free cyanide in the liquid phase of the pulp.

Ore distinguished by the presence of silver and gold tellurides and also by a substantial content of silver, bismuth, lead, copper and antimony in the sulphide part are processed at one of the gold-extracting plants of Central Asia. The treatment of these ores by the sorption method secures high extraction of gold but leads to complete loss of valuable sulphides and also a considerable amount of the silver. Since washing out of the cyanide and lime from the sorption tailings before flotation is completely excluded under the conditions of ions-exchange technology, it seemed of interest to study the conditions for the extraction of noble metals and valuable sulphide minerals from the tailings by flotation.

Experiments were carried out under laboratory conditions on two samples of ore, the composition of which is given in table 1. The sulphide part of these ores was largely represented by pyrite, chalcopyrite, grey copper ores, bismuthite and tellurobismuthites. Samples of the ores weighing 1kg were ground in rod mills with a liquid-solid ratio of 1:1 to 75% of the -0.08mm class with a rod

SUBJ
MNG
ENM

load of 8kg. Sorption cyaniding was realised under conditions close (in time and anion-exchanger consumption) to those used in the operating plant. The consumption rates of the cyanide and lime were varied within wide limits.

Table 1: Chemical composition of the gold-containing ores %

Sample	SiO ₂	Al ₂ O ₃	CaO	MgO	Fe	Cu	Pb	Bi	Te	S	Aug/t. Ag, g/t
A	84.92	5.77	0.90	0.55	2.60	0.04	0.066	-	-	1.28	11.3
B	74.88	12.94	1.13	0.08	3.75	0.07	0.23	0.01	0.007	2.94	9.7

After separation of the anion exchanger on a screen the pulp from the sorption cyaniding tailings was diluted in the cell of the flotation machine from a liquid-solid ratio of 1.5 to 3.5 and submitted to flotation with a butyl xanthate consumption rate of 100-150g/t and a frother T-66 consumption rate of 60-100g/t. Depending on the conditions of the preceding sorption process, the yield of the crude concentrate varied between 7 and 12% with an overall flotation time of 12-18 min. From table 2 it is seen that variation of the amount of cyanide delivered to the cyaniding process has little effect on its final concentration in the liquid phase of the pulp. This is due to sorption of the cyanide by the anion exchanger, as a result of which the consumption of cyanide approximates to the amount loaded. The alkalinity of the liquid phase of the pulp after sorption (% CaO) increases in a number of cases on account of the passage of hydroxide ions into the solution from the anion exchanger, previously loaded in the OH form. Since this is undesirable for the flotation of sulphides, other forms of anion exchanger were tested. Here, however, no substantial difference in the results from flotation of the sorption cyaniding tailings was observed, although the alkalinity of the pulp differed (Cl form, pH ≈ 6.0; NO₃ + OH form, pH ≈ 7; OH form, pH ≈ 8.0).

The results from flotation of the sorption cyaniding tailings (figs. 1, 2 and 3) show that the extraction of noble metals in the flotation cycle decreases sharply with increase in the consumption of cyanide in the sorption cyaniding cycle. However, as seen from figs. 1 and 2, such an effect from the cyanide is due not to its depressing action but to a decrease in the amount of gold and silver delivered to flotation, since their extraction in the sorption cycle increases with increase in the cyanide consumption. Increase in the lime consumption acts similarly, but to a considerably lesser degree. (In fig. 1 the effect of CaO is reflected by the vertical lines, the ends of which correspond to the minimum and maximum consumption rates).

From figs. 1 and 2 it follows that, irrespective of the conditions of sorption cyaniding, the overall extraction of gold and silver (into the anion exchanger and the flotation concentrate) remains constant, and only their distribution among the products changes. With the optimum cyanide consumption rates for the sorption process (0.4-0.6kg/T) flotation of the cyaniding tailings makes it possible to increase the extraction of gold by 5-10% and the extraction of silver by 25-30% (from sample B). In sample A, which differs in the increased silver content, the increase in its extraction on account of extraction from the sorption tailings by flotation is also sig-

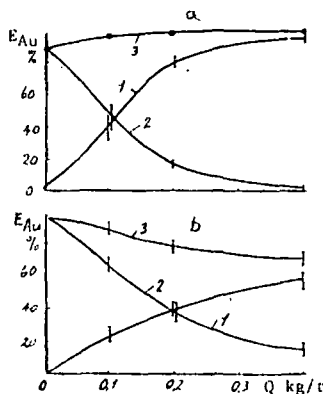


Fig. 1 The effect of the cyanide consumption (Q) in the cyaniding of the ore A on the extraction of noble metals: 1 - anion exchanger; 2 - flotation concentrate; 3 - overall extraction.

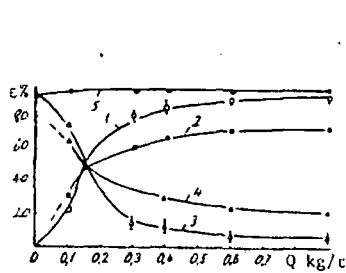


Fig. 2 The effect of the cyanide consumption (Q) in the cyaniding of ore B on the extraction of noble metals: 1 - gold into the anion exchanger; 2 - silver into the anion exchanger; 3 - gold into the flotation concentrate; 4 - silver into the flotation concentrate; 5 - overall extraction of gold.

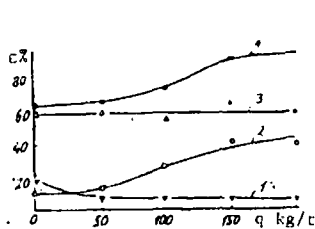


Fig. 3 The effect of the amount of copper sulphate (Q) on the extraction of sulphur (1), silver (2), and gold (3) during the flotation of tailings from the sorption cyaniding of ore A. The overall extraction of silver by sorption and flotation (4).

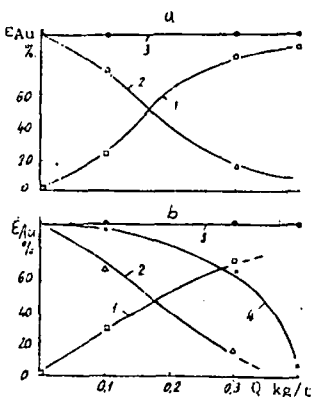


Fig. 4 The effect of the cyanide consumption (Q) on the extraction of noble metals from the tailings from sorption cyaniding by flotation in a closed cycle: 1 - into the anion exchanger; 2 - into the recycled concentrate; 3 - overall extraction; 4 - extraction of sulphur.

Table 2: The variation of the concentration of the reagents during the sorption cyaniding of the ores

Sample	Delivered for cyaniding kg/t		Concentration in liquid phase of pulp %				Total consumption of NaCN kg/t	pH value before flotation
	NaCN	CaO	After cyaniding		After sorption			
			NaCN	CaO	NaCN	CaO		
A	0.1	2.0-4.0	0.002-0.006	0.002-0.023	0.001-0.001	0.003-0.008	0.085-0.085	7.0-8.0
A	0.2	2.0-4.0	0.011-0.011	0.002-0.030	0.002-0.003	0.002-0.010	0.17-0.16	7.0-8.0
A	0.4	2.0-4.0	0.022-0.025	0.002-0.026	0.007-0.008	0.003-0.011	0.29-0.28	7.0-8.0
B	0.4	2.2-4.5	0.014-0.018	0.002-0.031	0.001-0.002	0.003-0.011	0.37-0.39	7.5-8.5
B	0.6	2.2-4.5	0.023-0.027	0.001-0.028	0.003-0.004	0.004-0.015	0.56-0.54	7.0-8.5
B	0.9	2.0-4.5	0.040-0.050	0.001-0.029	0.008-0.010	0.003-0.013	0.75-0.78	7.0-9.0

Note: Cyaniding was realised with a liquid-solid ratio of 1.5:1; cyaniding time 12h, sorption time 12h; amount of anion-exchanger in OH form 15kg/t of ore.

efficient (fig. 1b), although its overall extraction is lower than in sample B and decreases with increase in the consumption of cyanide in the sorption cycle. During the investigation it was established that the extraction of silver during the flotation of the tailings from sorption cyaniding of sample A can be increased considerably by activation of the silver-containing minerals with copper sulphate. With a copper sulphate consumption rate of about 150g/ton the extraction of gold and sulphur here remains practically unchanged (fig. 3).

The results from balancing trials with recleaning of the concentrates in a closed cycle confirmed the data from the single experiments (fig. 4, sample B). Irrespective of the sorption cyaniding conditions, the overall extraction of gold and silver into the anion exchanger and concentrate amounts to 95-97%. The yield of the recleaned concentrates and their content of noble metals are determined by the consumption of the cyanide during cyaniding. The compositions of the typical concentrates obtained with various sorption cyaniding conditions are given in table 3, from the data of which it is seen that the sulphur content in the concentrates decreases sharply with increase in the cyanide consumption. This is due to depression of the pyrite by the cyanide and the lime (fig. 4b). The content of the noble metals in the concentrate also decreases. However, as shown by statistical treatment of the results from the trials, there is no significant relation between the extraction of the noble metals into the flotation concentrate and the extraction of the sulphide (sulphur).

Table 3: Composition of the recleaned flotation concentrates %

Sample	NaCN consumption kg/t.	Yield of concentrate %	Au g/t	Ag g/t	S	Pb	Cu	Bi
A	0.2	1.66	105.0	1274.4	32.61	-	-	-
A	0.4	3.41	3.2	213.2	1.01	0.10	0.06	-
B	0.1	6.80	105.0	539.2	-	-	-	0.045
B	0.3	5.01	23.0	251.6	34.78	-	-	0.035
B	0.4	3.01	26.5	515.0	6.92	4.49	1.88	0.052

The regression equations have the following form:

$$\text{for sample A } E_{Au} = 55.56 + 0.2819 E_s;$$

$$E_{Ag} = 45.25 + 0.4022 E_s;$$

$$\text{for sample B } E_{Au} = 74.75 + 0.0260 E_s;$$

$$E_{Ag} = 74.24 + 0.2156 E_s.$$

The correlation coefficients are 0.35, 0.45, 0.05 and 0.49 respectively, and the coefficients at E_s are statistically insignificant. It can be supposed that the free gold and also the gold-containing minerals not depressed by the cyanide (lead, antimony) are floated after sorption cyaniding.

Conclusions

1. The flotation of the sorption cyaniding tailings makes it possible significantly to increase the extraction of gold (by 5-10%) and particularly of silver (by 25-30%), since the latter is extracted quite unsatisfactorily in the sorption process, and also to extract non-ferrous metal sulphides, which are completely lost in the sorption process.
2. By variation of the conditions of sorption cyaniding (the cyanide consumption rate) it is possible to obtain any desired distribution of the noble metals between the anion exchanger and the flotation concentrate. With increase in the cyanide consumption rate the proportion of gold extracted by the anion exchanger increases, and its proportion in the flotation concentrate decreases accordingly.

References

- 1) M A Fishman and V N Zelenov: Practice in the concentration of ores of non-ferrous and rare metals: Nedra, Moscow Vol. 5 1967.
- 2) V V Lodeishchikov: Technique and technology of the extraction of gold from ores abroad: Metallurgiya, Moscow 1973.
- 3) Concentration of ores in Australia (ed. V Yu Brand): Metallurgizdat, Moscow 1958.
- 4) S I Mitrofanov: Selective flotation: Metallurgizdat, Moscow 1958.

UDC 669.733.872

Investigation of the kinetics of the cementation of indium

G E Avakyan and I F Khudyakov (Ural Polytechnic Institute - Department of the Metallurgy of Heavy Non-Ferrous Metals)

Summary

The kinetics of the cementation of indium on zinc was investigated by the rotating disc method. The effects of the agitation rate of the solution, the temperature, the pH of the solution and the indium and cadmium concentrations on the rate of the cementation process were determined. Fig. 1 shows the dependence of the cementation rate on the intensity of agitation. It confirms that the cementation process changes from the diffusion to the kinetic region at an agitation rate of 7.2-7.8 rps.

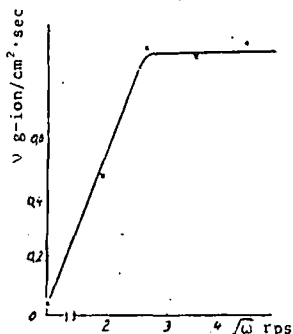


Fig. 1
The dependence of the cementation rate of indium on the square root of the agitation rate of the solution. $t = 90^\circ\text{C}$; $\text{pH} = 2.0$; initial concentration of indium 68 mg/l.

The effect of the temperature on the cementation process is shown on the polarisation diagram in fig. 2. The cementation rate increases with increase in temperature. By comparison of the anodic and cathodic curves for the corresponding temperatures it can be seen that the cementation process is under cathodic control, where the limiting factor is the rate of approach of the indium ions to the cathode.

Determination of the effect of the acidity of the solution on the cementation rate gave a linear relationship. The increase in the cementation rate with increase in pH from 1.0 to 2.8 is explained by an increase in the hydrogen overpotential with decrease in the acidity of the medium.

The effect of cadmium in the initial solution on the cementation rate is shown in fig. 3. To check the possibility of the recovery of indium from the solutions after the leaching of zinc cakes experiments were carried out on the cementation of indium with zinc dust. Copper and arsenic were first removed from the solution in order to eliminate the release of arsine and to produce a concentrate richer in indium. The cementation was carried out

experimentally for the concentration of an ilmenite product.

The results show that one of the methods for increasing the productivity of roll-type dry separators with bottom

feed is to increase the roll diameter with a simultaneous increase in its rotation rate. The equations obtained can be used to determine the rotation rate.

Method for determining the consumption of underscreen water in the settling of coarse-grained material

I D Raivich (Kazakh Polytechnical Institute. Department of the Metallurgy of Noble Metals and the Concentration of Minerals)

SUBJ

Summary

Equations are proposed for determining the consumption of underscreen water and the variation of the water level in a jigging machine. The amount of under-screen water is greater the higher the frequency of the pulsations, the size (and particularly the length) of the machine, and the

velocity of the ascending water stream.

The consumption of underscreen water depends little on the amount of transporting water delivered with the feed (or does not depend on it with dry delivery of the material).

*Doc. Non-Fe
1977 v. 5 NY*

2 articles

UDC 699.3-404.5:547.491.135.2

Electrode processes in cyanide-thiocyanate solutions of copper

G N Shvirin, E M Shvirina, and V S Klimchenko (Krasnoyarsk Institute of Nonferrous Metals - Department of the Metallurgy of Heavy and Noble Metals)

Ion exchange is finding wider and wider use for the extraction of noble and nonferrous metals from cyanide solutions and pulps¹⁻⁴). Solutions of thiocyanates are used for the elution of certain metals from ion exchangers^{1, 2}), and for the re-extraction of metals from organic solvents⁴). The thiocyanate eluates and re-extracts contain the following main anions: NCS⁻, CN⁻, Cl⁻, and complex cyanide anions of the metals.

The reduction of dissolved oxygen at the copper cathode in a cyanide solution is a diffusion process, as a result of which the first wave is characterised by the presence of a limiting current. The reduction of hydrogen is a kinetic process. From the form of the polarisation curves shown in fig.1 it can be concluded that the CN⁻ ion is hardly reduced at all at the copper cathode in the investigated concentration limits.

For the majority of metals the stability of the cyanide complexes is many orders of magnitude higher than the stability of the thiocyanate complexes, and for the actually obtainable concentrations of the thiocyanates in the solution gold, silver, zinc, copper, iron, and other metals are present almost entirely in the form of cyanide complexes.

In thiocyanate solutions the form in which the copper is present in the solution depends on the concentration of NCS⁻, and the equilibrium potential of the copper electrode depends on the activity of the NCS⁻ ions (a_t) and the activity of the copper thiocyanate complex (a_c):

In view of the fact that one of the most promising methods for the treatment of thiocyanate eluates and re-extracts is electrolysis, it seemed of interest to examine the electrode processes in cyanide-thiocyanate solutions. The investigation of the electrode processes in cyanide-thiocyanate solutions of copper was carried out on apparatus with a rotating copper disc cathode with the cathode and anode compartments separated by the anion-exchange membrane described in⁵).

$$\varphi_{i=0} = E_{\text{Cu}^{2+}/\text{Cu}}^0 - \frac{0.0592}{n} \text{p}K_d + \frac{0.0592}{n} \lg a_c - \frac{m}{n} 0.0592 \lg a_t \quad (2)$$

where m is the coordination number of the thiocyanate complex.

Measurement of the equilibrium potential of the copper electrode in pure cyanide solutions shows that the Cu(CN)₃²⁻ anion is formed and is present in 0.02-0.32 M solutions of sodium cyanide in 0.25 M sodium hydroxide since,

In thiocyanate solutions copper is present mainly in the form of thiocyanate complexes of monovalent copper, such as Cu(NCS)₂⁺ with pK_d = 12.11⁶), since the probability of the formation of complexes of divalent copper is many orders of magnitude lower [for the Cu(NCS)₃⁺ complex, pK_d = 5.18⁷].

$$\varphi_{i=0} = \text{const} - 3 \cdot 0.0592 \lg a_{\text{CN}^-} \quad (1)$$

Two polarisation waves appear on the log i-φ diagram during the polarisation of the copper cathode in cyanide solutions (fig.1).

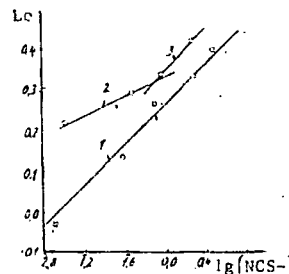


Fig.2
Dependence of the equilibrium potential of the rotating copper disc electrode on the activity of NCS⁻ ions in a solution of sodium thiocyanate¹) and in a 0.06M solution of Na₂Cu(CN)₃²)³).

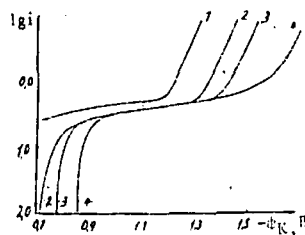


Fig.1
The dependence of the current density on the potential of the rotating copper disc electrode in a 0.25M solution of sodium hydroxide in the presence of sodium cyanide (mole/cm³): 1 - 0; 2 - 0.02; 3 - 0.08; 4 - 0.32.

Our investigations showed (fig.2) that in 0.1-3.5M solutions of NaNCS the equilibrium potential of the copper electrode is determined by the formation of the Cu(NCS)₂⁺, since

$$\varphi_{i=0} = \text{const} - 4 \cdot 0.0592 \lg a_t \quad (3)$$

The first of them is due to reduction of dissolved oxygen at the cathode. The second is due to reduction of hydrogen.

In thiocyanate solutions of copper complex anions of monovalent copper of the general form Cu(NCS)_m^{1-m} can evidently

form, depending on the concentration of NCS^- . In the presence of the cyanide complex of copper $\text{Cu}(\text{CN})_2^-$ (0.06 g-ion/dm³) in the thiocyanate solution the equilibrium electrode potential of copper in a solution containing 0.12-1.1 mole/dm³ of NaNCS is determined by the formation of the $\text{Cu}(\text{NCS})_2^-$ ion. In fig.2 line 2 corresponds to the equation

$$\varphi_{i=0} = \text{const} - 2 \cdot 0.0592 \lg a_c \quad (4)$$

With a concentration of NaNCS above 1.1 mole/dm³ the equilibrium potential of the copper electrode depends on the activity of NCS^- in accordance with Eq.(3), and this indicates the formation of the $\text{Cu}(\text{NCS})_2^-$ ion (fig.3, line 3). During the polarisation of the copper cathode in thiocyanate solutions three waves (fig.3) corresponding to the reduction of dissolved oxygen, NCS^- ions, and hydrogen, appear on the $\lg i - \varphi_c$ diagram.

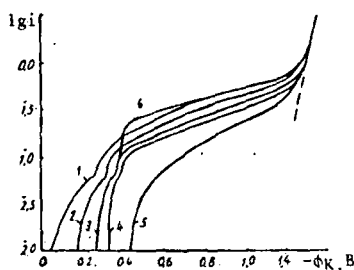
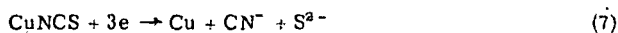


Fig.3
The dependence of the current density on the potential of the rotating copper disc electrode in solutions with various concentrations of NaNCS (mole/dm³):
1 - 0.104; 2 - 0.56;
3 - 1.11; 4 - 2.41;
5 - 3.53; 6 - 0.2 g/dm³ of $\text{NaCu}(\text{NCS})_2$ in a 1.1M solution of NaNCS .

The reduction of the NCS^- ions at the copper cathode depends on the concentration of NaNCS in the solution. If the NCS^- ion were the oxidised form in this electrode process, a shift of its reduction potential to the positive side would be expected in a solution of NCS^- . However, as seen from the $\lg i - \varphi_c$ diagram in fig.3, the potential corresponding to the beginning of the reduction of NCS^- ions is shifted towards the negative side with increase in the concentration of NaNCS in the solution. This is possible if the reduction of the NCS^- ions at the copper cathode takes place not directly but through the formation of a copper thiocyanate complex in accordance with Eq.(2). In this case the oxidised form is the compound $\text{Cu}(\text{NCS})_2^-$.

If the activity of the NCS^- ions is lower than 2.0 g-ion/dm³ the $\varphi_{\text{decomp.}} - \lg a_c$ relation is linear with the tangent of the gradient equal to -0.0592, which indicates reduction of the NCS^- ions through a stage involving the formation of the compound CuNCS .

The mechanism of the electrochemical reduction of NCS^- ions at copper can be represented as follows:



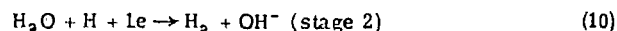
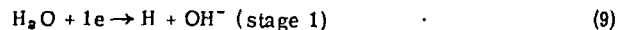
The slow stage of the overall process (8) is the reduction (decomposition) of the compound CuNCS (5).

If the activity of the NCS^- ions is higher than 2.0 g-ion/dm³, and also in the presence of considerable amounts of cyanide and thiocyanate complexes of copper in the solution, reduction of the NCS^- ions by a different mechanism is possible. The adsorption of CN^- , NCS^- , and $\text{Cu}(\text{CN})_2^-$ ions at the copper cathode does not significantly affect the electrode potential of copper.

It is known that the adsorption of anions on the cathode leads to a strong shift of the half-wave potential for the reduction of dissolved oxygen towards the negative side⁹). A shift of the half-wave potential for the reduction of oxygen towards the negative side is also observed during the adsorption of CN^- , NCS^- , and $\text{Cu}(\text{CN})_2^-$ ions on the copper cathode. The shift is considerably smaller during the adsorption of

NCS^- and $\text{Cu}(\text{CN})_2^-$ ions than during the adsorption of CN^- ions.

Let us consider the effect of the adsorption of anions on the reduction of hydrogen in a cyanide-thiocyanate solution. The mechanism of the reduction of hydrogen in an alkaline medium can be represented by the transition reactions⁹):



The cathode potential in this case is a function of the current density and the ζ potential:

$$\varphi_c = -\frac{RT}{(1-a)F} \ln |i| + \zeta + \text{const} \quad (11)$$

The adsorption of anions on the cathode leads to an increase in the negative ζ potential and, consequently, to an increase in the hydrogen overpotential. As shown by our investigations, the adsorption of the CN^- ion on the copper cathode results in an increase of the hydrogen overpotential, whereas the adsorption of the NCS^- ion does not affect the hydrogen overpotential (figs.1 and 3).

In an alkaline cyanide solution the overall degree of surface coverage of the copper cathode is composed of the degree of surface coverage with hydrogen atoms (θ_H) and CN^- ions (θ_{CN^-}), and the density of the exchange current for the reduction of hydrogen can be expressed in terms of the following equation:

$$i_0 = k[\text{H}_2\text{O}](1 - \theta_H - \theta_{\text{CN}^-}) \cdot e^{-\frac{(1-a)F}{RT} \varphi_0} \quad (12)$$

where k is the rate constant of the cathode process.

If the reciprocal of the adsorption constant of the CN^- ions at copper is considerably lower than the activity of the CN^- ions in the solution, then (as we showed earlier for the case of the adsorption of thiourea¹⁰) the exchange current density must be inversely proportional to the activity of CN^- ions in the solution:

$$i_0 = \frac{k_2}{B} a_{\text{CN}^-}^{-1} + k_2 \theta_H \quad (13)$$

Here k_2 combines the constant values in Eq.(12).

$$k_2 = k[\text{H}_2\text{O}] \cdot e^{-\frac{(1-a)F}{RT} \varphi_0} \cong i_0(a_{\text{CN}^- \rightarrow 0}) = 2.09 \cdot 10^{-4} \text{ A/dm}^2$$

We confirmed the linearity of the relation between i_0 and a^{-1} experimentally for NaCN concentrations of 0.02-0.32 mole/dm³ in the solution. Experimentally it was found that $k_2/B = 2.08 \cdot 10^{-7}$ and $k_2 \theta_H = 1.0 \cdot 10^{-9}$. Consequently, the adsorption constant of the CN^- ions on copper is $B = 1.0 \cdot 10^7$, and the free enthalpy for the adsorption of the CN^- ion on copper (at 298°K) under the investigated conditions amounted to:

$$-\Delta G_a = RT \ln B = 1365 \lg 1000 = 4095 \text{ cal/g-ion}$$

The degree of coverage of the active centres on the surface of the copper by hydrogen atoms under the experimental conditions was determined as $\theta_H = 4.78 \cdot 10^{-3}$. Variation in the concentration of the NCS^- ion in the solution within the limits of 0.1-3.5 g-ion/dm³ had practically no effect on the hydrogen overpotential (fig.3). On this basis it can be considered that the adsorption of NCS^- ions on the copper cathode is extremely insignificant.

References

- 1) I N Plaksin et alia: Hydrometallurgy with the use of ion-exchangers. Metallurgiya, Moscow 1964.
- 2) F Habashi: Principles of applied metallurgy. Vol.2 Hydrometallurgy. Metallurgiya, Moscow 1975.
- 3) B N Laskorin et alia: Ion exchange for the treatment of gold-containing clay ores. Tsvetnye Metally 1967, (3).
- 4) G N Shvirin: Technology of the extraction of the valuable components from the effluents of concentration plants.

SUBJ
MNG
EPF

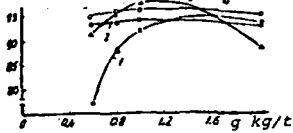


Fig. 3 The effect of the Na_2CO_3 (1,2) and CaO (3,4) consumption rates on the extraction of gold (1,3) and sulphur (2,4) by the flotation of ores A and B.

Thus, the foregoing once again confirms the expediency of using lime instead of soda as a medium regulator in

200. Non-Fe
1978 v.6 N2

the flotation of low-sulphide quartz-clay gold-containing ores. An appropriate dosage of lime, not permitting the attainment of the depression threshold, not only does not reduce but, on the contrary, helps somewhat to increase the extraction of gold and sulphides. Moreover, lime, being a coagulant, facilitates the thickening of the pulps and eliminates the need for the use of expensive coagulants of the polyacrylamide type.

References

- 1) N V Svistunov: Kolyma 1964, (1).
- 2) S M Anisimov et alia: Tsvetnye Metally 1965, (11).
- 3) S I Mitrofanov: Selective flotation. Metallurgizdat, Moscow 1958.
- 4) V V Lodeishchikov: Technique and technology of the extraction of gold from ores abroad. Metallurgiya, Moscow 1973, p.88.
- 5) A P Kreshkov: Principles of analytical chemistry. Khimiya, Moscow 1965, 1.

UDC 546.77'215:542.61

Extraction of peroxomolybdates from sulphate solutions by a tetraoctylammonium salt

G M Vol'dman, A N Zelikman and I Sh Khutoretskaya (Moscow Institute of Steel and Alloys. Department of Rare and Radio-Active Metals and Powder Metallurgy)

Extraction from peroxide solutions may provide an effective method for the separation of molybdenum and tungsten^{1,2}), spectral analysis of high-purity tungsten and molybdenum^{3,4}) and for other purposes. In recent years several papers have been devoted to the relationship and mechanism of the extraction of peroxomolybdates from nitrate solutions with tri-n-butyl phosphate⁵), trialkylbenzylammonium salts⁶), trioctylamine⁷), and alkylenediphosphine dioxides⁸). In the present work we investigated the relationships governing the extraction of peroxomolybdates from sulphate solutions with tetraoctylammonium sulphate.

To prepare the solutions we used sodium molybdate of analytical grade, hydrogen peroxide, and sulphuric acid of chemically pure grade. The amount of hydrogen peroxide in the solutions was 5 mole for 1g-atom of molybdenum.

The extraction was realised in separating funnels with a 0.005M solution of tetraoctylammonium sulphate (i.e. containing 0.01g-ion/l of NR_4^+), obtained from pure tetraoctylammonium bromide, in toluene with the organic and aqueous phases in a volume ratio of 1:1. The aqueous solution was brought into contact with the extractant at room temperature ($20 \pm 2^\circ\text{C}$) for 15 min, which ensured the attainment of equilibrium. The distribution of molybdenum between the equilibrium phases after extraction was monitored by analysis of the refined product and the alkaline re-extract. The molybdenum was determined by a colorimetric method⁹) after removal of the hydrogen peroxide by treatment of the solutions with hot concentrated hydrochloric acid and decomposition of the organics by evaporation of an aliquot portion with concentrated nitric and sulphuric acids.

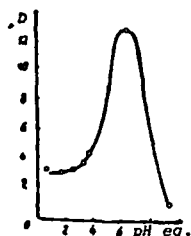


Fig. 1 The dependence of the distribution coefficient of molybdenum on the pH of the equilibrium aqueous phase. Initial concentration of molybdenum 0.01g-atom/l; extraction with 0.005M solution of tetraoctylammonium sulphate in toluene.

Fig. 1 shows the dependence of the distribution coefficient of molybdenum on the pH of the equilibrium aqueous phase during extraction from solutions with an initial concentration of 0.01g-atom/l. The distribution coefficient has a

maximum value at pH 5-7. The reason for the decrease in the distribution coefficient in the region of higher pH values is evidently the increasing competition from OH^- ions. The decrease in the distribution coefficient of molybdenum with decrease in pH is due to two factors. The first is the fact that the concentration of SO_4^{2-} increases simultaneously with the concentration of H^+ ions when sulphuric acid is added to the solution. The second is the additional effect at pH values below 3 and is due to the conversion of HMoO_4^- or $\text{HMo}_2\text{O}_{11}^{2-}$ ions, which predominate in the solution in the range of pH 3-9, into the form of the undissociated acids H_2MoO_5 or $\text{H}_2\text{Mo}_2\text{O}_{11}$ respectively. During the extraction process the undissociated peroxomolybdic acids are exchanged for the stronger sulphuric acid, as a result of which there is an increase in the aqueous solution of the concentration not only of the SO_4^{2-} ions but also of H^+ ions, and an increase in the concentration of the latter in the initial solution must impair the extraction.

The data required in order to present the extraction equation were obtained by the methods of saturation and displacement of equilibrium. In both methods the pH of the equilibrium aqueous phase was 2. As seen from fig.2, the highest content of molybdenum in the extract amounted to 0.01 g-atom/litre, which corresponds to an $\text{NR}_4^+:\text{Mo}$ ratio of 1:1 in the saturated organic phase (and, consequently, in the compound formed during extraction).

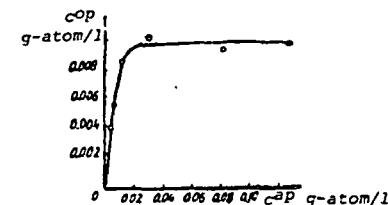


Fig. 2 The dependence of the concentration of molybdenum in the organic phase on its content in the equilibrium aqueous solution. Concentration of extractant in toluene 0.005M.

In contrast to the saturation method, the equilibrium displacement method (dilution method) makes it possible to determine not the ratio of the number of molecules of extractant

and metal in the compound which forms but the stoichiometric coefficient for the extractant in the extraction equation (11). During the investigation of extraction by amines and quaternary ammonium salts the use of the equilibrium displacement method is made difficult on account of polymerisation of the extractant, the degree of which increases with increase in its concentration^{1,2}). However, polymerisation can be prevented by the use of a diluent with a high dielectric constant³). We therefore used solutions of tetraoctylammonium sulphate in nitrobenzene [dielectric constant $\epsilon = 35.75$ at 20°C⁴)] to study the dependence of the distribution coefficient of molybdenum on the concentration of the free extractant. The use of various diluents and the associated difference in the degree of polymerisation of the extractant in the experiments on saturation and displacement of the equilibrium does not prevent comparison of the results obtained, since with full saturation of the organic phase the ratio of the weights of metal and extractant does not depend on the degree of polymerisation.

The initial concentration of the quaternary ammonium compound (QAC) was varied between 0.005 and 0.04 g-eq/litre NR_4^+ ; the concentration of molybdenum in the initial aqueous solutions was varied in line with the concentration of the QAC between 0.0013 and 0.0104 g-atom/litre. Parallel variation of the concentrations of the extractant and the metal made it possible in all the experiments to secure practically the same ratio between the concentrations of the free and combined extractant. Moreover, in all cases a sufficient amount of molybdenum for analysis remained in the refined product with increase in the concentration of the extractant in spite of the increase in the distribution coefficient. The concentration of the free extractant was obtained as the difference between the initial concentration (g-eq/litre) and the molybdenum content of the extract (g-atom/litre), since 1 g-ion of NR_4^+ is combined with 1 g-atom of molybdenum in the compound which forms.

The relationship obtained

$$\lg D = f\{\lg [QAC]_{free}\}$$

is plotted in fig.3 (curve 1). For comparison the same figure gives curve 2, characterising the dependence of log D on $\log [QAC]_{free}$ when the low-polarity solvent toluene is used. Whereas curve 2 indicates clearly defined polymerisation of the extractant, which increases with increase in the concentration of the QAC in toluene (a curvilinear relationship where the gradient of the tangents decreases with increase in the concentration of the QAC), the use of nitrobenzene as diluent completely eliminates the polymerisation over the whole range of investigated concentrations of the extractant; the dependence of log D on $\log [QAC]_{free}$ in this case is linear. The gradient of line 1, equal to 0.5, therefore corresponds to the stoichiometric coefficient for the tetraoctylammonium sulphate in the extraction equation.

The formulation of the extraction equation is complicated by the fact that there is no published view in the literature about whether there are monomeric or dimeric peroxomoly-

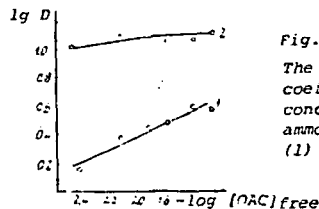
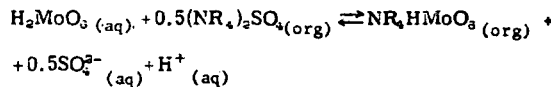
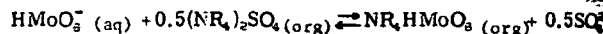


Fig.3

The dependence of the distribution coefficient of molybdenum on the concentration of free tetraoctylammonium sulphate in nitrobenzene (1) and toluene (2).

bdates in the solutions, and this does not make it possible unambiguously to go for the MoO_4^{2-} or the $Mo_2O_7^{4-}$ anion. It was found, however, that the results obtained by the saturation method ($NR_4^+ : Mo$ ratio in the extracted compound 1:1) and the equilibrium displacement method (stoichiometric coefficient for $(NR_4)_2SO_4$ 0.5) correspond to only one combination of the forms of molybdenum in the aqueous solution and in the organic phase, i.e., the monomer in the aqueous solution, while the extracted compound has the composition NR_4HMoo_3 .

Thus, the equations for the extraction of molybdenum from peroxide solutions with pH values of 3-6 and less than 2.5-3 by tetraoctylammonium sulphate without polymerisation in the organic phase can be represented in the following form:



References

- 1) A N Zelikman et alia: U S Patent No.3969478.
- 2) G M Vol'dman et alia: Dokl. Akad. Nauk SSSR 1977, 232, (3), 660.
- 3) I M Ivanov et alia: Izv. SO Akad. Nauk SSSR, Ser. Khim. Nauk 1972, No.3, No.7, 90.
- 4) L S Zolotareva et alia: Izv. SO Akad. Nauk SSSR, Ser. Khim. Nauk 1973, 1, (2), 92.
- 5) A N Zelikman et alia: Zh. Neorgan. Khim., 1972, XVII, (3), 783.
- 6) A N Zelikman et alia: Zh. Neorgan. Khim., 1974, 14, (4), 1040.
- 7) Z A Berkman et alia: Zh. Neorgan. Khim., 1974, 14, (10), 2839.
- 8) L B Zaichikova: Zavod. Lab., 1949, 15, 1025.
- 9) J Chanyi: J. Acta Chem. Acad. Scient. Hung., 1958, 14, 71.
- 10) W P Griffith: J. Chem. Soc., 1953, 5345.
- 11) V V Fomin: Chemistry of extraction processes. Atomizdat, Moscow 1960
- 12) A M Rozen et alia: Chemistry of extraction processes. Nauka, Moscow 1972, p.41.
- 13) V S Shmidt: Extraction with amines. Atomizdat, Moscow 1970.
- 14) F Eme: Dielectric measurements. Khimiya, Moscow

than 60% of reduced hydrazo compound capacity of 250 compartments with a temperature of 70°C. The experiments were carried out in the form of an anodeless cell as best as fibres retained under the cathode adhering tightly to the anode. The difference in the potential was measured through a salt bridge. The reduction of tin from the solution at the cathode of the solution at the anode was constant.

As cathode and anode (about 20 cm² each) the initial density of the solution was changed through the current yield of 100%. The potential of the electrodes of the initial solution was kept the same and thus kept the reduction products of tin, free tin, the dissolution rate of tin, the tin content was constant. The concentration of the solution of the initial solution was kept the same and thus kept the reduction products of tin, free tin, the dissolution rate of tin, the tin content was constant. The concentration of the solution of the initial solution was kept the same and thus kept the reduction products of tin, free tin, the dissolution rate of tin, the tin content was constant.

Hydrometallurgy

Economics provide motive for growth of bacteria leaching

Microbiological leaching of sulphide ores will enjoy increased use in the future, according to British Columbia Research Council's (BCRC) scientists, D. W. Duncan, C. C. Walden, P. C. Trussel and E. A. Lowe, in a paper delivered at the 1966 annual meeting of AIME.

They disclosed that a team of scientists and engineers at BCRC has been studying bacterial leaching of metals from ores for 10 years, and now have an extensive program underwritten by 16 prominent mining companies.

Although their immediate interest centers on copper recovery from low-grade dumps, similar leaching methods are feasible for zinc, nickel and uranium. Copper leaching solutions, concentrated enough for recovery by electro-deposition, can be obtained.

Bacteria have to be trained to be resistant to a particular mineral. How-

ever, their tolerance for high-metal concentrations builds up rapidly except for certain metals like molybdenum.

Thiobacillus ferrooxidans is the leaching "bug" used. This bacteria oxidizes ferrous iron to ferric-iron producing ferric sulphate and sulphuric acid for dissolving the wanted metal.

Kennecott Copper Corp. pioneered in this field and was granted U.S. Patent 2,829,964, dated April 8, 1958.

Equipment for the process must be constructed of materials that do not kill the microbes. Also important for healthy multiplication of bacteria is temperature control at 40°C maximum and a pH above 1.5 with optimum conditions at about 2.

Further information regarding this patent appears in *E/MJ*, June, 1958.

BCRC scientists prefer the shake-flask technique for rapidly evaluating

biological leaching variables. Different forms of agitation were used in order to determine their potential for laboratory and development work. On a laboratory scale, the only method compatible with the gyratory shaking technique used in the tests, was stirring with a magnetic bar. The magnetic stirring rod had to be operated at a speed that prevented mineral particles from splashing out of suspension and one that would limit frothing. Results indicated leaching rate can be enhanced by this method.

Previously reported, in-situ bacteria leaching underground continues. One report gives a cost to spray, pump and neutralize worked-out stopes as \$1.065 Canadian per pound U_3O_8 .

Work proceeds on investigating economics behind in-place leaching, improving leaching rate, and making process more efficient.

Three new patents show promise for cyaniding refractory ores

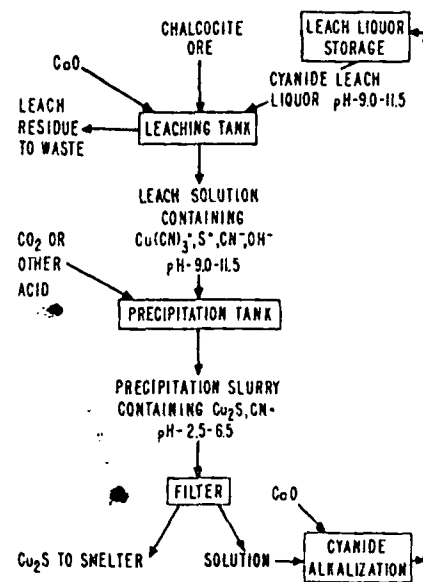
The precipitation of copper from its solutions by means of iron is the accepted method for treating weakly acid and neutral solutions, as well as discarded electrolytic cell liquors.

A new invention particularly concerned with improving copper value recovery from solutions derived from mine waters and leaching copper ores is the subject of U. S. Patent 2,390,450, assigned to Dow Chemical Co., by C. H. Keller.

Patent claims list these advantages for the water-soluble thiocyanate (uses alkali and alkaline earth metal and ammonia type thiocyanates) technique: (1) can be applied equally well to acid or neutral copper solutions; (2) reagents are recovered and reused; (3) copper can be completely extracted from solution; (4) copper product produced is commercially pure, suitable for smelting or other processes; (5) ordinary metallurgical equipment is used and does not require heavy capital investments.

In practice, copper leach solutions are treated with a solution of water-soluble thiocyanate and a reducing agent (sulphur dioxide, sulphites, bisulphites, zinc, iron, etc.) to change cupric to cuprous compounds. Cuprous thiocyanate is precipitated almost instantaneously from cold or warm, neutral or acid solutions, using stoichiometric proportions of thiocyanate.

Separation of precipitate from so-



U. S. PATENT 3,224,835 tells about above cyanidation process for treating flotation tailings of Copper Range.

lution is followed by contacting precipitate with an aqueous solution of a water soluble alkaline agent. Thiocyanate is solubilized leaving an insoluble copper residue behind. This copper residue is said to be suitable for smelting according to standard practice.

Another invention assigned to American Cyanamid Co. relates to a "Process of extracting precious metals

from their ores by the use of alpha-hydroxynitriles," and is covered by U.S. Patent 2,829,045.

Currently, inorganic cyanides, such as white cyanide (96-98% NaCN) or crude calcium cyanide (48-50% NaCN equivalent), used in very strongly alkaline circuits, (pH 11, 12 or higher) is employed to extract gold and silver from ores.

However, use of organic cyanides, instead of inorganic cyanides, namely, alpha-hydroxynitriles, may offer remarkable advantages over current practice. Organic cyanides of this type can be generally used. According to the patent, test work failed to reveal an ore that could not be leached with alpha-hydroxynitriles, if it was first of all amenable to inorganic cyanide.

Lactonitrile ($CH_2CH(OH)CN$), a colorless liquid, is listed by the patent as being preferred because it has a very high percentage of CN in comparison to other alpha-hydroxynitriles. In fact, crude lactonitrile, a by-product of acrylonitrile manufacture is spotlighted. Crude lactonitrile is represented as often being available at very low cost, and since it is just as effective for a given CN content as pure chemicals, it may find a place for economic reasons.

An example compared results using crude lactonitrile and 96-98% white, sodium cyanide. Essentially, it represented the following:

(Continued on p 544)

EXTRACTION OF PLATINUM METALS
FROM SOLUTIONS WITH MECHANICALLY ACTIVATED PYRRHOTITE

UDC 661.183.5:546.9:669.23

N. A. Dragavtseva, E. G. Avvakumov, and N. I. Matveeva

In view of the fact that extraction of platinum metals from solutions to the ultimate permissible concentrations presents particular difficulties, it is essential to seek new ways of solving this problem. The use of mechanically activated precipitating agents is one of the lines to be followed.

In the present work, pyrrhotite mechanically activated in a planetary centrifugal mill designed by S. I. Golosov was used for extraction of platinum metals from solutions [1]. Corundum balls and drums were used to avoid cementation of the platinum metals by iron. The drum volume was 120 cm³, the diameter of the balls was 5 mm, their mass 90 g, and the speed was 800 rpm. The weighed portion of pyrrhotite was ground in the mill for a prescribed time, then 10 ml of water was added and the material was ground again for 1 min to break up the powder. The activated material was mixed with solution containing the platinum metal (pH = 2), using a magnetic mixer. The experiments were at room temperature.

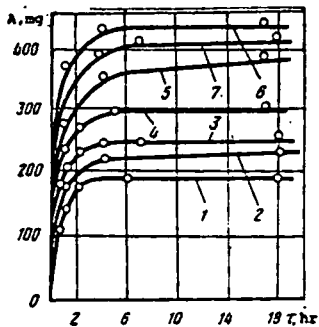


Fig. 1. Kinetics of dissolution of pyrrhotite activated over various periods of time (min) in hydrochloric acid (pH 2):

- 1 - without activation; 2 - 1; 3 - 2; 4 - 5; 5 - 10; 6 - 15; 7 - 20.

The amount of dissolved Fe from 1 g FeS (mg) is shown on the A axis.

the amount of iron passing into solution goes through a peak corresponding to a solubility of ~ 63% when the mechanical treatment time increases.

The variation in the solubility of pyrrhotite according to its surface is almost linear. The deviation from the linear relationship observed at a surface value of > 60 m²/g is apparently caused by the formation of aggregates whose inner surface is relatively inaccessible to the solvent but accessible to inert gas (when the surface is measured).

Kinetic data on palladium precipitation by activated pyrrhotite are given in Fig. 2. The initial palladium concentration was 350 mg/liter. Preliminary experiments showed that the capacity of the pyrrhotite was practically independent of the initial metal content of the solution. The ultimate capacity, which is achieved in 6-10 hr, is 2300 mg/g in the case of palladium. Similar kinetic data were also obtained for osmium. The ultimate capacity for osmium is 3000 mg/g.

The Table gives data on precipitation of platinum and

Solutions of platinum, palladium, and osmium were prepared by dissolving the compounds H₂PtCl₆, PdCl₂, and OsCl₄ in 0.5 N hydrochloric acid. Solutions of Rh(III) were obtained from the metals by melting them with sodium chloride in a quartz tube in a current of chlorine at 650-700°C.

The concentration of platinum metals and iron in the solutions was determined by colorimetric methods [2,3]; the surface of the powders was found by gas-adsorption chromatography [4]. The pyrrhotite used had a hexagonal structure [sulfur content 52.9% (at.)].

It is apparent from Fig. 1 that

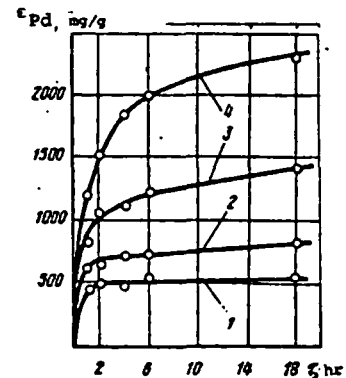


Fig. 2. Kinetics of palladium precipitation by pyrrhotite activated over various periods of time (min):

- 1 - without activation; 2 - 2; 3 - 10; 4 - 20; E_{Pd} is the capacity of FeS for Pd.

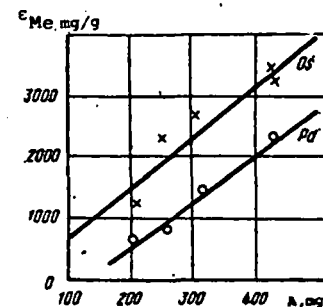


Fig. 3. Amount of platinum metal passing into the solid phase related to the solubility of pyrrhotite (A is the amount of dissolved Fe from 1 g FeS, mg).

rhodium with activated pyrrhotite which show that the capacity of pyrrhotite for these metals is much less than for palladium and osmium.

The low extraction of platinum and rhodium compared with palladium and osmium is apparently due to the fact that the capacity of these metals for sulfide formation and reduction is less marked. Thus whereas palladium and osmium can be extracted from solutions with hydrogen sulfide under normal conditions, the precipitation of platinum and rhodium calls for heating and a large excess of reagent. These metals are not reduced to the elementary state by bivalent iron [2].

Certain conclusions as to the mechanism of platinum metal extraction into the solid phase can be drawn from the results obtained.

It seems to us that there is precipitation in sulfide form, reduction to metals by the ions of bivalent iron which have passed into solution, and surface sorption on pyrrhotite and the platinum metal sulfides.

Evidence in support of palladium and osmium precipitation as a result of reaction with S^{2-} and Fe^{2+} ions is provided by the linear relationship between the amount of precipitated metals and the amount of pyrrhotite converted to soluble form (Fig. 3), and also by kinetic data showing that the curves for platinum metal precipitation and pyrrhotite dissolution emerge simultaneously onto a plateau.

The pyrrhotite and freshly precipitated sulfides have a large surface and are active as regards sorption. The adsorption of considerable amounts of platinum metals on them is therefore possible. Thus ~200 mg Pd is necessary to form one monolayer on a 100 m² surface.

The area of ground pyrrhotite is fairly large, amounting to 60-80 m²/g.

Adsorption increases with a rise in the valence of the element being adsorbed. Osmium ions have a +4 charge in solution, and palladium ions under these conditions have +2, and indeed the amount of sorbed osmium is much greater than the amount of sorbed palladium. These results provide indirect evidence of the fact that surface adsorption may be one of the factors in platinum metal extraction from solutions, in addition to precipitation of sulfides and reduction to metals.

The data on extraction of platinum metals with activated pyrrhotite indicate that the precipitation agent is high effective; this apparently explains the accumulation of platinum metals in natural pyrrhotite. The data obtained may be used in the purification of effluents containing platinum metals.

Precipitation of Pt and Rh with Activated Pyrrhotite

τ, min	S, m ² /g	P _{Me} , mg/g	
		Pt	Rh
0	0.22	19.0	8.0
2	—	20.5	10.0
5	34.2	21.0	9.5
10	61.5	20.5	10.0
20	89.0	23.2	14.0

REFERENCES

1. S. I. Golosov, Inventor's Cert. No. 101874, Byulleten' Izobretenii, 1955, No. 11, 45.
2. Guide to Chemical Analysis of Platinum Metals and Gold, Moscow, Nauka, 1956, 314 pages, illustrated. Authors: S. I. Ginsburg, K. A. Gladyshevskaya, N. A. Ezerskaya, et al.
3. Z. Marchenko, Photometric Determination of Elements, Moscow, Mir, 1971, 502 pages, illustrated.
4. N. E. Buyanova and A. P. Karnaukhov, Chromatographic Determination of the Specific Surface of Solids by Thermal Desorption of Argon, Novosibirsk, Nauka, 1965, 610 pages, illustrated.

ENERGY AND PARTICLE SIZE EFFECTS IN THE FRAGMENTATION OF OIL SHALE
WITH A TORSIONAL SPLIT HOPKINSON BAR*

D. Grady, J. Lipkin, L. Costin

Sandia National Laboratories**
Albuquerque, New Mexico 87185

1980

UNIVERSITY OF UTAH
RESEARCH INSTITUTE
EARTH SCIENCE LAB.

SUBJ
MNG
EPSE

I. INTRODUCTION

Underground processing of oil shale offers potential economic and environmental benefits sufficient to warrant a sizeable investment in research time and money to develop the necessary engineering capabilities. A critical aspect of the retort process relies on efficient explosive rubblization of the "in place" oil shale. Consequently, considerable effort is being focused on understanding and improving the explosive fragmentation process and in developing analytic methods and computational fracture models to guide the selection of blasting schemes.

One aspect of the fracture and fragmentation process for which a fundamental understanding is lacking is concerned with the fragment size distribution resulting from explosive loading. Material properties related to differences in oil shale grade and kinematic properties such as the strain rate influence the mean fragment size and the relative ratio of fine to large fragments in ways which are not well understood. Lack of a clear perception of these effects is currently frustrating further modeling and analysis.

A further concern relates to the energy requirements of explosive rock breakage. Calculation of the energy needed to achieve a desired fracture surface area through measured fracture toughness values is recognized to provide an unrealistic lower limit. Both practical and fundamental constraints prohibit the complete conversion of explosive-induced stress-wave energy into fracture energy. The energy required to achieve a specific particle size is not yet clearly known and further study directed toward an understanding of the energetics of dynamic fracture is necessary to optimize explosive blasting.

In the present work, a torsional split Hopkinson bar was used to conduct an experimental investigation of the particle size distribution and energy aspects of dynamic fragmentation of oil shale. Although recognized as being unrepresentative of explosive blasting the method allows for controlled experimentation in which input parameters can be accurately varied and output parameters, such as stress and strain, continuously resolved. Earlier studies by Lipkin and Jones (1979) with a torsional bar focused on the stress states achieved in dynamic fracture of oil shale and Gauna (1979) used a compressional split Hopkinson bar to study fracture energy requirements.

In this study both strain rate and oil shale grade were varied to investigate the influence on the fragment size distribution and fracture energy. Fracture energies were determined with active instrumentation on the Hopkinson bar and standard sieving methods were used to evaluate the fragment size distributions. In section II the experimental approach and

methods used to analyse the data are described. In section III the experiments conducted with various grades of oil shale are presented and the results for a specified oil shale grade loaded at different imposed strain rates are described in section IV. Discussion and comparison with earlier work is provided in section V.

II. EXPERIMENTAL METHODS AND ANALYSIS

Test Apparatus

The torsional split Hopkinson bar used in the present experiments is the same as that used by Lipkin and Jones (1979). The sudden opening of a friction clamp releases the torque stored in the input bar. Elastic shear waves propagate from the clamping point and interact with the test specimen which is bonded to both the input and output bars. Wave interaction at the specimen gives rise to transmitted and reflected waves which are monitored with strain gages during loading and failure of the specimen. The time-resolved measurements of these stress waves are used to evaluate the stress and strain history applied to the sample (Lipkin, et al., 1979).

Specimen Preparation

Both solid cylinder and thin-walled tubular samples of oil shale were studied. Tubular specimens were used when the loading strain rate was the parameter of interest. The solid specimens were used in the variable oil shale grade study where only energy effects were considered and a larger sample volume was desired.

The tubular samples of 80 ml/kg oil shale were machined with the axis of the tube perpendicular to the bedding planes of the sample. The tubes were 2.5 mm in length with an inner and outer diameter of 18 mm and 20 mm, respectively. This geometry was selected so that stress and strain rate would be approximately uniform in the strain rate regime, between about 80/s and 420/s. The finished specimens had machined flanges for bonding to the input and output bar. A more detailed description of the tubular specimen geometry has been provided by Lipkin and Jones (1979).

The solid cylinder specimens were 10 mm in length and 15 mm in diameter. Again the cylinder axis was perpendicular to the bedding planes. Samples were selected from four nominal oil shale grades of 32, 76, 124, and 156 ml/kg (~ 8, 19, 31, and 39 gal/ton). These are correlated with actual sample densities in Table I.

* This work was supported by the U.S. Dept. of Energy (DOE) under Contract DE-AC04-76-DPO0789.
**A U.S. DOE Facility.

TABLE I

TORSION FRAGMENTATION EXPERIMENTS

Shot Number	Density* (kg/m ³)	Fracture Energy (J)	Fracture Strain-Rate (s ⁻¹)	Fragment Mass (g)	Fracture Area (10 ⁻³ m ²)	Fracture Energy/Area (J/m ²)	Regression Coefficients "a" (g·mm ⁻ⁿ)	"n"
BF-02	2050	0.45	--	1.36	0.52	851	.0050	1.54
BF-04	2050	0.52	--	2.42	1.09	479	.0082	1.72
BF-14	2030	0.42	--	0.99	0.79	534	.0087	1.73
BF-15	2060	0.55	--	0.81	1.02	537	.0185	1.57
BF-16	2060	0.52	--	2.26	1.68	310	.0130	1.95
BF-8	2160	0.76	--	2.51	2.75	275	.0474	1.62
BF-9	2140	0.69	--	2.07	1.80	383	.0200	1.85
BF-10	2130	0.35	--	0.35	0.41	840	.0028	2.49
BF-1	2360	0.62	--	2.36	2.63	235	.0363	2.02
BF-3	2360	0.38	--	2.45	2.73	139	.0421	1.91
BF-11	2340	0.76	--	2.46	3.00	253	.0436	2.04
BF-12	2370	0.69	--	2.80	3.65	189	.0701	1.83
BF-13	2360	0.14	--	1.09	0.25	559	.0034	1.31
BF-5	2580	1.11	--	3.10	4.12	269	.1042	1.67
BF-6	2590	0.69	--	2.60	3.52	196	.0845	1.79
BF-7	2610	1.25	--	3.00	4.34	288	.1111	1.79
SR-1	2320	--	85	0.082	--	--	--	--
SR-2	2320	--	180	0.146	--	--	--	--
SR-3	2320	--	210	0.250	--	--	--	--
SR-4	2320	--	420	0.098	--	--	--	--

*A direct correlation between oil shale grade and density has been obtained by Smith (1956). Using this relation the four groups of increasing density oil shale samples correspond to oil shale grades of 156, 124, 76 and 32 ml/kg, respectively.

Energy and Strain-Rate Evaluation

Energy or strain-rate conditions characteristic of each test were determined by analyzing the strain gage records from both the input and output bars. In addition to the shear strain gage instrumentation, longitudinal strain gages were placed on one bar. This was to account for a mode transfer of shear energy to longitudinal energy occurring during the failure of the oil shale specimen (Lipkin and Jones, 1979).

Shear strain rate specific to a particular test follows from the usual analysis of Hopkinson bar response. Shear strain amplitudes are related to the corresponding elastic torque levels in the bar system. The torque history measured in the output bar, $T_2(t)$, is directly related to the specimen shear stress history. Assuming that the shear strain is uniform in the gage length, the relation between the shear stress, τ , and T_2 is given by

$$\tau(t) = \frac{T_2(t)}{2\pi r_m^2 h} \quad (1)$$

where r_m is the mean radius of the specimen and h is the wall thickness. Similarly, analysis of the elastic wave propagation characteristics of the bar system leads to the following relation for the average specimen shear strain rate,

$$\dot{\gamma} = \frac{r_m}{l} \frac{2}{J\rho C} (T_1 - T_2) \quad (2)$$

where l is the specimen gage length and $T_1(t)$ is the input bar torque history. The product $J\rho C$ is the torsional acoustic impedance of the bar, with J the polar moment of inertia, ρ the mass density and C the shear wave velocity.

The energy expended during inelastic deformation and failure of the specimen is the difference between the wave energy incident on the specimen, and the wave energy reflected from, and transmitted through, the specimen. An analysis of the elastic shear wave characteristics results in an expression for the energy expended in fragmentation of the specimen,

$$\epsilon = \frac{2}{J\rho C} \int_0^{\infty} T_2(T_1 - T_2) dt \quad (3)$$

Contributions due to axial mode conversion were also calculated for several tests and found to be only a few percent of the shear energy. This contribution was therefore neglected in subsequent data reduction and the expressions in Equations 2 and 3 were used to classify the dynamic tests performed in the present study.

Fragmentation Analysis

In each test a soft plastic container was placed around the specimen to collect the fragments resulting from the impulsive fracture event with a minimum amount of secondary breakage. Fragments from each test were sieved to determine the fragment size distribution. Standard sieves ranging from number 4 (4.75 mm aperture) to number 100 (0.15 mm aperture) were found adequate for the purpose.

The measured size distribution curves were found to be well described by an expression of the form (Schuhmann, 1940)

$$m = ax^n, \quad (4)$$

where m is the cumulative mass passing size x . Parameters a and n are determined by a statistical fit to the distribution.

The fracture surface area created during fragmentation was determined by an analytic method due to Gaudin (1939). The expression for the fracture surface area corresponding to cumulative mass m is,

$$A(m) = 1.75 \frac{6a}{\rho} \frac{n}{n-1} \left(\frac{m}{a}\right)^{\frac{n-1}{n}}, \quad (5)$$

which follows directly from Equation 4 and geometric considerations. In this case ρ is the oil shale mass density and the factor of 1.75 is an empirical factor determined by Gaudin to account for geometric irregularities in particle shapes.

III. VARIABLE OIL SHALE GRADE EXPERIMENTS

Sixteen tests on solid cylinders of oil shale were conducted with oil shale grade as the controlled variable. The input amplitude of the incident pulse was maintained within the range of 95-125 Nm and, in view of the scatter in the data, can be regarded as approximately constant loading conditions. The energy dissipated in fragmentation was determined from the time-resolved incident and transmitted strain records by the method discussed in Section II. The results are presented in Table I and are shown in Figure 1. The energy dissipated in fragmentation was found to correlate with sample density (oil shale grade). A linear regression indicated approximately a factor of two increase in energy dissipated over the density range of the samples tested (2030-2610 kg/m³). The large scatter in the higher density samples (leaner oil shale) is thought to be due to the increased difficulty in preparing samples without major flaws.

Fragment size distributions were determined for each of the 16 tests. Representative distribution curves from each of the four oil shale grades are shown in Figure 2. The results indicate the difference in fragmentation with grade under specified loading conditions. The size distribution curves were well described by a distribution of the form $m = ax^n$ where m is the cumulative mass passing fragment size x . A linear regression was obtained for each distribution and the regression coefficients, a and n , were plotted as a function of the sample density in Figure 3. A strong correlation with density was found for the scale parameter, a , indicating the sensitive dependence of fragment size on oil shale grade. A weaker correlation with density was found for the shape parameter, n , with values ranging from about 1.5 to 2.0.

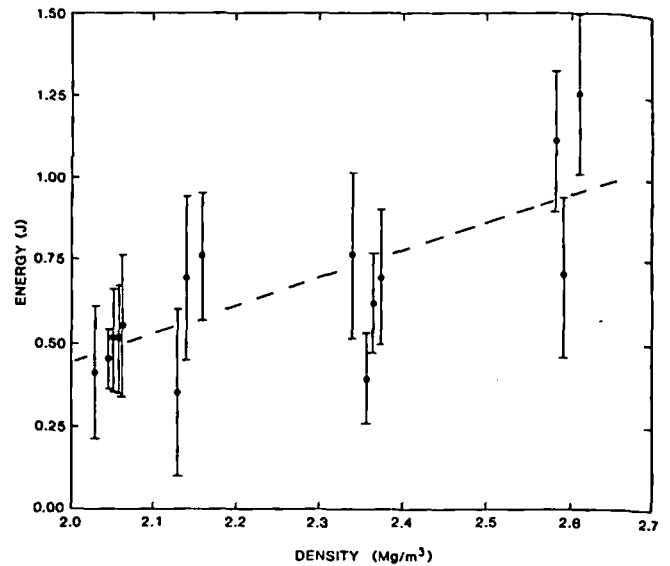


Fig. 1. Energy dissipated in fragmentation of solid oil shale cylinders under dynamic torsion loading. The dashed line is a linear regression to the data.

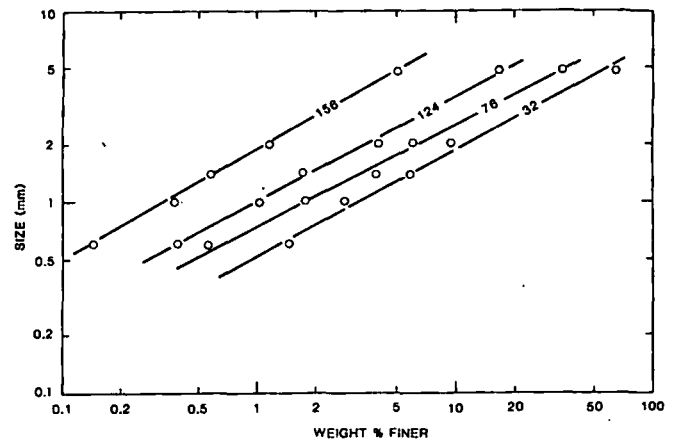


Fig. 2. Fragment size distribution curves for different grade oil shale samples. The numbers indicate the approximate grade in ml/kg.

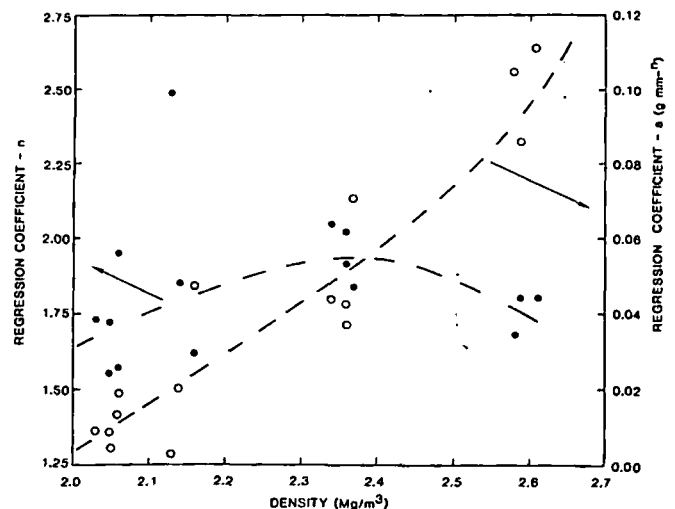


Fig. 3. Dependence of regression coefficients on density for $m = ax^n$ of fragment size distribution.

Further analysis focused on evaluation of the new fracture surface area created in dynamic fragmentation. An analytic method due to Gaudin (Equation 5) provided the fracture surface area values given in Table I.

The ratio of the energy dissipated in fragmentation to the new surface area created provides a useful index of the effectiveness of fragmentation. This fracture energy/area value is plotted as a function of oil shale density in Figure 4. The fracture energy/area achieves a minimum of about 200 J/m^2 at densities above about 2200 kg/m^3 ($\sim 100 \text{ ml/kg}$) but becomes significantly more dissipative at lower densities. At the lowest density studied (corresponding to about 160 ml/kg) values in excess of 500 J/m^2 were obtained. Comparisons with the strain energy release rates determined from studies on quasistatic single crack propagation (also shown in Figure 4) will be discussed in Section V.

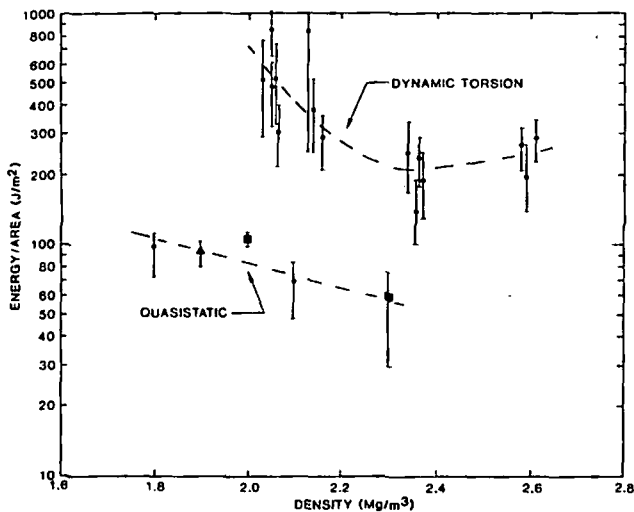


Fig. 4. Dependence of fracture energy/fracture area on sample density for both dynamic torsion and quasistatic loading.

IV. VARIABLE STRAIN-RATE EXPERIMENTS

Four fragmentation experiments were performed on thin-walled tubular specimens of 80 ml/kg oil shale under approximately uniform strain-rate loading conditions. Strain rates ranged from $85/\text{s}$ to $420/\text{s}$ or about a factor of 5. Strain gage data for each test provided the time-resolved stress and strain history. Fragments created during dynamic breakage were soft recovered and size distribution curves were determined by sieving.

The size distribution curves for each of the four different strain-rate experiments are plotted in Figure 5. Points greater than about 10% mass fraction are excluded from this plot. Small sample volumes associated with the thin-walled tubular geometry resulted in erratic values for the larger mass fractions and no clear trend was noted. The distribution curves for the finer fragments are seen to be nearly linear and parallel in a logarithmic plot. The slope of the data correspond to a shape parameter of approximately $n = 2$. Increasing strain-rate experiments are shifted consistently downward or to finer fragment sizes.

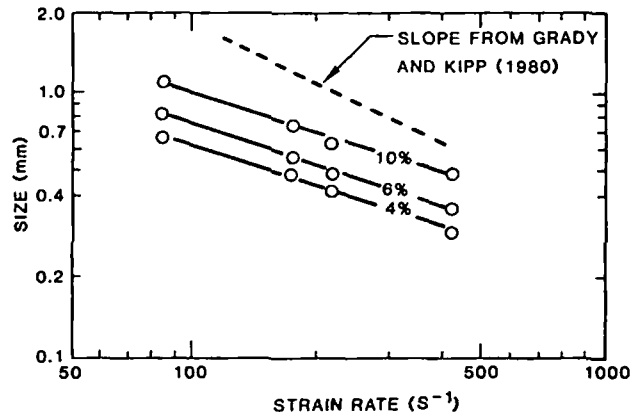
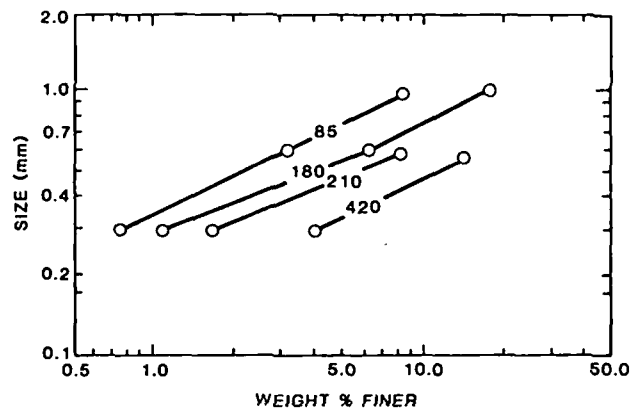


Fig. 5. Dependence of fragmentation on loading strain rate. (a) fragment size distribution curves for each strain rate test, (b) cross plot at fixed weight % finer showing the dependence of fragment size on loading strain rate. The slope of the dashed line is predicted by the fracture model of Grady and Kipp (1980).

The dependence of fragmentation on strain rate is more clearly illustrated by a cross plot of the fragment distribution curves corresponding to points of constant weight percent finer. These results are also plotted in Figure 5 and show the significant decrease in fragment size with increasing loading strain rate.

V. DISCUSSION

Oil shale is not ideally suited to a controlled study of dynamic fragmentation. Anisotropic properties and compositional variations along with major cracks and flaws make reproducible specimen preparation difficult. These problems probably account for the large degree of scatter observed in the present work. Oil shale does, however, offer the unique opportunity of investigating the effect of material property variation on dynamic fragmentation through sample to sample differences in oil shale grade. The results obtained clearly illustrate the importance of oil shale grade in fragmentation with the higher grades exhibiting increased resistance to fragmentation and energy dissipation. The loading conditions are also important in determining the outcome of fragmentation. More intense or higher strain-rate loading conditions lead to smaller average fragment size and increased fracture surface area.

A model of dynamic fracture and fragmentation has been developed recently by Grady and Kipp (1980) and applied to oil shale. Comparison of the present data with the predictions of that theory is useful. The fracture model is based on the concept of activation, growth and coalescence of fracture producing flaws. (Shockey et al. 1974) during dynamic tensile loading. Cracks are assumed to activate, grow at a constant fracture velocity and arrest when coalescence occurs. Crack activation is governed through concepts developed by Weibull (1939) in the sense that flaws are characterized by the tensile stress level at which crack growth initiates. A fundamental result of the model is a dependence of both fracture stress and average fragment size on the tensile strain rate. Model material parameters were determined from experimental results on both fracture stress and average fragment size for nominal 80 ml/kg oil shale.

With these material parameters the fracture model predicted that fragment size would depend on strain rate as $\dot{\epsilon}^{-0.73}$. This dependence is compared with the torsional bar fragment-size strain-rate data in Figure 5b and found to over predict the observed $\dot{\epsilon}^{-0.5}$ behavior. At this early stage of investigation there are numerous possible reasons for the discrepancy. We currently consider the finite sample size of the torsional bar specimens, which constrain the fragment distribution curves to smaller fragment sizes, to be the most likely explanation. The experiments which were used to determine the material parameters for the model used specimens substantially larger than the dominant fragment sizes expected at each loading strain rate which is not the case for the present experiments. It is quite possible, however, that the Hopkinson bar results are illuminating complexities in the fragmentation process not incorporated in the model.

The Hopkinson bar fracture energy/fracture area results for the variable oil shale grade experiments shown in Figure 4 indicate a minimum resistance to fracture for the higher density (leaner) specimens. Below a density of about 2100 to 2200 kg/m³ a dramatic increase in fracture resistance is noted, approaching about three times the minimum value for the richest oil shale samples studied. This break in material property response at an oil shale grade of about 100 ml/kg suggests a basic change in the oil shale microstructure. Ultrasonic studies on oil shale by Olinger (1978) also indicate a substantial change in material response at approximately the same density.

The fracture energy/area data shown in Figure 4 are compared with quasistatic strain energy release rate data for oil shale (Costin, 1980). The trend of the quasistatic data is also toward increasing fracture resistance with decreasing density although the change is not as dramatic as the dynamic data. Also the dynamic fracture energy is about a factor of five higher than the quasistatic strain energy release rate, a result typical of dynamic fragmentation.

The exponent, n , characterizes the shape of the fragment size distribution, $m = ax^n$, and consequently, the relative ratio of fine to large fragments. Rosin and Rammler (1933) and Bennett (1936) have shown that smaller n implies a weighting of the distribution toward the finer fragments while larger n implies an increasingly more uniform distribution in fragment size. In crushing and grinding applications n typically ranges from about 0.5 to as high as 1.3.

Extensive studies on point loaded spheres of brittle materials (Gilvarry and Bergstrom, 1961; Bergstrom, 1962) consistently provide values of n equal to unity within experimental error. In the present study the shape parameter, n , was found to range between about 1.5 and 2.0. High values of n seem to be characteristic of impact or impulsive fragmentation of solids where minimal crushing or secondary breakage occurs. Spall fragmentation due to high velocity impact appears to lead to similarly high values of n (Shockey et al. 1974).

VI. SUMMARY

The torsional split Hopkinson bar apparatus has been used to study the fracture energy and fragment size distributions resulting from controlled impulsive fracture of oil shale. Both strain rate and oil shale grade were varied to assess the influence of these parameters on energy dissipation and fragment size distributions.

Variations in oil shale grade under specified loading conditions showed increasing resistance to fracture for the higher oil shale grades. The fracture energy/area is significantly larger than predicted from quasistatic fracture toughness data and increases dramatically with oil shale grade above about 100 ml/kg (25 gal/ton). The mean fragment size also increased for the higher grade oil shale.

Fragmentation was found to depend on the strain rate for a specified oil shale grade. The mean fragment size decreased with increasing strain rate.

All fragment distribution curves were found to be adequately represented by a power law, $m = ax^n$, where m is the fragment mass finer than size x . The shape parameter, n , was found to be large (1.5 to 2.0), a feature which seems to distinguish dynamic fragmentation from other comminution processes. In general, variations in both strain rate and oil shale grade seemed to have little effect on n . In contrast, the scale parameter, a , was observed to depend sensitively on both variables.

REFERENCES

- BENNETT, J. G., 1936, Broken Coal, Journal Institute of Fuel, Vol. 10 pp. 22-39.
- BERGSTROM, B. H., 1962, Energy and size distribution aspects of single particle crushing, Proceedings 5th Symposium on Rock Mechanics, C. Fairhurst, Ed., pp. 155-172.
- COSTIN, L. S., 1980, in Oil Shale Programs 16th Quarterly Report, A. L. Stevens, ed., Sandia National Laboratories.
- GAUDIN, A. M., 1939, Principles of Mineral Dressing, McGraw-Hill, New York.
- GAUNA, M., 1979, Oil Shale Dynamic Toughness Measurements, 20th U. S. Symposium on Rock Mechanics, Austin, Texas, pp. 591-600.
- GILVARRY, J. J. AND B. H. BERGSTROM, 1961, Fracture of Brittle Solids. II. Distribution Function for Fragment Size in Single Fracture (Experimental), Journal of Applied Physics, Vol. 32 pp. 400-410.
- GRADY, D. E. AND M. E. KIPP, 1980, Continuum Modelling of Explosive Fracture in Oil Shale, International Journal of Rock Mechanics and Mining Science, Vol. 17 pp. 147-157.
- LIPKIN, J. AND A. K. JONES, 1979, Dynamic Fracture Strength of Oil Shale under Torsional Loading, 20th U. S. Symposium on Rock Mechanics, Austin, Texas, pp. 601-606.

- LIPKIN, J., et al, 1979, Dynamic Torsional Failure of Limestone Tubes, Proceedings, Conference on Mechanical Properties of Materials at High Rates of Loading, Oxford, U.K..
- OLINGER, B., 1978, Oil Shales Under Dynamic Stress, in Explosive Produced Fracture of Oil Shale, Los Alamos Scientific Laboratory Progress Report, LA-7357-PR, W. J. Carter, Editor.
- ROSIN, P. AND E. RAMMLER, 1933, The Laws Governing the Fineness of Powdered Coal, Journal Institute of Fuel, Vol. 7 pp. 29-36.
- SCHUHMAN, R., 1940, Principles of Comminution, in Size Distribution and Surface Calculations, AIME TP 1189, Mining Technology, pp. 1-11.
- SHOCKEY, D. A., et al, 1974, Fragmentation of Rock under Dynamic Loads, International Journal of Rock Mechanics and Mining Science, Vol. 11 pp. 303-317.
- SMITH, J. W., 1956, Specific Gravity -- Oil Yield Relationships of Two Colorado Oil Shale Cores, Industrial and Engineering Chemistry, Vol. 43 No. 3 pp. 441-444.
- WEIBULL, W., 1939, A Statistical Theory of the Strength of Materials, Ing. Vetensk. Akad. Handl. 151.

1976 v.17 N 8

BRIEF COMMUNICATIONS

ELECTROCHEMICAL REMOVAL OF CHROMIUM FROM PICKLING SOLUTIONS

UDC 669.2:628.334

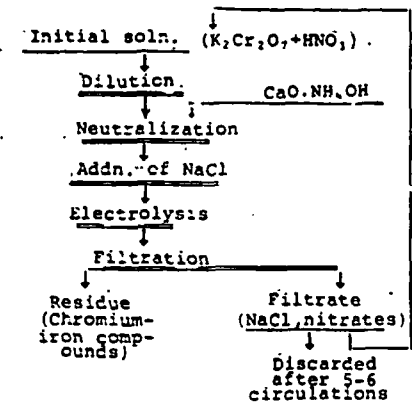
A. N. Zelikman, I. G. Kalinina, and L. M. Chemeris

An electrochemical method which involves reduction of Cr^{+6} to Cr^{+3} with simultaneous anodic dissolution of an iron electrode and precipitation of chromium as a relatively insoluble residue like iron chromite is used to remove chromium from pickling solutions containing potassium bichromate (60-70 g/liter Cr^{+6}) and concentrated nitric acid. As in the case of sulfuric acid solutions¹, the electrolytic removal of chromium from nitric acid solutions is possible only in the presence of substances which depolarize the iron anode. Sodium chloride was used as the anode depolarizer.

Preliminary studies established that a large quantity of residue formed during the electrolysis of solutions with a Cr content of 60-70 g/liter, impeding the process. Previously-diluted solutions were therefore studied subsequently.

A scheme has been worked out (see Fig.) and the following optimum routine for purification has been established: dilution of the initial solution in a ratio of 1:8, addition to the electrolyte of 40-50 g/liter NaCl as a depolarizer, neutralization of the solution with ammonia or calcium oxide to pH 2.5-4.0 and electrolysis with an iron anode at $i_a = 0.1 \text{ A/cm}^2$ for 1.5 hr

Recirculation has been tested, to prevent the dumping of solutions containing chlorides which have been stripped of most of their chromium. After separation from the residue the filtrate is sent to dilute the solution coming fresh to the purification stage. It is not necessary to add sodium chloride for a period of five cycles when initial NaCl content of the electrolyte is 40 g/liter.



Purification scheme for the $\text{K}_2\text{Cr}_2\text{O}_7 + \text{HNO}_3$ solution.

¹E. Buchilo, Purification of Effluents from Pickling and Electroplating Departments, Moscow, *Metallurgiya*, 1974, 200 pages, ill.; A. F. Bogoyavlesnkii, M. I. Garkavi, G. Z. Afanas'ev, et al, *Uchenya Zapiski, Khimiya, Kazan'*, Kazan' State University, 1953, vol. 111, No. 8, pp. 23-26.

EFFECT OF RHENIUM IONS UPON ZINC ELECTROLYSIS FROM SULFATE SOLUTIONS¹

UDC 669.849:669.537

A. Ya. Laikin and G. D. Budon

Periodic disturbances in the electrolysis process occur in practice at hydrometallurgical zinc plants; current efficiency in terms of zinc decreases sharply, electric power consumption increases, and stripping of the zinc deposit becomes difficult. It has been established that the chemical composition of solutions coming in for electrolysis during such periods is practically unchanged, i.e., the Co, Ni, Ge, Se, Te, Sb, and Cu concentrations in the solution are at the same level.

Investigations at the V. I. Lenin Ust'-Kamenogorsk Lead-Zinc Combine showed that the disturbances in the electrolysis process were linked to some extent with an increased intake into the hydrometallurgical process of weak acid containing from 1 to 3 mg/liter of rhenium ions [1].

Having regard to the fact that the rhenium is present in the solution as a complex anion and that hydrogen evolves on it at a very slight overvoltage [2,3], the effect of rhenium ions upon the zinc electrolysis process was studied under laboratory conditions.

Plant neutral solution containing (g/liter) 142 Zn, 0.002 Cd, 0.0001 Cu, 0.0001 Sb, 0.002 Co, 5.8 Mn, and 0.23 Cl was used for the experiments. Rhenium was added to the electrolyte in the form of aqueous sodium perhenate solution.

The experimental results (Table 1) showed that current efficiency in terms of zinc was drastically reduced, the sulfuric acid concentration decreased, and the zinc concentration rose when the rhenium concentration in the electrolyte increased. In the electrolysis of a solution with $C_{Re} = 5$ mg/liter, the zinc deposit dissolved completely in some experiments.

Table 1
Progress of Zinc Electrolysis when Rhenium Ions and Wash Acid are Added to the Electrolyte

Test conditions		Electrolysis to strip electrolyte			Electrolysis for 20 hours		
addition	concentration	H ₂ SO ₄ , g/l	Zn, g/l	η, %	H ₂ SO ₄ , g/l	Zn, g/l	η, %
Without additions		142,0	50,3	95,4	156,2	41,0	92,2
Re, mg/l	1,0	139,2	53,0	86,2	153,5	42,2	82,3
	3,5	135,4	55,2	82,6	141,6	50,4	60,7
	5,0	132,3	56,2	80,1	136,7	55,3	45,1
Wash acid, mg/l	1,0	135,1	55,4	83,4	152,6	43,2	81,3
	2,0	130,3	57,1	79,1	140,2	49,5	75,5

due to the presence of the acid of both rhenium ions and other impurities which adversely affect the zinc electrolysis process.

Having regard to the fact that the wash acid is added at the head end of the process and passes through the stages of calcine leaching and solution purification, experiments were carried out in which the wash acid was added to the solution prior to calcine leaching and solution purification.

It was established (Table 2) that current efficiency in terms of zinc was reduced by 2% when 1.5 ml/liter of wash acid was added. An increase in the amount of wash acid of more than 2.1 ml/liter reduces current efficiency drastically. The re-use of spent electrolyte (experiment 6) also reduces current efficiency.

It is known that reduction of rhenium takes place with a considerable excess of active hydrogen atoms and that rhenium is precipitated on metallic zinc in the form of hydrated oxides of $Re_mO_n \cdot H_2O$ type, while solution acidification is required in cementation on iron chips [3].

A study was therefore made in a subsequent series of experiments of the effect of rhenium ions added to the solution prior to copper-cadmium removal. The upper discharge from neutral thickeners of the following composition (g/liter) was used for the experiments: 141 Zn, 1.01 Cu, 0.65 Cd, 0.006 Co, 0.007 Ni, and 0.002 Sb.

The experimental results showed that there was fairly thorough reduction of rhenium when zinc sulfate solutions were purified with zinc dust, but in this case also the current efficiency in terms of zinc is drastically reduced when the initial solution rhenium ion concentration increases; a reduction in electrolyte acidity is observed in these circumstances, indicating dissolution of the zinc deposit on the cathode.

¹ L. M. Molchanova took part in the work.

Table 2
Zinc Electrolysis Figures with Addition of Rhenium Ions and Wash Acid to the Hydrometallurgical Cycle

Test no.	Test conditions		Electrolysis for stripping			Electrolysis for 24 hrs			Remarks
	addition	concentration	H ₂ SO ₄ , g/l	Zn, g/l	η, %	H ₂ SO ₄ , g/l	Zn, g/l	η, %	
1	Wash acid, mg/l	—	139,5	42,2	94,7	143,0	40,5	93,1	Acid added to solution prior to calcine leaching
2		1,5	132,0	43,5	92,5	135,0	41,0	90,8	
3		2,1	135,0	45,5	86,7	135,5	43,2	82,9	
4		10,1	121,5	46,1	80,1	124,0	42,5	72,4	
5		20,5	115,2	45,8	79,8	118,0	44,0	63,1	
6*		—	140,2	43,1	91,6	140,0	43,2	86,2	
1	Re ⁺⁺⁺ , mg/l	—	140,1	51,2	95,7	155,1	42,0	93,1	Rhenium added to solution prior to copper-cadmium removal
2		1,86(<0,1)	138,5	52,3	90,1	152,3	43,5	87,6	
3		3,72(<0,1)	134,7	55,0	85,3	149,4	47,1	80,0	
4		37,2(0,63)	133,2	56,0	80,3	145,0	51,5	69,7	

*Spent electrolyte from experiment 3 used for leaching

**Rhenium concentration after purification shown in parentheses.

zinc production figures at the Ust'-Kamenogorsk Lead-Zinc Combine.

REFERENCES

1. M. A. Vinogradova and B. S. Zadova, in: The Metallurgy of Rhenium (Proceedings of Third All-Union Conference on Rhenium), Part I, Moscow, Nauka, 1970, pp. 33-35.
2. M. M. Lakernik and G. N. Pakhomova, The Metallurgy of Zinc and Cadmium, Moscow, Metallurgiya, 1969, 488 pages, illustrated.
3. K. B. Lebedev, Rhenium, Moscow, Metallurgizdat, 1963, 206 pages, illustrated.

Thus removal of rhenium ions from zinc sulfate solutions is relatively ineffective when the parameters of the zinc dust cementation process adopted at Soviet plants are adhered to; it is therefore essential to close all the routes by which rhenium enters the hydrometallurgical zinc production process and to define the optimum conditions for thorough rhenium removal from the solutions.

Improved checking of the standard of copper and cadmium removal from the solutions and the withdrawal of wash acid from the process have stabilized electrolytic

EFFECT OF SOLUTION COMPOSITION AND ELECTROLYSIS CONDITIONS
ON GAS CONTENT OF NICKEL

UDC 669.24

N. F. Mamontov, V. V. Zenkevich, R. K. Alekseeva,
B. N. Lozovskii, and V. I. Nedashkovskii

A series of papers [1-5] have dealt with the gas content of electrolytic nickel. Up to the present the effect of the acidity and temperature of normal electrolytes, their organic impurities concentration, and current density on the metal hydrogen, oxygen, and carbon content has been ascertained.

Experience gained at the Yuzhuralnikel' Combine shows that the intensification of nickel electrolysis inevitably involves a substantial change in electrolyte composition and in particular a considerable increase in the concentration of nickel and chlorine ions.

In its turn the implementation of industrial electrolysis at a current density of 350 A/m² has given rise to quite an abrupt increase in the cathode metal gas content.

It was therefore a matter of particular interest to ascertain the reasons for the comparatively high gas content of electrolytic nickel produced at high

current density, using the results of previous researches as a basis.

The relationship of nickel gas content to the electrolyte Cl⁻ concentration was studied under laboratory conditions. The solutions for the experiments were prepared on the basis of industrial catholyte from the Severonikel' Combine electrolysis shop by the appropriate addition of nickel chloride solution (see Table).

The experiments were conducted in titanium baths 1 liter in volume. These baths were enclosed in hot water jackets to maintain the prescribed electrolyte temperature in the course of the experiment. The cathode and anode spaces in the baths were separated by a Kuralon fabric diaphragm. Electrolytic nickel was used for the anodes, and the cathodes were built up on nickel bases. Solution circulation was kept constant at the rate of 1 lit/hr.

The cathode deposit hydrogen and oxygen content was found by vacuum reduction melting in a Balzers EA-1 exhalograph. The sensitivity of the method for hydrogen was 0.00005% (wt.), and 0.0003% (wt.) for oxygen.

The experiments showed that the cathode gas contents remained almost unchanged and were at the level 6 ml/100 g of metal at a current density of 350 A/m² in the 30-45 g/liter Cl⁻ range of concentrations. An increase in the Cl⁻ concentration in the solution from 45 to 60 g/liter leads to the production of deposits with a total gas content of ~ 8 ml/100 g. A further increase in the Cl⁻ concentration to 75 and 90 g/liter causes a proportionate increase in the electrolytic nickel gas content, to 11.5 and 14 ml/100 mg respectively.

With a Cl⁻ concentration > 45 g/liter the curve shows a strong upward tendency (Fig. 1); an increase in the solution nickel content from 80 to 113.6 g/liter has little effect on the nature of this relationship. Obviously the increase in the solution Cl⁻ concentration has the decisive effect on forming the composition of the catholyte layer and so on forming the cathode deposits.

It is known that cathode nickel obtained from chloride solutions has a finer structure than the metal obtained from sulfate-chloride solutions. Consequently, when the Cl⁻ concentration increases the crystal dimensions are reduced and the adsorptive capacity of the deposit

Composition of Initial Solutions

Constituents, g/l							pH
Ni	Co	Cu	Fe	Cl ⁻	SO ₄ ²⁻	Na	
80.77	0.018	0.00047	0.0110	31.55	130.88	19.5	2.62
90.33	0.018	0.00110	0.0050	45.94	126.87	19.0	2.74
94.61	0.018	0.00130	0.0080	57.51	109.10	18.1	2.56
110.07	0.018	0.00160	0.0028	76.86	104.69	16.0	2.56
113.60	0.016	0.00062	0.0051	89.59	87.60	13.5	2.60

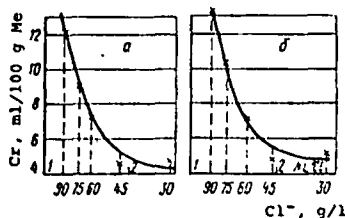


Fig. 1. Relationship of cathode nickel gas content (C_g) to Cl⁻ and Ni concentration in catholyte at various current densities: a) 250 A/m²; b) 350 A/m².

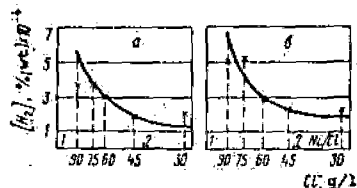


Fig. 2. Relationship of cathode nickel hydrogen content to Cl^- and Ni concentration in catholyte at various current densities: a) 250 A/m²; b) 350 A/m².

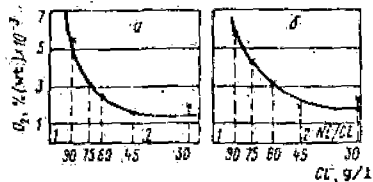


Fig. 3. Relationship of cathode nickel oxygen content to Cl^- and Ni concentration in catholyte at various current densities: a) 250 A/m²; b) 350 A/m².

increases relative to the organic impurities and colloidal particles of nickel hydroxide, with which gases also enter the nickel. The sharp increase in the gas content of electrolytic nickel obtained from high-chloride solutions at high current density may be regarded as due to the combined effect of these factors.

The nature of the relationship between total gas content and the Cl^- concentration in the solutions

was confirmed at normal current density (250 A/m²). A tendency toward some reduction in the total gas content was observed under these conditions (see Fig. 1a).

Determining the gas composition showed that the electrolytic nickel contained 0.0023% (wt.) H_2 and 0.0024% (wt.) O_2 in the 30-45 g/liter range of solution Cl^- concentrations (Figs. 2 and 3). A further increase in the catholyte Cl^- concentration leads to a sharp rise in the gas content; for example, at 90 g/liter Cl^- the cathodes contain 0.0050% H_2 and 0.0058% O_2 respectively. The level of the nickel hydrogen and oxygen content is reduced somewhat at a current density of 250 A/m².

It was demonstrated under conditions of nickel electrolysis from normal sulfate-chloride electrolyte that the gas content of the metal did not depend on solution pH in the 2.5-5.0 range [3]. Using an electrolyte with a high concentration of Cl^- and nickel substantially alters the process of deposit formation, especially at the increased current density. Finding the relationship of the metal gas content to electrolyte pH was therefore a matter of some interest. The appropriate experiments were conducted with solutions containing 30 and 75 g/liter Cl^- at a current density of 300 A/m² and a temperature of 68-72° C. The acidity of the solutions varied from pH 2.5 to pH 5.0. The prescribed pH was maintained with an accuracy of ± 0.1 units. The cathodes were built up over a period of 50 hr. The experimental results are given in Fig. 4.

It was demonstrated previously in [6] that when the Cl^- concentration in the electrolyte increases, the pH at which colloidal particles of nickel hydroxide form is much lower than the pH at which they begin to form in normal sulfate-chloride electrolyte. Taking this and the high current density into account, there is an entirely logical explanation for the increase in the gas content of nickel when the pH of the electrolyte entering the baths increases. The reduction in the gas content in the electrolyte pH range 4.3-4.7 is apparently due to clumping of the nickel hydroxide micelles [7-8]. The sharp increase in the gas content of the cathodes at electrolyte

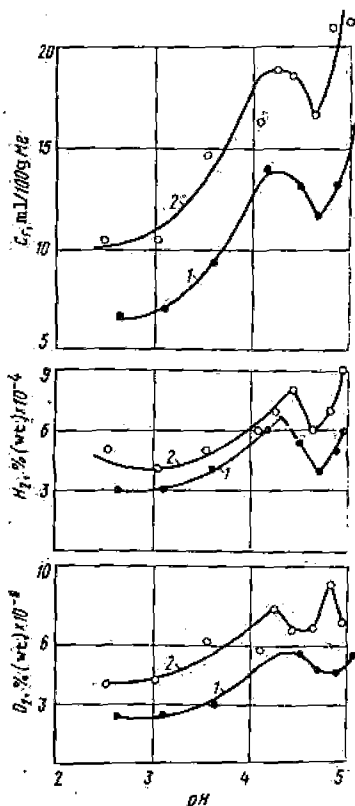


Fig 4. Relationship of cathode nickel gas content to acidity of catholyte:

- 1) 30 g/liter Cl^- ;
- 2) 75 g/liter Cl^- .

pH > 4.7 is explained by the abrupt increase in the number of nickel hydroxide particles in the catholyte layer.

REFERENCES

1. A. L. Rotinyan and E. Sh. Ioffe, *Zhurnal Prikladnoi Khimii*, 1960, 33, No. 2, 362-368.
2. A. L. Rotinyan, V. Ya. Zel'des, and I. A. Shoshina, *Zhurnal Prikladnoi Khimii*, 1962, 35, No. 7, 1542-1546.
3. A. L. Rotinyan and E. Sh. Ioffe, *Tsvetnye Metally*, 1964, No. 11, 42-46.

4. V. A. Zinov'ev and S. A. Nikolaeva, Tsvetnye Metally, 1964, No. 4, 18-21.
 5. A. I. Zhurin, Electrometallurgy of Non-Ferrous Metals, Moscow, Metallurgizdat, 1964. (M. I. Kalinin Leningrad Polytechnical Institute, Issue 239), pp. 82-107.
 6. A. L. Rotinyan and V. Ya. Zel'des, Zhurnal Prikladnoi Khimii, 1950, 23, No. 7, 717-723.
 7. A. I. Zhurin and M. G. Shoikhet, Zhurnal Prikladnoi Khimii, 1956, 29, Issue 4, 583-588.
 8. A. L. Rotinyan and E. S. Kozich, Zhurnal Prikladnoi Khimii, 1959, 32, Issue 12, 2678-2681.
-

N6, 1975

EFFECT OF SIZE OF COPPER-ZINC MATERIALS
ON THEIR ACID AUTOCLAVE LEACHING CHARACTERISTICS

SUBJ
MING
ESCZ

UDC [669.33+669.53]:66.046.8

S. S. Naboichenko, V. I. Neustroev, and I. F. Khudyakov

The basic characteristics of sulfuric acid autoclave leaching of copper-zinc materials have been established by previous investigations [1-3].

Supplementary grinding of the initial material is desirable, in order to intensify autoclave leaching. This is particularly effective with an increased sulfide mineral concretion and gangue constituent content.

Table 1
Results of Mineralogical and Petrographic Analysis
of Initial Materials

Sample	Fraction, %	Pyrite				Chalcopyrite				Sphalerite			
		free grains	concretions with chalcopyrite	concretions with sphalerite	complex concretions	free grains	concretions with pyrite	concretions with sphalerite	complex concretions	free grains	concretions with chalcopyrite	concretions with pyrite	complex concretions
0	—	65	7	25	3	20	60	10	10	45	—	50	5*
№ 2	—56+40	70	10	20	Sing. gr.	40	45	10	5	55	5	40	Sing. gr.
	—40+20	80	5	15	Sing. gr.	65	20	10	5	75	—	20	5*
	—20+10	95	—	5	—	90	5	5	—	90	Single grains	10	—
	—10	No concretions found											

* Including concretions with chalcopyrite

tions is achieved by grinding the material to -20μ; 40-70% of the ground material is attributable to this product. The specific surface of the material increases as a result of supplementary grinding; the surface is more than doubled after 35 min of treatment.

Leaching was carried out at 105 ± 2° C with a liquid-to-solid ratio of 2:1, an oxygen pressure of 4 atm, and a mixing rate of 2.43 g-mole Na₂SO₃/(liter.atm.hr) with solutions of a model electrolyte: CH₂SO₄ = 125-130 g/liter, CZn = 30-50 g/liter. The leaching time was 1-5 hr.

At the conclusion of leaching, the pulp was subjected to "granulation": the oxygen feed was shut off and the temperature raised to 130° C and maintained there for 15 min during mixing. All the experiments were balance experiments.

The results of the experiments (see Fig.) show that preliminary grinding of the material raises zinc extraction by 10-20% and increases the speed of the process considerably.

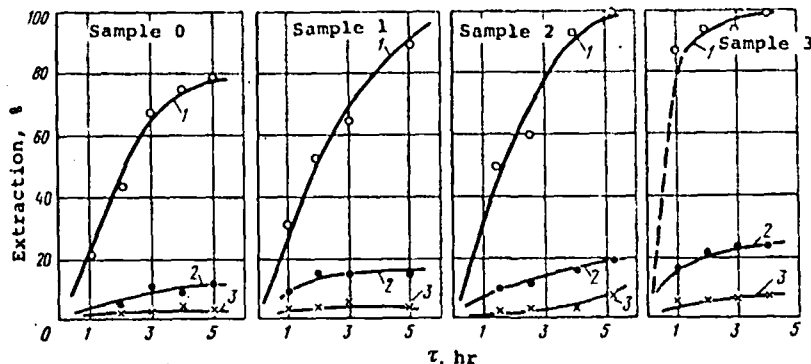
Calculations have established that the leaching of zinc in the first 1-2 hr increases in proportion to the increase in the specific surface of the material. According to our data the specific surface gives a fairly objective picture of the degree of dispersion of the initial raw material and correlates closely with the characteristics of solution.

As might have been expected, the passage of copper and iron into solution increased somewhat when material was leached after supplementary grinding. Attempts to reduce the oxygen pressure to 2-3 atm (all other conditions being equal) did not give good results: extraction of zinc in the 3-hour leaching of material No. 2 did not exceed 40-60%.

A study was also made of the speed of pulp settling after leaching materials of various sizes. The experiments were conducted at 60° C, with addition of surface-active agents at the rate of 340 mg per kg of solid material. Pulp from experiments with the initial material and with the finest material after treatment under strongly oxidizing conditions were used in comparative

Table 2
Particle-size Composition
(%) and Specific Surface
of Materials

Fractions, μm	Sample No.			
	0	1	2	3
+80	19.84	1.94	0.44	1.10
-80+40	33.40	11.30	23.83	4.27
—40	46.76	86.76	75.17	94.63
Including:				
+20	—	14.18	30.38	55.38
-20	—	72.56	44.79	39.25
Specific surface, cm ² /g	760	1035	1600	2000



Extraction of Zn (1), Cu (2), and Fe (3) into solution with various leaching times.

teristic of more dispersed materials and also to the increased content of hydrated forms of iron.

Thus the investigations established that supplementary grinding of materials for a short time can intensify the process appreciably and increase zinc extraction. This will make it possible to reduce the capacity of the autoclave apparatus required which, according to a preliminary economic assessment, offsets the additional expenditure involved in the preliminary grinding and in the slight deterioration in pulp settling and filterability.

REFERENCES

1. S. S. Naboichenko, E. I. Eliseev, and I. F. Khudyakov, Tsvetnye Metally, 1969, No. 1, 39-43.
2. S. S. Naboichenko, V. K. Pinigin, and I. F. Khudyakov, Tsvetnye Metally, 1972, No. 8, 20-23.
3. S. S. Naboichenko, V. K. Pinigin, and I. F. Khudyakov, Tsvetnye Metally, 1973, No. 10, 23-24.

experiments. In both cases rapid separation of the pulp constituents took place after 2-3 min, but the depth of the clarified layer of pulp in the experiment with the ground material was 40% less than that of the initial material pulp. The rapid settling of the pulp was due to the granulated nature of the solid phase (due to fusion of the elementary sulfur and pelletizing of the dispersed sulfide particles). The increased depth of the solid phase when pulp from ground product leaching settled may be regarded as due to the increase in bulk mass charac-

UDX

en
si
la
na
co
la2-
1
-
5
4

J

F

f
ri
w
t
T
G
2

f

s

T

f

c

References

- 1) A Brenner Proc. Amer. Electroplaters' Soc. 1941, 28.
- H G Read and A K Graham, Trans. Electrochem. Soc., 1940, 78, 279.
- V Hauf and U Grigul' Optical methods in heat transfer (Russian translation), Mir, Moscow, 1973.
- H Laitinen and W Ferguson Analyt. Chem., 1957, 29, 4.
- A N Baraboshkin and O N Vinogradov-Zhabrov Tr. Inst. Elektrokhimii UF Akad. Nauk SSSR 1970, No. 15, 118.
- A S Lifshits, Author's abstract of Thesis Sverdlovsk, 1968.

- 7) G N Agar Disc. Faraday Soc. 1947, No. 1, 20.
- 8) V G Levich Physicochemical hydrodynamics Fizmatgiz, 1959.
- 9) E Schmidt Forsh Ind. Wes., 1932, No. 3, 181.
- 10) N Ibl et alia Helv. Chim. Acta 1954, 32, 583.
- 11) G H Keulegan J. Res. Nat. Bureau Stand. 1951, No. 3, 47.
- 12) N Ibl et alia Z. Electrochem. 1955, 59, 671.
- 13) N L Gron' et alia, Izv. Vuz, Tsvetnaya Metallurgiya, 1972, No. 6
- 14) R I Goldstein et alia Internat. J. Heat. Mass Transfer 1960, No. 1, 1.

*Sov. Nauka
1975 v. 3 N6*

UNIVERSITY OF UTAH
RESEARCH INSTITUTE
EARTH SCIENCE LAB
UDC 66.061.3.665.213.6

Effect of some diluents on the liquid extraction of gold from cyanide media

M D Ivanovskii, M A Meretukov and V D Potekhin (Moscow Institute of Steel and Alloys - Department of the Metallurgy of Heavy Non-Ferrous Metals).

The salts of aliphatic amines and quarternary ammonium bases, usually employed in the extraction of gold from cyanide media by liquid extraction, are used in the form of solutions in low-polarity diluents, immiscible with the aqueous phase, which have an effect on the degree of extraction^{1,2}.

In view of the fragmentary nature of these data investigations were carried out into the effect of a series of diluents on the extraction of gold cyanide complexes under the conditions of normal and "Poroplast" (foamed plastic) liquid extraction³). As applied to the latter method it was the first time that the effect of diluents had been studied.

The organic diluents usually employed in liquid extraction processes were tested. The distribution coefficients for gold between a 0.01 M solution of trialkylbenzyl-ammonium chloride (TABAC) in an appropriate solvent and an aqueous phase containing 850 mg/l of Au, 0.1% KCN, and 0.05% NaOH were determined by the normal extraction method. The volume ratio of the organic and aqueous phase was 1:2.2, and the agitation time was 30 min.

The results and some of the physicochemical characteristics of the employed diluents are given in Table 1. The most polar solvents chloroform, dichloroethane, and o-dichlorobenzene give higher distribution coefficients, and this agrees with data obtained for the first two solvents in the extraction of platinum, palladium, and rhodium⁴).

It is known that the action of the diluent during extraction with amines is determined by which part of the molecule of the amine salt is solvated by it, i.e., the anion, the cation, or the whole molecule⁵). Solvation of the cation of the TABAC salt, where the positive charge is largely screened by the alkyl chains, is only possible when strongly polar nucleophilic diluents are used and is not very typical of the diluents.

More likely is solvation of the anion of the salt by electro-

philic diluents such as chloroform, where the hydrogen atom is capable of forming a donor-acceptor bond with the ion of the extractant. Since the anion is a group which takes part in the formation of the extracted compound, its solvation leads to a deterioration in the degree of extraction. For the solvation of ions previous authors⁶) developed the SE (solvent effect) scale, by means of which it is possible to calculate the extraction constant:

$$\lg K = \lg K_0 + \rho BP$$

where:

- K = the extraction constant in the given diluent;
- K₀ = the extraction constant in a diluent adopted as standard;
- ρ = a coefficient which is constant for a series of identical extraction systems with a variable diluent and is determined from the tangent of a slope of the straight line obtained against the extraction constant and the SE value as coordinates; the SE value is a parameter which only depends on the nature of the diluent.

With the use of the SE values given in the above-mentioned paper it can be expected that the diluents will be arranged in the following order depending on the magnitude of this parameter: p-xylene > toluene > o-dichlorobenzene > chloroform, i.e., the extraction should deteriorate in the transition from p-xylene to chloroform. The data from our experiments show that the distribution coefficients of gold increase with decrease in the SE parameter. Consequently, it can be supposed that in the present case a more important role is played by the overall solvation of the polar salt of the extractant, due to interaction of its dipole with the polar molecules of the solvent. In this case it is also possible to establish a relationship of type (1) but with the use of a different scale for the parameters of the diluent- the SE scale⁶). The parameter δ (Table 1) is equal to the square root of the change in internal energy during evaporation, related to unit volume, and provides a measure of the internal pressure of the substance.

Table 1: Dependence of the extraction characteristics of gold by TABAC on the nature of diluent

Diluent	Molecular weight	Density g/cm ³	Dipole moment D	Dielectric constant	Viscosity at 20°C cP	Solubility in water g/l	δ J/m ³	D
Chloroform	119.4	1.49	1.15	4.81	0.57	6.2	9.3	134.4
Dichloroethane	98.9	1.25	2.06	10.36	0.83	9	9.9	122.0
p-Dichlorobenzene	147.0	1.30	-	7.5	-	0.08	11.0	93.1
Toluene	92.1	0.87	0.38	2.4	0.58	0.5	8.9	25.9
p-Xylene	106.2	0.86	0	2.27	0.64	0.19	8.8	24.1
n-Decane*	142.3	0.73	0	1.99	0.92	-	7.7	14.2
Petroleum ether*	-	-	-	-	-	-	-	8.6
Kerosene*	-	-	-	-1.8	1.8-1.9	-	-	6.6

* - for complete dissolution of the extractant the diluents were used in a mixture with vol.% decyl alcohol.

The obtained experimental data are consistent with certain known values for the SE parameters: Chloroform 4.5 ($D = 134.4$) > 1.8 ($D = 25.9$) > p-xylene 0.8 ($D = 24.1$). It has been suggested (1) that the overall solvation increases with increase in the Hildebrand solubility parameter δ of the diluent. In the investigated series of diluents such a relationship is observed from decane to o-dichlorobenzene, where the distribution coefficient of gold increases from 14.2 to 93.1 with increase of δ from 7.7 to 11.0 (Table 1).

The increase in the distribution coefficient with increase in the polarity of the diluents is probably due to depolarisation and to increase in the activity of TABAC, where decrease in the association is promoted both by the general and by the specific solvation of the salt.

The fact that better extraction results are obtained with chloroform ($\epsilon = 4.81$) as diluent compared with dichloroethane ($\epsilon = 10.36$) and o-dichlorobenzene ($\epsilon = 7.5$) can be explained by the fact that the ionisation of the solute can be due not only to the overall polarity of the diluent but also to a series of other factors, e.g., the presence in the diluent molecule of an atom capable of interacting fairly actively with one of the atoms forming the given polar bond⁷).

Since quarternary ammonium compounds (QAC) and the obtained complex have limited solubility in kerosene and certain other hydrocarbons, additions of polar solvents and, in particular, high-molecular aliphatic alcohols (which in addition help to give better separation of the phases on standing) are made to the organic phase.

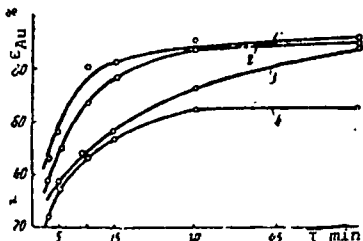


Fig. 1 The rate of extraction of gold by "Poroplast" extraction as a function of the nature of the alcohol and its composition (vol.%): decyl alcohol 40 (1) and 100 (2); isoamyl alcohol 40 (3); butyl alcohol 40 (4).

Since alcohols contain the polar hydroxyl group, they are more similar to water than other solvents; this group can solvate both cations and anions of the extractant by co-ordination, and this leads to increase in the activity of the extractant on account of a decrease in the degree of association in the organic phase.

The action of solubilising additions, which promote mutual solubility of two other substances, is determined on the basis of the Winsor theory⁸) by the quantity R. This quantity in the present case is the ratio of the affinity of the addition in the low-polarity phase (the diluent) to the affinity of the addition to the more polar phase (the extractant). The greatest effect is secured by additions with $R = 1$.

The interaction of the alcohol with the diluent, due largely to van der Waals forces, is considerably weaker than the interaction with the more polar extractant, as a result of which R is considerably less than unity in this system. Therefore, in the homologous series of alcohols a stronger solubilising action must be possessed by those alcohols which are less similar to water in nature and whose R values are close to unity.

Since the dielectric constant of alcohols and their solubility in water decrease with increase in the length of the alkyl chains (i.e., their affinity to the nonpolar phase increases), it can be expected that their solubilising ability will increase in the same direction. The effect of alcohols with various hydrocarbon chain lengths was investigated with the organic phase PPE-200 as porous support. The granules of the foamed plastic, measuring 5 x 5 x 5mm, were impregnated

with a 0.2 M solution of TABAC in a mixture of kerosene and 40 vol. % of the respective alcohol. The concentration of gold in the aqueous phase was 90 mg/l, the volume of the aqueous phase was 40 ml, and the organic-aqueous ratio was 1:70.

According to the experimental results (fig. 1), the effectiveness of the extraction of gold in the presence of aliphatic alcohols increases with increase in the length of the organic radical in the following order: Butyl ($\epsilon = 17.7$) < isoamyl ($\epsilon = 14.7$) < decyl ($\epsilon = 8.1$). This confirms the considerations given above.

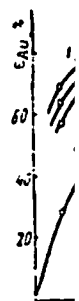
Table 2: Dependence of the extraction of gold in "Poroplast" extraction on the nature of the diluent in the presence of decyl alcohol in the organic phase (TABAC 0.2M)

Diluent	Extraction of gold %						D
	Time min						
	3	5	10	15	30	60	
n-Decane	52.4	63.6	80.8	88.2	90.4	93.2	959.0
o-Dichlorobenzene	44.0	54.6	79.3	89.4	90.4	91.5	753.2
p-Xylene	44.0	55.2	80.4	83.8	88.2	89.9	623.1
Kerosene	42.0	52.4	78.7	80.6	86.6	91.0	713.3
Benzene	41.8	54.6	71.5	75.5	85.4	93.8	1058.4
CCl ₄	40.6	52.4	71.4	74.2	88.2	92.6	875.0
Dichloroethane	39.0	50.2	68.6	72.6	83.2	89.9	623.1
Petroleum ether	50.2	55.8	64.2	67.0	72.6	86.4	444.5

Table 2 gives the results from "Poroplast" extraction of gold as a function of the nature of the diluent with the organic phase decyl alcohol (10-20%) in its composition. Under these conditions the position of the diluents in the extraction effectiveness series differs considerably from their position in the series given in Table 1. In the extraction rate of gold certain nonpolar diluents (p-xylene, kerosene, carbon tetrachloride) are not inferior to the polar diluents (o-dichlorobenzene, dichloroethane), while others (decane, benzene) are even superior.

Such an effect is probably due to interphase phenomena, since the alcohols belong to compounds capable of weakening or destroying the interphase barrier, which in this case can be constructed from the molecules of the extracting phase⁹). For our diluents the existence of such a barrier must be supposed primarily in decane, kerosene, carbon tetrachloride, p-xylene, and benzene, i.e., compounds distinguished by a low dielectric constant, since in polar solvents the added substances are distributed more readily in the volume of the solution and do not accumulate at the surface. Additions of alcohol should then lead to an increase in the rate of mass transfer on account of elimination of the interphase barrier, and this is observed in the experiments. For such solvents as o-dichlorobenzene and dichloroethane, where the interphase barrier is absent or very weak, it is clearly not possible to expect an improvement in the extraction characteristics with the addition of alcohols. Moreover, these additions can have a negative effect on the rate of extraction of the metal owing to an increase in the viscosity of the organic phase and also on account of decrease in the activity of the diluent and the alcohol resulting from the formation of hydrogen bonds between them, which is possible, for example, in dichloroethane¹⁰). The effect of the concentration of decyl alcohol in the organic phase on the extraction results was investigated with PPE-9 and with the other experimental conditions the same as during investigation of the effect of the nature of the alcohols. The results are given in fig. 2. The solubilising effect of the alcohol becomes considerably stronger with variation of its content in the organic phase from 1 to 10 vol. %. Further increase in the content of the alcohol to 40 vol. % has a considerably smaller effect on the rate and on the degree of extraction of gold. The increase in the viscosity of the organic phase probably begins to have an effect on the extraction rate, and this reduces the rate of diffusion of the extracted complex and the reaction products. This conclusion is confirmed by experiments on the extraction of gold with pure decyl alcohol as diluent (fig. 1). It should be noted that, in addition to viscosity, the extraction results can in this case also be affected by the susceptibility of the molecules of the

alcohol of a hydro molecule and solv



Solubilit

A P Nac Metallu

One of concentrated molybdi acid amably if r present separate no publi acid-pe: results acid in f

The st nitric a 1.099, by an is thermo: fluctuat The sol was add the ves: vessel Schott l determ: metric

By pr contact attainm time w:

To ob H₂O-H₂ design a lattic respon: 1-6, T:

In the molybd respect mixture mean: coeffic from th

$\gamma = 1,$

alcohol itself towards association on account of the formation of a hydrogen bond with the oxygen of a neighbouring molecule¹⁰); this effect leads to a decrease in the activity and solvating capacity of the alcohol.

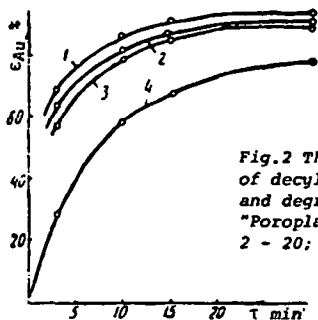


Fig.2 The effect of the concentration of decyl alcohol (vol.%) on the rate and degree of extraction of gold by "Poroplast" extraction: 1 - 40; 2 - 20; 3 - 10; 4 - 1.

Solubility of Molybdic Acid in the H₂O-H₂O₂-HNO₃ System

A P Nadol'skii, V N Fedosov, A D Mikhnev and S S Nechaeva (Irkutsk Polytechnical Institute - Department of the Metallurgy of Heavy and Rare Metals.

One of the methods for the treatment of molybdenum concentrate is to decompose it with nitric acid to produce molybdic acid. The solubility of molybdic acid in nitric acid amounts to 93 g/l^{1,2}). This value increases considerably if molybdic acid is dissolved in nitric acid in the presence of hydrogen peroxide. Molybdenum can be separated from such solutions by extraction³). There are no published data on the solubility of molybdic acid in nitric acid-peroxide solutions. The present article sets out the results from an investigation into the solubility of molybdic acid in the H₂O-H₂O₂-HNO₃ system at 26°C.

The starting materials were molybdic acid of pure grade, nitric acid with density 1.335, hydrogen peroxide with density 1.099, and distilled water. The solubility was investigated by an isothermal method on an apparatus including a thermostated glass vessel with a stirrer. The temperature fluctuations in the thermostat were not greater than ±0.5°C. The solvent was poured into the vessel, and molybdic acid was added in an amount such that solid phase remained in the vessel after dissolution. A sample was taken from the vessel with a thermostated pipette and filtered through a Schott No. 4 filter. The molybdenum concentration (g/l) was determined in a specific volume of the filtrate by a colorimetric method.

By preliminary experiments it had been established that 4-h contact between the solid and liquid phases secures the attainment of equilibrium with any solvent composition. This time was subsequently used in the experiments.

To obtain data on the solubility of molybdic acid in the H₂O-H₂O₂-HNO₃ system we used the method of experimental design proposed by Scheffe^{4,5}). In the first stage a simplex - a lattice plan of the [3, 2] type - was realised to describe the response surface by a polynomial of second degree (trials 1-6, Table).

In the first three trials data are given on the solubility of molybdic acid in water - 54.27% HNO₃, and 30% H₂O₂ respectively, and in the following trials data are given for mixtures of these reagents. Each trial was repeated. The mean-square error in the results amounted to 1.844. The coefficients of the second-degree polynomial were evaluated from the obtained data and from well-known equations (5):

$$\gamma = 1,194X_1 + 44,044X_2 + 288,438X_3 + 177,856X_1X_2 +$$

References

- 1) V S Schmidt: Extraction by amines Atomizdat, Moscow, 1970.
- 2) V F Borbat: Use of extraction with amines for the extraction and separation of metals, Tsvetmetinformatsiya, Moscow, 1967.
- 3) M D Ivanovskii et alia: In: New methods in extraction-sorption processes for the treatment of metal-containing materials, Tsvetmetinformatsiya, Moscow, 1970.
- 4) V F Borbat et alia: Izv. Vuz. Tsvetnaya Metallurgiya 1967, No. 4, 84; 1965, No. 6, 47; 1967, No. 2, 75.
- 5) V S Shmidt et alia: Radiokhimiya No. 9, 1967, 700.
- 6) V S Shmidt et alia: Radiokhimiya No. 2, 1970, 12.
- 7) L McClean et alia: Chemistry of nuclear fuel (Russian translation) Goskhimizdat, Moscow, 1956.
- 8) P Winsor: Solvent properties of amphiphilic compounds, Butterworth Sci. Bull. London, 1954.
- 9) Z Zyulkovskii: Liquid extraction in the chemical industry (Russian translation) Leningrad, Izd. Khim. Lit., 1963.
- 10) R Treibal: Liquid extraction (Russian translation) Khimiya, Moscow, 1966.

UDC 669.28

$$+ 247,244X_1X_3 - 116,236X_2X_3$$

To check the adequacy of the obtained model trials were carried out at three check points, one of which was located at the centre of the simplex (table, trials 7-9).

Table: Conditions and results of trials

Trial No.	X ₁	X ₂	X ₃	V
	H ₂ O	54.27% HNO ₃	30% H ₂ O ₂	Solubility of MoO ₃ , g/l (arithmetic mean of 2 parallel trials)
1	1	0	0	1.194
2	0	1	0	44.044
3	0	0	1	288.438
4	0.5	0.5	0	67.083
5	0.5	0	0.5	206.627
6	0	0.5	0.5	157.182
7	0.333	0.333	0.333	109.981
8	0.5	0.2	0.3	110.624
9	0.3	0.2	0.5	159.259

By substituting the corresponding experimental conditions in Eq. (1), we obtained calculated values for the solubility, which amounted to 145.073, 143.866, and 189.520 g/l for trials 7, 8, and 9 respectively. The greatest difference between the experimental values and the values calculated by means of Eq. (1) was 35.056 in the seventh trial.

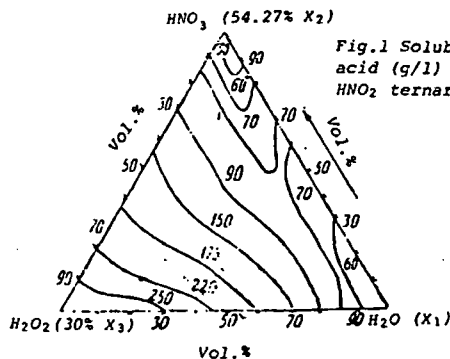


Fig.1 Solubility of molybdic acid (g/l) in the H₂O-H₂O₂-HNO₃ ternary system.

The calculated value for the Student criterion at this point amounted to 20.6, and the tabular value was 3.36,

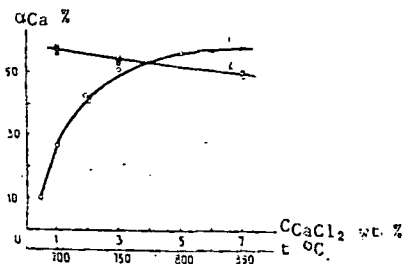


Fig. 3

Effect of the CaCl_2 content (1) and temperature (2) on the degree of extraction of calcium ($\frac{g_{\text{alloy}}}{g_{\text{salt}}} = 0.84$; $C = 5\text{wt.}\%$, $C_{\text{Na}} = 0$). 1 - 700°C , 2 - $5\text{wt.}\%$ CaCl_2 .

800. Nou-Fe...

1980 v. 8 N1

UDC 669.2

Extraction of sulphur from solutions by sulphide-containing cellulose fibre

S P Kiseleva, L S Chernikova, K A Malyshevskaya, V N Parshikova, N P Nazarova and V I Krotova (Siberian Technological Institute - Department of Chemical Fibres)

In recent years ion-exchange materials have found wide use in the extraction of non-ferrous and noble metals. In addition to ion-exchange resins, it is possible to use poorly soluble hydrated metal sulphides¹⁾²⁾ and also materials containing water-insoluble sulphides such as mercury, silver, and copper sulphides³⁾ as ion-exchangers.

At the Siberian Technological Institute a method has been developed for the production of a cellulose fibre containing finely dispersed zinc sulphide, which is formed in the pores of the fibre during the formation process and is held there fairly strongly⁴⁾. The content of zinc sulphide in the fibre amounts to 6.9-10%. In the present report we examine the possibility of using the sulphide-containing cellulose fibre for the extraction of various non-ferrous and noble metals (table 1), based on an exchange reaction between the metal ions of the solution and the zinc sulphide in the fibre.

A 0.2-1-g sample of the fibre was mixed with a solution of the salt of the corresponding metal and stirred periodically for one hour. The solution was separated from the fibre, and the equilibrium concentration of the elements in the solution was determined.

As can be seen from the data presented, the fibre possesses a high absorption capacity with respect to the bismuth, silver, and platinum ions, i.e. the fibre sorbs the ions of the metals whose sulphides are less soluble than zinc sulphide.

An investigation was undertaken into the extraction of silver from various technological solutions with the sulphide-containing cellulose fibre. For this

Table 1: The results from the sorption of metals from solutions by the sulphide-containing cellulose fibre (weight of fibre 0.5g, volume of solution 100ml)

Extracted element	Initial compound of metal	Acidity of solution	Concentration of metal in solution		Content of metal on fibre
			Initial	Equilibrium	
Copper	Copper sulphate	pH = 6	1.14	0.91	46
			1.43	1.39	8
Molybdenum	Sodium molybdate	pH = 8	1.29	1.23	12
			1.50	1.48	4
Tungsten	Sodium tungstate	pH = 8	1.50	1.40	20
			0.79	0.24	104
Bismuth	Bismuth chloride	1.0 N HCl	2.0	1.46	108
			0.45	0.09	72
Silver	Silver nitrate	0.1 N HNO ₃			
Platinum	Potassium chloro-phthalate	0.2 N HCl			

Table 2: Results from the sorption of silver from technological solutions

Solution	pH of equilibrium solution	Wt. of fibre g	Vol. of sol. l	Concentration of silver g/l		Content of metal on fibre	Static exchange capacity $\frac{\text{mg-eq}}{\text{g}}$	Degree of extraction %
				Initial	Equilibrium			
Thiosulphate	8.80	1.0	0.1	4.6	1.0	360	3.4	78
	8.80	1.0	0.1	4.5	1.0	350	3.3	78
	8.75	1.0	0.1	13.0	9.1	390	3.7	30
	9.50	1.0	0.1	2.4	0.007	239	2.2	99.7
Cyanide	11.35	0.25	0.5	0.025	0.003	44	0.4	88
	11.50	0.25	0.5	0.020	0.001	38	0.3	95
Chloride-sulphate	8.40	0.5	1.0	0.059	0.017	84	0.8	71
	8.40	0.75	1.0	0.059	traces	79	0.7	100

Table 3: The effect of the pH value of the medium on the sorption of silver from chloride-sulphate solutions
(Weight of fibre 0.5g, volume of solution 1 l)

pH of equilibrium solution	Concentration of silver mg/l		Content of metal on fibre mg/g	Static exch. capacity mg-eq/g	Degree of extraction %
	Initial	Equilibrium			
9.70	57.5	11.0	93	0.87	81
8.55	56.2	19.0	92	0.86	66
8.40	43.5	0.2	87	0.81	99.5
6.5	57.5	14.0	87	0.81	76
4.35	57.5	13.0	89	0.83	77
2.5	43.1	0.1	86.0	0.80	99.8
2.0	62.5	19.0	87	0.81	70
1.0*	54.9	34.4	20	0.19	37
0.9*	50.0	30.1	20	0.18	40

*) The volume of the solution amounted to 0.5l.

purpose we used spent thiosulphate solutions from the photographic industry, cyanide solutions obtained during the concentration of copper-molybdenum ores, and chloride-sulphate solutions from the electrochemical leaching of molybdenum intermediates⁵). The results are given in table 2.

The data in table 2 show that the sulphide-containing cellulose fibre can be used successfully for the extraction of silver from various solutions. The exchange capacity of the fibre varies within wide limits and depends to a significant degree on the concentration of silver in the solution. During the sorption of silver from concentrated thiosulphate solutions the absorption capacity of the fibre is significantly higher. It should be noted that under optimum conditions the fibre secures a high degree of extraction (95-100%), irrespective of the composition of the silver-containing solutions.

The possibility of using the fibre for the extraction of silver from chloride-sulphate molybdenum-containing solutions was investigated in greater detail for solutions with the following compositions, g/l: 2.0-5.0Mo, 0.01Cu, 80-100Na, 130-150Cl, 30-50SO₄²⁻, (43.1-65.2) · 10⁻³ Ag. In connection with the fact that both alkaline and acidic solutions can be obtained during electrochemical leaching of molybdenum intermediates, the effect of the pH value of the medium on the absorption capacity of the fibre was studied (table 3).

The exchange capacity of the fibre in the range of pH 2.0-9.7 varies little and amounts to 86.0-93.0 mg/g. In the transition to a more acidic region the absorption capacity of the fibre decreases. It should be noted that molybdenum, the content of which exceeds the concentration of silver by tens of times, is hardly sorbed at all under these conditions, i.e. the sulphide-containing cellulose fibre secures the selective isolation of silver from solutions with a complex salt composition.

Fibrous materials, possessing a more developed active surface than granulated ion-exchange resins, give a high process rate. As shown by the investigations (fig. 1), the sorption equilibrium is established after 5 min and the capacity of the fibre remains practically constant with further increase in the contact time.

Thus, the investigations showed that a cellulose fibre containing finely dispersed zinc sulphide can be used for the selective isolation of silver from various solutions. It secures a high degree of extraction of the metal even from very poor solutions. The isolation of the silver from the spent sorbent is realised in the smelting process. Technical and economic calculations showed that the cost of the extraction of silver (for the case of thiosulphate solutions) amounts to 10-12% of the cost of the extracted metal.

References

- 1) V V Vol'khin et alia: Zh. Prikl. Khim., 1967, 40, (5), 988-992.

- 2) A V Ukhina et alia: Ion-exchangers and ion-exchange. Nauka, Moscow 1975, p. 49.
- 3) Author's Certificate No. 247867, class CO2B 1/56.
- 4) Author's Certificate No. 547483, class DO1G 2/08.
- 5) L S Chernikova et alia: Tsvetnaya Metallurgiya (Tsvetmetinformatsiya), 1975, (2), p. 32.

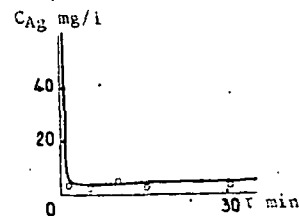


Fig. 1

Absorption of silver by sulphide-containing cellulose fibre from chloride-sulphate solutions (weight of fibre 1g, volume of solution 0.15l, pH = 7.85, initial concentration of silver mg/l).

UDC 66.094.33

Oxidation of pyrite by sulphur trioxide

L N Makedonova and N V Svistunov (North-Caucasian Mining-Metallurgical Institute - Department of the Metallurgy of Noble, Rare, and Light Metals)

The action of sulphur trioxide on various materials, including sulphides, has been investigated by a series of investigators at relatively high temperatures¹). Reactions between sulphur trioxide and sulphides at low temperatures have not yet been sufficiently studied. We put forward the suggestion²) that pyrite is decomposed by sulphur trioxide according to the following reactions:



Calculation of the temperature dependence of the isobaric-isothermal potentials of these reactions showed that they can occur in the range of 25-350°C. In this connection it seemed of interest to confirm experimentally that reactions occur between SO₃ and FeS₂ and also to establish the necessary conditions.

The need to study the conditions for the decomposition of pyrite by sulphur trioxide is dictated by the increasing interest in SO₃ as one of the strongest oxidizing agents. Sulphur dioxide, formed by reactions (1) and (2), is used for the production of sulphur trioxide. In addition, as is known, interest in the development of new economic methods for the complex treatment of sulphide materials has increased sharply throughout the world, and this is

deciding role in the sorption processes at least in its initial period. Here the role of the blocks increases with increase in their size. However, the role of the blocks is particularly large in the concluding stage of the sorption processes. This is shown by the dependence of α on τ , obtained for the ZnS-CuCl₂-H₂O system (fig. 4)

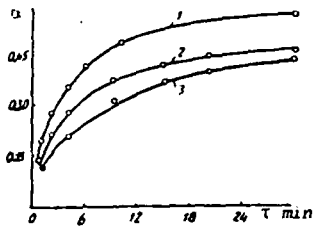


Fig. 3 The dependence of the sorption rate of sulphide ions on the density of Cd(OH)₂ g/cm³:
1 - 4.09; 2 - 4.23; 3 - 4.56.

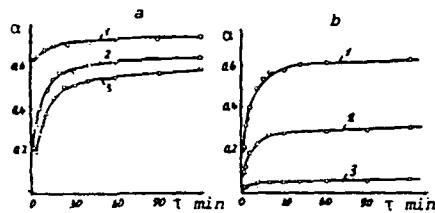


Fig. 4 The dependence of the sorption rate of Cu²⁺ on ZnS on the size of the granules (a) and crystalline blocks (b). 1-ungranulated sorbent. Size of sorbent granules mm: 2 - 0.2-0.3; 3 - 0.5-0.6. Size of blocks Å: 1 - 60; 2 - 70; 3 - 270.

As can be seen, the process is greatly retarded when $\alpha > 0.5$, and a state of apparent equilibrium then begins. Here special attention is drawn to the fact that a sharp decrease in the rate of the sorption process also occurs when ungranulated finely dispersed sorbent is used (fig. 4, curve 1). Consequently, the role of the crystalline blocks in the retardation of the sorption process at the concluding stage is determining.

This point is further confirmed by the experimental data shown in fig. 4b. Increase in the size of the crystalline blocks from 60 to 270 Å leads to a considerable decrease in the value of α (from 0.6 to 0.05) at which the state of apparent equilibrium is established. The retardation of the sorption process begins as a result of the very low rate of diffusion of the ions in the solid phase of the blocks. However, systems are possible where the state of apparent equilibrium

Soov. Non-Fe...
1978 v. 6 N3

Effect of sodium salts on the technology of the leaching of hydrargillite bauxites

A I Timoshenko (Irkutsk Branch, All-Union Aluminium and Magnesium Institute)

Sodium carbonate, sulphur ions and fluoride ions mostly enter the solutions of alumina production in the leaching of bauxites. The quantitative ratio of the impurities in the solutions varies and depends on the mineralogical composition of the bauxites¹). The presence of many impurities has an unfavourable effect on the production of alumina. Caustic alkali is used up in their dissolution. Part of the impurities enters the aluminium hydroxide, contaminating the alumina. The process is complicated by evaporation of the mother solutions²) etc.

In the present work the effect of sodium salts (sulphate, carbonate and fluoride) on the leaching of hydrargillite bauxites was investigated. The investigations were carried out on synthetic aluminate solutions with the salts of chem-

is less clearly defined. For example, in the reaction of Zn and CdS with Ag⁺ ions such high values of α as 0.99 are easily achieved (sorbents with blocks of 60 and 245 Å respectively). The extremely full realisation of the sorption process in these systems is explained by the high rate of diffusion of Ag⁺ ions in the crystal lattice of the sulphides.

In spite of the fact that the obtained experimental data demonstrate the important role of the crystalline blocks in the establishment of the apparent equilibrium, the effect of the size of the granules here must evidently not be ignored. A considerable reduction in the rate of the sorption process can occur as a result of blockage of the channels in the granules on account of a change in the number, the mutual arrangement, and the density of the crystalline blocks in the course of the reaction. Diffusion limitations can also arise as a result of separation of a loose deposit of reaction products in the channels, and this can be promoted by supersaturation of the solution in the respectively ions, e.g. in the presence of an excess of acid (the ZnS-CuCl₂-HCl-H₂O system).

Conclusions

1. The sorption on granulated sorbents, which occur with the formation of new crystalline phases, are accompanied by retardation as the sorption products form. Existing mathematical models do not make it possible to describe the kinetics of such sorption processes from the beginning to the end within the scope of any unified scheme.
2. It was established experimentally that the sorption processes in such systems develop at two levels, i.e. in the granules, and in the crystalline blocks. At the initial stage the sorption rate is mainly limited by diffusion in the granules. In the concluding stage the sorption rate decreases sharply, and a state of apparent equilibrium, brought about by the low rate of diffusion of the ions in the crystalline blocks, is established.

References

- 1) V V Vol'khin et alia: Izv VUZ Tsvetnaya Metallurgiya 1966, 9, 28.
- 2) O G Zhendareva and Z S Mukhina: Methods of analysis of electrolytic baths: Oborongiz 1963.
- 3) V F Gillebrand et alia: Practical manual of inorganic analysis: Goskhimizdat, Moscow 1960.
- 4) B Del'mon: Kinetics of heterogeneous reactions: Mir, Moscow 1972.
- 5) Yu A Kokotov and V A Pasechnik: Equilibrium and kinetics of ions exchange: Khimiya, Leningrad 1970.
- 6) Physics and chemistry of Ag^IBiV compounds: Mir, Moscow 1970.

ical purity.

The bauxite for leaching was ground by a dry method to a particle size of less than 0.074 mm. The sample of bauxite was calculated so that an aluminate solution with $\alpha_{\text{caustic}} = 1.7$ was obtained when all the aluminium oxide had been dissolved and the silicon dioxide had been combined into the compound Na₂O·Al₂O₃·1.7SiO₂·nH₂O. A sample of the ground bauxite was added to recycled solution which had been heated to 90°C, stirred vigorously for 2 min, and heated to 105°C. At this temperature the pulp was leached with a solution having a concentration of 185g/l Na₂O_{caustic}. In the work we used a sample of bauxite from the Turgai deposit having the following composition %: 42.86 Al₂O₃, 18.13 Al₂O₃, 12.63 SiO₂, 0.31 SO₃, 0.65 CaO, 2.46 TiO₂,

UNIVERSITY OF
RESEARCH INSTITUTE
EARTH SCIENCES
SUBJ
MNG
ESS



The extract during the bauxite with following: 10 Na₂O_{caustic}; 4 - 10 Na₂O; 4 NaF; 7 - Na₂SO₄; 8 - Na₂SO₄ + 5

Soda is a salt hydrolyses in an Na₂CO₃ + H₂O

As a result of... es the caustic sulphate in the... For example, with... of aluminium against 74.2%.

The X-ray... sible to explain... duct obtained aft... of hydrargillite Al₂O₃·2SiO₂·2H₂O, detected, i.e. in the... position process... sence of sodium... ising process is... for sodalite app... noted that the di... appreciably with... kaolinite lines a

Investigation... tained in the re... of the Turgai... reduced extract

UDC 669.2

2.29 CO₂ and ~2.67 calcination loss.

We investigated the effect of impurities, present in the following amounts g/l: 30 and 45 Na₂O carbonate, 10 and 20 Na₂SO₄, 4 NaF. We also investigated the joint effect of the following salts g/l: 30 Na₂O carbonate and 10 Na₂SO₄; 30 Na₂O carbonate, 10 Na₂SO₄, and 5 NaF.

The results (fig. 1) show that the presence of carbonate at concentrations of 30 and 45g/l increases the extraction of alumina from the bauxite to an approximately equal degree. After 30 min the extraction of aluminium oxide in the presence of the additions is 1% higher than without the additions. This difference is maintained after leaching for 2h. On the X-ray pattern of the solid phase obtained from the leaching of the bauxites with solutions containing 30g/l Na₂O carbonate no lines characteristic of hydrargillite and partly of kaolinite were found after leaching for only 30 min. The increase in the leaching rate in the presence of carbonate alkali is explained by some increase in the caustic ratio of the solution.

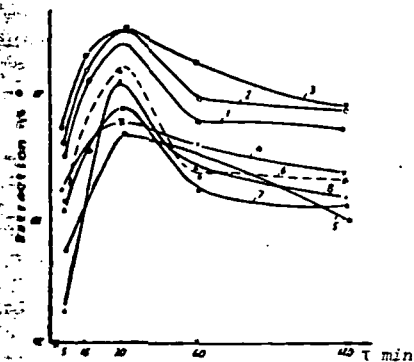
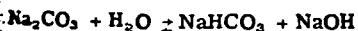


Fig. 1 The extraction of Al₂O₃ into solution during the leaching of hydrargillite bauxite with solutions containing the following impurities g/l: 1 - 0, 2 - 30 Na₂O carbonate, 3 - 45 Na₂O carbonate, 4 - 10 Na₂SO₄; 5 - 20 Na₂SO₄; 6 - 4 NaF; 7 - 30 Na₂O carbonate + 10 Na₂SO₄; 8 - 30 Na₂O carbonate + 10 Na₂SO₄ + 5 NaF.

* Figures on diagram unreadable in Russian text

Soda is a salt formed by a weak acid and a strong base and hydrolyses in an aqueous medium:



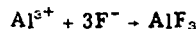
As a result of hydrolysis NaOH is formed, and this increases the caustic ratio of the solution⁽³⁾. The present of sodium sulphate in the leaching solutions impairs the process (fig. 1). For example, with 10g/l Na₂SO₄ in the solution the extraction of aluminium oxide after 30 min amounts to 67.64% against 74.2%.

The X-ray characteristics of the solid phase make it possible to explain the decrease in the leaching rate. In the product obtained after leaching for 30 min lines characteristic of hydrargillite Al(OH)₃ (d/n Å: 4.36, 2.43) and kaolinite Al₂O₃·2SiO₂·2H₂O (d/n Å: 7.25, 4.36) are still clearly detected, i.e. in the presence of sulphate the bauxite decomposition process takes place more slowly than in the presence of sodium carbonate. At the same time the desilicating process is more intense. On the diffractogram lines for sodalite appear (d/n Å: 6.37, 3.66, 2.66). It should be noted that the dissolution of kaolinite is only suppressed appreciably with sodium sulphate in the solution. The kaolinite lines are more intense.

Investigation of the effect of sodium fluoride (4g/l), contained in the recycled solution, showed that the leaching of the Turgai bauxite is less complete in this case. The reduced extraction of aluminium oxide results from the

formation of aluminium fluoride compounds. To confirm this the diffractogram of the red mud obtained after leaching of the bauxite with the recycled solution containing 10g/l of sodium fluoride was recorded. Apart from the lines for haematite and sodalite the red mud gave lines for AlF₃ (d/n Å: 3.55, 2.13).

The presence of aluminium fluoride and not cryolite in the mud is explained by the fact that the fluoride ion dissolved in the aluminate solution should first react completely with the aluminium ion according to the reaction



and then, on the attainment of a certain concentration of AlF₃, the latter reacts with sodium fluoride to form cryolite.

Drozhev's equation⁽⁴⁾, used earlier for the treatment of kinetic data on the leaching of monohydrate bauxites, satisfactorily describes the leaching of hydrargillite bauxites (fig. 2). The experimental points lie fairly close to a straight line:

$$\frac{1}{\tau} \ln \frac{100}{100-\epsilon} - \beta \frac{\epsilon}{\tau} = M$$

where: τ is time and ϵ is the extraction of Al₂O₃

$$\beta = \frac{kV}{\text{DSMB} + KV}, \quad M = \frac{K\text{DSBM}}{\text{DSMB} + KV}$$

where: D is the average coefficient of diffusion of the reagent through the film, S is the surface area of the interface, K is the rate constant of a first-order reaction, V is the volume of the reagent, B is the amount of reagent passing in unit volume of solid phase, and M is a coefficient which allows for conversion from surface to volume concentration.

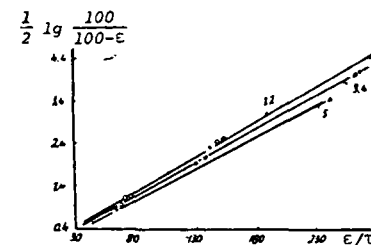


Fig. 2 The results from mathematical treatment of data on the leaching of hydrargillite bauxite with the pure solution (1) and with solutions containing g/l: 2 - 30 Na₂O carbonate, 3 - 10 Na₂SO₄; 4 - NaF; 5 - 30 Na₂O carbonate + 10 Na₂SO₄ + 5 NaF.

Drozhev's formula was derived for self-retarding reactions on the condition that the rates of the chemical reaction and diffusion are equal. It can be considered that the rate of the process is limited by external diffusion only in the initial period, and dissolution of the alumina-containing minerals then occurs in the thickness of the solid phase without disrupting its main structure and without a large excess of solvent. Here the magnitude of the dissolving surface remains constant, and this is one of the conditions for the applicability of Drozhev's equation.

The practical interest lies mainly in the final section of the kinetic curves, which gives an idea of the maximum possible level of extraction of alumina under the conditions of a restricted process time. The exception is the beginning of the kinetic line. Here, in the bauxite the open surface of the alumina-containing minerals has not yet been blocked by secondary reaction products. The same can be said about the section of limiting extractions of aluminium oxide, where the leaching rate is so

low that side processes (e.g. desilicising) play a perceptible role.

Conclusions

1. The effect of sodium salts (sodium carbonate, sodium sulphate, sodium fluoride) on the leaching of hydrargillite bauxite of the Turgai deposit was investigated.
2. The positive role of sodium carbonate and the negative role of sodium sulphate and sodium fluoride on the extraction of aluminium oxide from bauxite into solution were demonstrated.

Decomposition of mixed zincate-aluminate solutions

N I Zabolotnov, V V Grachev, V K Kuznetsova, T V Bogacheva and N G Vinogradov (Urals Polytechnical Institute - Urals Branch, All-Union Aluminium and Magnesium Institute)

In the earlier work¹) it was established that supersaturated alkaline zincate solutions possess the ability to decompose comparatively rapidly when mixed with a seed of zinc oxide. Here, if the concentration of Na₂O amounts to 90g/l or more zinc oxide separates from the solutions; and with a concentration of Na₂O below 90g/l zinc hydroxide separates. At low concentrations the solutions decompose at a high rate without a seed. The length of the decomposition of alkaline zincate solutions containing about 100g/l Na₂O amounts to 3-4h. After stirring for 4h the degree of decomposition of the solutions amounts to 50-55%, and it remains practically unchanged with increase in the length of stirring. Since the solubility of zinc oxide in alkaline solutions varies little with variation of temperature, it can be considered with some fraction of error that the degree of decomposition of the solutions with not change on heating. However, the decomposition rate increases with increase in temperature. The decomposition of alkaline zincate solutions is greatly retarded by silica impurity.

It is of great interest to investigate the decomposition of mixed zincate-aluminate solutions. For the technology of alumina production it is important to know the behaviour of the zinc impurity during the decomposition of aluminate solutions. It was established that aluminium hydroxide contaminated with zinc oxide separates during the decomposition of aluminate solutions containing zinc as impurity. The decomposition rate of the aluminate solutions decreases with increase in the zinc oxide content. Here, more coarse-grained aluminium hydroxide is obtained²).

We set out to investigate the decomposition of mixed zincate-aluminate solutions from the standpoint of determining the possibility of combining the production of zinc oxide with the production of alumina. The hydrometallurgical method for the production of zinc oxide from materials containing it, i.e., the concentrates of oxidised zinc ores and the slimes from the wet gas purification of blast furnaces, is well known³). The method consists in the leaching of the zinc-containing material with strong alkali followed by dilution and separation of the undissolved parts of the slime. The zincate solution is decomposed by mixing with a seed of zinc oxide. The mother solution separated from the obtained zinc oxide is evaporated and passed on for leaching the zinc-containing material. This method is distinguished by its great simplicity and by the low cost of the obtained zinc oxide.

It is also possible to use recycled alkaline aluminate solutions from alumina production for the extraction of zinc oxide. In this case mixed zincate-aluminate solutions will be obtained. The higher decomposition rate of the zincate solutions compared with aluminate solutions gives hope for the production of pure zinc oxide from the mixed solution. In the first series of experiments we studied the leaching of zinc oxide with aluminate solutions having various concen-

3. The kinetics of the leaching of hydrargillite bauxites are described by Drozdov's equation for self-retarding reactions.

References

- 1) S I Beneslavskii: Mineralogy of bauxites: Gosgeoltekhizdat, Moscow 1963.
- 2) F I Tsybal: Tr. VAMI, Glavalyumintii 1945, 28, 66.
- 3) Ya I Mikhailenko: Course of general and inorganic chemistry: Moscow 1966.
- 4) N S Mal'ts and L F Verbov: Tsvetnye Metally 1972, 5, 35.

UDC 669.371

trations: The aluminate solutions were obtained by dissolving aluminium hydroxide of analytical grade in alkaline solutions. The prepared solutions had one and the same caustic ratio, equal to 3.4, but different concentrations: 50, 100, 150, 200, 250, 275, 300, and 325 g/l Na₂O. With these solutions we leached zinc oxide, which was used in a small excess calculated on its solubility in alkaline solutions. The leaching was carried out in glass flasks, which were placed in an air agitation-type thermostat at 90-105°C for 1h. During leaching we obtained zincate-aluminate solutions containing various amounts of zinc oxide (tables 1 and 2).

Table 1: The results from the leaching of ZnO in synthetic recycled aluminate solution. $\alpha_{caustic} = 3.4$; $t = 95^\circ\text{C}$; $\tau_{leach} = 1\text{h}$

Na ₂ O _{in} , g/l	Al ₂ O ₃ _{in} , g/l	Na ₂ O _{fin} , g/l	Al ₂ O ₃ _{fin} , g/l	ZnO, g/l	α_{in}	α_{fin}
51.21	26.72	51.36	24.99	4.88	3.2	1.6
101.55	49.98	100.59	48.96	8.13	3.4	1.6
155.68	78.54	154.97	75.99	19.52	3.3	1.6
197.04	103.02	199.58	99.96	34.17	3.2	1.6
245.6	125.45	255.08	127.5	50.45	3.2	1.6
279.49	138.73	275.96	137.5	61.02	3.3	1.6
296.85	148.92	296.18	148.92	73.23	3.3	1.6
323.51	159.12	325.14	159.12	78.92	3.3	1.6

Table 2: The results from leaching of ZnO with synthetic recycled aluminate solution. $\alpha_{caustic} = 3.4$; $t = 105^\circ\text{C}$; $\tau_{leach} = 1\text{h}$

Na ₂ O _{in} , g/l	Al ₂ O ₃ _{in} , g/l	Na ₂ O _{fin} , g/l	Al ₂ O ₃ _{fin} , g/l	ZnO, g/l	α_{in}	α_{fin}
39.98	18.36	39.33	18.36	0.8	2.95	1.3
79.29	38.25	79.08	37.71	3.58	3.4	1.4
118.84	60.18	120.22	59.67	13.12	3.2	1.3
164.54	79.56	161.89	81.09	25.55	3.4	1.4
204.47	97.92	204.60	100.77	35.8	3.4	1.4
213.39	105.08	223.8	110.36	43.12	3.31	1.4
232.0	116.28	246.35	123.42	48.00	3.28	1.3
256.74	124.44	267.35	131.07	56.14	3.4	1.4

From the data in tables 1 and 2 and in the figure it follows that the extraction of zinc oxide into aluminate solutions increases greatly with increase in the concentration of Na₂O. With Na₂O concentrations of 300-325 g/l it is possible to obtain zincate-aluminate solutions with a high content of zinc oxide (73-79 g). In the range of 90-105°C the temperature has practically no effect on the extraction of zinc oxide into aluminate solutions. The curves for the extraction of zinc oxide are curved towards the abscissa axis. This makes it possible to obtain supersaturated solutions with respect to zinc oxide by dilution of strong zincate-aluminate solutions. The strong zincate-aluminate solutions obtained during the leaching of zinc oxide were diluted with distilled water to 100, 150, 200, and 250 g/l Na₂O and were then analysed for zinc oxide content. A seed of zinc oxide

SUBJ
MNG
ESSL

IN SITU, 2(2), 75-92 (1978)

UNIVERSITY OF UTAH
RESEARCH INSTITUTE
EARTH SCIENCE LAB.

EFFECT OF SODIUM SILICATE ON LEACHING URANIUM
ORES WITH HYDROGEN PEROXIDE

Bernard C. Lawes
E. I. du Pont de Nemours & Company, Inc.
Chemicals, Dyes and Pigments, Department
Wilmington, DE 19898

ABSTRACT

Hydrogen peroxide has been widely used as an oxidant for in-place solution mining of low-grade uranium ores with ammonium bicarbonate. Recent laboratory column leaching experiments have shown that hydrogen peroxide--under accelerated conditions--at least appears to ~~be~~ ~~more~~ ~~effective~~ ~~than~~ ~~ammonium~~ ~~bicarbonate~~ ~~in~~ ~~the~~ ~~leaching~~ ~~of~~ ~~low~~ ~~grade~~ ~~uranium~~ ~~ores~~. ~~The~~ ~~rate~~ ~~of~~ ~~leaching~~ ~~varies~~ ~~with~~ ~~different~~ ~~ores~~. ~~With~~ ~~some~~ ~~ores~~, ~~the~~ ~~rate~~ ~~of~~ ~~leaching~~ ~~is~~ ~~prevented~~, ~~or~~ ~~even~~ ~~reversed~~. ~~With~~ ~~some~~ ~~ores~~, ~~the~~ ~~rate~~ ~~of~~ ~~leaching~~ ~~is~~ ~~helped~~ ~~to~~ ~~stabilize~~ ~~hydrogen~~ ~~peroxide~~ ~~against~~ ~~decomposition~~.

BACKGROUND

In-place solution mining of uranium ore is the only viable option for recovery of uranium from low-grade deposits. Figure 1 shows a simplified diagram for this mining technique.

Figure 2 shows the basic chemistry of in-situ leaching. Oxygen gas, and, to a lesser extent, sodium chlorate have also been used in the first step, to convert the insoluble +4 uranium in ore to soluble +6 uranium. In this oxidized state the uranium is complexed with carbonate to form the anion shown in the second step. The last step shows the decomposition of hydrogen peroxide to oxygen, catalyzed by contact with the insoluble uranium.

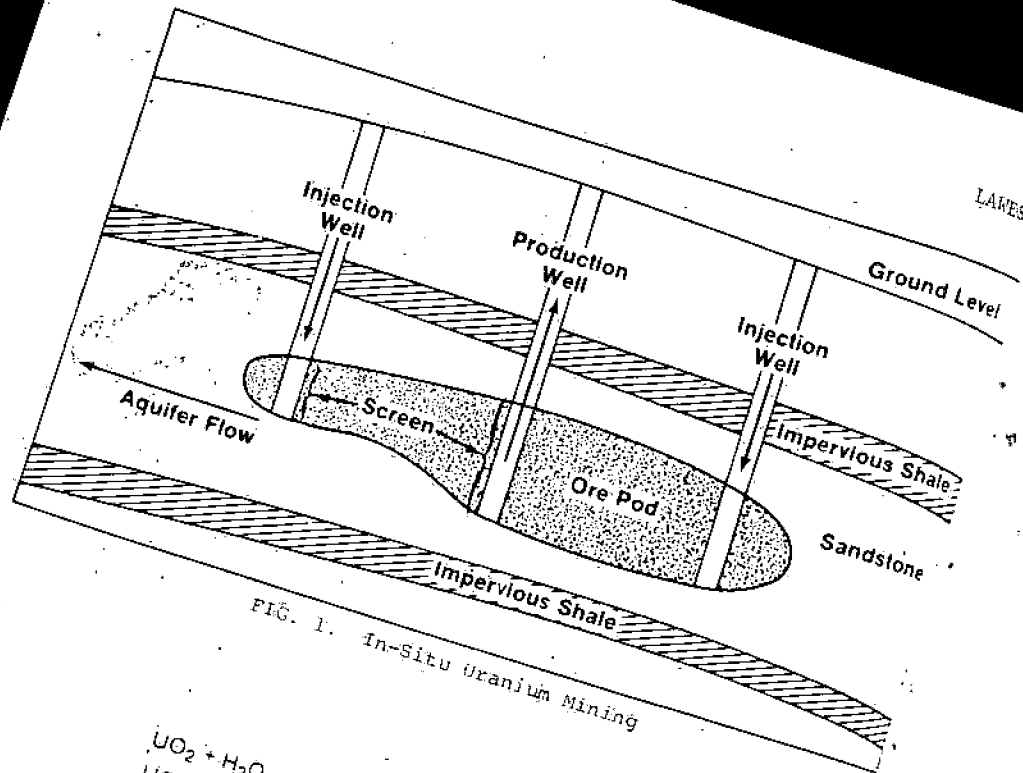


FIG. 1. In-Situ Uranium Mining

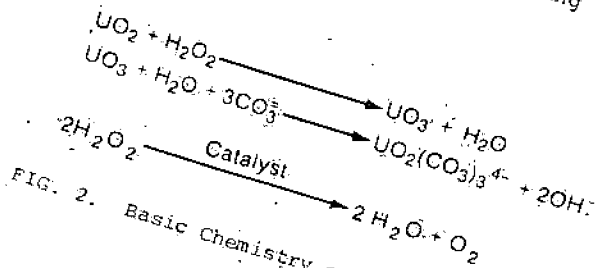


FIG. 2. Basic Chemistry of In-Situ Leaching.

PURPOSE AND HIGHLIGHTS OF PAPER

Table 1 lists some qualities of the ideal oxidant, and the corresponding properties of H₂O₂. On point 6, there have been reports that some operating mines have experienced a loss of permeability, particularly after prolonged operation, irrespective of the oxidant used. It is known that the direct injection of oxygen into an ore can cause permeability loss by vapor blinding, which in extreme cases

EQUIPMENT AND PROCEDURES

Referring to permeability, or resistivity, or resist energy nee

LEACHING URANIUM ORES

Table 1. Qualities of Ideal Oxidant and Corresponding H₂O₂ Properties

Ideal Oxidant

1. Fast, complete oxidation
2. Easy to handle
3. Concentration easily variable
4. Minimal ecological impact
5. Minimal investment for using
6. No undesirable side effects

H₂O₂ Properties

- Furnishes perhydroxyl and O₂ for oxidation
- Safe, liquid system
- Can be diluted with water
- End products are H₂O and O₂
- Doesn't use pressurized gas feed
- None reported from field use

can lead to separate flow channels. Since hydrogen peroxide decomposes into water and oxygen, a laboratory study was undertaken to assess the effects of this oxidant on permeability. With certain ores and under accelerated laboratory conditions, losses in permeability were noted when leaching with hydrogen peroxide as compared to leaching with oxygen. However, it was demonstrated that the loss of permeability was prevented or substantially reversed with the addition of silicate to the leach. An additional finding was that silicate acted as a peroxide stabilizer. It is not clear whether this was a key

the pressure drop across the bed, say between an injection well and a production well. Both ways were used in the laboratory in glass leach columns. The first method is shown in Figure 3. A 2.5 to 10 cm high ore bed (50-200g of ore) in a 42 or a 22 mm diameter glass column--on top of a glass wool plug--was first wetted the top by leach feed from the inlet pump. Then leachate liquor was pumped from the bottom of the column to a collection reservoir by a Masterflex peristaltic outlet pump, using for most runs a pump with a range of 5 to 120 rpm, capable of delivering 0.21 cc/min/rpm. When two such set-ups were run side-by-side--one a control and the other using a test chemical in the leach--the number of rpms on the outlet pump was recorded as a measure of the resistance to flow, i.e., permeability. A vacuum gage was used in a few runs in the air space below the ore-bed support to measure permeability changes. The

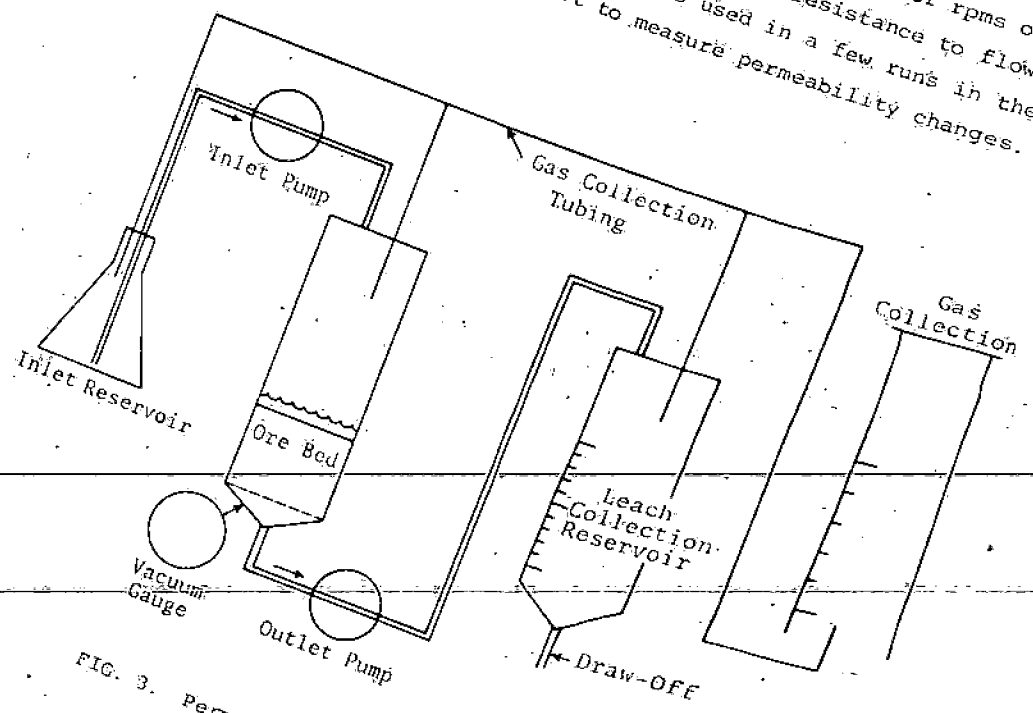


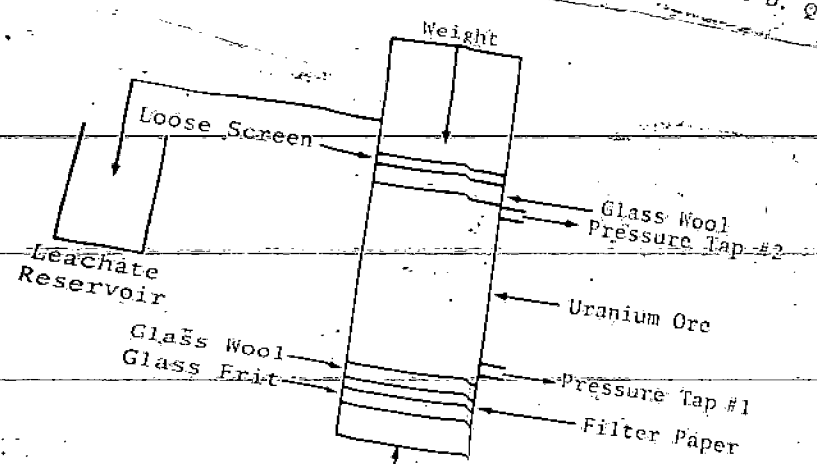
FIG. 3. Permeability from Outlet Pump RPMs

LEACHING URANIUM ORES

system was manifolded with tubing so that oxygen released by peroxide decomposition was measured by displacement of water in the inverted cylinder.

The other column flow technique, shown in Figure 4, provides permeability in millidarcys, from the ΔP monitored for upflow passage of leach through ore bed between two pressure taps. Column diameter requirements were: overflow values of 2000 lbs/(hr ft²) mass velocity, and 15 particle diameters. The ΔP data, from these experiments were converted to millidarcy units by computation, and the amount of residual peroxide was measured by permanganate titration of leachate samples taken at 15-minute intervals.

Equation: $K = Q \frac{(1)}{(A)} = \frac{\Delta P}{\Delta X} = 1000 = \text{milli D.}$
 $Q = \text{flow rate, cc/sec; } A = \text{cross sec. area, cm}^2$
 $\Delta X = \text{bed depth, cm}$



The ore is first wet with peroxide-free and silicate-free leach, and the hydraulic part of the system is then degassed by aspirator vacuum. Leach solutions (Note: Distilled water was used for all solutions reported in this work.) contained 8-12g of carbonate salt, 1.2 or 1.8g H₂O₂/l for "Albone" 50 hydrogen peroxide and sufficient Grade F du Pont sodium silicate to provide 0.2-4.0 g/l of a silicate containing 28.4% SiO₂ having a weight ratio SiO₂:Na₂O = 3.25. Most solutions were pH 8.0-8.6, but the range 7-10 was also explored. Freshly prepared solutions were made for the start of each experiment and replenished daily, unless otherwise specified. Calcium and molybdenum were measured by atomic absorption spectroscopy, and sulfate by turbidimetry, and uranium by a dibenzoylmethane colorimetric procedure provided by the U. S. Bureau of Mines at Salt Lake City, Utah. Batch leach experiments were run under vigorous agitation using 4-1/4" x 2" (285-cc) screw-top polyethylene jars in a platform or wrist shaker.

It is important to emphasize that to make sure effects could be seen in lab tests of limited duration, accelerated conditions were used to magnify effects. For example, flow rates were used that corresponded to superficial linear velocities of 0.7-1.4 ft/hr, much higher than would be encountered in actual downhole operation. Furthermore, as can be seen, relatively high oxidant levels--up to 1.8 g/l H₂O₂--were used, along with composite ore samples that probably only poorly represented the undisturbed underground condition of the ore. Therefore data should not be extrapolated to field needs but rather viewed more as a barometer of the general directions that permeability changes might take, and, as a starting point on how to deal with permeability reduction should it become an operational problem.

Ores from four different sources were used, and are shown in Table 2. Hereafter these names will be used to identify ores. (Note: Even though these samples in some cases were lower in uranium content than ore bodies usually mined, the permeability phenomena described in this paper are unlikely to be affected by this fact.)

Table 2. Uranium Ores Used

Identification	Uranium Content
Rich Texas Ore	0.85%
Weak Texas Ore	0.03%
Wyoming Ore	0.02%
Mt. States Ore	5 ppm

The first two were from different sites in south Texas, the third from a Wyoming in-situ site and furnished by the United States Bureau of Mines at Twin Cities, Minnesota, and the fourth, from a Grant's, New Mexico, site, was furnished by Mountain States Research & Development, Tucson, Arizona. All were dry and free-flowing composite samples from corings, except for the weak Texas ore, which was wet and contained about 13% moisture. The screen analysis for the Wyoming ore was 26% above 20 mesh, 48% at -20 to +60 mesh, 19% at -60 to +200 mesh, and 7% below 200 mesh. This screen analysis was reasonably typical of other ores used.

EFFECT OF HYDROGEN PEROXIDE ON PERMEABILITY

It was observed that if an ammonium bicarbonate leach solution was pumped through small beds of ore, the amount of outlet pumping energy, or rpms needed to maintain a flow, generally increased if peroxide was added to the leach. The effect was fairly strong for the rich Texas and the Mountain States ores, but very weak for the other two.

Using as an example a leach flowing down through a 50g ore bed of the rich Texas ore, at 5-10 cm/min--as in Figure 4--with no peroxide, flow rate doesn't change substantially with time--outlet pump speed remains only slightly higher than inlet pump speed. However, about 20-40 minutes after peroxide is added to the leach feed, flow decreases markedly, more than 5-fold, even if outlet pump speed is increased to its maximum value.

The effect apparently is not related to the uranium content of the ore, because the two ores showing the largest effect had the highest (0.85%) and the lowest (5 ppm) uranium contents. Permeability loss was also shown by vacuum gage readings taken at the outlet to the leach column. For example, in a run using Mountain States ore, vacuum increased from 0-5 inches up to 21 inches of mercury over a 40-minute period after peroxide was added.

EFFECT OF SILICATE IN PREVENTING LOSS OF PERMEABILITY

Now, of course comparing permeability for leaches with and without peroxide sets up a kind of artificial control because the oxidant, after all, is an essential ingredient for in-situ leaching of uranium. Without an oxidant, no uranium is removed unless it is already in the oxidized state. A more meaningful comparison, in Table 3, shows how adding small amounts of sodium silicate to peroxide-containing ammonium bicarbonate leaches at pH 8-9 can greatly improve permeability.

The rich Texas ore, which had shown the greatest loss of permeability with peroxide, showed a very large reversal of this loss with sodium silicate. The 5-fold increase indicated by the 5.9 vs. 1.2 cc/min flow rates is really larger than that because higher outlet pumping energy was needed to maintain 1.2 cc/min. The effect of

Table 3. Permeability Improvement With Silicate

Ore	g/l Silicate Added	Flow Rate and Pump Speed cc/min	
		Silicate	No Silicate
Rich Texas	4.0	5.9 @ 62 rpm	1.2 @ 112 rpm
Weak Texas	1.0	2.8 @ 115 rpm	0.9 @ 110 rpm
Wyoming	1.5	2.5 @ 112 rpm	1.2 @ 116 rpm
Mt. States	3.0	6.1 @ 50 rpm	3.6 @ 50 rpm

adding silicate for the other three ores was less dramatic, flow rates increasing from 1.7 to three times at roughly constant pump speed. In most cases--using outlet pump energy to measure permeability--it appeared that flow rates for peroxide and silicate-containing leaches were as good as or almost as good as for leaches containing no peroxide, i.e., by this method at least, silicate seemed to restore all or most of the permeability decrease caused by the addition of peroxide.

Although this figure shows silicate being used at 1-4 g/l--and all of these concentrations were effective--there were important concentration factors. First, as little as 0.2 g/l was found to be effective in this case improving flow through Mountain States ore almost one and a half times at constant pumping energy. Second, no more than 1-1.5 g/l was needed in column experiments to get the maximum silicate effect. Furthermore, solutions containing up to 2.0 g/l of silicate and up to 16 g/l of ammonium carbonate, at pH 6.6-9, remained free from any gelled silicate for at least 11 days, as was evidenced by lack of cloudiness or Tyndall effect. Turbidity measurements on these solutions showed generally less than 2 ppm of solids expressed as SiO₂. Silicate concentrations much above 2 g/l should be avoided because these can lose their clarity on aging, indicating gelling which can actually decrease permeability if pumped into ore deposits. Leach solutions containing 3 g/l actually deposited gel on 11-day standing.

Three other relevant parameters worth mentioning are the following: First, the silicate effect worked in the pH 7 to 10 range normally used in in-situ carbonate leaching. Second, the effects were less certain if the leach contained too much sodium ion. For example, sodium silicate improved permeability for a peroxide leach solution containing 5 g/l of NaHCO₃ but not for one containing 11 g/l. Third, the effect is apparently reversible. When silicate was removed from a free-flowing peroxide-containing leach, the flow rate maintained itself for 2 hours or longer--before decreasing, essentially to values seen for peroxide-containing leaches without any silicate.

The next three figures, starting with Figure 5, show more quantitatively for three ores how peroxide and silicate effect permeability as a function of run time, using the upflow column technique that measures ΔP . Leaches contained 4g of ammonium bicar-

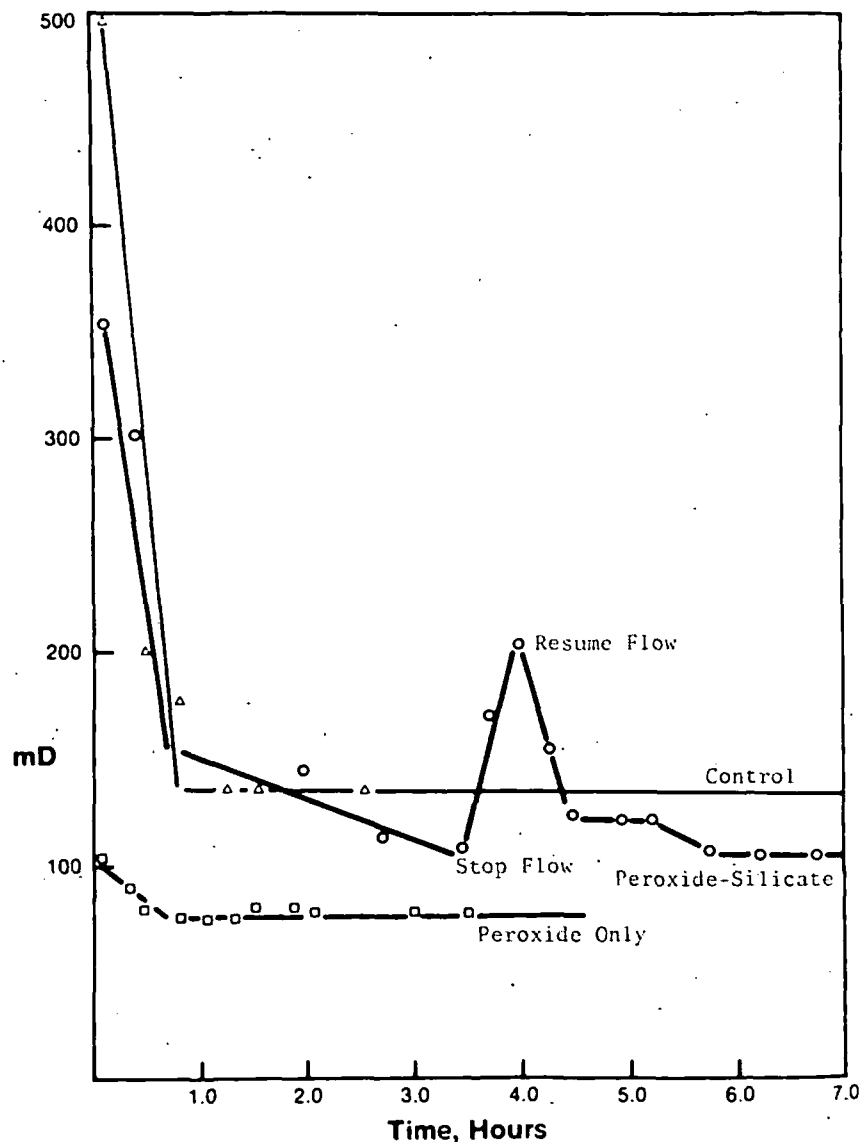


FIG. 5. Permeability for Wyoming Ore

bonate per liter (pH 8.0); peroxide was used at 1.2 g/l, and silicate at 1.5 g/l.

Figure 5 shows data for the Wyoming ore. Here a 45% loss of permeability caused by peroxide was about half offset by silicate.

Again, the caution should be raised that the top curve, labelled "no oxidant", is not really a control because in-situ leaching is not done without an oxidant. The very sharp decrease in permeability in the peroxide-silicate curve at about 3.5 hours, occurred when flow was stopped. This seemed to be a rather general finding, namely, that some sort of interrupted, or stop-flow mode of applying the silicate solution increased the effectiveness of silicate.

Similar results were obtained for two other ores, though the actual magnitude of the effects differed. See Figures 6 and 7.

For Figure 5 and 6 superficial linear velocities of 0.35 ft/hr were maintained in 2.4 x 1.5" diameter beds.

For Figure 7, a smaller bed (1.2 x 1.0" diameter) of more finely divided ore (100% -80 mesh) was used to get a superficial linear velocity of 0.39 ft/hr.

EFFECT OF MODE OF ADDITION OF SILICATE

Some experiments showed that post-addition of silicate to a leach can partially reverse an adversely-induced loss of permeability. For example, this was shown by a column leaching sequence using 50g charges of the rich Texas ore. This bed was partially plugged during a 56-minute leach period with peroxide. Leach flow fell to < 5 cc/min at 350 outlet pump rpms (using a larger pump head than usual). A subsequent 45-minute flow period with silicate added did not change leach flow rate. However, following a no-flow period of 72 minutes, leaching was resumed and a flow rate was observed that was essentially equivalent to flows obtained for a peroxide-free leach (12.5 cc/min at 85 rpm). In the no-silicate control, the 72-min. no-flow period caused only a very temporary, short-lived relief from low flow rate. Thus, benefits from stop-flow operation seem to apply only when silicate is present along with the peroxide. With another ore just a 10-minute no-flow period was sufficient to provide benefit.

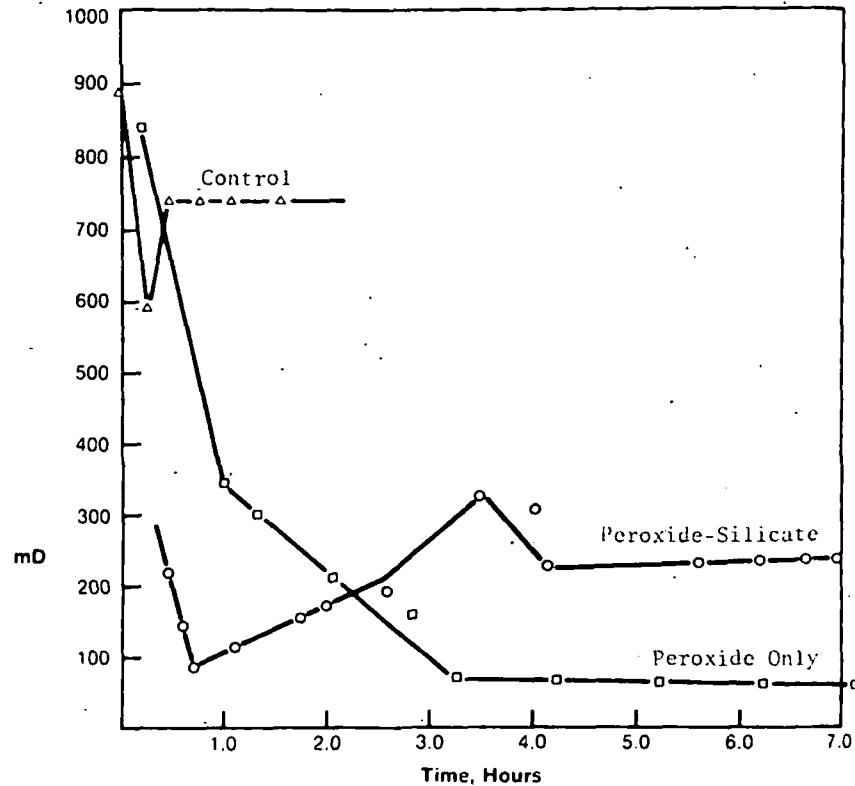


FIG. 6. Permeability for Mountain States Ore

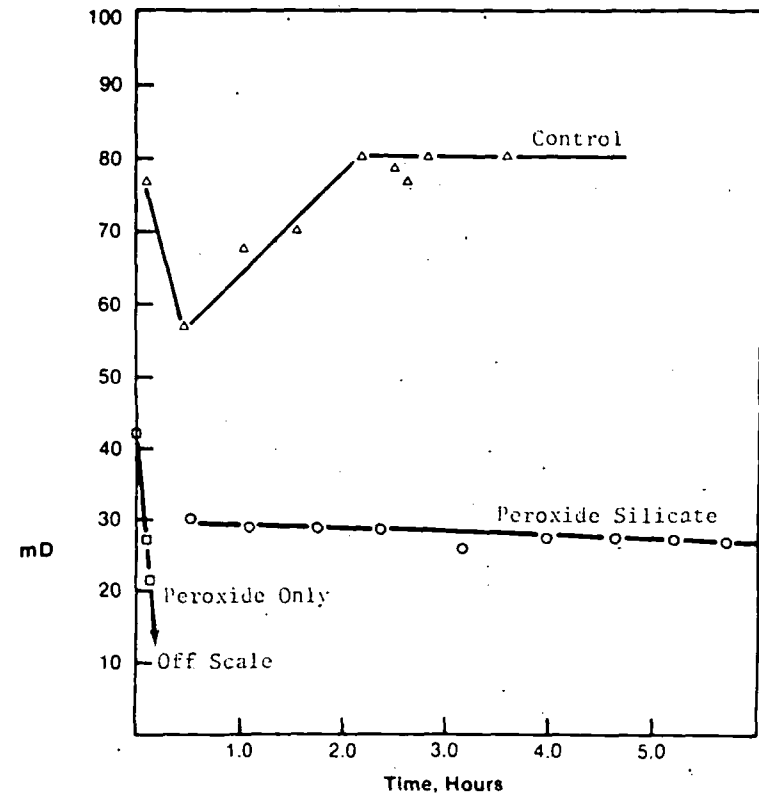


FIG. 7. Permeability for Rich Texas Ore

EFFECT OF SILICATE ON ORE EXTRACTIONS

Preliminary experiments showed that silicate may or may not effect ore extractions, depending on the ore used. Table 4 summarizes column leaching results for the weak Texas ore, and shows that 3 g/l of silicate in the leach had no substantial effect for an exhaustive uranium extraction (that also extracted only 1-2% of the calcium and 3-4% of the sulfate in the ore). An exhaustive batch leaching experiment for ore gave the same result for uranium. It was observed that the calcium content of silicate-containing leachate was somewhat lower for 2 of 3 other column leach experiments, thus suggesting the

Table 4. Effect of Silicate on Column Leaching

Constituent	mg in Leachate	
	No Silicate	With 3 g/l Silicate
Uranium	58.7	56.3
Calcium	12.7	5.37
Sulfate	134	161
Molybdenum	11.9	13.6

difference noted in Table 4 for calcium may be real. The difference in sulfate seen in Table 4 was probably not real, as illustrated by not being reproducible in other experiments. The single molybdenum result at least suggests no unusual silicate effect.

Batch leaching of rich Texas ore similarly showed that silicate did not affect leaching of uranium, though leaching of a weak ore showed small losses in the rate of uranium leaching when silicate was in the leach.

Work in this area is continuing because evidence was developed that the use of additives, including hydrogen peroxide stabilizers, can have profound effects on the laboratory extraction of uranium from some ores, and that even the mode of lab test extraction--whether batch or column leaching--can influence the kind of comparative results one gets.

Before leaving the subject of the effect of silicate on uranium extraction, what about its effect on the subsequent ion-exchange removal of the complex uranium-carbonate anion from the leachate? It is not expected that silicate anions would seriously compete with the more highly charged uranium complex anions during ion exchange. However, because individual pregnant liquors and ion exchange resins can vary so, ion exchange performance should be evaluated on individual leaches rather than be trusted to theory.

MECHANISM CONSIDERATIONS

Factors, or mechanisms, that could explain permeability changes are: (1) clay swelling, (2) slimes migration, (3) particle redistribution, (4) vaporblinding, (5) precipitation, and (6) viscosity changes. Various data and observations from this study support some of these, but the picture is far from clear.

First, as to clay swelling of water sensitive clays, it is well known that chemicals like sodium silicate can change the nature of clay surface charges--and, thus, their swelling characteristics--depending on factors such as silicate concentration and the presence or absence of other chemicals. In these experiments there was no

visible bulk expansion of the ore bed volume when leach containing peroxide--with or without silicate--was being pumped through the ore bed. When flow was stopped, however, the bed would typically expand 10-20%--from release of O_2 by peroxide decomposition--but would quickly shrink to about its original volume when flow was resumed. Any improvement in flow rate associated with this expansion for a silicate-free leach was quickly lost when the bed shrank again on resuming flow. Silicate seemed to enhance this expansion on flow stoppage--even though less oxygen was evolved--and the shrinkage with resumed flow did not appear to be as complete.

Second, the migration of very finely divided particles, or slimes, can contribute to loss of leach flow by blinding flow channels. Column experiments indicated that silicate tended to retard such migration because the glass wool plugs under the ore bed and the leachates themselves seemed to be freer of finely divided particles when silicate was in the leach. However, this is at most a partial answer because flow which had already been diminished by peroxide showed substantial recovery with post-addition of silicate.

Third, as to gross particle redistribution, packing columns with the moist weak Texas ore left about 5-10% of the ore bed volume as small voids, which did not change in number or shape when peroxide-free leach was pumped through the bed. However, when the leach contained hydrogen peroxide, the voids disappeared completely within about a half hour, with no visible difference in the bulk volume of the ore bed. This local redistribution of loose-packed ore--presumably by the action of oxygen gas from peroxide decomposition--raises an interesting question; namely, could decomposing peroxide in actual downhole operation have a similar effect and lead to less channelling of leach flow, and better distribution of oxidant, at least in the critical area near an injection well?

Fourth, as to vapor blinding, the data are mixed and indirect as to whether minute oxygen bubbles from peroxide decomposition can cause this. An indirect piece of evidence was that an oxidant that did not release a gas--sodium chlorate--did not cause any apparent

loss of permeability over several hours during column leaching through a bed of the rich Texas ore. To get a similar effect with peroxide, silicate also had to be present. However, such a potential advantage for chlorate was offset by poorer column leaching as shown by comparative column leaching experiments run at 5 cc/min. Even though the peroxide leach contained only half the number of moles (0.05 moles/l) and one-sixth the number of oxidizing electrons as the chlorate leach, the peroxide leach extracted about 120% more uranium than the chlorate leach did during a 500-minute period. This followed an earlier 80-minute period where uranium mostly in the already-oxidized state was leached out. For the total 580 minutes, peroxide leaching removed 73% of the ore's uranium, chlorate leaching 43%.

A more direct piece of evidence was that for some ores silicate substantially decreased the rate of decomposition of peroxide to oxygen gas, and this is summarized for the Mountain States ore in Figure 8.

For the rich Texas ore, however, about 90% of the peroxide was decomposed by a single pass through an ore bed, whether or not silicate was present. Another thing to keep in mind is that lab tests greatly exaggerated the amount of oxygen gas in contact with ore, because tests were run at atmospheric pressure. Higher downhole pressures would solubilize much of this oxygen gas.

As to the last two points--precipitation and viscosity changes affecting permeability--there was no direct evidence to bear. Precipitation of the highly insoluble $UO_4 \cdot 4H_2O$ was probably not involved in this study, because most permeability effects occurred with leaches strongly buffered at pH 8-9. Separate experiments showed that this compound did not precipitate above pH 6-7. As to viscosity, since 1 g/l of silicate worked as well as 4 g/l, bulk solution viscosity would not appear to be involved. This does not, however, rule out the possibility of subtle non-Newtonian effects being operative.

Silicate chemistry is exceedingly complex. Even though leach solutions containing less than 2 g/l of silicate remain clear, silicate can exist as a complex mixture of monomeric sodium silicate, soluble polymeric condensation products, or sub-visible colloids.

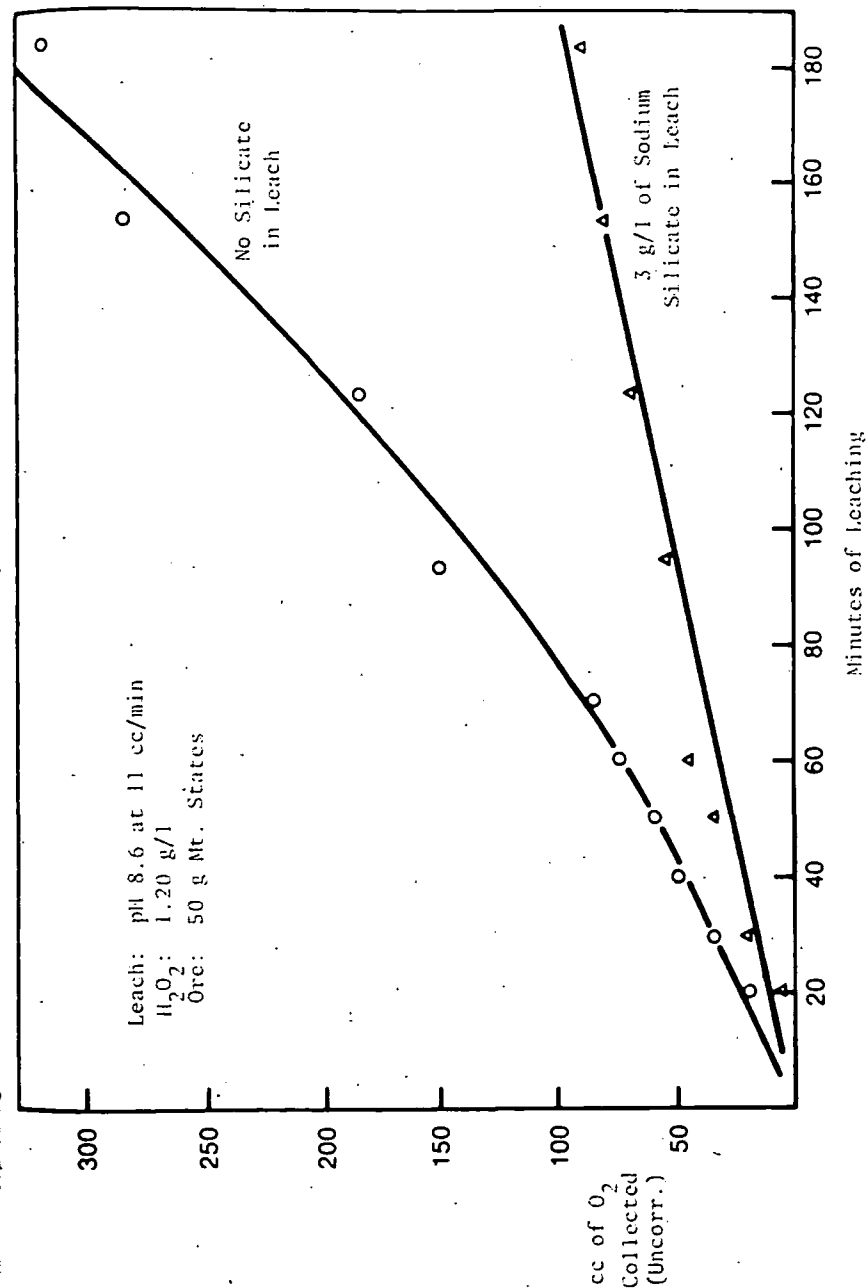


FIG. 8. Effect of Silicate on H_2O_2 Decomposition

SUMMARY AND CONCLUSIONS

From accelerated lab tests, non-gelling silicate concentrations can be very helpful in improving the permeability of peroxide-containing ammonium carbonate leaches at pH 7-10. The mechanism needs further clarification, but because the effects and process parameters can vary so with individual ores, the information from this paper would be put to best use by field testing in an in-situ mine where solution flow is likely to be, or has turned out to be a problem.

ACKNOWLEDGEMENT

The author wishes to express his appreciation to his many associates at du Pont who helped in or encouraged the preparation of this publication, particularly to Frederick W. DeVries, John C. Watts, John L. Fitzjohn, Paul C. Yates and Chris Needes for invaluable technical discussions, to Bonnie Griffiths for her skillful direction of work measuring permeability, and to Edwin S. Cooke for skillful execution of experimental protocol; also to Dean Milton Wadsworth of the University of Utah for early invaluable suggestions and continuing interest.

This paper was presented at the American Nuclear Society Meeting, Golden, CO, 4/14/77.

Th
by the
this e.
seven
These t
(therma
and dis
(b) rer
induce
real-t
contro
respec
develop
were of
detail
based
fielde

INTRODU

S:

quire
mechan
and ge
of cons
tion.

Copyrig
may be r
photoco
without

EFFECT OF SEEDING UPON PURITY OF ALUMINUM HYDROXIDE EVOLVING IN CARBONIZATION OF PREDOMINANTLY POTASSIUM ALUMINATE SOLUTIONS

UDC 669.712.1.051

A. A. Khanamirova and B. V. Nikogosyan

According to the scheme now adopted at Soviet alumina plants processing aluminosilicate material, the aluminate solutions enter the carbonizing process after full two-stage desiliconizing. Only thus can the production of high-purity alumina from predominantly sodium aluminate solutions be maintained.

Predominantly potassium aluminate solutions will be produced at the Razdansk Mining and Chemical Combine by integrated processing of nephelitic syenites. Two-stage desiliconizing conditions for these aluminate solutions have been worked out at the Institute of General and Inorganic Chemistry, Academy of Sciences of the Armenian SSR.

According to the proposed scheme [1], the first stage of desiliconizing is at 130°C, with a duration of 3 hr and addition of 30 g/liter alkaline aluminosilicate ("potassium chemical concentrate"), while the second stage is at 100°C, with a duration of 2 hr and addition of 15 g/liter CaO.

The investigations in [2] showed that carbonizing of predominantly potassium aluminate solutions produced aluminum hydroxide of much higher purity than carbonization of predominantly sodium aluminate solutions under analogous conditions.

High-grade alumina can be produced in carbonization without seeding of predominantly potassium aluminate solutions with various silicon ratios by incomplete or complete carbonizing [2].

This work gives the results of research under laboratory conditions on carbonizing synthetic predominantly potassium aluminate solutions with various silicon ratios obtained after the first and second stages of desiliconizing with seeding (Tables 1 and 2).

The use of seeding in carbonizing predominantly potassium aluminate solutions after the first

Table 1
Carbonization of the Predominantly Potassium Aluminate Solutions After the First Stage of Desiliconization

Serial no.	Solution des-composition, %	Seeding ratio	Impurities content (converted to alumina), %								Grade of alumina produced from aluminum hydroxide	
			seeding aluminum hydroxide				aluminum hydroxide produced by carbonizing					
			SiO ₂	R ₂ O ₂ tot (in Na ₂ O)	K ₂ O	Na ₂ O	SiO ₂	R ₂ O ₂ tot (in Na ₂ O)	K ₂ O	Na ₂ O		
1	84.1	—	—	—	—	—	—	—	—	—	—	GAB
2	60.5	0.5	0.008	0.28	0.14	0.19	0.030	0.31	0.15	0.21	0.24	GAB5
3	84.1	0.5	0.04	0.57	0.29	0.38	0.028	0.36	0.18	0.24	0.25	GAB5
4	73.7	0.5	0.008	0.28	0.14	0.19	0.070	0.33	0.15	0.23	0.30	GAB5
5	88.8	0.5	0.006	0.28	0.14	0.19	0.105	0.48	0.27	0.30	0.31	GAB5
6	98.0	0.5	0.04	0.57	0.29	0.38	0.110	0.48	0.26	0.31	0.27	GAB5
7	61.9	1.0	0.006	0.28	0.14	0.19	0.017	0.27	0.11	0.20	0.25	GAB5
8	62.8	1.0	0.04	0.57	0.29	0.38	0.010	0.36	0.17	0.25	0.25	GAB5
9	77.7	1.0	0.006	0.28	0.14	0.19	0.027	0.30	0.14	0.21	0.25	GAB5
10	86.8	1.0	0.008	0.28	0.14	0.19	0.054	0.38	0.20	0.25	0.25	GAB5
11	92.1	1.0	0.008	0.32	0.15	0.22	0.080	0.38	0.15	0.25	0.25	GAB5
12	98.0	1.0	0.04	0.57	0.29	0.38	0.060	0.43	0.24	0.27	0.27	GAB5

Test conditions: The solutions to be carbonized contained (in g/liter): 147-152 R₂O (tot) (in terms of K₂O); 132-137 R₂O₂caust (in terms of K₂O); 14-15 R₂O₂carb (in terms of K₂O); R₂O:Na₂O ratio by mass ~ 8:2; 80-83 Al₂O₃; 0.3-0.55 SiO₂; α_{CR} = 161-147; t = 80°C; speed of passage of gas-air mixture 15 liters/hr.
Note: The seeding aluminum hydroxide was produced by carbonizing the predominantly potassium aluminate solutions with α_{CR} = 1023, 1180, and 2634 at a gas passage rate of 15 liters/hr and a solution decomposition rate of 60-64%.

Table 2
Carbonization of the Predominantly Potassium Aluminate Solutions After the Second Stage of Desiliconization

Serial no.	Solution des-composition, %	Seeding ratio	Impurities content (converted to alumina), %								Grade of alumina produced from aluminum hydroxide		
			seeding aluminum hydroxide				aluminum hydroxide produced by carbonizing						
			SiO ₂	R ₂ O ₂ tot (in Na ₂ O)	K ₂ O	Na ₂ O	SiO ₂	R ₂ O ₂ tot (in Na ₂ O)	K ₂ O	Na ₂ O			
1	82.1	—	—	—	—	—	—	—	—	—	—	—	GAB5
2	75.2	—	—	—	—	—	—	0.010	0.48	—	—	—	GAB5
3	81.7	—	—	—	—	—	—	0.013	0.55	—	—	—	GAB5
4	97.4	—	—	—	—	—	—	0.028	0.71	—	—	—	GAB5
5	82.4	0.5	0.008	0.33	0.16	0.23	0.008	0.31	0.16	0.22	0.25	0.25	GAB5
6	98.1	0.5	0.008	0.33	0.16	0.23	0.025	0.36	0.19	0.23	0.25	0.25	GAB5
7	81.5	1.0	0.008	0.33	0.16	0.23	0.005	0.25	0.12	0.19	0.25	0.25	GAB5
8	98.1	1.0	0.008	0.33	0.16	0.23	0.008	0.26	0.12	0.18	0.25	0.25	GAB5

Test conditions: The solutions to be carbonized contained (in g/liter): 146-153 R₂O₂total (in terms of K₂O); 133-137 R₂O₂caust (in terms of K₂O); 14-16 R₂O₂carb (in terms of K₂O); K₂O:Na₂O ratio by mass ~ 8:2; 78-80 Al₂O₃; 0.05-0.08 SiO₂; α_{CR} = 1531-932; t = 80°C; gas-air mixture passage rate 15 liters/hr.
Note: The seeding aluminum hydroxide was produced by carbonizing predominantly potassium aluminate solutions with α_{CR} = 1202 at a gas passage rate of 15 liters/hr, and a solution decomposition rate of 72.4%.

desiliconizing stage gives a larger amount of high-purity aluminum hydroxide, and under optimum conditions (decomposition 60-64%, speed of gas passage 15 liters/hr) it helps to produce aluminum hydroxide of higher purity than in carbonizing without seeding (see Table 1).

Single-stage carbonizing without seeding of predominantly potassium aluminate solutions after the second desiliconizing stage at a speed of gas passage of 15 liters/hr produces aluminum hydroxide corresponding to GA8 and GA85* grade alumina with up to 82% aluminate solution decomposition (see Table 2).

The use of pure aluminum hydroxide seeding in carbonizing these solutions makes it possible to produce aluminum hydroxide conforming to GA85 grade alumina with practically complete aluminate solution decomposition (98%) at seeding ratios of 0.5 and 1.0 (see Table 2).

It is apparent from Table 3 that alumina produced under optimum conditions of carbonization with seeding is coarse-grained, and its density, which is an indirect indication of phase composition (α -Al₂O₃ content), is within the same limits as production alumina from Soviet plants¹.

Thus the alumina produced from predominantly potassium aluminate solutions under laboratory conditions by carbonizing with seeding conforms both in impurities content and in structure to the requirements imposed upon alumina from Soviet plants.

CONCLUSIONS

In carbonization with seeding of predominantly potassium aluminate solutions after the first desiliconizing stage, GA8 grade alumina evolves at a decomposition rate of 74 and 87% and GA85 grade at a decomposition rate of 64 and 78% (at seeding ratios of 0.5 and 1.0); after the second stage, alumina of the highest grade (GA85) evolves with practically complete solution decomposition (98%).

REFERENCES

1. M. G. Manvelyan and A. A. Khanamirova, Desiliconizing of Alkaline Aluminate Solutions, Erevan, Izd. Akad. Nauk Arm. SSR, 1973, 299 pages, illustrated.
2. A. A. Khanamirova and B. V. Nikogosyan, Tsvetnye Metally, 1976, No. 8, 44-48.

*The matching of aluminum hydroxide produced under laboratory conditions with alumina grades according to GOST 6912-64 takes no account of contamination during calcining, as is customary under production conditions.

¹In continuous carbonizing of predominantly potassium aluminate solutions at the Razdansk Mining and Chemical Combine the alumina will have somewhat different particle-size characteristics.

Table 3
Particle-Size Analysis and Density of Aluminas Produced by Carbonizing Predominantly Potassium Aluminate Solutions with Seeding

Sample no.	Composition of aluminas, % (by mass)								Density, g/cm ³	
	Fraction, μ m									
	+100	-100+80	80+63	63+55	55+36	36+25	25+17	17+10		-10+7
Sample 10 (Table 1)	86.8	20.8	12.9	1.3	0.7	1.6	2.2	2.9	0.5	3.7
Sample 11 (Table 1)	80.0	28.9	9.9	1.6	1.2	1.6	3.3	3.2	0.9	3.6
Sample 6 (Table 2)	48.0	32.9	8.0	1.7	1.2	1.4	3.0	4.8	1.3	3.6
Sample 8 (Table 2)	68.3	8.3	16.9	1.3	0.9	0.8	1.3	1.5	0.6	3.6

Elastic and Transport Properties of an *In Situ* Jointed Granite

H. R. PRATT*
H. S. SWOLFS*
W. F. BRACE†
A. D. BLACK*
‡ W. HANDIN‡

UNIVERSITY OF UTAH
RESEARCH INSTITUTE
EARTH SCIENCE LAB.

In situ elastic and transport properties were measured as a function of compressive stress to 200 bars for a variety of load paths on a 3-m cube of jointed granite near Laramie, Wyoming. The specimen contained 3 vertical joints which are parallel to a set of well-developed microfractures. Measurements were made parallel and normal to the joints across the entire block and within intact areas containing only microfractures. The loads were applied by eight 1.2 × 2.4 m flatjacks, 2 on each of the 4 sides. The measured properties included deformation, compressional velocity, electrical resistivity and fluid permeability. Load paths included uniaxial, biaxial and proportional stress and uniaxial 'strain'. 'Direct shear' tests were also conducted at 2 normal stresses. Field data were compared with measurements made on oriented specimens in the laboratory.

Results based on differences in rate of change of fluid flow, elastic modulus and on seismic wave propagation indicate that the joints close at 15-30 bars normal stress, but that microcracks remain open at the highest stresses attained. Changes in fluid permeability along the joint and elastic modulus with stress are greater than those of either seismic velocity or electrical resistivity. Modulus and velocity increased with stress while permeability decreased by a factor of 4. Even when 'closed' permeability along the joint is 3 orders of magnitude greater than for intact granite. Intact granite exhibits a marked anisotropy with respect to both modulus and seismic velocity.

INTRODUCTION

Structural discontinuities such as joints, faults and bedding plane partings are widespread in rock near the surface and, perhaps locally, to several kilometers depth. Such discontinuities strongly affect elastic properties, mechanical strength, and phenomena which involve mass transport through pore space. The exact contribution of such discontinuities, however, although vital in predicting the response of a rock mass to, say, the loads and hydraulic conditions imposed by a dam, remain obscure. Indeed, this question of how to formulate the *in situ* contribution of joints and other discontinuities, is one of the most critical in rock mechanics.

There are a number of ways of approaching this problem [see reviews in 1,2] and most involve modeling the discontinuity in some way. This may take the form of mathematical analysis of idealized block sys-

tems [3-6], observation of scaled-down analogues of real jointed systems [7,8] or study of sawcuts and other artificial discontinuities introduced into small rock samples [9-12]. It is often unclear just how closely these models reflect the actual behavior of the jointed rocks they are supposed to represent.

Still another approach, and the one adopted here, is the study of actual discontinuities *in situ* [13-15]. Here at least, the uncertainty of modeling and scaling the results are avoided and, if the experiment is well conducted, the role of a particular set of discontinuities can be precisely determined. Of course, the difficulty of extrapolation to other sets remains, but there is a possibility that with continued study, certain common characteristics of all discontinuities will emerge.

Most *in situ* studies have been devoted to a single property, such as shear resistance [14], elastic deformation [16], fracture strength [17] or fluid flow [18,19]. We have devised an experiment in which a variety of characteristics could be observed while a large *in situ* block was subjected to nearly homogeneous stress. These included both static and dynamic elastic response as well as electrical resistivity and fluid permea-

*Terratek Inc., University Research Park, 420 Wakara Way, Salt Lake City, UT 84108, U.S.A.

†Department of Earth and Planetary Sciences, Massachusetts Inst. of Technology, Cambridge, MA 02139, U.S.A.

‡Texas A and M University, College Station, TX 77843, U.S.A.

UNIVERSITY OF UTAH
RESEARCH INSTITUTE
EARTH SCIENCE LAB.

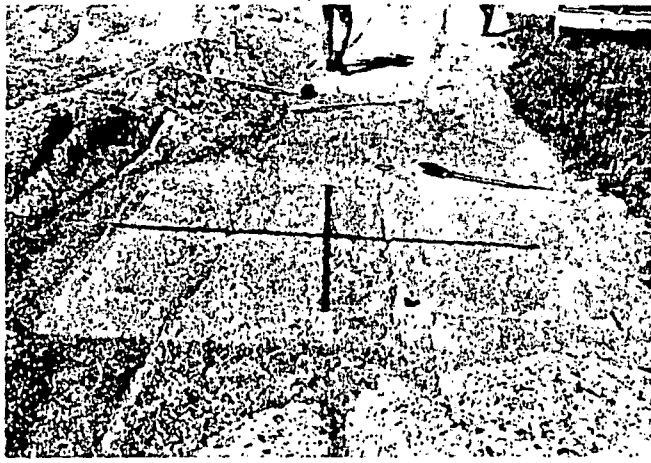


Fig. 1. Photograph of test site in massive granite. View is typical of outcrop in area. Shovel gives scale.

bility. Stress was sufficient to close the larger joints so that changes in these properties could be observed simultaneously, as the joints closed, for a wide range of load paths. To our knowledge, an *in situ* experiment of this complexity and size had never been attempted before.

SITE SELECTION

Several factors dictated the selection of the site. We felt it particularly important, in this first experiment, to have simple joint geometry, ideally 3–6 vertical parallel joints. We wished to avoid intersecting joints, as these might introduce unnecessary complications. The rock had to be unweathered, homogeneous and massive. Because of the procedure used for preparation of the *in situ* sample, the outcrop surface had to be fairly flat. We also wished to find rock which was dry in the natural state, so that properties when dry could be compared with properties after saturation. After some search we chose outcrops of the Sherman granite [20] near the town of Tie Siding, 32 km south of Laramie, Wyoming. The rock is fresh, coarse-grained granite which, at the site selected, is cut by single sets of vertical joints spaced about 1 m apart (Fig. 1). The joints have a strong preferred orientation, approx N 55° E, which is parallel to innumerable mesoscopic fractures up to 1 cm long which cut the intact rock between the joints. An additional Northwest-Southeast set of joints is found in the area but is not prevalent in the outcrop studied. The Sherman granite contains potash feldspar, quartz, plagioclase and biotite, has a density of 2.715 g/cm³ and a porosity of 0.42%.

PROCEDURE

The test block, shown diagrammatically in Fig. 2 was 2.8 m square and 2.6 m deep; it was cut out using the techniques we have developed for large *in situ* samples [13]. The vertical sides of the specimen were formed by line drilling. Near the center of each slot a small enlargement was excavated to accommodate the seismic transducers. Oriented samples of rock were removed during this process and saved for future labor-

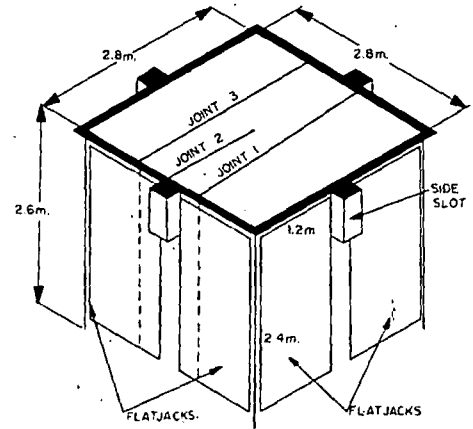


Fig. 2. Schematic diagram of the experimental block and the positions of the flatjacks used to load the specimen. The three joints are visible in Fig. 1.

atory comparison with *in situ* measurements. The final sample (Fig. 2) was a rectangular prism containing 3 parallel vertical joints, 2 of which cut the entire block, the third joint went approximately halfway through the block. The entire block remained attached at the bottom.

In each of the 4 slots, two 1.2 m wide by 2.4 m long stainless steel flatjacks were inserted and grouted in place. The flatjacks were coated with PVC plastic to provide electrical insulation. These 8 flatjacks constituted the loading system. A hydraulic pumping system was used to pressurize the flatjacks and apply a uniform load to the sides of the specimen. Two opposite sides of the block could be loaded simultaneously but independently of the 2 adjacent sides; that is, the block could be subjected to different loads in 2 directions. Because the surface area of a pair of flatjacks was smaller than the surface area of the sides of the block the flatjack pressure, known to ± 0.3 bar, was multiplied by a calibration factor of 0.89 to obtain the actual stress in the block. An elastic analysis of the stress distribution in the block when loaded by the flatjacks showed that the stresses in the upper two thirds of the block were quite uniform; all physical properties were measured in this part of the block.

The top surface of the block (Fig. 3) was the site of most measurements. Strains were detected with 5 sets of 5.1 cm gage length 45° rosettes and displacements with 6 DCDTs. Short gage length DCDTs, D₁, D₄, D₅, D₆, gave the displacements across the joints while long gage length DCDTs, D₁, D₂, included sections of unjointed rock. Strains were measured by a Vishay strain indicator with an accuracy of $\pm 1 \times 10^{-3}$ and displacements with a digital voltmeter with an accuracy of $\pm 40 \mu\text{m}$, which over a meter is equivalent to a strain of 4×10^{-5} .

Ultrasonic velocity transducers (45 kHz) were mounted on the sides of the block in the 4 side slots, about 60 cm below the surface. Two shallow 5 cm diameter holes (marked V₂ and V₄ in Fig. 3) were drilled in the surface of the block 1 m in from the sides, for additional velocity transducers (100 kHz). Compressional

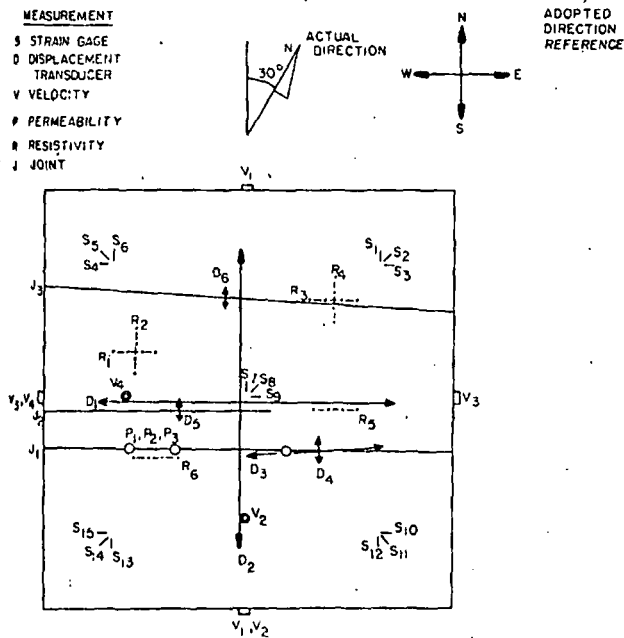


Fig. 3. Sketch of the top surface of the block showing the points at which various measurements were made relative to the three joints.

velocity was measured both across the entire width of the sample (paths V_1 and V_4). Travel times were measured with an oscilloscope; accuracy of reported velocity is $\pm 0.025 \text{ km sec}^{-1}$.

Electrical resistivity was measured by the 4 electrode Wenner method at 6 locations, marked R_1 – R_6 in Fig. 3. Electrical contact was made through thin lead strips inserted in 1.6 cm dia by 20.3 cm deep holes drilled in the rock and kept full of water. Constant current was applied to one pair of electrodes by a 15 Hz signal generator and voltage across the other pair was measured with a solid state a.c. voltmeter. Resistivity could be determined to about $\pm 30 \Omega$ meters.

Fluid permeability along joint 1 (Figs. 2 and 3) was measured between pairs of holes 7.6 cm dia by 1.8 m deep drilled along the plane of the joint. Water was injected under 4 bars pressure into one hole (Fig. 4) and flow along the joint measured by several methods:

(1) direct observation of the volume flowing into the second hole as pressure drop across the hole was held constant. (2) decay of pressure in the first hole as water flowed outward at constant system volume, or (3) through transit time of a dye tracer introduced into one hole. Accuracy of these different methods was comparable, approx $0.2 \text{ cm}^3 \text{ sec}^{-1}$.

We had hoped to study the effect of saturation during our tests, based on the likelihood that the outcrop chosen would, at the site selected, be initially unsaturated. The slots remained dry as the block was excavated, in support of this idea. However, when *in situ* resistivity was measured it became clear that saturation of the microfractures at least, was fairly complete. We were, of course, unable to materially alter this *in situ* state, so this phase of our study became somewhat secondary.

Since our experiments lasted several months it was necessary to insure that neither the block surface, nor the instruments attached to it suffered from environmental changes. A tent-like enclosure was built over the entire test site to mitigate the effects of temperature changes, precipitation, drying and roving livestock. We tried to maintain the block as close as possible to its original water content during the first tests; later, water was flushed over the surface and injected into the joints, to see if properties changed. Since we were also interested in long term changes in the block, after completion of our measurements during the first summer, the block was left exposed to the elements for about 10 months. Static deformation and compressional velocity were then remeasured.

A number of laboratory experiments complemented our field measurements: (i) stress-strain behavior and fracture strength was observed for 5 cm diameter samples, unconfined, in directions parallel and perpendicular to jointing (Fig. 2); (ii) compressional velocity in the same 2 directions was measured, as a function of pressure, both air-dried and saturated on a rectangular block 10 cm by 15 cm by 12 cm; (iii) electrical resistivity (10 Hz) was measured on 2.5 cm dia saturated samples in a direction normal to jointing, at a confining

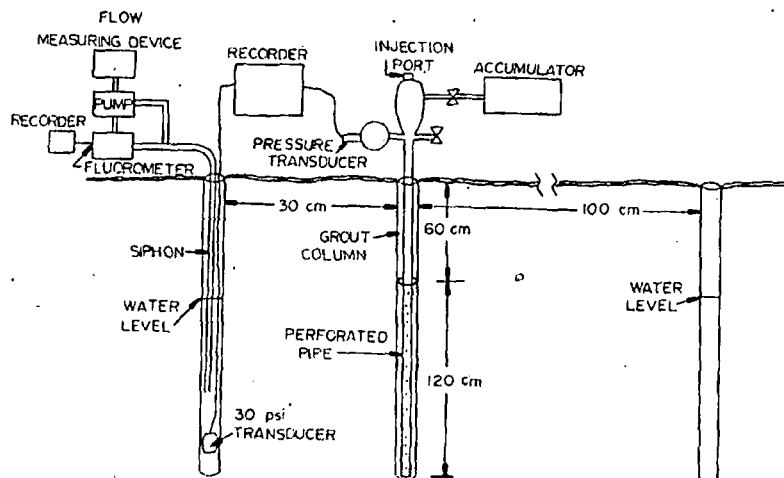


Fig. 4. Schematic cross-section of the permeability experiment along joint J_1 .

UNIVERSITY OF CALIFORNIA

TABLE 1. SUMMARY OF *in situ* TESTS

Test No.	Load path	Saturation	Maximum stress (bars)		Measurements
			E-W	N-S	
1	Biaxial EW/NS = 1	Dry	30.7	30.7	S ₁₋₁₅ , D ₁₋₆ , V ₁₋₄ , R ₁₋₆
2	Uniaxial strain E-W	Dry	61.4	4.2	"
3	Uniaxial strain N-S/Dry	Dry	3.1	24.6	"
4	Biaxial proportional EW-NS = 2	Dry	49.1	24.6	"
6	Uniaxial stress E-W	Dry	92.1	0	"
7	Uniaxial stress N-S	Dry	0	33.8	"
8	Biaxial EW/NS = 1	Wet	36.8	36.8	S ₁₋₁₅ , D ₁₋₆ , P ₁₋₃ , R ₁₋₆
9	Biaxial proportional EW/NS = 2	Wet	73.7	36.8	"
10	Uniaxial stress E-W	Wet	147.3	0	"
11	Uniaxial stress N-S	Wet	0	61.4	"
12	Shear $\sigma_N = 0$	Wet	54	0	"
14	Reload biaxial EW/NS = 1	Dry	41.7	41.7	S ₁₋₁₅ , D ₁₋₆ , V ₁₋₄
15	Reload uniaxial stress N-S	Dry	0	41.7	S ₁₋₁₅ , D ₁₋₆ , V ₁₋₄
16	Reload uniaxial stress E-W	Dry	69	0	"

pressure from 10 bars to several kbars; (iv) permeability parallel and perpendicular to jointing, density and porosity were determined for 2.5 cm dia samples. Samples for all these tests came from the blocks which were produced by excavation of the 4 side slots of the large block (Fig. 2).

Finally, for comparison with both jointed rock and laboratory values, seismic velocity was measured along several 100 m profiles centered on the test block. Geophone spacing was about 8 m and the profiles were made along directions parallel and perpendicular to the joints in the test block.

OBSERVATIONS

Sixteen experiments were conducted at the field site along with a variety of load paths and at different stress levels (Table 1). In a typical experiment a single load path, for example uniaxial stress parallel to the joints (test 6), was followed stepwise while deformations (S and D), resistivity (R) and velocity (V) were recorded. Except for test 13 the stresses were kept below 150 bars, the level at which we felt permanent changes might be induced in the block. In tests 12 and 13 we measured shearing resistance along joint 1 for 2 values of normal stress; presumably at that time we may have damaged the rock locally close to the joint. In tests 14, 15 and 16 we repeated certain measurements made in tests 1, 6 and 7, after the block had been exposed to the elements for 10 months. In Table 1, *biaxial* refers to 2 equal horizontal stresses, and *proportional biaxial* to the load path along which horizontal stresses were maintained at a constant ratio. *Uniaxial strain* was achieved by adjusting the least stress so that one horizontal strain remained zero, as recorded by the DCDTs. For simplicity, directions in the block were referred to a local East-West taken along the joints (Fig 3), which in reality strike N.55° E.

Static deformation and strain

The stress-strain behavior of intact rock, that is, rock between the joints, is shown for one pair of gages in

Fig. 5. The anisotropy of the rock is evident, as is the effect of loading condition. The rock is considerably less compliant under biaxial than under uniaxial stress. If we compare gage sets all over the block (Fig. 3) the parallel with the jointing agreed within about 10%. In the other direction, however, the strains at different points in the block varied unsystematically by a factor of 2.

The average stress-strain response of 3 sample measured in the laboratory with gages having a gage length of 2.5 cm is shown in Fig. 6 in comparison with

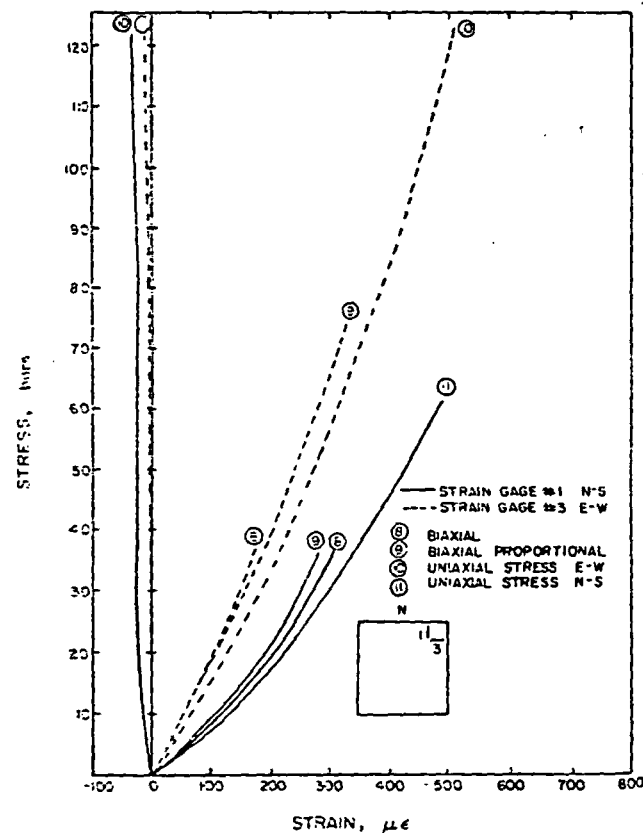


Fig. 5. Stress-strain behavior for rock between the joints, for a single set of perpendicular strain gages, for a variety of load paths. This behavior is fairly typical of all the strain gages. Note the anisotropy of the joint-free rock as well as the greater stiffness under biaxial

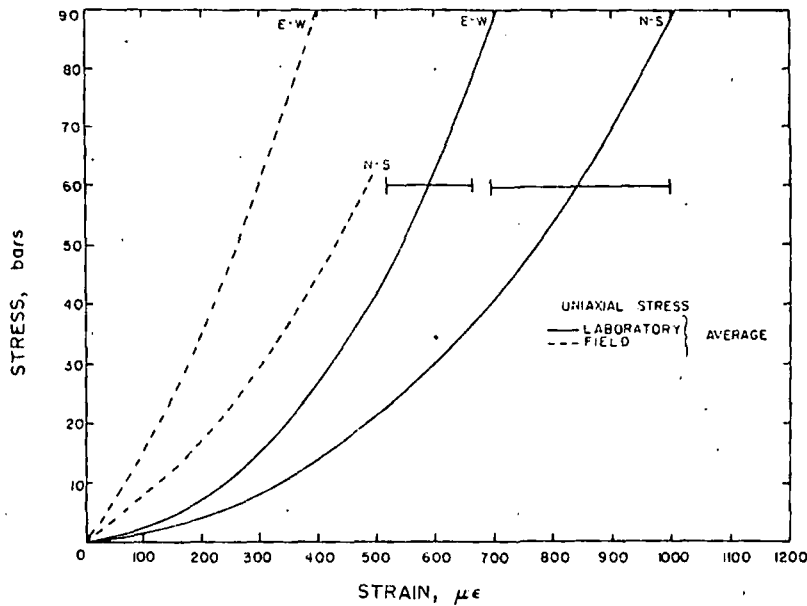


Fig. 6. Comparison of laboratory and *in situ* stress-strain behavior under uniaxial stress. The stress direction is indicated on each curve. These are average values. The spread is given by the set of error bars shown. Note the approximate agreement of elastic moduli of laboratory and field values at high stress; at low stress the laboratory samples are much more compliant.

field values taken from Fig. 5. The strong anisotropy is evident in both sets of curves. In addition, the laboratory samples were initially much more compliant than the *in situ* block.

Displacement across the joints and deformation of rock plus joints was measured by short and long gage length DCDTs respectively. Depending on the direction of loading and stress ratio, joints were observed both to open and to close. Hysteresis during stress cycling was pronounced, and joints rarely returned to their original opening (Fig. 7). The stress-displacement behavior of the 3 joints (Fig. 8) indicates that they were not equally compliant. Deformation of all 3 joints plus intact rock is given by curve D_2 .

Our measurements of joint closure as a function of stress enabled *joint stiffness* to be determined. The

values close to zero stress were taken from curves such as those in Fig. 8 for a number of load paths and are tabulated in Table 2.

Compressional velocity

Compressional velocity measured across the entire block typically increased with stress (Fig. 9) both parallel and normal to jointing. The increase with stress was greatest for load paths in which both stresses were increasing, that is, biaxial and biaxial-proportional loading (Fig. 10). The effect of stress normal to jointing was quite dramatic: signals could not be detected across the block (curve V_1 , Fig. 9) until stress reached about 12 bars.

Velocity was also measured along approx 1 m paths (Figs. 9 and 10). The observed velocity was lower than

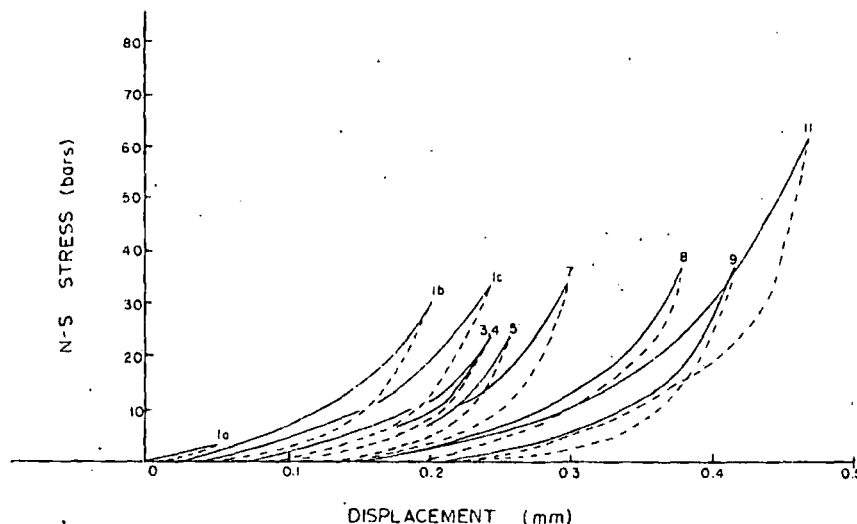


Fig. 7. Displacement across joint 3 as recorded by DCDT 6 as a function of N-S stress. Loading curves are solid, unloading curves dotted; the number above each curve gives the load path from Table 1. Note the cumulative closure of the joint with each cycle. Paths 1a, 1b and 1c are reloads of the biaxial load path.

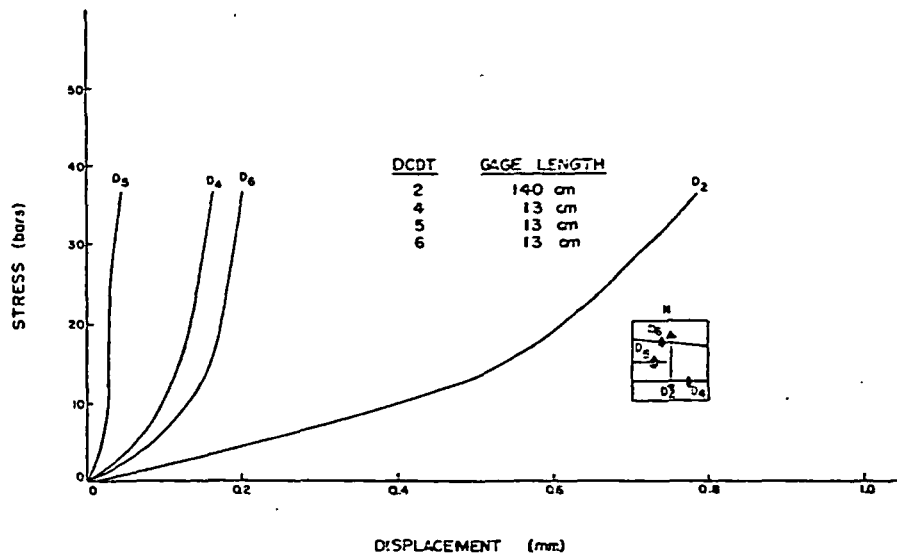


Fig. 8. Stress-displacement curves across joints. The output of DCDTs 4, 5 and 6 show closure of joints 1, 2 and 3 as a function of stress. D_2 gives the contraction of the entire block. The load path was 9, biaxial-proportional.

TABLE 2. NORMAL AND SHEAR STIFFNESS OF JOINTS

Test No.	Test	Direction	DCDT 4	DCDT 5	DCDT 6	DCDT 3
1	Biaxial	$P_{EW}/P_{NS} = 1$	29.66 ^a	326.28	19.68	
2	Uniaxial strain	$N-S = 0$	12.23	—	—	
3	Uniaxial strain	$E-W = 0$	25.37	207.63	17.57	
4	Proportional stress	$P_{EW}/P_{NS} = 2$	29.66	207.63	20.76	
5	Uniaxial strain	$EW = 0$	27.52	253.78	12.15	
6	Uniaxial stress	$P_{NS} = 0$	—	—	—	
7	Uniaxial strain	$P_{EW} = 0$	24.04	253.78	14.46	
8	Biaxial	$P_{EW}/P_{NS} = 1$	25.95	326.28	14.64	
9	Proportional stress	$P_{EW}/P_{NS} = 2$	24.83	265.58	16.31	
10	Uniaxial stress	$P_{NS} = 0$	—	—	—	
11	Uniaxial stress	$P_{EW} = 0$	24.83	228.4	11.77	
12	Shear	$\sigma_n = 0$				7.82
13	Shear	$\sigma_n = 69$ bars				15.42

^a A secant value taken early in the loading phase (kbar/mm).

^b Shear stiffness: slope of shear stress-displacement curve.

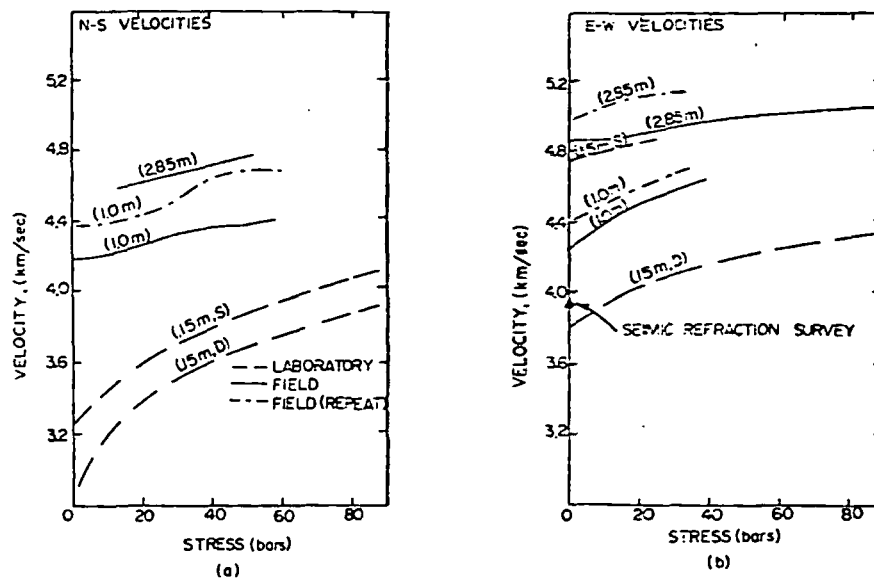


Fig. 9. Velocity as a function of stress for both *in situ* and laboratory tests. (a) North-South velocities, (b) East-West velocities. Paths lengths (e.g. 2.85 m) are given in meters. Moisture content: D = lab dry; S = saturated.

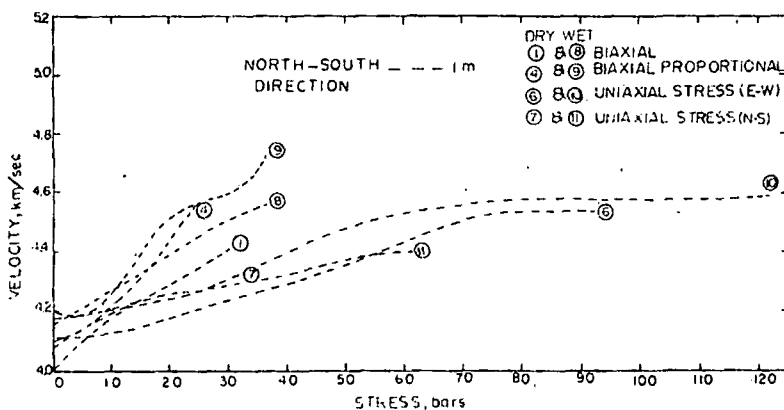


Fig. 10. Velocity-stress diagram showing the effect of applied loading conditions on the rate of change of velocity with increasing stress.

that for the 2.8 m paths, but the change with stress was similar for both path lengths.

As noted above, the *in situ* block was evidently nearly saturated from the very beginning. Nevertheless, we explored the effect of further wetting of the surface and the joints. At all stresses velocity increased uniformly by about 0.1 km/sec (curves 9 vs 4 and 8 vs 1, Fig. 10).

Velocity along 15 cm paths in the laboratory samples as a function of uniaxial stress in the N-S direction is given in Fig. 9. Two cases are compared: the specimen air dried, and the specimen saturated at atmospheric pressure. For both directions relative to jointing, saturation increased the velocity; evidently the increase in velocity in the E-W direction due to saturation was much greater than in the N-S direction.

The velocities observed during reloading after a period of 10 months are also given in Fig. 9 for load path 15 (uniaxial stress N-S). The new values seem to be about 0.1 km/sec higher for the 3 paths studied.

The seismic refraction measurements gave a value of 3.9 km/sec parallel to jointing in the *in situ* block. This value is also included in Fig. 9 for comparison with zero stress values measured in the block.

Permeability and resistivity

Flow rate along joint 1 is shown in Fig. 11 for various loading paths. Under biaxial load the rate decreased by a factor of 2 with stress to about 26 bars, where it remained constant. Flow rate increased under E-W uniaxial stress, due to opening of J_1 , but then decreased by a factor of 4 as the load was applied N-S, normal to the joint.

Permeability in 2 directions relative to jointing was measured for small core samples. Samples were about 2 cm dia by 4 cm long. Permeability was $100 \pm 10 \mu\text{darcies}$ parallel with jointing and $40 \pm 4 \mu\text{darcies}$ normal to jointing.

Changes in resistivity with stress are shown in Fig. 12 for 2 loading paths. The mean resistivity of 4 apparently identical laboratory samples as a function of hydrostatic pressure is also included for comparison. We did not know the resistivity of pore fluids at the field

site so we resaturated the laboratory samples with tap water of approx 50 Ω meters resistivity. Frequency was 10-15 Hz and temperature 23°C.

DISCUSSION

Variation of modulus with stress, size and direction

Our results, Figs. 5 and 6, clearly show that modulus of the Sherman granite on all scales depended on stress and direction. Modulus always increased with stress and modulus under biaxial was always greater than modulus under uniaxial load. At a given stress level E-W directions were always stiffer than N-S, reflecting both the E-W joints and the pervasive E-W microfractures. These microfractures were not entirely uniform in length and distribution, judging from the factor of 2 variation in observed strains at different N-S strain gage points. The variation in microfracture density is probably also responsible for the large variation we found for both laboratory and *in situ* resistivity (Fig. 12); this variation is larger than normal for small laboratory samples of granite [21].

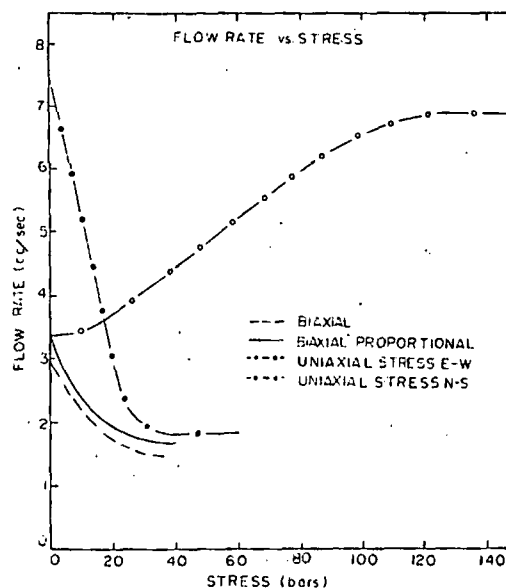


Fig. 11. Loading path dependence of flow rate of fluid along joint J_1 .

UNIVERSITY OF CALIFORNIA

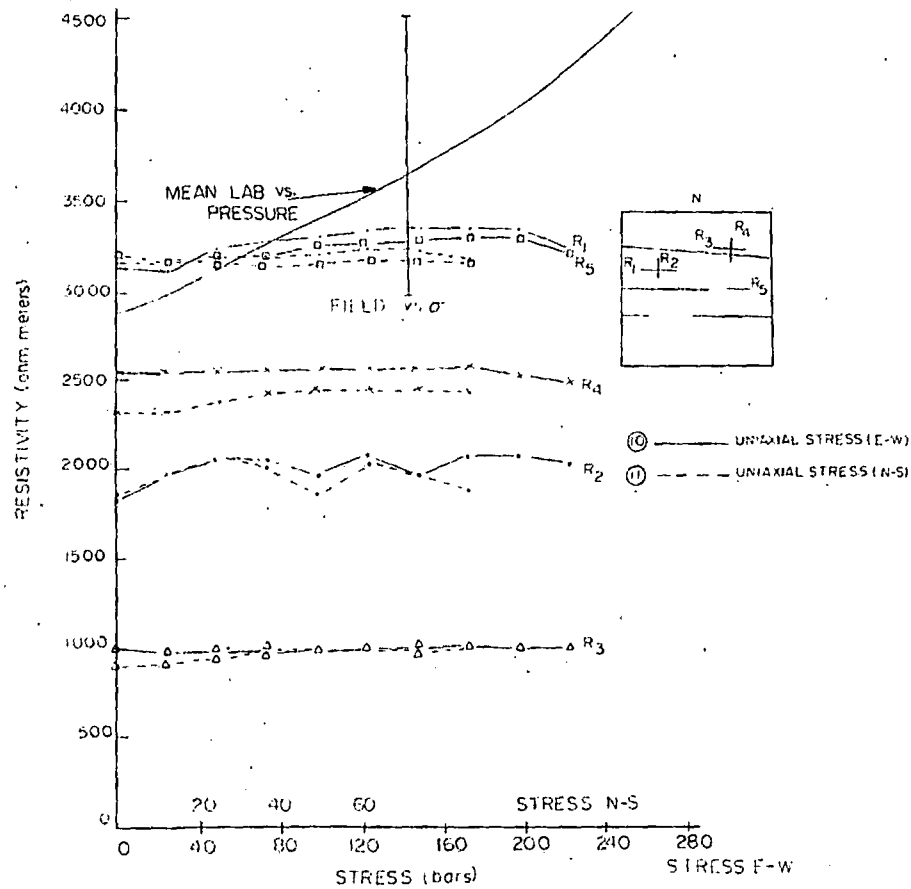


Fig. 12. Laboratory and field resistivity. Field values at points 1-5 are shown as a function of stress, for two load paths. The mean and spread of 4 laboratory samples as a function of hydrostatic pressure are also given for comparison. Frequency was 10-15 Hz. Pore water for the laboratory samples was 50 Ω meters and for the *in situ* block, the natural ground water, of unknown resistivity.

The dependence of modulus on scale (Fig. 6) is somewhat puzzling. The large intact portions of the block are stiffer than small cores of the same material at stresses below about 40 bars. The laboratory samples behaved as though they had acquired new larger cracks after removal from outcrop. One possibility is that the *in situ* Sherman granite contained high residual stress and that this stress was relieved for the small cores through formation of cracks. This conclusion may be supported by the electrical measurements: for resistivity of small samples increased much more rapidly than that of the *in situ* block, as pressure or stress was increased (Fig. 12). However, there are several complicating factors. For one thing, absolute comparison of laboratory and *in situ* resistivity measurements is clouded by uncertainty as to pore water resistivity in the outcrop. Also, the effect of stress is known to be somewhat less than the effect of hydrostatic pressure on resistivity [22].

Joint closure

Displacement of the joints with stress also had some interesting aspects. Although the joints predictably increased the compliance of the *in situ* block over the value it would have had were only microfractures present (Fig. 8), the contribution of individual joints varied

considerably (compare D_4 , D_5 and D_6 in Fig. 8, as well as joint stiffnesses in Table 2). Also, joint 3, at least, displayed marked hysteresis, even for uniaxial stress normal to the joint plane. This is hard to explain unless the joint surface was highly irregular and interpenetrating; residual stress in the block may also have forced some shearing motion as we opened and closed the joint. As transducer D_6 included very little intact rock, the usual explanation [23] of sliding on inclined cracks probably does not hold here.

From the contribution of individual joints and the overall deformation (Fig. 8) it is possible to determine average strain across the entire 140 cm of intact rock between the joints. From the 4 curves in Fig. 8 this strain is about 230 $\mu\epsilon$ at a stress of 30 bars, which is quite close to the value shown for gage 1, loading path 9, in Fig. 5.

The displacement of individual joints typically accounted for more than half of the total shortening of the block at a given stress (Fig. 13). As most of the microfractures are E-W, the E-W stress strain curve gives something close to the intrinsic elastic response of the granite. The difference between it and the N-S curve for intact rock gives the *microcrack contribution*. The difference between the N-S strain gage curve and curve showing the response of the entire jointed block gives the *joint contribution*.

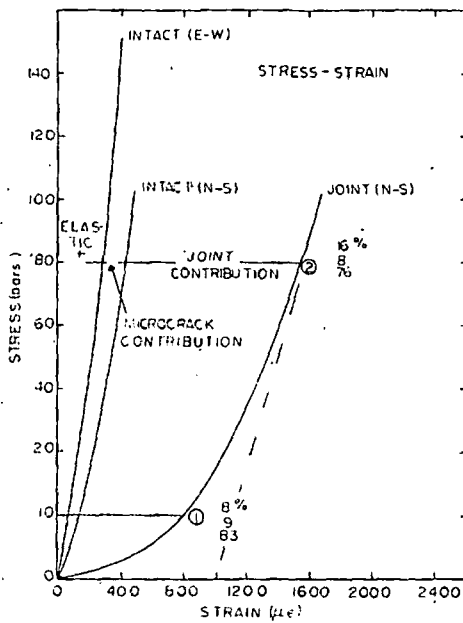


Fig. 13. Stress-strain curves, showing the relative contributions of elastic, microfracture and joint deformation. This is the response of joint 1 as measured by DCDT-4.

Actual joint closure, at least as reflected in stress-displacement curves seemed to require about 15 bars (Fig. 8). This is also close to the stress at which N-S velocity signals could be first detected (Fig. 9). Above about 15 bars the N-S modulus of the block as a whole (Fig. 13) seemed to approach a value somewhat less than half that of the intact rock in the N-S direction. Some additional closure or slip of small sections of the joints must have continued in this region.

Compressional velocity

Velocity at all path lengths, directions, and loading paths increased with stress but often in a somewhat unexpected manner. Based on well-known saturation effects, velocity for curves 7 and 11 in Fig. 10 ought to have increased with stress more rapidly than for curves 6 and 10. The fact that all 4 are similar suggests, as did the resistivity, that the block was nearly saturated from the outset, although we generally raised the velocity by about 0.1 km/s by further wetting of the surface.

The variation with both path length and between field and laboratory is quite significant. Both effects are in the same direction, namely, both laboratory and short field path give lower velocity (Fig. 9). The cause, as suggested above for static modulus, may be cracking due to residual stress combined with some irreversibility in crack closure. Here velocities do not seem to approach a constant value at high stress, as did the static moduli. It has been observed that appreciable residual stress can remain in blocks the size of ours [24]. A zone of partly relieved stress around the periphery of the block could be reflected in higher crack density and therefore lower velocity along the 1 m paths. The 1 m paths probably contained more stress-relieved rock than the 6 m paths.

The effects of saturation are confusing and difficult to explain. Saturation raised all velocities in both laboratory samples (Fig. 9) and *in situ* (Fig. 10) relative to what was assumed to be the dry state. As noted above, this was in accord with previous studies. Also, the greater effect for the laboratory samples is probably understandable in terms of their greater initial under-saturation. However, increase in velocity for the E-W laboratory samples was about 4 times that for the N-S samples. Based on the crack orientation, this order ought to be reversed. Also the saturated laboratory values ought, based on the arguments presented above, to fall below the values for the 1.0 m paths in the *in situ* block. In one case (N-S) they do, in the other they do not. This could perhaps be explained by material inhomogeneity or elastic inhomogeneity due to local differences in the degree of stress relief. Clearly this is a matter for further more detailed study for it leaves unresolved the important question of how laboratory and *in situ* velocities are related.

Reloading the *in situ* block appeared to uniformly raise compressional velocity for both path lengths and both directions by the same relative amount, namely about 5%. The reason is not clear. It could be due to differences in saturation during the 10 month period, or even to a small systematic error in either set of velocity measurements.

Permeability

The permeability along a joint is approximated from the Navier-Stokes equation by:

$$Q = -k_p \frac{\partial P}{\partial s} = \frac{\rho g (2b)^n}{\mu 12} \frac{\partial P}{\partial s}$$

where k_p = area permeability, ρg = unit weight, μ is the viscosity, $2b$ is the aperture width, P is the pressure, s the length of the fracture and $1 \leq n \leq 3$ where the limiting cases are filled and hydraulically smooth joints, respectively [25]. In our case n is equal to 3.

The equation assumed laminar flow between 2 frictionless plates. The initial joint aperture in our experiment can be derived from the point at which the slope of the stress displacement curves stiffens to a deformation equivalent to the elastic deformation (Fig. 13). The initial aperture is about 0.1 mm and flow rate for the biaxial test was about 3.0 cm³/s. It is obvious that the flow rate does not rigorously follow equation (1) (Fig. 11). In fact, significant flow, approx 2.0 cm³/s occurs after the joint apparently closes. This is equivalent to a permeability of 1.2 mdarcies assuming a joint spacing of 1 m. This compares with a permeability of 100 μ darcies measured for the intact rock in the same direction. The flow is, therefore, an order of magnitude greater through this volume of rock even after apparent closing of the joint. The joint, thus, must be bridged allowing flow along paths in the plane of the joint.

A comparison of the flow rate, displacement and velocity data as a function of stress indicates that all three properties are highly dependent on the aperture of the

UNIVERSITY OF TORONTO LIBRARY

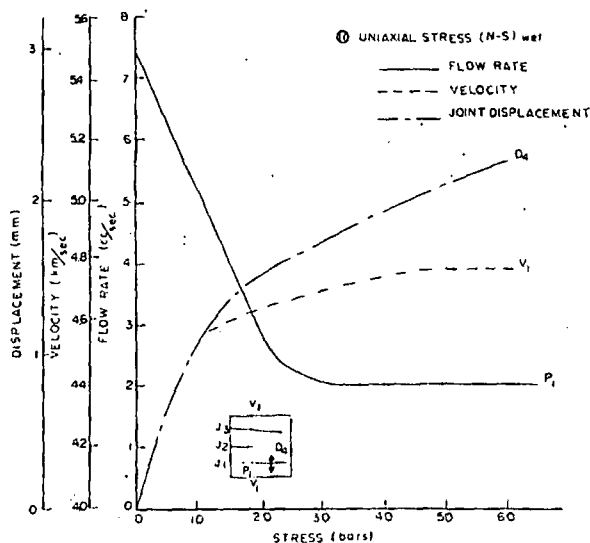


Fig. 14. Comparison of the effect of joint closure on displacement, sonic velocity and fluid flow.

joints in an intact rock mass (Fig. 14). Once the aperture closes at reasonably low stresses, the rates of change of velocity and deformation are close to the elastic properties of the intact rock; fluid permeability decreases rapidly to approx 25 bars after which it remains constant.

TIME EFFECTS

The changes that occurred in velocity and deformation during the 10 months between tests were minimal. The increase in velocity was small and perhaps even within the data scatter. The fact that the velocity increased is surprising as one would expect the velocity to decrease because of stress relief as a function of time. The increase may be due to increased water content over the previous year.

CONCLUSIONS

Field and laboratory tests were conducted in Sherman granite, a massive anisotropic rock. These tests suggest the following conclusions:

(1) Results from this *in situ* test can be scaled to larger rocks of the same rock type because the specimen was representative of a rock out-cropping over a large area, was tested *in situ*, and contained several discontinuities with sufficient surface area to allow measurement of bulk mass properties rather than intact properties. These discontinuities are part of the regional geologic environment.

(2) Seismic velocity, displacement and resistivity all increase with stress while permeability typically decreases.

(3) The granite block in the field appears elastically stiffer than a laboratory specimen of the same rock material. This is especially true at low stresses where crack closure plays a more subordinate role in very large specimens than in very small ones.

(4) Initial velocities in the unstressed granite block are higher than in unstressed laboratory samples. Factors that contribute to the differences in wave propagation include: *in situ* and/or residual prestress and *in situ* moisture content of the rock.

(5) The directional dependence or anisotropy in rock properties is nearly independent of applied loads. The rate of change in strain and velocity with stress depends on the boundary load conditions.

(6) The displacement of individual joints accounts for only a portion of the total displacement of the granite block under compression. The contribution of the joints to the total deformation is especially significant at the lower stresses. The remainder is attributed to the closure of the ubiquitous microfractures.

(7) Permeability of fluid along a joint is the most sensitive property to joint closure at very low stresses. It decreases by a factor of 4 for uniaxial stresses up to 25 bars. Once the joint is closed, flow rate along the joint remains nearly constant and is insensitive to further increase in load. At these pressures, permeability along the joint is still significantly greater than the permeability of the intact rock.

Acknowledgements—This work was performed for the Army Research Office, Contract DAH CO4-72-C-0049 under the technical direction of Mr. Finn Bronner, for whose guidance and encouragement we are indebted. We also acknowledge the support of A. S. Orange, K. Gronseth, D. Norton and R. B. Smith for their assistance in conducting the resistivity, permeability and seismic experiments. Mr. H. Robertson assisted in conducting the field and laboratory experiments. Some preliminary seismic surveys were performed by Dr. S. Smithson of the University of Wyoming. J. B. Walsh of the Massachusetts Institute of Technology carried out an elastic analysis of the *in situ* test configuration.

Received 10 March 1976.

REFERENCES

1. Jaeger J. C. & Cook N. G. W. *Fundamentals of Rock Mechanics*. Methuen, London (1969).
2. Muller L. Die Mechanischen Eigenschaften der Geologischen Körper. *Carinthia* 11, 28, 177-191 (1971).
3. Malina H. Berechnung von Spannungsumlagerungen in Fels und Boden mit Hilfe der Elementenmethode. *Veröff. Inst. Boden. Feib. mech.* Univ. Karlsruhe, Heft 40, p. 1-25.
4. Cundall P. A computer model for rock mass behavior using interactive graphics for the input and output of geometrical data. University of Minnesota, U.S. Army Corps of Engineers Contract DACW 45-74-C-006, (July 1974).
5. Goodman R. E., Taylor R. L. & Brekke T. L. A Model for the mechanics of jointed rock. *J. Soil Mech. Fdn. Div. Am. Soc. Civ. Engrs* 94, 637-659 (1968).
6. Barton N. R. A model study of rock-joint deformation. *Int. J. Rock Mech. Min. Sci.* 9, 579-602 (1972).
7. Einstein H. H. & Hirschfeld R. C. Model studies on mechanics of jointed rock. *J. Soil Mech. Fdn. Div. Am. Soc. Civ. Engrs* 99, 229-248 (1973).
8. Muller L., Tess C., Fecker E. & Muller K. Kriterien zur Erkennung der Bruchgefahr geklüfteter Medien. *Rock. Mech. Suppl.* 2, 71-92 (1973).
9. Byerlee J. D. Frictional characteristics of granite under high confining pressure. *J. geophys. Res.* 73, 6031-6037 (1968).
10. Goodman R. E. & Ohnishi Y. Undrained shear testing of jointed rock. *Rock Mech.* 5, 129-149 (1973).

11. Hoskins E. R., Jaeger J. C. & Rosengren K. J. A medium scale direct friction experiment. *Int. J. Rock Mech. Min. Sci.* 5, 143-153 (1968).
12. Logan J. M., Iwasake T., Friedman M. & Kling S. A. Experimental investigation of sliding friction in multilithologic specimens. *Geologic Factors in Rapid Excavation*, Geol. Soc. Am. Eng. Geol. Case History No. 9, pp. 55-67 (1973).
13. Pratt H. R., Black A. D. & Brace W. F. Friction and deformation of jointed quartz diorite. *Proc. 3rd Congr. Int. Soc. Rock Mech.* Vol. 2, Part A, 306-310 (1974).
14. Wallace G. B., Slebir E. J. & Anderson F. A. Foundation testing for Auburn Dam. *Proc. 11th Symp. Rock Mech. University of California, Berkeley*, pp. 461-498 (1969).
15. Eydokimov P. D. & Sapozhnik D. D. A large scale field shear test on rock. *Proc. 1st Congr. Int. Soc. Rock Mech.* Belgrade, pp. 3-17 (1970).
16. Wallace G. B., Slebir E. J. & Anderson F. A. *In situ* methods for determining deformation modulus used by the Bureau of Reclamation. In *Determination of the In Situ Modulus of Deformation of Rock*. ASTM spec. publ. 477, pp. 3-261 (1970).
17. Bieniawski Z. T. The effect of specimen size on compressive strength of coal. *Int. J. Rock Mech. Min. Sci.* 5, 325-335 (1968).
18. Maini Y. N. T. *In situ* hydraulic parameters in jointed rock—their measurement and interpretation. Unpublished Ph.D. Thesis, Imperial College (1971).
19. Jouanna P. Seepage tests under stress *in situ*. *Proc. Symp. Int. Soc. Rock Mech.—Percolation through fissured rock*. Paper T2-G, Stuttgart (1972).
20. Darton N. A., Blackwelder E. & Siebenthal C. E. U.S. Geological Survey. Geological Atlas, Laramie-Sherman Folio (1910).
21. Brace W. F., Orange A. S. & Madden T. R. The effect of pressure on the electrical resistivity of water-saturated crystalline rock. *J. Geophys. Res.* 70, 5669-5678 (1965).
22. Brace W. F. & Orange A. S. Further studies of the effect of pressure on electrical resistivity of rocks. *J. Geophys. Res.* 73, 5407-5420 (1968).
23. Walsh J. B. The effect of cracks on the compressibility of rocks. *J. Geophys. Res.* 70, 381-390 (1965).
24. Swalls, H. S., Handin J. & Pratt H. R. Field measurements of residual strain in granitic rock masses. *Proc. Third Congr. Int. Soc. Rock Mech.* Vol. II, Part A, pp. 563-568 (1974).
25. Gale J. S. A numerical field and laboratory study of flow in rocks with deformable fractures. Ph.D. Dissertation, University of California, Berkeley (1975).

UNIVERSITY OF VERMONT LIBRARIES

The purpose of the investigations was to develop a method for the production of K_2ZrF_6 not contaminated with other reaction products. The method involved the sintering of zirconium dioxide with fluorine-containing compounds of potassium and ammonium. Pure baddeleyite, obtained under semi-industrial conditions, potassium fluoride, and ammonium fluoride were used.

To investigate the reaction process derivatograms of the charge were recorded. The reaction loading to the forma-

tion of K_2ZrF_6 clearly takes place at $400^\circ C$. At this temperature 95% of K_2ZrF_6 is formed from baddeleyite in 10 min.

It was also shown that K_2ZrF_6 can also be obtained from potassium fluoride and ammonium fluoride. Replacement of ammonium fluoride by ammonium bifluoride does not affect the degree of formation of potassium fluorozirconate from baddeleyite.

500-Non-Fe
1975 N3 N3

UDC 524.61:661.833

Extraction of tantalum (V) with tributyl phosphate from chloride solutions in the presence of potassium, magnesium, aluminium and iron (III) salts

E V Prudnikov and Yu I Levchenko (Leningrad Technological Institute)

SUBJ
MNG
ETT

Effect of HCl concentration on the degree of extraction of tantalum and iron (III) by solutions of TBP in kerosene ($Ta_{init} = 2.12 \cdot 10^{-4}$ g-ion/l)

HCl _{init} mole/l	Equilibrium concentration in aqueous phase (1) and organic phase (2)						V _w /V _o	ε _{Ta} %	ε _{Fe} %
	HCl mole/l		Fe ³⁺ · 10 ² mole/l		Ta · 10 ⁴ g-ion/l				
	1	2	1	2	1	2			
50% TBP in kerosene									
1.02	1.02	0.01	0.40	0.63	2.13	-	0.98	-	61.2
2.96	3.74	0.21	0.19	0.82	2.11	-	0.94	-	81.2
4.94	4.58	0.36	0.05	0.93	2.12	-	0.92	-	84.9
6.86	6.39	0.47	-	1.02	2.12	-	0.89	-	100.0
9.85	9.12	0.73	-	1.01	1.26	0.82	0.87	38.9	100.0
10.85	10.05	0.81	-	1.02	1.07	0.95	0.85	47.0	100.0
75% TBP in kerosene									
1.02	1.01	0.01	0.16	0.86	2.12	-	0.89	-	84.3
2.96	2.63	0.33	0.04	0.98	2.11	-	0.85	-	96.1
4.94	4.32	0.61	0.03	0.99	2.12	-	0.81	-	97.1
6.86	6.02	0.85	-	1.01	2.12	-	0.77	-	100.0
9.85	8.62	1.23	-	1.02	0.68	1.45	0.72	68.4	100.0
10.85	9.5	1.36	-	1.02	0.53	1.53	0.68	74.3	100.0
100% TBP									
1.02	1.0	0.02	0.06	1.0	2.11	-	0.76	-	95.8
2.96	3.63	0.32	0.009	1.01	2.12	-	0.71	-	99.4
4.94	4.31	0.63	-	1.02	2.11	-	0.67	-	100.0
6.86	6.0	0.85	-	1.02	2.13	-	0.61	-	100.0
9.85	8.59	1.25	-	1.02	0.43	1.69	0.56	79.7	100.0
10.85	9.48	1.36	-	1.02	0.39	1.81	0.54	82.3	100.0

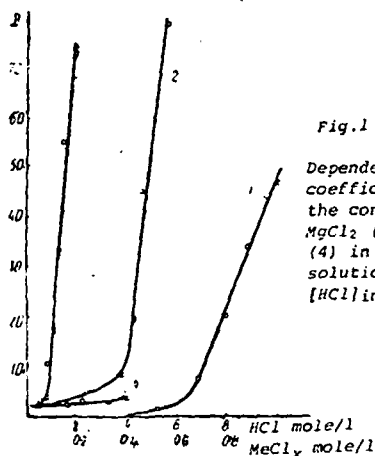


Fig. 1
Dependence of the distribution coefficients of tantalum D on the concentration of HCl (1), MgCl₂ (2), AlCl₃ (3) and KCl (4) in the initial aqueous so solution. For curves 2-4 [HCl]_{init} = 7 mole/l.

Summary

As a result of the susceptibility of tantalum (V) ions in solution towards hydrolysis and the formation of hydrolytic polymers, its behaviour in extraction systems is complicated. The extraction of tantalum(5⁺) from metals associated with it was investigated.

To determine the composition of the extracted chloride complexes of tantalum the electronic absorption spectra of the aqueous solutions and extracts were determined at 210-400 nm. The results indicate that tantalum passes into the organic phase in the form of tetrachloro-oxotantalate ions and in the form of undissociated hydrolytic complexes of the Me(OH)_xCl_{4-x} type.

Reaction of lanthanum chloride with magnesium oxide

UDC 546.131+546.634

P G Permyakov, B G Korshunov and V A Korkhin (Moscow Institute of Steel and Alloys - State Research Institute of Rare Metals)

Summary

Rare-earth metal chlorides obtained in the treatment of

complex ores by the chlorination method enter into a complex reaction with the oxygen-containing components of the and refractories. The oxychlorides which form are poorly

N12, 1975

EXPERIENCE WITH TITANIUM EQUIPMENT IN HYDROMETALLURGICAL PROCESSES AT THE NORIL'SK MINING AND METALLURGICAL COMBINE AND PROSPECTS FOR ITS ADOPTION

UDC 669.295

I. A. Travnichek

UNIVERSITY OF UTAH
RESEARCH INSTITUTE
EARTH SCIENCE LAB.

Many years of experience in the use of titanium at the Noril'sk Combine have demonstrated its advantages over corrosion-resistant steels and polymers.

The process liquids in hydrometallurgical processes at the Noril'sk Combine have a wide range of working temperatures, pressures, and abrasiveness and various degrees of acidity; sulfuric acid, metal sulfides, sulfates, and chlorides, and dissolved gases (O_2 , Cl_2 , H_2S , H_2) being present in them simultaneously.

Comparative tests in various hydrometallurgical process liquids at the Combine showed that the resistance of titanium brand VT1-0 is practically the same as that of VT3, VT4, OT4, VT6, VT14, and AT3 titanium alloys. This is in accordance with the conclusions of other authors that in most cases titanium alloys are less resistant than unalloyed titanium [1,2]. These factors predetermined the use of VT1-0 brand titanium at the Combine (VT1-1 had been used previously).

As early as 1960, 12 titanium bases for starting sheet production were manufactured in the nickel electrolysis shop and successfully tested.

Comparative Resistance of Titanium and Steel
12Kh18N10T Equipment

Process liquid	Equipment	Service life, years	
		12Kh18N10T	VT1-0
150-180 g/l H_2SO_4 ; 80 g/l Cu^{2+} ; 50 mg/l Cl^- ; Fe^{2+} , Ni^{2+} , and precious metal ions; $t = 40-60^\circ C$	Header tank Segregation tank EKHM20-35 pumps TN-70 pumps	1.5-2 0.5 0.5-1 —	5 year operation 1.5 yr operation — 2
120-140 g/l H_2SO_4 ; 50 g/l Cu^{2+} ; 28 g/l Ni^{2+} ; 55 mg/l Cl^- ; Fe^{2+} ; $t = 60^\circ C$	Candle-type filter	—	Operating from 1967
20 g/l H_2SO_4 ; Ni^{2+} , Cu^{2+} , and Fe^{2+} ; sol; liq = 1:100; $t = 60^\circ C$	Filter press	—	4 year operation
Thiourea+NaCl+"Ekstra" glue	Colloid tank	3	5 year operation

not capable of consistent operation in the copper electrolysis shops, because of the relatively high sulfuric acid content of the electrolyte. However, a comparison of the resistance of certain types of titanium and steel 12Kh18N10T equipment (see Table) indicates that titanium could be adopted more extensively in copper production.

The range of titanium equipment in the hydrometallurgical production of precious metals has been considerably extended in recent years. For example, in the electrolysis department (20-100 g/liter H_2SO_4 , up to 50 g/liter Cu^{2+} , Fe^{2+} , Fe^{3+} , and precious metal ions present, $t = 20-90^\circ C$) the life of steel 12Kh18N10T valves does not exceed 6 months and the life of 75Kh28L alloy pumps is 9-10 months. Titanium pumps have been operating consistently under the same conditions for more than two years. Titanium valves, pipework, and trays give outstanding reliability in these processes.

Titanium proved to be a reliable structural material when the autoclave method of producing precious metals was introduced. It proved to be exceptionally stable, for example, in acid chloride solutions during reduction with hydrogen ($t = 150^\circ C$, PH_2 up to 20 gauge atmospheres, 30 g/liter Ni^{2+} , 26 g/liter Cu^{2+} , 225 g/liter Cl^- , 40 g/liter SO_4^{2-} , up to 30 g/liter HCl). Chrome-nickel steels corrode under these conditions. In this case a protective layer of platinum group metals and hydrides forms on the surface of the titanium.

The consistent operation of pumps of various types, pipework, and sealing equipment made from titanium in process stages in the chlorine-cobalt shop is evidence of its efficiency in this section.

Research has revealed the sections where (for one reason or another) titanium equipment cannot be used. In particular operations (production of copper sulfate

SUBJ
MNG
EWT

attent:
electro
in the
these p
solid-t
20 days
bush ma
The t
carburi
layer w
covers,
tance a
their s
ties wa
The r
experie
nium as
Combine
stage in
tial ou
reduces
intensi
obtaine
has save
The No
complex
in diame
vacuum f

1. N.
Mashgiz,
2. V.
(seminar
3. V.
urgy of
19.
4. V.
1974, No

and sulfuric acid) titanium is not capable of consistent passivation, and in this case the use of high-alloy chrome-nickel steels and titanium with increased corrosion resistance [4200 (Ti + 0.2 Pd) and 4201 (Ti + 33% Mo)] is justified.

Titanium equipment such as pump covers, the working parts of seals, and angle sections in pipework which are exposed to considerable erosive action require special attention. For example, the service life of titanium pumps installed in the nickel electrolysis shop in the catholyte feed line is 8 years, whereas in one of the stages in the chlorine-cobalt shop where the pulp solids content is 30% the service life of these pumps does not exceed 8 months. In the pilot autoclave installation, where the solid-to-liquid ratio is 1 : 1, the service life of pump covers is not more than 10-20 days. There is also steady wear, due to the poor antifriction properties of the bush material in titanium pumps.

The titanium surface carburizing technology developed at the Combine using a solid carburizing agent and hard facing with carburized titanium wire give a dense surface layer with a hardness of up to 90 Rockwell C. Experimental titanium bushes, pump covers, and valve seatings have shown an increase of several times in erosion resistance and antifriction properties. Oxidizing titanium components did not increase their service life in erosion-active media. The increase in their antifriction properties was less marked than in carburized titanium components.

The results of corrosion tests on titanium and other metals in aggressive media and experience in the use of titanium equipment indicate the desirability of using titanium as a basic construction material for hydrometallurgical equipment at the Noril'sk Combine. Thus titanium is recommended for equipping the whole of the sulfur-processing stage in phase I at the Nadezhda Nickel Plant [4]. In spite of the considerable initial outlay on manufacture, the use of titanium is economically justified because it reduces equipment idle time and expenditure on all types of repairs, processes can be intensified and new advanced technology can be mastered, and high product purity is obtained. The use of titanium equipment in hydrometallurgical process stages in 1974 has saved the Combine ~ 3 million rubles.

The Noril'sk Combine has experience in the manufacture and erection of large and complex process equipment such as a sulfuric acid washing tower (8 m high and 3.4 m in diameter), an electrostatic precipitator (11.2 m high and 3.4 m in diameter), a vacuum filter with a fully immersible disk, and autoclaves.

REFERENCES

1. N. D. Tomashov and R. M. Al'ovskii, Corrosion and Protection of Titanium, Moscow, Mashgiz, 1963, 168 pages, illustrated.
2. V. B. Zhilkin, in: Applications of Titanium in the National Economy of the USSR (seminar reports), Moscow, Tsvetmetinformatsiya, 1967, 84-91.
3. V. N. Toporkov and I. A. Travnichek, in: Uses of Titanium in Industry ("Metallurgy of Light Non-Ferrous Metals" series), Moscow, Tsvetmetinformatsiya, 1970, 16-19.
4. V. A. Gutin, I. A. Travnichek, S. M. Salei, and N. A. Adugina, Tsvetnye Metally, 1974, No. 6, 27-29.

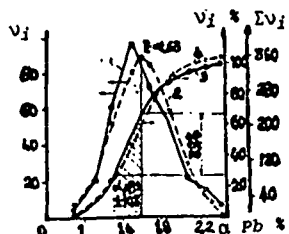


Fig. 1 The curves for the distribution of lead in the feed of the first stage of flotation: empirical (1, 3) and theoretical (2, 4). v_i and Σv_i are the frequency and sum of the frequencies of the empirical distribution; E is the mathematical expectation of the lead content in the ore %.

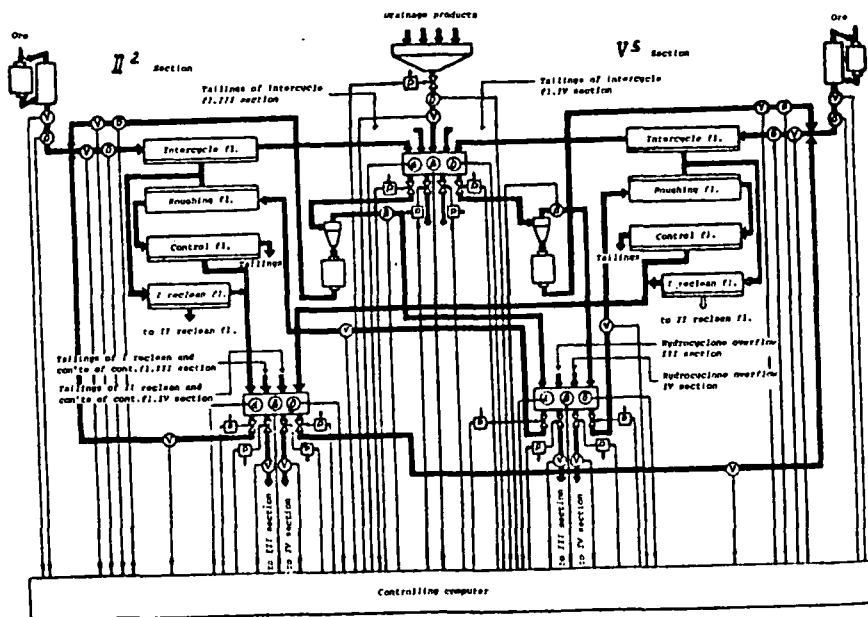


Fig. 2 Schematic diagram of the system for automatic control of the bulk flotation production lines:

- V = the volume consumption rate of pulp
- δ = the density of the pulp
- α = the content of lead and zinc in the flotation product
- β = the content of the -0.074mm class in the flotation products
- O = the stopping point of the automatic control indicators
- P = the regulator of the local control system

Features of the movement of free-flowing material in a revolving drum in the "cascade" regime

G I Sverdlik and G G Grigor'ev (North-Caucasian Mining-Metallurgical Institute. Urals Polytechnical Institute)

Summary

The "cascade" regime is one of the main high-speed operating regimes for revolving drum units widely used in the metallurgical industry (drum mills, mixers, etc.). Determination of the relationships governing the movement of the load in this regime is important for optimisation of the industrial processes of grinding and mixing. A distinguishing feature of the "cascade" regime is the presence of a region in which the particles are in a state of free flight.

The characteristics of the movement of material in the upper section of the load were investigated on a model with a drum diameter of 100mm by means of cine photography. The transition of the particle into the state of free flight is only possible on the descending section of its trajectory. It is preceded by slip of the particle in relation to the particles situated below.

*Res. Non-Fe...
1979 N. 2 N 1*

UDC 669.2

Electrolysis of zinc solutions to exhaustion in an electrolysis cell with an anion-exchange membrane

A D Pogorelyi, V S Saval'skii and G M Tysh (North-Caucasian Mining-Metallurgical Institute - Department of General Metallurgy)

In the hydrometallurgical production of zinc the problem of maintaining the accumulated impurities (Na, K, Mg, Mn) at a specific level is solved by a single method, i.e. by withdrawal of part of the solution from the cycle. Zinc or zinc and sulphuric acid are extracted from the withdrawn solution in various ways.

One of the methods¹⁾ involves subsequent electrolysis of the spent electrolyte to exhaustion in zinc (to approximately 12g/l) and evaporation of the residue to recover the sulphuric acid as a 75% solution and produce a mixture of crystalline zinc sulphates and impurities, which are treated separately.

The problem of extracting the zinc and recovering the sulphuric acid from the spent electrolyte can be solved more simply by electrolysis to exhaustion in a cell with anion-exchange membranes, which separate the cathode and

anode compartments. The purpose of the anion-exchange membranes is to pass the anions and keep the cations in the cathode cell²). It was proposed to obtain a compact deposit of zinc at the cathode, to transfer the free SO₄²⁻ ions and sulphuric acid combined with zinc into the anode compartment, and to produce a catholyte as free as possible from zinc and sulphuric acid.

In this method the final product will be the spent catholyte, in which the sulphate of alkali metals and magnesium (and manganese) are retained. The process of periodic electrolysis was modelled in a three-compartment plastic electrolysis cell with anion-exchange membranes separating the cathode and anode compartment, as shown in fig. 1.

The working volume of the central cathode cell amounted to 150ml, and that of the two outer anode cells amounted to 100ml each. We used MA-41 membranes. The cathode was made from aluminium, and the anodes were lead. Synthetic solutions of zinc sulphate were prepared from ZnSO₄ conforming to GOST 4114-69 and sulphuric acid of chemically pure grade.

The concentrations of the components of the solution simulated the neutral and spent electrolytes of zinc production. Balancing trials were undertaken on the electrolysis with the anion-exchange membranes in order to determine the selectivity of the selected membrane in relation to the Zn²⁺ and SO₄²⁻ ions and to establish the presence of oxidation reduction side reactions in the process and the limits of removal of zinc and sulphuric acid from the solution. The procedure involved the application of a potential to the cell filled with measured volumes of the catholyte and anolyte and electrolysis without interruption. Every hour the characteristics of the process were recorded, and the catholyte and anolyte were analysed for zinc and sulphuric acid content.

The initial solutions were as follows: catholyte 150ml, containing 40.75g/l and 117g/l H₂SO₄, density 1.195; anolyte 200ml, density 1.270 containing 120.7g/l Zn, pH = 5. The results from a representative experiment on the electrolysis of the zinc solution with anion-exchange membranes under the published conditions²) at a current density of 500A/m² a cell potential of 4.2V, and a final temperature of 30°C are given in table 1.

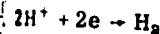
Table 1: Results from electrolysis in the three-chamber electrolysis cell

Time h	Number of ampere-hours after each hour A · h	Catholyte				Anolyte		
		Zn g/l	Zn g	H ₂ SO ₄ g/l	H ₂ SO ₄ transferred g	H ₂ SO ₄ g/l	H ₂ SO ₄ transferred g	Zn g
0		40.75		117.0		pH=5		120.7
1	3.152	22.18	2.786	119.9	+ 0.237	21.7	4.34	120.7
2	3.197	9.60	1.89	114.0	- 0.885	32.4	2.14	115.6
3	3.419	4.0	0.795	97.8	- 2.430	59.1	5.34	115.6
4	2.93	3.03	0.190	78.5	- 2.895	77.22	3.64	111.6
5	3.019	1.71	0.198	50.1	- 4.260	88.11	2.18	111.6
	15.72		5.859		-10.233		17.64	

At the end of the experiment we obtained 5.62g of cathode deposit of satisfactory quality with 94.75% extraction of Zn, 117ml of spent catholyte with density 1.012, and 206ml of anolyte with density 1.305, and we had taken 10.5ml each of the catholyte and anolyte for analysis. The material balance had a discrepancy of 0.53% with respect to zinc and 1.68% with respect to the acid.

The selectivity of the membrane was estimated by the size of the discrepancy for the transfer of Zn²⁺ and SO₄²⁻ ions in the balance. In the first case the imbalance amounted to 2.3%, and in the second 1.6%. Thus, the MA-41 membrane has fairly high selectivity with respect to Zn²⁺ and SO₄²⁻ ions.

The current yield of SO₄²⁻ transferred into the anode compartment from the deposition of 5.62g of zinc on the cathode and the amount of SO₄²⁻ from decomposition of H₂SO₄ to the amount of SO₄²⁻ ions, calculated from the direct current consumption (15.72A · h), amounts to only 67.4%. The low current efficiency indicates that side reactions occur at the anode and that OH⁻ ions pass through the membrane. The current yield of zinc (5.62 · 100/15.72 · 1.22) amounts to only 29.36%, and this indicates development of the reaction



at the cathode and the transfer of OH⁻ ions into the anode compartment. In fact, 100 - 29.36 = 70.64% of the direct current or 11.09A · h is used on the evolution reaction, and this corresponds to the formation of 0.417g of hydrogen. Of this amount 0.237g of hydrogen was formed on account of the 1.4g of SO₄²⁻ transferred from the cathode to the anode compartment, and 1.8g was produced from decomposition of H₂O.

After compilation of the material balance for the anode cell the amount of water passing into the anode part of the cell was 13.81g, while the amount of water calculated from the current consumption (32.8% of 15.72A · h) for the transfer of OH⁻ was only 3.25g. Evidently, not SO₄²⁻ and OH⁻ ions but O₂ · nH₂O and OH⁻ · nH₂O ions pass through the membrane.

Fig. 2 shows the curve for the variation of the volume of the catholyte during electrolysis. From the curve it follows that the deposition of a large amount of zinc and the transfer of SO₄²⁻ ions and of part of the water into the anode cell lead to a reduction of 15% in the final volume of the catholyte. For this reason the concentration of sulphate impurities in the waste catholyte increases in work with industrial solutions.

On account of the change in volume the concentration of zinc in the anolyte increases insignificantly (from 120 to 111g/l). In our case the sulphuric acid concentration amounted to 88.11g/l and can be increased by continuing electrolysis until it has been completely transferred from the cathode cell.

Under production conditions it is important to retain the sulphuric acid in the cycle, and its concentration is not important if the anolyte into which the

acid is being extracted is directed to the main electrolysis process. For the reason in subsequent experiments we stabilised the composition of the anolyte with respect to the acid, by replacing it each hour with new portions of neutral solution so that the sulphuric acid concentration was not higher than 20g/l and studied the possibility of complete transfer of the sulphuric acid into the anolyte. In other respects the procedure and the control of the process remain as before.

The operating conditions were as follows: current density 550A/m²; cell voltage 3.8-4.0V; temperature up to 30°C; catholyte containing 31.24g/l Zn and 120.64g/l H₂SO₄; anolyte containing 78.1g/l Zn at pH ≈ 5. Electrolysis continued to exhaustion with respect to zinc and sulphuric acid. The main characteristics of the process are given in table 2.

In experiment 3 (table 2) in order to define the limits of the region of chemical corrosion of the cathodic zinc more precisely the solution in the cathode cell was strengthened to 10.88g/l Zn by the addition of the concentrated solution 3h after the beginning of electrolysis.

Table 2: Results from electrolysis of the solution to exhaustion with respect to zinc and sulphuric acid

Electrolysis characteristics	Experiment		
	1	2	3
Residual content in catholyte g/l:			
a) Zinc	0.46	0.92	1.5
b) Sulphuric acid	0.05	10.05	30
Current yield of zinc %:			
a) Calculated from the composition of the catholyte after:			
first hour	77.62	87.58	84
second hour	61.85	58.88	62
third hour	31.44	26.98	30
fourth hour	4.87	9.81	45
fifth hour	14.42	-8.56	12
sixth hour	2.17	7.44	6
seventh hour	4.85	8.56	
b) Calculated from the weight of the cathodic zinc in the experiment %	27.21	28.37	37
Current yield of H ₂ SO ₄ % calculated from the composition of the catholyte after the first hour:			
second hour	80.90	90.98	99
third hour	94.19	79.80	76
fourth hour	86.31	75.84	81
fifth hour	76.21	82.01	101
sixth hour	82.16	75.69	31
seventh hour	76.73	83.03	72
eighth hour	83.00	76.30	
Extraction %:			
a) Zinc	98.53	97.05	91
b) Sulphuric acid	99.9	91.6	71
Electricity consumption kWh/t:			
a) for deposition of zinc	12917.5	10988.0	8278.1
b) for transfer of H ₂ SO ₄ into anolyte	2191.1	2206.2	2154.1

The electricity consumption during electrolysis to exhaustion in cells with membranes considerably exceeds the usual norms for zinc electrolysis practice. With allowance for regeneration of sulphuric acid this excess must be attributed to losses on the technique of purification of a small volume of the electrolyte, amounting to 1% of the total volume, from accumulating impurities.

The change in the content of zinc and sulphuric acid in the catholyte after each hour of operation is shown in fig. 3. From these data it follows that the region of chemical corrosion of the deposit is observed with a residual zinc concentration of 2-3g/l and an acidity of 75-85g/l H₂SO₄. The expediency of continuing electrolysis for extraction of free sulphuric acid is determined by economic calculation.

Conclusions

1. The possibility of using electrolysis of zinc solutions with anion-exchange membranes for fairly complete isolation of zinc and sulphuric acid from the solution is demonstrated. It may find use for the separation of these components from the accumulating sulphates of alkali metals and magnesium (and also manganese) in zinc production solutions.
2. In the method 95-98% of the zinc is obtained as a cathode deposit suitable for remelting. Practically all the free sulphuric acid and sulphuric acid combined with zinc sulphate can be returned to the production process.

References

- 1) Z. Syrychinskii: Materials of scientific-technical conference in Warsaw on the improvement of the production technique for zinc, lead and accompanying metals: Moscow 1957.
- 2) F. Helferich: Ion-exchange resin: IL1962.
- 3) A. A. Salin and M. E. Syroeshkin: Electrolysis of zinc sulphate: Metallurgizdat, Moscow 1955.

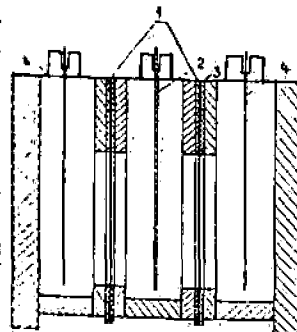


Fig. 1

Diagram of the three-chamber electrolysis cell. 1) Anion-exchange membranes, 2) aluminium cathode, 3) insert (rubber), 4) lead anodes.